

CHAPTER ONE

INTRODUCTION

1.0 Background to the Study

The use of geospatial information is growing continuously and needs to be updated frequently with the highest possible metric or thematic accuracy. Remote sensing offers the possibility of a fast and area-wide assessment of urban changes and developments. Remote sensing uses the visible, infrared and microwave sections or regions of the electromagnetic spectrum to record information about earth features under study (Igbokwe, 2010).

Recently the possibility of Very High Resolution (VHR) images and LiDAR (Light Detection and Ranging) data which are complementary by each other's types of information have proved to be reliable source of updates especially for land use land cover (LULC) information. Remote sensing data and digital image processing techniques have helped to reduce this burden of manual interpretation by making available continuously precise data for an automatic, systematic and efficient territorial and urban management. With increasing availability and wide utilization of sub-meter imagery, object-based image analysis (OBIA) has become the most basic means to process VHR imagery (Blaschke, 2010). The recent launch of many commercial VHR sensor systems (such as GeoEye-1, Pléiades-2, and WorldView-3) greatly improved the spatial resolution of imagery remotely sensed, with several 1–4 m multispectral bands and a sub-meter panchromatic band.

Urban landscapes are characterized by a complex spectral mixture of materials that are predominately made up of impervious surfaces, vegetation and soil. This heterogeneous composition of urban landscapes is difficult to map using traditional per-pixel classification (Mhangara et al 2015,) Digital image processing techniques are either pixel- or object-based (Soille, 2003,). Due to the high internal variance of high resolution imagery, previous urban mapping efforts using the per-pixel method have often produced unsatisfactory results (Blaschke and Strobl, 2001; Blaschke, 2009). The main drawback of per-pixel classification in a multi-dimensional feature space is that it doesn't make use of any spatial concept (Blaschke and Strobl, 2001). Especially in high-resolution images it is very likely that neighboring pixels belong to the same land cover class due to spatial patterns of differing complexity or texture. The application of traditional automatic classification systems, based on the pixel's spectral value, have been showing very unsatisfactory results when applied to high resolution images (Rego and Koch, 2003; Blaschke et al., 2001). In high resolution imagery each pixel is related not to the character of object or area as a whole, but to the components of the image. As a result, a lot more classes are detected when it is classified (Smith et al., 2000).

Recently, classification technology has progressed from traditional pixel-based statistical methods to knowledge- and object-based classification (OBC) approaches (Hodgson et al., 2003; Taubenböck et al., 2006). Object-oriented image processing overcomes these difficulties by first segmenting the image into meaningful multi-pixel objects of various sizes, based on both spectral and spatial characteristics of groups of pixels. According to Gamanya et al. (2007), the use of image segmentation and image understanding

algorithms replace classification based on entire pixel dominant classes hence providing a robust and reliable way to automate the classification processing chain. Object-oriented classification using multi-resolution image segmentation technique facilitates extraction of object primitives necessary for good classification results (Nausbaum and Menz, 2008). Furthermore, the fractal nature of remotely sensed imagery allows for object-oriented classification as they consider the geometric, spectral and topologic properties of image objects (Blaschke and Strobl, 2001). These unique characteristics offer great potential in the often diverse and dynamic nature of urban land cover classes (Zhou and Troy, 2008).

Remotely sensed data from airborne and space borne platforms offer global coverage at varying spatial, spectral, and temporal resolutions, and are the major sources of geospatial information (Baltasvias and Gruen, 2003). The emergence of new technologies in remote sensing which provide valuable data in various forms and scales for mapping and monitoring land cover features has created new research focus in the research community. It provides an opportunity for fast update of urban spatial classifications to match the dynamic transformations that characterize urban environments. For instance, its use has increased dramatically due to availability of high-density LiDAR data as well as high spatial/spectral resolution airborne imageries. The diverse sensor technologies allow to measure different aspects of objects on the Earth, from spectral characteristics in multispectral and hyperspectral images (HSIs), to height information in Light Detection and Ranging (LiDAR) data, to amplitude and phase in Synthetic Aperture Radar (SAR) systems. In other words, the passive sensing of

hyperspectral systems can be effective in describing the phenomenology of the observed scene over a continuum of spectral channels, whereas the active sensing of LiDAR systems can be exploited for characterizing topographical information of the scene.

The main goal of classification is to be able to effectively discriminate ground features. Even when the horizontal information for categories, shapes, and boundaries of ground features can be determined, urban features are so complex that multispectral imagery and traditional classification techniques are not sufficient for classifying them, e.g. while it is generally easy to distinguish vegetation and man-made objects using NIR (Near Infrared) images, it is still very difficult to discriminate between trees and grass. Again, sometimes in using the traditional method buildings are classified into other categories because of spectral variations caused by apparent differences in roof composition and shadow effects. However, such misclassification may be resolved by adding height information. So, even without NIR, using color images (containing only RGB bands) together with LiDAR data may improve classification accuracy.

Although highly capable in their own right, LiDAR and spectral information still lack certain details. LiDAR provides detailed information regarding geometries such as spatial distances, heights and canopy penetration but lacks any information concerning the particularities in the electromagnetic spectrum. Spectral provides highly detailed electromagnetic information to the point of material identification, but it is limited to two dimensions without spatial information in the 'z' or height dimension. These technologies are uniquely matched to lead to fusion opportunities. LiDAR has a unique advantage of being able to penetrate through foliage to capture some aspects within and

below vegetation. Hyperspectral imaging is a passive system that captures distinct spectra of ground features, exploiting electronic characteristics and molecular vibrations to identify and classify materials. Studies have shown that these two datasets complement each other and optimize classification capabilities. LiDAR data provides accurate measurement of landcover structures in the vertical plane; however, current LiDAR sensors have limited coverage in the horizontal plane. Multispectral data provide extensive coverage of landcover classes in the horizontal plane but are relatively insensitive to variation in their height. Therefore, the integration of LiDAR and multispectral data can greatly improve the measurement and mapping of landcover classes. New approaches such as the use of height information have been developed given the growing demand for accurate geospatial information (Potsiou et al 2010). A variety of Extremely High Spatial Resolution (EHSR) sensors and platforms are now available. This data combined with complementary data such as DSM, are suitable for the detection of buildings (Ioannidis, Psaltis & Potsiou 2009).

It is obvious that no single technology can be always sufficient for reliable image interpretation. For example, hyperspectral imagery should not be used to differentiate objects composed of the same material, such as roofs and roads both made of concrete. On the other hand, LiDAR data alone cannot be used to separate objects with the same elevation, such as roads with the same height but made of asphalt or concrete. In mapping and analyzing land cover features, the integration of LiDAR and high-resolution satellite imagery has a promising future. LiDAR provides very accurate position and height information, but less direct information on the object's geometrical shape, while high-

resolution imagery offers very detailed information on objects, such as spectral signature, texture, shape etc. Combining these two kinds of complementary datasets is quite promising for building extraction, 3D city modelling etc. (Tao and Yasuoka, 2002). Rottensteiner et al. (2003) integrated LiDAR and high-resolution multispectral data for the automatic detection of buildings with heterogeneous appearances; a hierarchic integration technique was adopted to detect buildings in urban settings. Hofmann (2001) used an object-based classification scheme to detect buildings and roads in IKONOS data using additional elevation information. Fusion of these two data sources is an obvious approach in order to capitalize on their respective advantages and compensate for their respective shortcomings for fine-scale land cover classification (Lee et al., 2008; Anderson et al., 2008).

1.1 Statement of the Problem

What is increasingly clear, however, is that urbanization is an important component of regional and global environmental change (Foley et al. 2005) and has significant implications for both environmental systems (Grimm et al. 2008) and human health and well-being (Patz et al. 2005). An understanding of emerging spatial patterns of urban form is a necessity as the spatial configuration of the urban landscape provides a snapshot of various economic, social and political factors that influence land use decisions (Netzband, Stefanov & Redman 2007). As metropolitan areas grow and change at an unprecedented rate (Fraser, Dial & Grodecki 2006), the provision of spatial and temporal data that illustrate where changes are occurring becomes imperative (Eurosense 2011). To this end, high quality, regularly updated information on the

patterns and processes within the urban environment – including maps that monitor location and extent – is essential (Potere and Schneider 2007). Mapping of urban land use/cover has therefore become an important requirement for urban land cover mapping, planning and management.

The study area has been carved out of River state of Nigeria. It is an area with high socio-economic activity especially because of the dominant oil exploration activities. All these, as a consequence bring about diverse and spatially dispersed land uses by all classes of the population. Unfortunately, Rivers State like many other similar places in Nigeria has not been given sufficient attention in the area of the regular environmental changes caused by natural and anthropogenic processes. Availability of up-to-date maps with their corresponding information will in no small measure help planners and other government agencies properly carry outplanning, monitoring and development of residential amenities, basic facilities, utilities and services. This study aims to evaluate the pixel and object based in order to determine more accurate and faster methods of analyzing land use and land cover features that undergo regular changes caused by these natural and human activities within the study area. The study will also give attention to the extraction of unpaved roads which has not been given much attention in urban features extraction.

There is no doubt therefore, that understanding the spatial distribution of human activities and physical environment at various levels will play critical role in sustainable planning and development.

1.2 Aim and Objectives of the Research

The aim of this study is to evaluate object and pixel based techniques in urban mapping using VHR image and LiDAR data. The aim was achieved through the following objectives:

(i) To carry out mapping of urban features (buildings, roads, vegetation, water bodies and bare soil.) from Geoeye-1 (VHR) image of 2012 using object-based and pixel-based techniques.

(ii) To statistically compare the results obtained from the two techniques and evaluate the capabilities of the nDSM to optimize the accuracy of urban features extraction.

(iii) To combine the Geoeye-1 image and LiDAR derived nDSM in the 3-D analysis of the features extracted.

(iv) To develop a technique for the extraction/identification of unpaved road

(v) To produce a digital urban map of the study site.

1.3 Research Questions

(i) Does object based method of classification achieve higher accuracy than the pixel based method in land cover classification using VHR image?

(ii) Does the addition of nDSM from LiDAR data improve the classification accuracy of urban land cover?

(iii) Does the addition of LiDAR derived nDSM to the VHR image effective in the 3-D analysis of features extracted?

1.4 Research Hypothesis

To statistically evaluate the research questions, the following hypotheses are drawn for investigation:

Ho: There is no significant difference between the accuracies of object based and pixel based methods of classification using high spatial resolution imagery.

Ho₁ The addition of nDSM does not significantly improve the accuracy of high resolution image classification of urban area.

Ho₂ The addition of LiDAR derived nDSM to the VHR image is not effective in the 3-D analysis of features extracted.

1.5 Justification of the Study

The traditional method of acquiring land use land cover information through ground survey method is not only labour intensive but time consuming. They may be suitable for small areas as opposed to when very large and complex areas are involved in large scale mapping. With the reduction in manual surveying techniques, remote sensing is a viable alternative for updating GIS databases. There is an increasing need to derive tangible image objects which can be imported in a GIS-ready form from the many images available for a particular area (Blaschke, 2010).

The use of VHR imagery in mapping and classification of land covers in urban areas has received great attention in recent times due to the availability of these images. With about half meter spatial resolution of VHR imagery (e.g. Geoeye, QuickBird and WorldView-2), small targets can be observed and detected. However, because of the

complexity of urban landscapes, the failure to consider spatial characteristics of the image in traditional pixel-based classifiers, and inconsistencies between scale of observation (i.e., pixel size) and the spatial characteristics of targets (e.g., buildings), conventional spectral-based classification approaches are ineffective (Weng and Quattrochi, (2006).

With regards to mapping of roads, it is also noteworthy that a great percentage of previous studies have mainly focused on the paved roads without much attention to unpaved roads which constitute a greater percentage of transportation networks in this part of the world. It is therefore important to exploit the use of object based classification method by integrating VHR image (Geoeye-1) and LiDAR data height information for better land use/land cover classification results. Furthermore the research will seek to design an algorithm that will be suitable for the mapping of unpaved roads. The findings in this study can be used to determine areas of attention as well as greatly assist stakeholders and other decision makers in implementing development programs and help to address security challenges particularly in this time of kidnapping and other forms of crime.

1.6 Scope of the Study

The scope of this study has been defined by the objectives outlined. It has focused on the mapping and analysis of land cover and land use features of the study area to highlight the efficacy of the object oriented classification method over pixel based method when VHR images are used. It has also investigated the value added when the height

information from LiDAR data (nDSM) is added to the VHR images in discriminating land cover features. Multiresolution segmentation and Rule-based classification have been used. The LiDAR derived nDSM was also utilized to develop a 3-D model of the study area with a view to ascertaining the strength of VHR image and LiDAR data in producing 3-D modeling. Google image and ground truth values were used to update the map.

As part of this research, effort was made to extract unpaved roads which are common features within the study area and as has been noted in the literature review, not much attention has been given to this, in previous research studies.

1.7 Limitations of the Study

It was hoped that the image to be acquired for this study will include a raw LiDAR data from which point clouds, intensity, DTM, DSM and point classification values can also be derived. However, what were available are 2012 Geoeye-1 image and 2012 LiDAR data which has been processed to DTM and DSM. Consequently, for the LiDAR, the researcher was limited to the use of nDSM value which is the difference between the DTM and DSM. LiDAR point has classification properties that can define the type of object that has reflected the laser pulse. They can be classified into a number of categories including bare earth, top of canopy and water. The intensity is a measure, collected for every point, of the return strength of the laser pulse that generated the point which is based on the reflectivity of the object struck by the laser pulse. The lack of other LiDAR values limited the researcher's analysis to the use of nDSM only. In order to effectively use the LiDAR derived nDSM, a corresponding GeoEye-1 image over the

same area and period was acquired for the analysis. The final results of the analysis which were based on the 2012 images were eventually updated using the latest Google image of the area as well as some ground truth values of the study area.

1.8 Significance of the Study

This growing phase of urbanization and Industrialization has presented emergent need of proper town planning. This study focuses on the production of an updated map, development of a technique for the extraction of unpaved roads and 3-D analysis of the features. The OBIA ruleset developed from this study can be applied to similar imaging sensors, similar applications, and similar elevations at different geographic locations, with reasonable classification accuracy. Consequently, the ultimate results from this study will to a great extent help planners and decision makers optimise the decision and planning process to enable them cope with the pace of urbanization and industrialization.

1.9 Study Area

The study area is located in Rivers State, Nigeria (see fig. 1a). Rivers State is one of the six states that form the Niger Delta, in the South South geo-political zone of Nigeria bordering the Atlantic Ocean (see fig. 1.1b). Having critically examined the data available for this study, seven study sites have been carved out from Ogba/Egbema/Ndoni and Emohua Local Government Areas (LGA) of Rivers State (see fig. 1.1c) and each with varying levels of urbanization. Effort was made to select sites on the image not covered by cloud and must be those areas that coincide with the LiDAR data coverage. This was to ensure that the study sites were areas free from cloud and also covered by the aerial image and the LiDAR data. These sites include Omoku, Osiakpu,

Ikiri, Obido, Ogbogwu and Akabuka towns in Ogba/Egbema/Ndoni LGA as well as Egbeda town in Emuoha LGA.

These sites were subsequently clipped from the Geoeye images and georectified using the LiDAR data. This process was performed using the Georeferencing tool in ArcGIS desktop software. Figure 1.1a, 1.1b and 1.1c present maps of Nigeria, Rivers State and the two local government areas (Ogba/Egbema/Ndoni and Emuoha LGAs) where the study has been carried out.

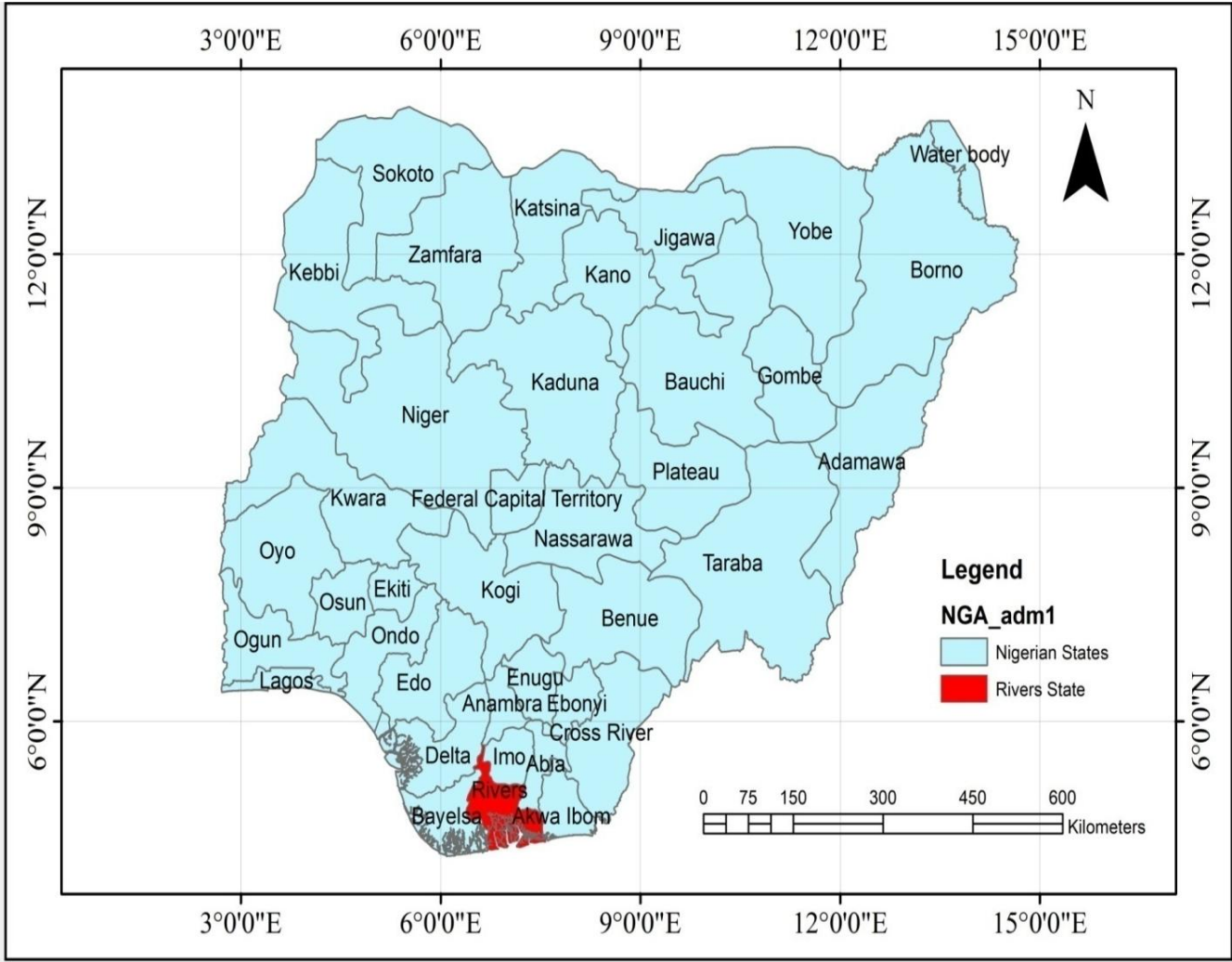


Figure 1.1a: Map of Nigeria showing location of Rivers State in red
Source: Ministry of Lands, Rivers State, Nigeria

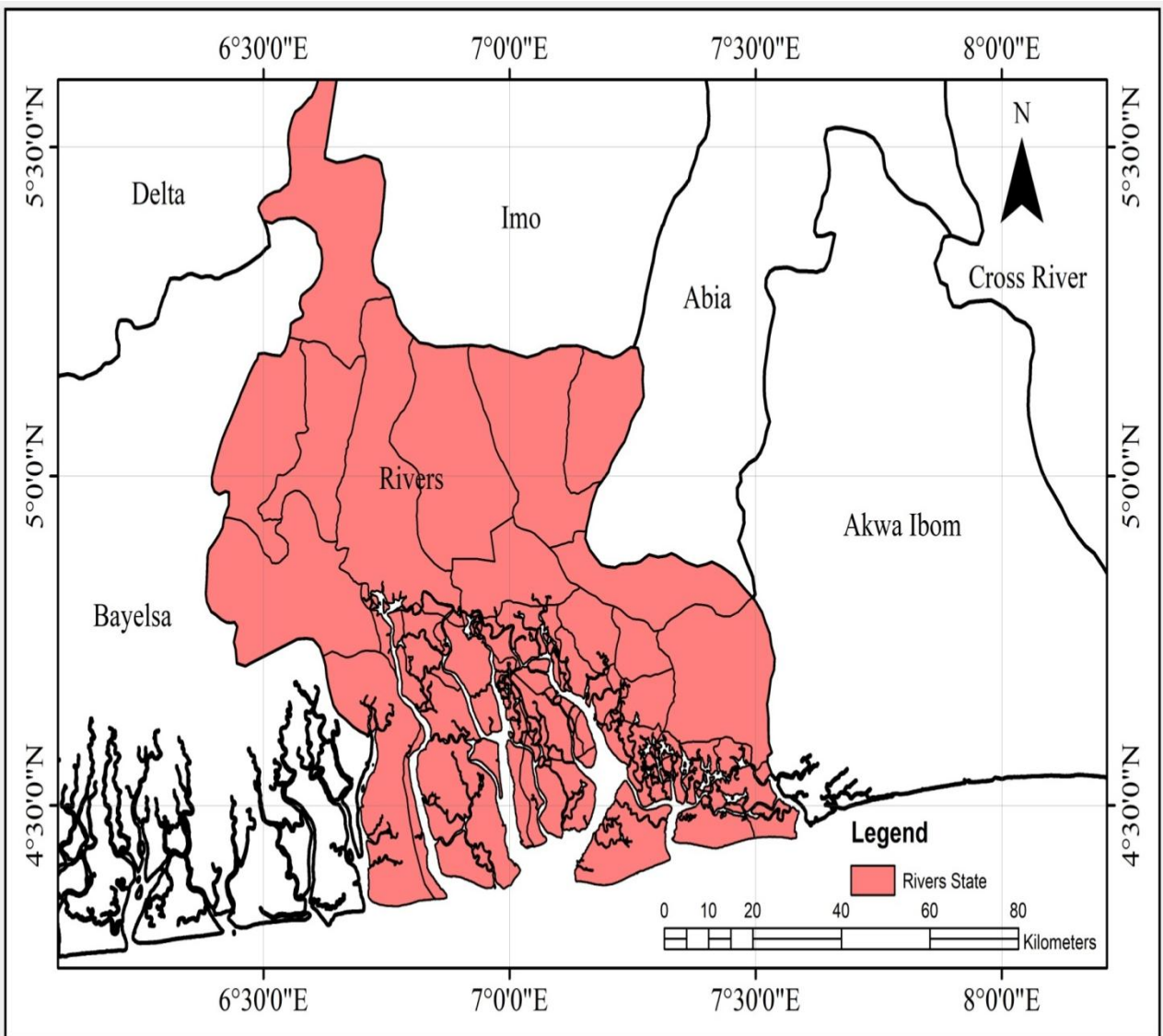


Figure 1.1b: Red patch shows map of River State, Nigeria.
 Source: Ministry of Lands, Rivers State, Nigeria

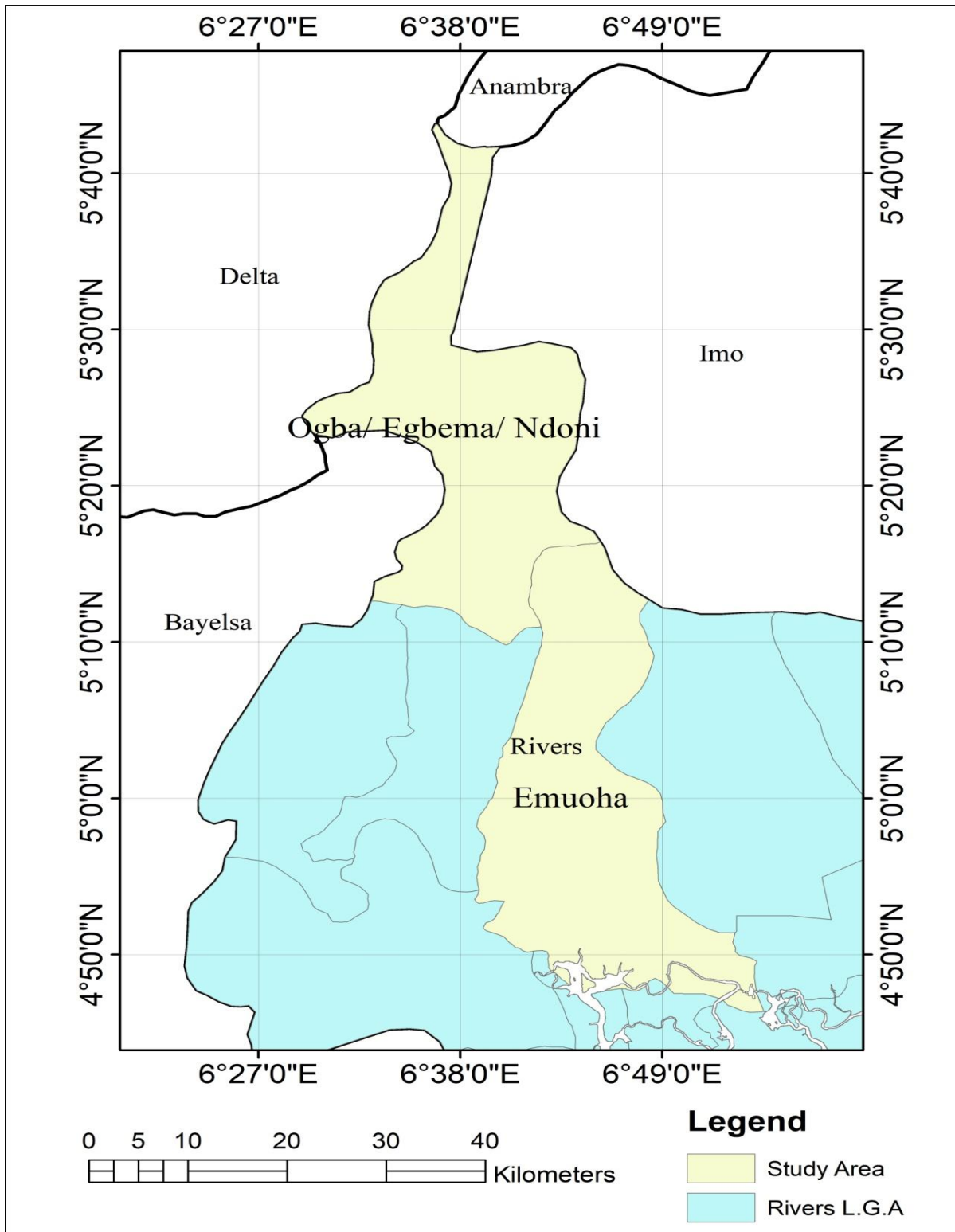


Figure 1.1c: Map of the Study Area from where seven (7) study sites were carved out
 Source: Ministry of Lands, Rivers State, Nigeria

The portion carved out as the study area has been covered by both the satellite imagery and the LiDAR data during the acquisition in 2012. This area is located approximately between Latitudes $04^{\circ} 35'$ and $05^{\circ} 40'$ North, and Longitude $06^{\circ} 30'$ and $06^{\circ} 59'$ East.

1.9.1 Geomorphological and Vegetation of the Area

The study area has a relatively well-drained land and rich soil, fresh water rivers, creeks, wetlands secondary forests and abundant sunshine and rainfall all year round (Ella, 1995). The vegetation is a typical rainforest, characterized by various plant species arranged in tiers or store. Common plant species include oil palm [*Elaeis guineensis*], mango [*Mangnifera indica*], Native pear [*Dacryodes edulis*], Oil bean tree [*penthracllethra macrophylla*], Avacado pear [*persea americana*], Musa Spp Cassava [*manihot esculenta*], Yam [*Dioscorea spp.*] African star apple [*chrystophyllum albidum*], Guava [*psidium guajava*], Paw-Paw [*cariaca papaya*], etc. The climatic conditions and topography support a wide variety of plant and animal life. The flora consists of economic trees especially oil palm trees and a variety of plants species of great pharmacological value as human elixir.(Ellah, 1995).Underneath the earth surface are pools of natural gas and oil. (Ellah, 1995).

According to Rivers State meteorological station in Port Harcourt, the climate of the study area is tropical and marked by two distinct seasons, the dry season (November – March) and the wet season (April – November). The wet season annual rainfall is between 49.5mm in January and 580mm in July and is usually interrupted by a short dry spell in August. Average temperature ranged from 27.1°C to 31.1°C , (Ellah, 1995)

In terms of land use in the study area, some sections of the land support forest growth, fallow lands and rivers, while roads, buildings (commercial and dwelling places) and other infrastructures are also notable features in the study area. In other words, apart from the places covered with fresh water rivers, creeks, wetlands secondary forests, significant sections of the land in the area are used for residential purposes and other social amenities such as roads, schools, hospitals and markets. The entire topography of the State is also characterized by a maze of rivers, lakes, creeks and swamps crisscrossing the low-lying plains in varying dimensions. This relatively low altitude gives the area its characteristic flat and monotonous low relief interspersed by many wetland (swamp /creek basins), which crisscross the central low lands and empty into the two main river systems Sombreiro and Orashi (Ellah 1995).

1.9.2 Economic Activity in the Study Area

Rivers State generally has maintained its importance as a leading supplier of wealth to the Nigerian nation because of its famous huge oil reserve and natural gas. From available records, the study area hosts the most of the oil exploration in Rivers State. According to current oil company records, no local government in Nigeria produces as much crude oil and gas as the Ogba/Egbema/Ndoni (ONELGA) local government (Ellah 1995).

The natural environment supports an agricultural economy based on fishing and farming for production of a wide variety of crops such as cassava, yam, maize, coco-yam, plantain and banana, including many vegetables such as okra, pepper and different types

of melon and a variety of fruits. Fishing and farming are therefore the dominant occupation of the local inhabitants.

The oil exploration activity in the area on the other hand has attracted the influx of people from various parts of the country to settle and carry out different classes of businesses since there is a huge guarantee of clientele for any type of business. It is also important to mention the other side of the economic and environmental side of the oil exploration in the area. The oil spill and gas flaring have direct consequences on the environment. Several studies carried out can confirm that Ogba/Egbema/Ndoni area is immensely polluted with various pollutants ranging from acid rain, carbon monoxides, heavy metals and lead compounds. This can easily be seen as all the surrounding vegetation is damaged and some are completely destroyed for as much as 50 meter or more from the pint of gas flaring (Efe, 2003). Likewise, the oil spill does a lot of damage to agriculture and fishing and most times the land and water affected by the spillare rendered completely useless for mostly farming and fishing.

CHAPTER TWO

THEORETICAL FRAMEWORK

2.0 Introduction

This section deals with a comprehensive insight into the concept of the research, its basis and the perspectives of the proposed analysis that will be made in the research. It will focus on the subject of remote sensing application of Very High Resolution (VHR) image and LiDAR data as well as investigate the pixel based and Object Based Image Analysis (OBIA) classification method and segmentation parameters. To do this, there is need to understand the operating principles of remote sensing with respect to VHR and LiDAR data properties and their applications in LULC urban mapping. 3-D modeling will also be achieved.

2.1 High Resolution Remote Sensing of Urban Areas using VHR and LiDAR

The analysis of urban areas demands for high spatial resolution supporting data. Although their spatial resolution enables the identification of urban and sub-urban objects, these images are difficult to classify on a pixel-by-pixel basis due to their high level of information (Van der Sande et al., 2003). Images of urban areas contain a complex spatial set of spectrally distinct land feature types, which require important spatial/semantic information for their classification. In these cases, object-oriented image classification algorithms are recommended as opposed to pixel based because the information necessary to interpret those images is represented by image objects and their mutual relationships (Gamanya et al ., 2007). Pixel-based classification techniques utilize spectral pattern value combinations associated with different feature types, each

assigned a unique Digital Number (DN), evaluating spectral reflectance values present within each pixel to find meaningful patterns.

Shadows cast by elevated objects also cause limitation on the use of high spatial resolution images. These shaded areas are usually left unclassified or simply classified as shadows (e.g., Shackelford and Davis, 2003), resulting in a significant loss of land features information. One possible approach to overcome this problem is to use spatial information, such as adjacency relations, for the classification of shaded areas in this kind of images (e.g., Yuan and Bauer, 2006; Zhou and Troy, 2008).

Object-oriented classification algorithms, that consider not only the spectral information but also several other image object features, such as shape, texture and spatial context, may be used to improve the classification in urban areas (Benz et al ., 2004; Zhou and Troy, 2008). Zhou et al. (2009) used both the spatial relations to neighbouring objects and the Normalized Difference Vegetation Index (NDVI), to distinguish “low shadows” into grass and pavement and “high shadows” into trees and buildings.

In addition, altimetry data from LiDAR may be helpful in the discrimination of image features of the same material at different heights, such as concrete buildings and road/vacant land in urban areas (Madhok and Landgrebe, 1999; Gamba and Houshmand, 2002; Chen et al., 2009; Zhou et al., 2009). However, LiDAR data itself is insufficient to distinguish between different features with the same height, such as buildings and trees (Vu et al., 2004). In such cases, spectral indices, such as the NDVI, can be used to first discriminate between vegetation and impervious surfaces and then at a low level of

segmentation, the LiDAR data can be used to discriminate among features with different heights.

Although highly capable in their own right, LiDAR and spectral information do lack certain details. LiDAR provides detailed information regarding geometries such as spatial distances, heights, and canopy penetration but lacks any information concerning the particularities in the electromagnetic spectrum. Spectral provides highly detailed electromagnetic information to the point of material identification, but it is limited to two dimensions without spatial information in the 'z' or height dimension. These technologies are uniquely matched to lead to fusion opportunities (Mesina, 2012)

2.2 Very High Resolution Images

VHR satellite imagery (spatial resolution $\leq 1\text{m}$) began with the successful launch of IKONOS-2 in 1999 with four multispectral bands of red (R), Green (G), blue (B), and near infra-red (NIR).

The requirement of an appropriate signal to noise ratio for the high spatial resolution data collection has restricted the spectral resolution to four bands for a decade since 1999 [Zhang, 2014]. Although, the successful launch of WorldView-2 with 8 MS bands (each with a spatial resolution of 1.8m) and 1 Pan Band (with maximum spatial resolution of 0.46m) has relaxed this restriction. These new generation of high spatial resolution satellite sensors have helped to acquire new images making it possible for new applications. Although their spatial resolution enables the identification of urban and sub-urban objects, these images are difficult to classify on a pixel-by-pixel basis due to their high level of information (Van der Sande et al., 2003). The images contain a

complex spatial set of spectrally distinct land feature types, which require important spatial/semantic information for their classification. In these cases, object oriented image classification algorithms are recommended because the information necessary to interpret those images is represented by image objects and their mutual relationships (Gamanya et al., 2007). Figure 2.1 presents the growth of optical VHR images since 1999.

Table 2.1: The growth of optical VHR satellite images since 1999.

Sensor Type	Spatial Resolution (in metres)		Number of Bands	Year	Country
	MS	Pan			
IKONOS-2	4.0	1.0	4MS + 1Pan	1999	US
Quickbird-2	2.44	0.61	4MS + 1Pan	2001	US
Kompsat-2	4	1.0	4MS + 1Pan	2006	South Korea
EROS-B	0.7		1Pan	2006	Israel
CartoSat-2	-	0.8	1Pan	2007	India
WorldView-1	-	0.5	1Pan	2007	US
Skymed-1		1.0	1Pan	2007	Italy
Skymed-2		1.0	1Pan	2007	Italy
GeoEye-1	1.65	0.41	4MS + 1Pan	2008	US
Skymed-3		1.0	1Pan	2008	Italy
WorldView-2	1.8	0.46	8MS + 1Pan	2009	US
Skymed-3		1.0	1Pan	2010	Italy
Pléiades-1	2.0	0.5	4MS + 1Pan	2011	Italy
Pléiades-2	2.0	0.5	4MS + 1Pan	2012	France
Kompsat-3	3.2	0.7	4MS + 1Pan	2012	South Korea
GeoEye-2	1.0	0.25	4MS + 1Pan	2013	US

Pan = Panchromatic, MS = Multi-Spectral, Source: [Stoney, 2008].

Apart from the problem mentioned above, the use of high spatial resolution images is related to the existence of shadows cast by elevated urban objects, particularly buildings. These shaded areas are usually left unclassified or simply classified as shadows (e.g., Shackelford and Davis, 2003), and this results in a significant loss of land features information. One possible approach to overcome this problem is to use spatial

information, such as adjacency relations, for the classification of shaded areas in this kind of images (e.g., Yuan and Bauer, 2006; Zhou and Troy, 2008). Object-oriented classification algorithms, that consider not only the spectral information but also several other image object features, such as shape, texture and spatial context, may be used to improve the classification in urban areas (Benz et al., 2004; Zhou and Troy, 2008). Alternatively, shadows may be classified by replacing the shadowed pixels by non-shadowed pixels of the same region from another image acquired at a different time and with different sun azimuth angles as proposed by Zhou et al. (2009).

In addition, altimetry data from LiDAR may be helpful in the discrimination of image features of the same material at different heights, such as concrete buildings and road/vacant land in urban areas (Madhok and Landgrebe, 1999; Gamba and Houshmand, 2002; Chen et al., 2009; Zhou et al., 2009). However, LiDAR data itself is insufficient to distinguish between different features with the same height, such as buildings and trees (Vu et al., 2004). A way around this problem is to use NDVI to differentiate between vegetation and non-vegetation areas.

There is no doubt that in spite of these noted problems, VHR images have provided high amount of data related to earth observation on a daily basis. This is because satellite images have wide ground coverage as well as high frequency of image acquisition [Konecny and Schiewe, 1996]. This improvement enabled the use of VHR satellite imagery in a rapidly growing list of new applications, e.g., urban security, urban disaster management, and urban planning [Blaschke, 2010].

2.2.1 Multispectral and Hyperspectral Satellite Images

Sensors measure reflected energy within sections of the electromagnetic spectrum. Multispectral imagery is produced by sensors that measure reflected energy within specific sections or bands. The sensors usually have between 3 and 10 different band measurements in each pixel of the images they produce. Examples of bands in these sensors typically include visible green, visible red, near infrared, etc. and Landsat, Quickbird and Spot satellites are well known to use multispectral sensors. Conversely, Hyperspectral sensors measure energy in narrower and more numerous bands. They can contain as many as 200 or more contiguous spectral bands that provide continuous spectral measurement across the entire electromagnetic spectrum, an example of hyperspectral sensor is Hyperion. The images produced from hyperspectral sensors contain much more data than images from multispectral sensors and have greater potential to detect differences among land and water features. For example, multispectral images can be used to map forested areas, while hyperspectral images can be used to map species within the same forest area.

2.3 LiDAR Imaging Systems

LiDAR system (Light Detection and Ranging) also known as airborne laser scanning (ALS) comprises a set of instruments: the laser device; an inertial navigational measurement unit (IMU), which continuously records the aircraft's attitude vectors (orientation); a high-precision airborne Global Positioning System (GPS) unit, which records the three-dimensional position of the aircraft; and a computer interface that manages communication among devices and data storage. LiDAR imaging system

actively sends light energy known as pulses to the ground and measures reflected light (return) back to the sensor. So pulses of light travel to the ground, they are reflected and the returns are detected by the sensor while using the timing of those return trips to measure distances and thus produce 3-D images. Figure 2 shows LiDAR components.

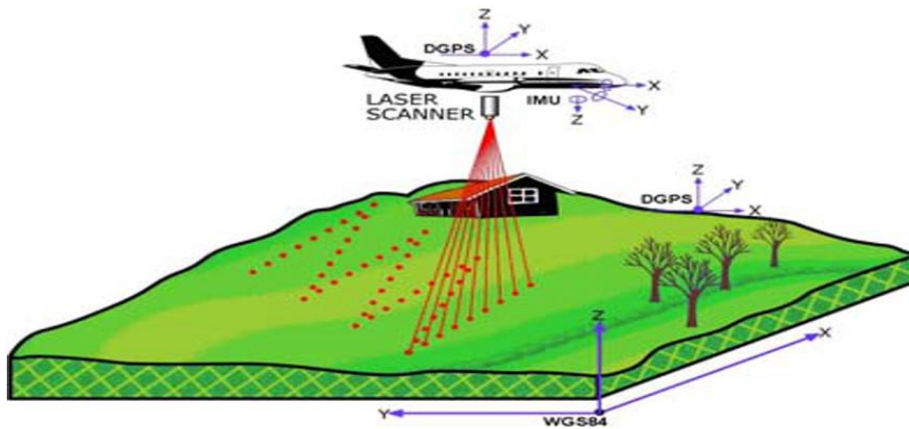


Figure 2.1: Components of LiDAR, Source McGaughey, (2007)

LiDAR is a remote sensing technology that operates on a similar fashion to RADAR sensing, but uses laser light instead of radio waves. LiDAR scanners, which can be either ground based or airborne/space borne, generate 3D models of their environment by emitting pulses of light and precisely timing their reflections from a target. This timing information is used to create a point cloud, a set of possibly millions of 3D coordinates that represent laser-target interactions. The system uses laser technology

enabled with an integrated inertial/GPS system to generate data.

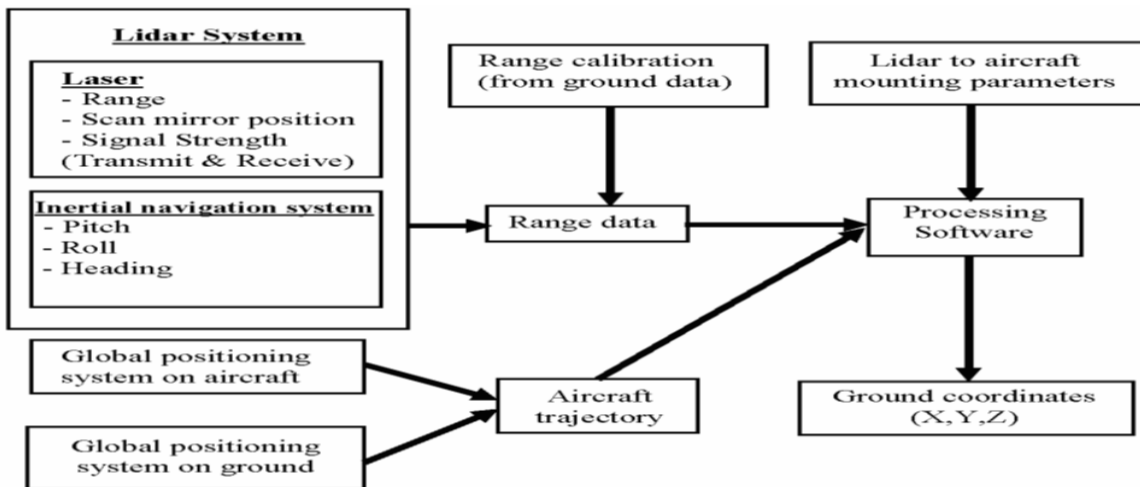


Figure 2.2: Various sensors employed in LiDAR system. (Lohani, 2010).

LIDAR offers tangible advantages, including nearly perfect registration of spatially distributed data and the ability to penetrate the vertical profile of a forest canopy and quantify its structure (Gatziolis, et al, 2008). There are two types of LIDAR acquisition differentiated by how backscattered laser energy is quantified and recorded by the system’s receiver. With waveform LIDAR, the energy reflected back to the sensor is recorded as a (nearly) continuous signal. With discrete-return, small-footprint LIDAR, reflected energy is quantized at amplitude intervals and is recorded at precisely referenced points in time and space. Popular alternatives to the term “point” include “return” and “echo.” The energy amplitude pertaining to each return is known as intensity. This article addresses only small-footprint, discrete-return LIDAR. The discrete return LiDAR returns multiple measurements from a pulse, but not tied to the specific pulses, see figure 2.3.

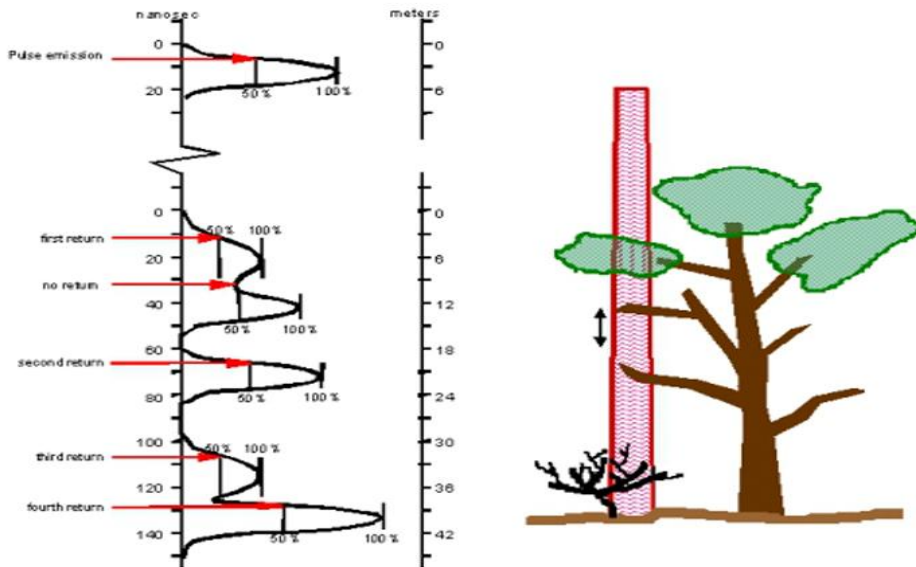


Figure 2.3: Multiple LiDAR returns, Source: Tiwari, (2011)

Whereas, waveform LiDAR represents multiple binned measurements associated with each pulse. The waveform data allows one to derive a continuous distribution of the laser energy for each pulse where discrete return does not, see figure 2.4.

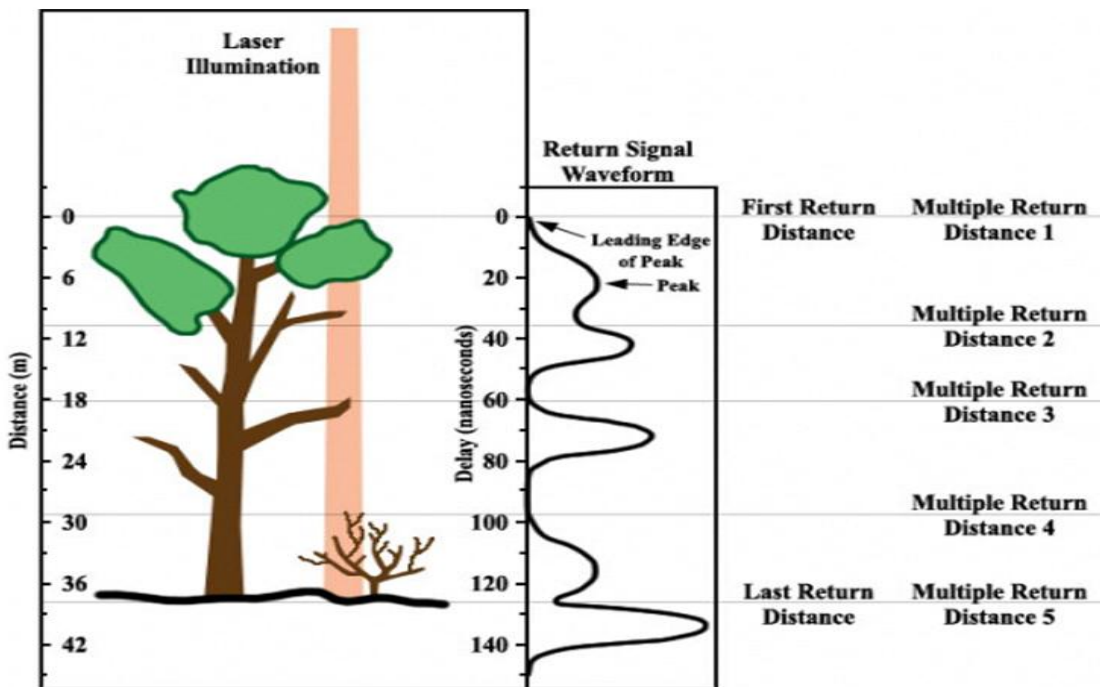


Figure 2.4: In a waveform LiDAR, the entire return pulse is digitized and recorded in a discrete multiple-return LiDAR. Source: Tiwari, (2011)

LiDAR has become an established technique for deriving geometric information in three dimensions. The system is seen to offer a relatively quick technique for extracting accurate surface models and thus offers the potential for the creation of DEMs and other mapping products (Kost, Loddenkemper & Petring, 1996; Lohr, 1998). LiDAR is considered to offer several potential benefits for the creation of DSMs:

1. Offers a cost-effective way of producing DSMs with an accuracy in the order of decimeters (Lohr, 1998), and is less prone than other remote measuring systems to difficulties in measurement due to variations in weather.
2. Offers precise definition of surface features through a very high density of recorded points, allowing the creation of gridded DSMs with cell resolutions of 1 ± 3 m (Lohr, 1998). Automatic DSM generation using digital photogrammetry has problems with feature definition because of surface smoothing and the difficulty of controlling the image-matching algorithms (Smith, 1997; Smith & Waldram, 1996; Smith, Tragheim & Holt, 1997).

2.4 LIDAR Positioning Principle

LiDAR survey data acquisition begins by flying an aircraft or helicopter over an area and operates the laser scan from side to side. The receiver picks up the laser pulses reflection value of the target and records the time it takes from emission to when it is received back at the receiver. The distance from the aircraft to the ground is calculated by dividing the time by two and multiplying by the speed of light. The inertial navigation system keeps track of the rotations of the aircraft in the three axes (along the

line of flight around the wings and crab) and the GPS keeps track of the actual location of the aircraft in space. After scanning an area, multiple returns and points are combined with each other in what is known as a point cloud. Point clouds are representative models of an area and are processed further to create products such as a digital surface model (DSM) and digital elevation model (DEM).

2.5 Characteristics of LiDAR data (Landmap Spatial Discovery, 2014)

- i. LiDAR data collection produces a geographic database with height and surface measurement information.
- ii. Collected by a laser at intervals of between 1m and 2m on the ground, the vertical accuracy of each height point is +/- 15 cm.
- iii. The LiDAR database is referenced to the British National Grid system which means that it can be easily integrated with other geographic databases and Ordnance Survey mapping.
- iv. The data collected can be used to produce both Digital Terrain Models (ground surface only) and Digital Surface Models (the ground and all features on it).
- v. LiDAR data is available in ERDAS Imagine format projected in British National Grid.

2.6 LiDAR and other DTM and DSM Building Technologies

For now there are three main known technologies of building DTM and DSM. The classical topographic survey remains the simplest and most uncomplicated way of building it. This is by obtaining a cloud of points and lineal elements with planimetric and altimetric coordinates (x, y and z), by means of some type of measurement

equipment (GPS, total stations, levels etc.). Besides being a precise system, it allows for the selection of the most representative points to be taken as the orographic characteristics of the terrain. However, this method can only be viable for a small area as it is very tedious and time consuming.

The second technology is the photogrammetric system and it is based on performing a photogrammetric flight, the area on which to base the Digital Terrain Model and apply either photogrammetric restitution or digital correlation of images. This has shown to be very reliable method of obtaining Digital Terrain Models. According to (Gomez et al, 2005), Photogrammetric restitution provides a DTM defined by a series of curves in level with a defined equidistance which, a priori, may be insufficient given that for flatland the distance between curves may be excessively large. Digital correlation of images provides a regular match of points with an associated altitude. The disadvantage here is that sometimes a DSM is presented rather than a DTM.

The third method which is increasingly being used for this purpose is LIDAR. This system uses laser to measure distances and it is similar to the more-familiar radar, but uses laser (or light) rather than radio waves, and is often referred to as "laser radar". The LIDAR system is complex and comprised of a transmitter/receiver and a high-power laser scanner, a GPS receiver provides the position and height of the aircraft at all times, and an inertial measurement system (IMU) provides information on the turns made by the aircraft and its trajectory. During the flight, measurements are taken independently with the three LIDAR subsystems: GPS, IMU and ALS (Airborne Laser Scanning) but applying labels with the GPS time. The labels will allow for the synchronization of all the measurements in post processing. In addition to the laser measurements, we must

also know the coordinates of the GPS antenna and the position of the ALS with respect to the antenna in order to assign WGS84 coordinates to the terrain points.

It should be noted that the LIDAR system can discriminate among multiple responses received by a single pulse (up to 5) allowing for the determination of intermediate surfaces, such as power lines or vegetation coverage. Currently there are various types of scanners which can recognize up to 7 echoes, other that can only recognize the first pulse, others that only recognize the last, and others that recognize both, etc. the type of scanners selected will depend on the type of job and level of data needed (Gomez et al, 2005). Based on the large amount of pulses received (current systems can broadcast up to 100,000 pulses per second and 95% of the pulses issued plus their echoes are received), a very high density Digital surface model is generated. A LIDAR based DTM is at least three times more dense than a photogrammetric DTM.

Accordingly, the primary goal of the airborne LIDAR system is to obtain precise digital terrain models which are applicable in a large number of fields and represent an efficient alternative to the traditional methods of obtaining Digital Terrain Models using photogrammetry (restitution or digital correlation of images). Another advantage is the speed in which the DTM is obtained thanks to the lack of any intermediate processes. In addition, it is possible to build a separate DTM and DSM, which would provide even greater information for analysis.

2.7 Advantages of LiDAR Technology

As mentioned earlier, the other methods of topographic data collection are ground survey methods, interferometry, and photogrammetry. LiDAR technology has some

advantages in comparison to these methods, which are being listed according to report by Indian Institute of Technology, Kanpur:

- i Higher accuracy: Vertical accuracy 5-15 cm (1s) and Horizontal accuracy 30-50 cm
- ii Fast acquisition and processing: Acquisition of 1000 km² in 12 hours and DEM generation of 1000 km² in 24 hours.
- iii Minimum human dependence: As most of the processes are automatic unlike photogrammetry, GPS or land surveying.
- iv Weather/Light independence: Data collection independent of sun inclination and at night and slightly bad weather.
- v Canopy penetration: LiDAR pulses can reach beneath the canopy thus generating measurements of points there unlike photogrammetry.
- vi Higher data density: Up to 167,000 pulses per second. More than 24 points per m² can be measured. Multiple returns to collect data in 3D.
- vii GCP independence: Only a few GCPs are needed to keep reference receiver for the purpose of DGPS. There is no need of GCPs otherwise. This makes LiDAR ideal for mapping inaccessible and featureless areas.
- viii Additional data: LiDAR also observes the amplitude of back scatter energy thus recording a reflectance value for each data point. This data, though poor spectrally, can

be used for classification, as at the wavelength used some features may be discriminated accurately.

ix Cost: It has been found by comparative studies that LiDAR data is cheaper in many applications. This is particularly considering the speed, accuracy and density of data.

Confusion has arisen from time to time over the difference between the terms DTM, DEM and DSM. Attempt will be made here to describe the terms based on several conclusions made by researchers.

Digital elevation model (DEM): Generic term covering digital topographic data in all its various forms as well as the method for interpreting implicitly of the elevations between observations (Maune et al., 2001). Digital Elevation Models are bare earth (topology) models of the Earth's surface. You can derive Digital Elevation Models (or Digital Terrain Models) by using the ground hits from LiDAR. Ground hits are the last return of the LiDAR.

Florinsky 1998, defined DTMs as digital representations of variables relating to a topographic surface, namely: digital elevation models (DEMs), digital models of gradient (G), aspect (A), horizontal (Kh) and vertical (Kv) land surface curvatures as well as other topographic attributes.

Digital surface model (DSM): Model depicting elevations of the top of reflective surfaces, such as buildings and vegetation (Maune et al., 2001). $DSM - DTM =$ Height of the objects standing in the surface of the earth that are either natural like trees canopy or

manmade like buildings, towers, electric poles etc. This difference is also referred to as Normalized Digital Surface Model (nDSM).

2.8 LiDAR data Application in Mapping Urban Features

While the need for large scale mapping of urban areas using EHRS imagery continues to grow, LiDAR technology offers the advantage of being used to derive accurate high-resolution digital surface models (DSMs) which can support the extraction of urban features (Gamba & Houshmand 2000; Renslow, Greenfiel & Guay 2000). Both airborne and terrestrial LiDAR are revolutionising the domain of EO for a wide range of applications including the mapping of canopy gaps in continuous cover forest (Gaulton & Malthus 2010), providing information about the ecosystem structure for understanding and monitoring of environmental change (Béland, Widlowski & Fournier 2014), the city modelling and surface reconstruction (Habib et al. 2005), and building extraction (Niemeyer, Rottensteiner & Soergel 2014).

It is reported that an accuracy of the order of 0.2 m horizontally (x,y) and 0.1 m vertically (z) can be achieved in the production of DSMs (Lohr, 1998) from LiDAR depending on the system used. A last pulse Digital Surface Model (DSM) is created from the original LiDAR points using inverse distance weighting. A gradient image is then created by differentiating the DSM. A DTM is created.

During the last two decades, DEM have been subsequently integrated into land feature classification from remotely sensed data (Weidner, 1997) due to the limitations of pixel-by-pixel classification based essentially on spectral information. DEM have since been used to extract buildings (Koc & Turker 2005,), roads (Clode, Kootsookos

&Rottensteiner 2004) and trees (Kim & Muller 2011), either as a single dataset or combined with remotely sensed imagery. The literature indicates that elevation data resolves the difficulties related to spectral similarities of land features having different height, for example parking lots and buildings, grass and trees (Koc & Turker 2005; Gamba & Houshmand 2000).

Urban planning, infrastructural development, and roof modelling require building footprints (Li et al. 2013; Wang, Lodha & Helmbold 2006), which are defined as the area within the perimeter of a building measured at the foundation. The generation of 3-D building models from point clouds provided by LiDAR has also gained importance (Wang, Lodha & Helmbold 2006). The DSM not only provides a geometric description for building extraction (Brunn & Weidner 1997), but also provides height information essential for distinguishing objects with similar spectral information, such as building, roads, water, coal piles, and different vegetation types (Yu et al. 2011). According to Koc & Turker (2005), the basic idea behind using a DSM for building extraction is that man-made objects with different heights can be detected by applying a height threshold to nDSM.

Extraction of vegetation is also another application of LiDAR data in urban features mapping. In some cases, DSM is used in conjunction with high resolution image and in some other cases, only DSM can be used depending on the nature of discrimination. For example, Iovan, Boldo & Cord (2008) extracted urban vegetation using high-resolution colour infrared (CIR) digital images and a DSM within a high density urban area. Priestnall, Jaafar & Duncan (2000) used the standard deviation of DSM to differentiate

buildings from trees after the study area was split into above-surface information and surface information.

Beyond the 3-D coordinates determination capability, LiDAR intensity data have proven beneficial in data registration, feature extraction, classification, surface analysis, and segmentation to name just a few examples. The primary benefit of LiDAR intensity lies in the fact that it is related to surface reflectance and other surface characteristics and several intensity processing techniques have been developed and implemented to calibrate, normalize, or otherwise correct the recorded intensity values to produce values that are more useful and more closely related to true surface characteristics. In order to accurately and comprehensively retrieve various tree properties, making full use of LiDAR data attributes is necessary (Moffiet et al, 2005). Laser return intensity is such a data attribute which is closely related to the spectral reflectance of object surfaces. This data attribute facilitates exposing object-inherent information such as tree biochemical and physiological properties (García et al, 2011). In combination with the common 3-D coordinates that show the spatial location of each laser point, laser return intensity can further derive the spatial distributions of object biophysical properties such as forest biomass carbon stocks (García et al, 2011). LiDAR intensity is particularly useful in distinguishing features in land use/cover. For example, impervious surfaces stand out in light intensity images. OBIA segmentation can separate these features using light intensity values. Hence, the data attribute of laser return intensity has long been stressed in the field of LiDAR-based forest remote sensing.

According to (Kongo, 2015) LiDAR application in feature extraction is undoubtedly very useful due to the following reasons:

(1) Dense LiDAR point clouds enable the generation of highly accurate high-resolution nDSM;

(2) Surface features can be extracted on the basis of a height context analysis of the LiDAR points, thus enabling accurate mapping of surface features like buildings, trees, power lines, and pipelines;

(3) Dense LiDAR point clouds provide the easiest way to identify small changes in elevation, hence making it easier to map regions with little textural variations, including variations in the surface of vegetation canopies;

(4) LiDAR pulses penetrate the vegetation canopy creating multiple returns which can be used to facilitate vegetation classification in different seasons;

(5) Multiple returns of LiDAR enable the mapping of ground elevations, even in regions of dense vegetation.

2.9 Land Cover Classification

The general aim of land cover classification is the associations of each pixel within the image with a specific land cover class to produce precise classification maps of the data.

The purpose of image classification is to label the pixels in the image with meaningful information of the real world (Jensen, 2006; Igbokwe, 2009). In other words image classification is performed in order to derive specific information on the amount and spatial distribution of various types of land use and land cover, from remotely sensed

data (i.e. satellite imagery, aerial photographs), and is generally regarded as the process of creating thematic maps from images (Campbell 1996, Lillesand and Kiefer 1994). Urban and environmental applications depend on these classification results. The major steps of image classification may include: determination of a suitable classification system; selection of training samples; image preprocessing; feature extraction; post-classification processing; and accuracy assessment (Lu and Weng, 2007). Before raw data image data is transformed into land cover image maps, a decision must be taken on what categories of land cover is needed. The only requirement for any land cover category is that it has a distinct signature that a satellite can record.

In remote sensing, pixel is the ground area corresponding to one number of a digital image data set. In a classification process unknown pixels are identified and assigned to a predefined class or they are combined to unknown clusters according to an appropriate decision rule. The decision rule is a mathematical algorithm that performs the actual sorting of pixels into distinct classes (Lillesand and Kiefer, 1994). The selection of a suitable classification method is significant for improving classification accuracy. A recent review of classification algorithms (Lu and Weng, 2007) grouped the large number of classifiers available to the remote sensing analyst into: supervised; unsupervised; soft; hard; parametric; non-parametric; pixel-based; object-based.

2.9.1 Classification Techniques

Based on the idea that different feature types on the earth's surface have different spectral reflectance and remittance properties, their recognition is carried out through the classification process. There are various classification approaches that have been

developed and widely used to produce land cover maps (Aplin, 2006). Satellite image classification plays a major role in extract and interpretation of valuable information from massive satellite images. Satellite image classification methods can be broadly classified into three categories (see figure 2.5) and all three methods have their own advantages and disadvantages

(1) **Automatic:** These classification methods use algorithms that applied systematically the entire satellite image to group pixels into meaningful categories. Automated satellite image classification methods can be further classified into two categories - supervised and unsupervised classification methods. The supervised classification requires that the analyst inputs training sets. These training samples are the most important factor in supervised classification. Accuracy of the methods highly depends on the samples taken for training. Training samples are two types, one used for classification and another for supervising classification accuracy. Major supervised classification method uses the following statistical techniques:

- i Artificial Neural Network (ANN)
- ii Binary Decision Tree (BDT)
- iii Image Segmentation

Unsupervised classification technique uses clustering mechanisms to group satellite image pixels into unlabeled classes/clusters. Later analyst assigns meaningful labels to the clusters and produces well classified satellite image. Most common unsupervised satellite image classification is

- i ISODATA (Al-Ahmadi, et al 2009)
- ii Support Vector Machine (SVM)

iii K-Means (Ahmed, et al, 2009)

(2) **Manual:** Manual satellite image classification methods are robust, effective and efficient methods. But manual methods consume more time. In manual methods the analyst must be familiar with the area covered by the satellite image. Efficiency and accuracy of the classification, depends on analyst knowledge and familiarity towards the field of study Sunitha, et al (2015).

(3) **Hybrid:** This method is a combination of the automated and the manual methods. Automated method is used for the initial classification before manual is employed to refine and correct the errors.

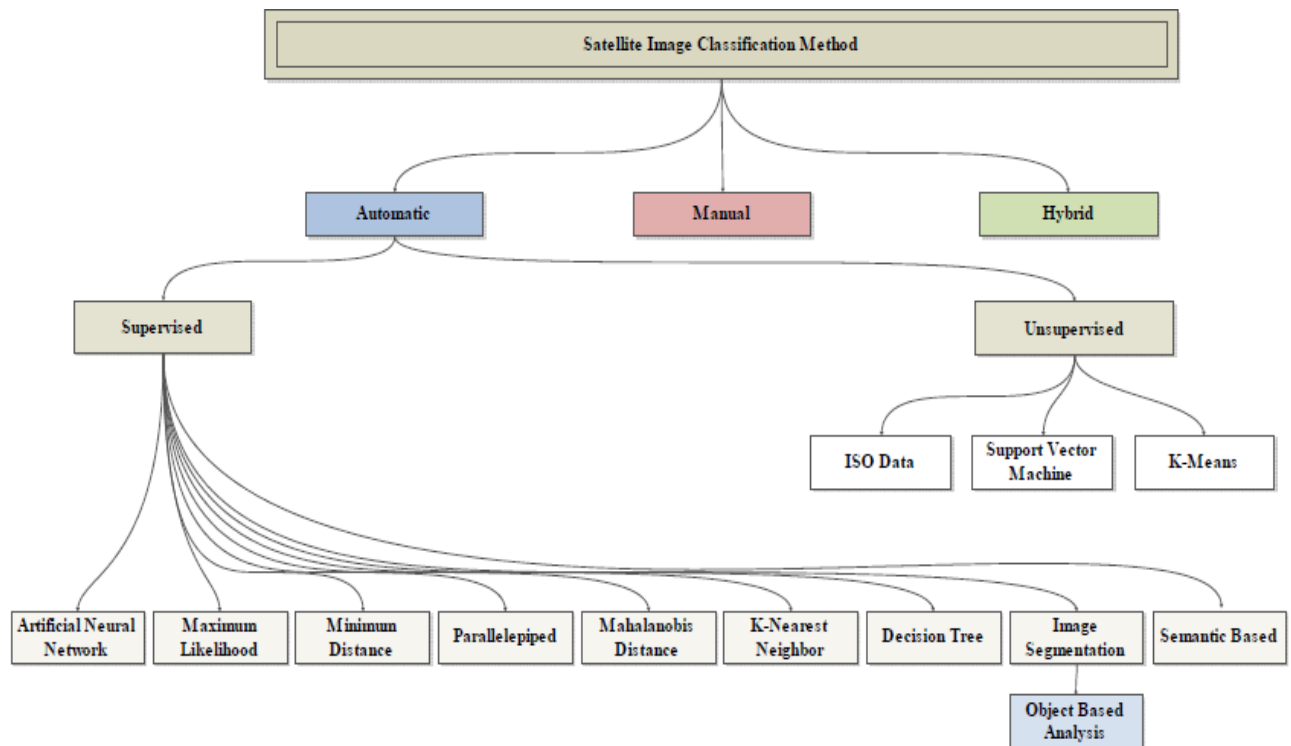


Figure 2.5: Satellite image classifications methods hierarchy, Source: Sunitha, (2015)

This research has used the Maximum Likelihood Classification (MLC) for the pixel-based classification method and the Rule based classification for the object-based method.

2.9.1.1 Maximum Likelihood Classification (MLC)

The MLC is one of the most popular supervised methods in which a pixel with the maximum likelihood is classified into the corresponding class. It is a parametric statistical method where the analyst supervises the classification by identifying representative areas, called training zones. The computer algorithm uses these zones to classify the pixels into spectral classes that are most alike. It is assumed that the distribution training data is Gaussian (normally distributed). During classification, all unclassified pixels are assigned class membership based on the relative likelihood of the pixel occurring within each class probability density function (Lillesand et al, 2004). Maximum likelihood classifier may have difficulty distinguishing the pixels that come from different land cover classes but have very similar spectral properties. As a result, may lead to 'salt and pepper' effects in classification maps especially when many mixed pixels are involved.

2.9.1.2 K-Nearest Neighbour (KNN)

K-NN is a non-parametric classification method and when you say a technique is non-parametric, it means that it does not make any assumptions on the underlying data distribution. It is one of simplest algorithms available for supervised learning. Despite its simplicity, k-NN can outperform more powerful classifiers and is used in a variety of applications (Zakka, 2016) It is called nearest neighbor because classification depends only on the nearest neighbor. The classification is based on a majority vote of the k-nearest neighbours, based on Euclidean distance in feature space, whereby 'k' specifies the number of neighbours to be used. In k-NN classification, the output is a class

membership. An object is classified by a majority vote of neighbours, with the object being assigned to the class most common among its 'k' nearest neighbours (k is a positive integer, typically small). If k=1 then the object is simply assigned to the class of that single nearest neighbor.

Some advantages of k-NN are that it is simple to understand and easy to implement. Furthermore, k-NN works just as easily with multiclass data sets whereas other algorithms are hardcoded for the binary setting. Finally, the non-parametric nature of k-NN gives it an edge in certain settings where the data may be highly “unusual”. On the other hand, k-NN has computationally expensive testing phase and can suffer from skewed class distributions if a particular class is frequent in the training set. Finally, the accuracy of k-NN can be severely degraded with high-dimension data because there is little difference between the nearest and farthest neighbor.

2.9.1.3 Supervised Object Based Classification

There are two main approaches in object based image classification – the supervised and the rule based methods. The supervised is very similar to pixel based supervised classification, based on selection of training samples that are used to train the classification algorithm. However for supervised object based method, instead of single pixels or random group of pixels, compact image objects with calculated features (statistics), which are result of image segmentation process, are selected. Supervised classification algorithms include Nearest Neighbor (NN) classification (e.g., Jensen, 2005), Standard Nearest Neighbor, Fuzzy membership functions (Benz et al., 2004) and others.

2.9.1.4 Rule Based Classification Method

The rule based classification method has been employed in the object based analysis of this research. This method does not use any samples for the classification, but is based purely on the expert knowledge of the user. The user assigns objects to classes based on expertise/prior knowledge. A set of conditions or rules commonly referred to as rule set is developed by the user for each target class. The rule set development makes use of image object features, such as spectral mean value, size, shape, texture, or different contextual image features are used in the rule set development to assign image objects that fulfill the criteria to the respective classes. One advantage of this method is that the users as a result, has full control of the classification process and able to confidently determine where image objects belong. Another advantage is that the rule set is transferable to another image, so it can be re-used again in another scene or project. The ability to reuse the rule set later completely as it is or with minor manual modifications makes it a very valuable approach.

Rules are created based on human knowledge and reasoning about specific land-cover types (ENVI-Zoom 2010). For example, dark building has a low NDVI, roads are elongated, buildings are rectangle in shape, water has a low mean value in NIR band, and vegetation has a high NDVI and trees are highly textured compared to grass. To extract specific features, multiple rules can be defined to separate unwanted features from targeted features, and assigning wanted objects to desired feature class (Hamedianfar 2014). In this research rule sets were defined for classification based on available spectral, spatial and textural characteristics.

2.10 Very High Resolution (VHR) Image Analysis

The main goal of the classification is to detect and name the elements (geographical objects and phenomena) on the Earth surface (fig. 2.6). With the use of visual (manual) interpretation (fig. 2.6a) the operator tries to define land use classes by selecting the closed groups of similar pixels. Digital (automatic) classification defines classes by the means of spectral and/or geometric, texture, context, temporal information combined with mathematical (statistical) grouping into classes (Navulur, 2007; Oštir, 2006).

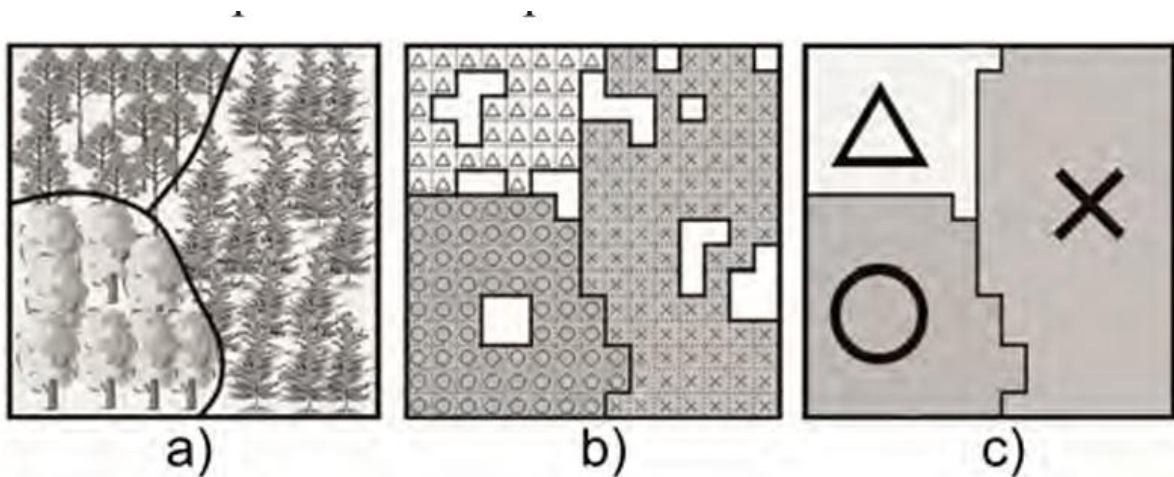


Figure 2.6: Different classification approaches, performed on a vegetation example (Blaschke et al., 2008): a) visual interpretation, b) pixel-based classification and c) object-based classification.

The next method in terms of evolution is the Digital Pixel-based method of classification (fig. 2.6b), uses the pixel's spectral signature to allocate each individual pixel to the most appropriate thematic class. This approach focuses on the individual pixel, which in general does not present the semantic unity of geographical reality (geographical object) and neglects the importance of the neighbouring pixels. The third and commonly in use today (fig 2.6c) is the Digital Object-based method. This one starts by grouping pixels with common structural characteristics, and then these segments are allocated into the

correct thematic classes based on several attributes. Thus, object-based classification combines the advantages of both, visual interpretation and pixel-based classification.

However, the key factor in the accuracy of satellite-data-based thematic information lies in the efficient procedures used to classify satellite images. The great importance of such procedures is revealed through numerous past studies and devoted research (Schowengerdt, 2007; Oštir, 2006). There is also a recognition of limitations with pixel-based image approaches (i.e., that pixels are not true geographical objects, that pixel topology is limited, that current remote sensing image analysis largely neglects the spatial photointerpretive elements (i.e., texture, context, shape), and that increased variability implicit within VHR imagery confuses traditional pixel-based classifiers resulting in lower classification accuracies).

One of the impressive challenges in land cover mapping comes from the increase in spatial resolution power of imaging sensors. Usually in the images acquired by these sensors, the size of objects is much smaller than the size of a single pixel. The availability of a range of Very high resolution (VHR) images offers an advantage for more precise extraction of information by developing advanced classification schemes. However the higher the resolution of an image the more inaccurate the pixel based classification method becomes. The challenge of classifying urban land cover from high resolution remote sensing data arises from the spectral and spatial heterogeneity of such imagery. The frequent alternation and coexistence of built-up structures, vegetation, bare soil or water areas and the heterogeneity of the objects themselves (for example roads with cars) result in distinct spectral variation within these areas of literal homogenous

land cover classes. Digital image classification is the process of assigning pixels to meaningful classes. It is a computer-assisted analysis of images for consequential information extraction. Thus, classification can also be termed as information extraction. A pixel is assumed to be an individual unit which carries several spectral band values (Campbell et al, 2011). In the field of RS, numerous attempts have been made for developing an effective approach for the information extraction processes.

In order to characterize this complex highly-structured urban environment, an object-oriented approach with shape parameters and neighborhood relations provides additional analysis potential from remote sensing apart from spectral information. Recent developments in “object-oriented” image classification (based on image segmentation) have taken advantage of the detailed spatial characteristics of high-resolution datasets. The research in this area has emphasized the reduction of spectral variability within the objects and the incorporation of additional information from spatial and contextual image/ object characteristics (Blaschke and Strobl, 2001).

2.11 LiDAR data for Image Analysis

Basically LiDAR data are used to generate DTM and DSM. They are also capable in many applications such as 3D city modeling and classification of land cover map. LiDAR data is just a data set of mass points with X-, Y-, Z- coordinates and possibly with attributes like amplitude or echo count so in order to extract information from it, it has to undergo further processing. Vosselman et al. (2010) stated that converting point cloud in raster image through interpolation algorithm or structuring laser scanner data by Delaunay triangulation, k-D tree or octree data structures can visualize LiDAR data and

make the point cloud organized. The availability of this structure makes it possible for the point cloud segmentation to be performed. During this process points that belong to the same planar, cylinder or smooth surface are grouped together corresponding to some criterion. Then, the extracted features by such point cloud segmentation are required for buildings modelling or terrain surface extraction. Traditionally, LiDAR point cloud has been frequently used in ground point extraction (Priestnall, Jaafar, & Duncan, 2000) and points of building or vegetation classification (Norbert & Claus, 1999). Song et al. (2002) evaluated the possibility of using LiDAR intensity data for land cover classification. In that case, interpolation and filtering methods were performed to reduce noise effect.

Antonarakis, Richards, & Brasington (2008) used airborne LiDAR data to classify planted forest and natural forest in sweeping meanders. Two methods of object-based classification were compared, one included the influence of the ground and the other excluded the ground point supplemented with the help of aerial digital photographs. The exercise was seen to be successful with accuracies of 95% and 94% respectively. Several primary features were generated from LiDAR data, vegetation height model, percentage canopy hits model, intensity models and skewness and kurtosis models. Brennan and Webster (2006) described the utilization of segmentation and rule-based object-oriented classification techniques based on LiDAR data. Land cover types like building, road, water vegetation, and so on were extracted by analyzing DSM, DEM, intensity, multiple echoes, and normalized height derived from LiDAR data.

2.12 Pixel-based Analysis of Satellite Images

Remote sensing uses the visible, infra-red, and micro-wave spectra to get information about the earth surface. Different land types reflect the sun energy in different ways, thus their spectral response varies, and this is what enables their analysis via the spectrometric processes. Pixel-based analysis has been a common praxis in the remote sensing data studies. Its classification method is based on the so called spectral signature, i.e. the characteristic reflection of electromagnetic waves from the Earth's surface which is wavelength dependent (Oštir, 2006). Most methods are based on cluster analysis, and the two most common approaches are: a) unsupervised classification in which the algorithm automatically finds the best pixel candidate (on the basis of a previously selected number of classes) and classifies them according to the statistically closest membership; b) supervised classification, which utilizes the training sample patterns and reference data for the statistically-based sorting into classes. Notable shortcomings of the pixel-based classification include:

- Confusion of target objects with other classes
- Visual quality, shadow and contrast features affect quality of object extractions
- Only the spectral values of features are used.

New high resolution sensors significantly increase the within-class spectral variability and, therefore, decrease the potential accuracy of a purely pixel-based approach to classification. So time went on with the advent of higher resolution images, the pixel based method of classification became more time consuming and less effective. The need for better results from the studies of the changes in the Earth surface ultimately

culminated in the necessity for a completely new approach (Blaschke in Strobl, 2001). According to (Veljanovski, 2011) the key motives behind the transition from pixel-based to object-based analysis of remote sensing data were: (1) the demand for improved interpretative values of remote sensing data in different applications (mostly in time comparison studies, and manifestations of remote sensing data used for planning); (2) increasing the availability of high resolution satellite data, on which one can observe surface objects in greater detail (including the increasing interest in the contextual validation of the image content); and (3) higher level of development of technological equipment and algorithms used for processing remote sensing data (accessibility to a wider user society; transfer of GIS object-based spatial analysis towards the field of raster remote sensing data and their particularities). Nowadays, object-based analysis of satellite data is well-established, and there is a common consensus that it is based on the concepts of segmentation, edge-detection, as well as object detection and classification, all of which have been present in the field of remote sensing already for decades (Johansen et al., 2011). Object based method provides a methodological framework of computer-based image analysis of a complex environment, possibly in a multi-level object hierarchy, based on spectral, spatial and structural information available in objects (Benz et al., 2004; Niemeyer and Canty, 2003; Hay et al., 2006).

2.13 Object Based Image Analysis (OBIA)

Research on urban mapping has gained momentum, chiefly due to the availability and accessibility of VHR imagery, and successful results using object-based image analysis (OBIA) (Pinho et al. 2008; Zhou 2013). The OBIA approach incorporates spatial

contexts and mutual relationships between objects, and is often referred to as GEOgraphic object-based image analysis (GEOBIA) when used in EO (Conchedda, Durieux & Mayaux 2008). According to Blaschke, Lang & Hay (2008: 78) GEOBIA is proposed to replace OBIA “because the term OBIA encompassed techniques used in many different disciplines such as biomedical imaging, Astronomy, Microscopy, Computer vision and others”. GEOBIA is defined by Blaschke, Lang & Hay (2008: 77) as “a sub-discipline of GIS devoted to developing automated methods to partitioning RS imagery into meaningful image-objects, and assessing their characteristics through spatial, spectral and temporal scales, so as to generate new geographic information in GIS-ready format”.

One of the key elements of the OBIA approach is that it can integrate all data types including DEM (DTM, DSM and nDSM), shapefiles, and LiDAR data in combination with image data as opposed to the traditional pixel-based approach (Koc & Turker 2005; Wang 2009; Zhou 2013). OBIA combine spectral information (tone and colour), with spatial arrangements (size, shape, texture and pattern) in association with neighbouring objects (Campbell & Vynne 2012; Laliberte et al. 2004).

One of the critical steps in image analysis is to determine the most relevant features and algorithms to be used in classification (BLASCHKE 2010). Image objects which are essentially made up from pixels have information like the spectral signature, the shape and size or context and eCognition software works well with objects for classification. Features use upper and lower range to define the characteristics of image objects. In this

study the following feature sets will be used to define limits of specified classes for classification. They include:

- i. Elevation
- ii. Colour: mean and standard deviation of each band, band ratios (NDVI, NDWI....)
- iii. Size: area, length to width ratio, relative border length
- iv. Shape: rectangular fit
- v. Texture: smoothness
- vi. Relation to neighbours (class level).

The next will be to classify the image objects created through the segmentation process. Rule based classification will be applied to classify using the feature sets. eCognition offers two types of classifiers: the Nearest Neighbour (NN) and Fuzzy Membership Function. These two classifiers act as class descriptors. The nearest neighbor (NN) which assigns classes to image objects based on minimum distance measurements has been chosen for the proposed method. NN classifier is appropriate for describing variation in fine resolution images.

Although many feature sets will be used, the nDSM derived from LiDAR for height difference and the NDVI for vegetation separation will be the prominent feature sets in use. Similarly, brightness will be used to classify shadow, whereas NDWI will be used to differentiate water bodies and impervious surfaces. Features such as homogeneity, standard deviation of nDSM, shape index, and rectangular fit will be used to refine the classification.

The aim of classification is to identify the image object as certain class. According to the researcher's proposal, seven categories of features classification have been defined for the proposed research. They include buildings, paved roads, bare soil, Trees, grass/low vegetation, water bodies and shadows. A rule-set based classification will be constructed to classify each object into certain class. Threshold of objects using their related characteristics will be determined in order to properly classify the image objects.

(a) Vegetation: The first phase in this rule based classification process aims to mask out vegetation. The normalized difference vegetation index (NDVI) has been widely used in the literature to separate vegetation from non-vegetation areas. Therefore, NDVI will be used to separate vegetation and non-vegetation.

$$NDVI = (NIR-R)/(NIR+R) \dots\dots\dots(1)$$

Where NIR and R are the mean values of all pixels (within the boundary of each object) in band near infrared and red for a given object in each level of segmentation and a threshold value of about 0.3 for classifying vegetation will be set. Having extracted vegetation area, it will further be classified into trees and grass. These two classes are distinguishable using their height difference or textural characteristics. In the proposed study, the ancillary data or height information (nDSM) from the LiDAR data will be used to separate trees from grasses by setting a height threshold. The result of LiDAR surface acquisition is in almost every case a Digital Surface Model (DSM) which represents the first pulse reflection and a Digital Terrain Model (DTM) which forms the surface after removal of vegetation and manmade structures. $nDSM = DSM - DTM$.

(b) Shadow: Shadows are dark features in optical imagery, and because the segmentation of such imagery is mainly based on the spectral structure of the image [Smith and Morton 2010]. Shadows influence segmentation shaded features. Furthermore, shadow is an important factor that reduces the spectral values of the shaded objects and thus influences the land cover classification [Lu et al., 2010]. As a result of this, it should be extracted from the non-vegetation and vegetation areas before further classification. Shadows can be extracted using two spectral properties (NDWI and Brightness) and two morphological features (Density and Area). The normalized difference water index (NDWI) [Mcfeeters 1996] is a metric used for masking out black bodies (water and shadow) in VHR imagery [Chen et al., 2009] and is defined as follows [Mcfeeters 1996]:

$$NDWI = (G-NIR)/G+NIR).....(2)$$

Where, G is the averages mean value of all pixels (within the boundary of each object) in each level of segmentation for the band green and NIR is the Near Infrared band. The morphological features Density and Area of objects help to fine tune the shadow areas. The size of shadows in optical imagery depends primarily on the height of objects but also on the sun elevation angle [Dare 2005].

(c) Water bodies: The Normalized Difference Water Index (NDWI) will be used to delineate water features and tarred roads. This index maximizes reflectance of water by using green light wavelengths and minimizes low reflectance of NIR by water features while taking advantages of the high reflectance of NIR by vegetation and soil features.

With this index water features are enhanced due to positive values and vegetation and soil are suppressed due to zero or negative values.

$$\text{NDWI} = \frac{G - \text{NIR}}{G + \text{NIR}} \dots \dots \dots (3)$$

(d) Buildings: For buildings, the determined object primitives in segmentation, such as scale parameter, shape, completeness, brightness, and statistical parameters, will be used to determine threshold values for classification in the analysis step to form the target object class. An object-based classification considering the characteristics of elevation, spectral, texture, roughness, and shape information is performed to detect the building regions (Hofmann, et. al, 2001).

For the elevation, the nDSM height information which is most relevant characteristics of buildings will be used to distinguish buildings in the non-vegetation area. Spectrally, the NDVI had earlier been used in this proposal to separate vegetation from the non-vegetation area from where the building is being extracted.

The shape attribute includes size and length-to-width ratio. An area threshold is used to filter out those small objects. That means the regions smaller than a minimum area (e.g., 10m² considering the locality of the study area) are discarded. The length-to-width ratio is suitable to remove the thin objects. The objects are eliminated when the length-to-width ratio is larger than a threshold.

(e) Paved Roads: After dark features, buildings, water and vegetation have been classified, roads will be extracted from the remaining ‘non-vegetated’ areas using rules that will be derived from spectral indices, geometry and texture. Therefore, for the

classification, a rule sets will be developed with thresholds on the spectral bands, spectral indices, geometric properties, texture related features to classify paved roads.

Note that the spectral signature features of paved roads in green and NIR band are similar with those of water, i.e., they both reflect green light more than reflected near infrared light. Instead the Built-Up Areas Index will be considered useful in detecting asphalt in this study.

$$BAI = B - NIR / B + NIR \dots\dots(4)$$

This multi-level object based hierarchical classification will successfully mask out irrelevant region, thereby greatly reducing complexity of classification which should occur in the next level.

2.14 Methodology of Object-Based Image Analysis

In object based image analysis, data homogeneous regions (segments) obtained from satellite images are used as basic entities. It has basic procedures for obtaining segments and their characteristics (attributes), for analyzing these segments, sorting them into classes or objects (classification), verifying them and for error removal (post-classification).

OBIA consists of the following steps:

- i. Segmentation and computation of spectral, geometric, textural, conceptual and temporal attributes,
- ii. Object (semantic) classification,
- iii. Post-classification (verification, error elimination) and result validation.

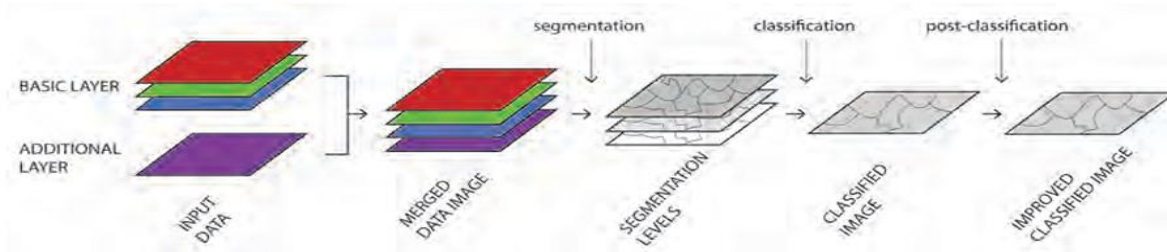


Figure 2.7. Processing steps in the object-based analysis of remote sensing data.

Segments produced within the first step of object-based classification influence the final classification results (Blaschke et al., 2008). There is a causal relationship between segmentation and classification, as the particularities and errors of the first transfer onto the latter. The character and quality of objects depends on the segments formed.

2.14.1 Segmentation

Image segmentation is a process of subdividing a digital image into distinct regions or segments containing pixels with similar attributes. These regions are strongly related and able to depict objects of features of interest. In other words, segmentation is the subdivision of an image into separated regions represented by basic unclassified image objects called image object primitives. Therefore, for a successful and accurate image analysis, defining object primitives of suitable size and shape is of utmost importance. Image object primitives serve as information carriers and as building blocks for all further image analysis. Therefore, when starting an image analysis, it is important to invest enough time on testing and improving the segmentation to be used. To analyze and capture the small variations within a dataset, multilevel segmentation with varying parameters that is scale, shape and compactness are thus used (Wang 2009). The work of

Gang et al (2010) indicated that a number of segmentations at various scales may need to be performed in order to get meaningful image objects that lead to improve classification. The selection of optimal parameters is usually a trial and error process and tedious. Image objects produced contain information about their spectral characteristics, their shapes, their positions and textures, as well as information about their neighborhoods. Thus, they are an essential prerequisite for the subsequent image analysis steps.

eCognition developer software is very popular for OBIA and can very well perform image segmentation. For the process of image segmentation there are many segmentation algorithms which are also available in eCognition:

- i. Chessboard: segments image into equal sized objects,
- ii. Contrast filter: segments image by contrast and gradient to create primitive image objects,
- iii. Contrast split: segments image with a given threshold into bright and dark objects,
- iv. Multi-resolution: segments image and consecutively merge objects at higher scales,
- v. Multi-threshold: segments image into user specified thresholds,
- vi. Quad tree based: segments image into a quadtree formed by square objects, and
- vii. Spectral difference: merges neighboring image objects from a previously segmented image.

Problems of over-segmentation and under-segmentation are usually faced in this process of segmentation. Nevertheless, segmentation is considered to be appropriate when no extreme prevails (Blaschke et al., 2008). Segment attributes describe the characteristics

of individual segments. They are (Navulur, 2007): geometric (e.g. area, perimeter, oblongness, compactness), spectral (e.g. mean value, standard deviation, minimal and maximal value of each band), textural (e.g. span, entropy, variability), attributes of the spectrum band proportions (e.g. vegetation index), contextual (e.g. proximity of the neighbouring pixels, distance), temporal (e.g. time span, date, stability) and other attributes.

2.14.2 Segmentation Parameters

Segmentations, and the resulting characteristics of object primitives and eventual image objects, are based on shape, size, color, and pixel topology controlled through parameters (scale, shape and compactness) set by the user. The shape and size of the image objects depend greatly on the influence segmentation parameters have on spectral and spatial characteristics of the image layers. Settings for segmentation parameters vary and are determined by trial and error and experience. Settings that work well for one image may not work at all for another, even if the images are similar. Colour and shape parameters are responsible for image objects spectral and spatial homogeneity. They both balance each other in such a way that if colour has a high value then shape must have a low value. The color/shape and the compactness/smoothness parameters are together known as homogeneity criterion (eCognition Reference Book, 2011). The scale parameter limits the maximum heterogeneity for combining adjoining image objects (eCognition Reference Book, 2011).

On the other hand, the value of the scale parameter affects image segmentation by determining the size of image objects. If the scale value is high, the variability allowed

within each object is high and image objects are relatively large. Conversely, small scale values allow less variability within each segment, creating relatively smaller segments. The optimization of these parameters is necessary for best segmentation result which guarantees high classification results. These three parameters are recommended to be changed in different studies to obtain optimized results. The default values are color/shape = 0.1, compactness/smoothness = 0.5, and scale = 10. Defining the criteria for minimum heterogeneity by specifying segmentation parameter constraints and deciding on the strategy of assembling homogeneous areas leads to a good segmentation result (Benz et al., 2004).

Minho (2012) divides segmentation qualities into three main categories:

1. Over-segmentation – the created objects are too small relative to features of interest
2. Optimal segmentation
3. Under-segmentation – inadequate low numbers of objects which lead to merging different features into one object.

2.14.3 Multiresolution Segmentation

The most widely used segmentation algorithm is MRS (Chen et al. 2007; Krause et al. 2004; Salehi et al 2012; Zhou 2013). The multiresolution algorithm which is a bottom up algorithm locally minimizes the average heterogeneity of image objects and maximizes the respective homogeneity of the respective objects. The segmentation produced begins with single image objects of one pixel and repeatedly merges them as long as an upper threshold of homogeneity is not exceeded locally. The homogeneity criteria are defined as a combination of both spectral and shape homogeneity which are influenced by the

scale parameter. Multiresolution segmentation has proved to be one of the most successful image segmentation algorithms in OBIA framework (Nuebert et al, 2008).

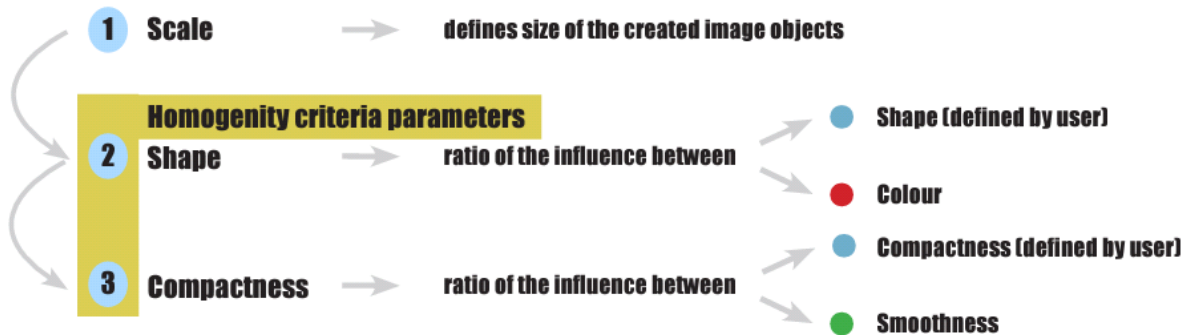


Figure 2.8: How Multi-resolution works, Source Benz (2004)

2.15 Object (semantic) Classification

After an image has been segmented into appropriate image objects, the image is classified by assigning each object to known and defined classes based on features and criteria set by the user. Each pixel in the data set is then compared numerically to each category in the interpretation key and labeled with the name of the category it looks more like (Igbokwe, 2008). To be assured of the final classified image's quality, the process of the accuracy assessment is carried out. The object (semantic) classification uses the segment characteristics to sort them into object classes. Individual segment characteristics (attributes) are compared, and membership in a particular class is established (Nussbaum and Menz, 2008). The two common methods of doing this are: defining training samples, and defining rules on the basis of representative threshold values (usually decision trees) that are usually defined for each target object class separately. The classification is done with the use of a classifier. Some of the more established classifiers are (Schowengerdt, 2007; Oštir, 2006; Lillesand et al., 2004):

- i. parametric and non-parametric statistical classifiers (e.g. K-Means, ISODATA, minimum distance method, maximal probability method, nearest neighbour, parallel-piped method, vector machine support (SVM variations)),
- ii. classifiers based on neural networks (with loop information, Kohonen method),
- iii. classifiers based on machine learning (decision trees, classification and regression trees),
- iv. classifiers based on fuzzy logic (membership) etc.

Classifications based on the decision tree are known to yield good results when analysing surface phenomena (mostly anthropological) that was built in compliance with certain standards and can therefore be relatively easily described by a set of rules (Lang and Blaschke, 2003). The same holds true when we analyse clearly distinguishable patterns on an image, e.g. water on a radar satellite image (Veljanovski et al. 2011a). The quality of the final classification definitions is linked directly to the quality of the segmentation and the quality of the classifier.

2.16 Post-classification

Post-classification serves to eliminate the evident errors (wrong classifications) and generalize the results. This error elimination is by visual control, field inspection and/or comparison with the reference source (if available), which are completely manual and therefore time consuming. Generalization of the obtained object classes helps to improve the visual quality of the final result. If, for example, we do not wish to keep the small objects, we can eliminate them by merging them with the dominant neighbouring classes using the ‘clump and sieve’ procedures (Kokalj, 2006). These methods only work for

raster images while line-smoothing is used as a post-procedure for finalizing vector thematic maps.

2.17 Advantages and Limitations of Object-based Classification

According to (Veljanovski, T et al, 2011), the advantages of OBIA include:

- i. It uses a vast variety of remote sensing data characteristics (spectral, spatial, temporal) and combines them with GIS functionalities in the various processing phases. Within the classification process: employment and consideration of additional information and data layers, additional relations such as distance, etc. expressed through various spatial functions. Within the post-classification process: smoothing and generalization.
- ii. Object-based classification uses all available and usable segment characteristics for their classification (e.g. shape, texture, relations with other segments).
- iii. Results (identified objects) are vectors, which demand easier post-processing than pixel-based classification results. To a certain degree the generalization can also be performed during the main processing phases (e.g. elimination of small objects based on their shape or size).
- iv. It classifies the image contents into objects in a way that is close to the human understanding of the environment. The results are already generalized, since the classification uses clear semantic rules that can also be used to enhance or omit certain typical object characteristics (e.g. linearity, length, width, rectangularity of buildings) or enhance their key differences (e.g. typical size in nature).

- v. The fact that the basic computation entities are objects (and not pixels) reduces the demand on computer algorithms and at the same time enables the users to utilize more complex computation techniques and a wider set of data characteristics (introduction of conceptual attributes).
- vi. Various free software for object-based analyses are on the increase, as is their compatibility and file format support.
- vii. It is an interactive multi-phase process. It enables the intermediate results to be checked, and immediate improvements can be made through immediate parameter fine-tuning.

The classical methodology for OBIA involves repeated segmentation, classification and refinement of image object until the desired land cover classification is achieved. This incorporates the elements of manual interpretation. Authors have evaluated the method of image classification with two approaches: Rule set method and Nearest neighbor (NN) classification (Shackelford, A. K. et al, 2003). eCognition is a software with powerful functionality that can create the objects with different scale parameters and at different levels. OBIA technique for image classification not only provides higher accuracy but also operational simplicity, time efficiency, effectiveness of replicating human visual system associated with it made it more popular. Figure 2.9, below shows typical methodology used for OBIA.

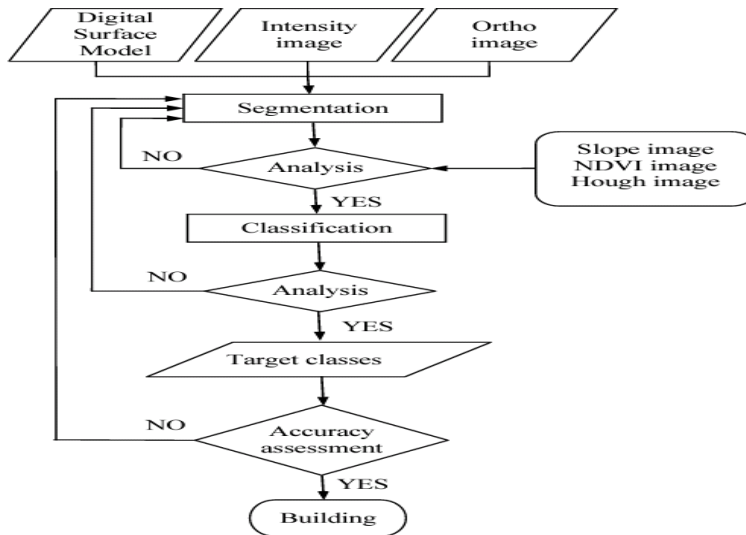


Figure 2.9: Typical methodology used for OBIA, Source: Uzar, (2013)

2.18 Accuracy Assessment

It is very important to evaluate classification results irrespective of the method of classification used. It's also important to appreciate that apart from the errors from the classification itself, there are other sources of error. In addition to errors from the classification itself, other sources of errors, such as position errors resulting from the registration, interpretation errors, and poor quality of training or test samples, all affect classification accuracy (Powell et al., (2004).

Accuracy assessment is an important part of any classification project. It compares the classified image to another data source that is considered to be accurate or ground truth data. Ground truth can be collected in the field; however, this is time consuming and expensive. Ground truth data can also be derived from interpreting high-resolution imagery, existing classified imagery, or GIS data layers.

In the process of accuracy assessment, different approaches may be employed (Foody, 2002). The error matrix approach is the one most widely used in accuracy assessment.

After generation of an error matrix, other important accuracy assessment elements, such as overall accuracy, omission error and commission error can be derived. In principal, this matrix provides a simple summary of classification accuracy and highlights the two types of thematic error that may occur, omission and commission. This not only summarizes the accuracy of the classification but also may convey useful information to enhance analyses based on the classification (e.g. Prisley and Smith 1987, Fang et al. 2006). The confusion matrix comprises two main components which are a kappa and the overall accuracy (OA) calculated by Congalton & Green (2009) as follow:

$$OA = \sum_i^n \frac{X_i}{n}$$

Where ‘ X_i ’ is the value of the i^{th} corrected classified sample units;

And ‘ n ’ is the number of sample units

$$Kappa = \frac{N \sum_{i=1}^r x_{ii} - \sum_{i=1}^r x_{i+} * x_{+i}}{N^2 - \sum_{i=1}^r (x_{i+} * x_{+i})}$$

Where r is the number of rows in the matrix;

X_{ii} Is the number of observations in a row I and column I ;

X_{i+} Are the marginal totals of row i

X_{+I} Are the marginal totals of column i

N is the total number of observations.

The kappa analysis is used in accuracy assessments to statistically determine if one error matrix is significantly different from another (Congalton & Green 2009). Additional details about the accuracy of the map are provided by the user and producer's accuracies. Gamba & Martin (2009) define the user and producer accuracies as: (1) the producer accuracy characterizes the error of omission incurred when the classified map misses an area of urban land; and (2) the user accuracy reflects the error of commission measuring the number of pixels erroneously labeled like urban land. Table 2 below from Jensen (2005) is a typical confusion matrix for a classification result from which the following accuracy values Overall, Producer, User and Kappa are calculated.

Table 2.2: Typical Confusion Matrix

	Residential	Commercial	Wetland	Forest	Water	Row total
Residential	70	5	0	13	0	88
Commercial	3	55	0	0	0	58
Wetland	0	0	99	0	0	99
Forest	0	0	4	37	0	41
Water	0	0	0	0	121	121
Column total	73	60	103	50	121	407

Overall Accuracy = $382/407 = 93.86\%$

Producer's Accuracy (omission error)
 Residential = $70/73 = 96\%$ 4% omission error
 Commercial = $55/60 = 92\%$ 8% omission error
 Wetland = $99/103 = 96\%$ 4% omission error
 Forest = $37/50 = 74\%$ 26% omission error
 Water = $20/22 = 100\%$ 0% omission error

User's Accuracy (commission error)
 Residential = $70/88 = 80\%$ 20% commission error
 Commercial = $55/58 = 95\%$ 5% commission error
 Wetland = $99/99 = 100\%$ 0% commission error
 Forest = $37/41 = 90\%$ 10% commission error
 Water = $121/121 = 100\%$ 0% commission error

Source: Jensen (2005)

Computation of K_{hat} Coefficient of Agreement

$$\hat{K} = \frac{N \sum_{i=1}^k x_{ii} - \sum_{i=1}^k (x_{i+} \times x_{+i})}{N^2 - \sum_{i=1}^k (x_{i+} \times x_{+i})}$$

$$\sum_{i=1}^k x_{ii} = (70 + 55 + 99 + 37 + 121) = 382$$

$$\sum_{i=1}^k (x_{i+} \times x_{+i}) = (88 \times 73) + (58 \times 60) + (99 \times 103) + (41 \times 50) + (121 \times 121) = 36,792$$

$$\text{therefore } \hat{K} = \frac{407(382) - 36792}{407^2 - 36792} = \frac{155474 - 36792}{165649 - 36792} = \frac{118682}{128857} = 92.1\%$$

(a) **Overall accuracy:** This is the total classification accuracy and it is obtained by dividing the total number of correct pixels (diagonal) by the total number of pixels in the error matrix.

(b) **Producer's accuracy:** This is also called Omission error and it occurs when pixels which should have been identified as belonging to a particular class were simply not recognized as present. The value is obtained by dividing the total pixels not correctly classified for each class in the reference data (column) by the total pixels for that class in the reference data/image (column total).

(c) User Accuracy: This is also referred to as Commission error and it occurs when pixels associated with a class are incorrectly identified as other classes or improperly separating a single class into two or more classes. The value is obtained by dividing the number of pixels not classified for each class in the classification (row) by the total number of pixels for that call in the classification (row total).

(d) Kappa Coefficient: This is a measure of agreement between the classification map and the reference data. It expresses the proportionate reduction in error generated by a classification process, compared with the error of a completely random classification. For example: a value of 0.82 would imply that the classification process was avoiding 82% of the errors that a completely random classification would generate. Table 3 below is strength of agreement of classification based on the Kappa coefficient as described by Landis and Kosh (1977).

Table 2.3: Landis and Kosh (1977) Scheme of Agreement based on Kappa

Kappa Co-efficient	Agreement
< 0.00	Poor
0.00 – 0.20	Slight
0.21 – 0.40	Fair
0.41 – 0.60	Moderate
0.61 – 0.80	Substantial
0.81 – 1.00	Almost Perfect

Source: Jiang and Liu, 2011

2.19 Hypothesis Test to Evaluate Research Questions

Hypothesis test is a procedure based on sample evidence and probability theory, used to determine whether the hypothesis is a reasonable statement and should not be rejected, or is unreasonable and should be rejected. In other words Hypothesis test is about

making an inference about how the value of a parameter relates to a specific numerical value.

According to University of California, Davis Department of Statistics, Summer Session II (2012), test of hypothesis has the following elements:

1. Null hypothesis (H_0): A theory about the values of one or more population parameters.

The theory generally represents the status quo, which we adopt until it is proven false.

By convention, the theory is stated as H_0 : parameter = value.

2. Alternative (research) hypothesis (H_a): A theory that contradicts the null hypothesis.

The theory generally represents that which we will accept only when sufficient evidence exist to establish its truth.

3. Test statistic: A sample statistic used to decide whether to reject the null hypothesis.

4. Rejection region: The numerical values of the test statistic for which the null hypothesis will be rejected. The rejection region is chosen so that the probability is that it will contain the test statistic when the null hypothesis is true, thereby leading to a Type I error. The value of α is usually chosen to be small (e.g, 0.01, 0.05, or 0.10) and is referred to as the level of significance of the test.

5. Assumptions: Clear statements of any assumptions made about the population(s) being sampled.

6. Experiment and calculation of test statistic: Performance of the sampling experiment and determination of the numerical value of the test statistic.

7. Conclusion:

a. If the numerical value of the test statistic falls into the rejection region, we reject the null hypothesis and conclude that the alternative hypothesis is true. We know that the

hypothesis-testing process will lead to this conclusion incorrectly (a Type I error) only 100 α % of the time when H_0 is true.

b. If the test statistic does not fall into the rejection region, we do not reject H_0 . Thus we reserve the judgment about which hypothesis is true. We do not conclude that the null hypothesis is true because we do not (in general) know the probability β that our test procedure will lead to an incorrect acceptance of H_0 (a Type II error).

2.19.1 T-test Method of Hypothesis Testing

The t-test which has been used in this research is probably the most commonly used Statistical Data Analysis procedure for hypothesis testing. Actually, there are several kinds of t-tests, but the most common is the "two-sample t-test" also known as the "Student's t-test" or the "independent samples t-test". The t-test can only be used when certain following conditions are met. When the population standard deviation, σ , is unknown and either the data is normally distributed or the sample size is greater than 30 ($n > 30$), we use the t-distribution (t-statistic).

The following steps are involved in hypothesis testing:

Step 1 State the null hypothesis and the alternate hypothesis.

Step 2 Select the appropriate test statistic and level of significance.

Step 3 State the decision rules.

Step 4 Compute the appropriate test statistic and make the decision.

Step 5 Interpret the decision.

Step 1: State the null hypothesis and the alternate hypothesis:-

Null Hypothesis, H_0 – statement about the value of a population parameter.

Alternate Hypothesis, H_1 –statement that is accepted if the evidence proves a null hypothesis to be false.

The null hypothesis (H_0) always contradicts the research hypothesis, usually stating that there is no difference between them while the substantive hypothesis or research hypothesis (H_1) states the relationship in which we are really interested.

Step 2: Select the appropriate test statistic and level of significance:-

The t- test value Statistic is used in this research and so the t-statistics for the data will be calculated. Choose the level of statistical significance, α . This stipulates the acceptable risk of a Type 1 error (rejecting H_0 when H_0 is true). Typical values for α are 0.05 and 0.01. Compare t_{calc} to the tabulated t-value, for the appropriate significance level and degree of freedom. If $t_{\text{calc}} > t_{\text{tab}}$, we reject the null hypothesis and accept the alternate hypothesis. Otherwise, we accept the null hypothesis.

Step three: State the decision rules:-

The decision rules state the conditions under which the null hypothesis will be accepted or rejected. The critical value for the test-statistic is determined by the level of significance. The critical value is the value that divides the non-reject region from the reject region.

Step four: Compute the appropriate test statistic and make the decision:-

T-test is computed and compare the computed test statistic with critical value. If the computed value is within the rejection region(s), we reject the null hypothesis; otherwise, we do not reject the null hypothesis.

Step five: Summarize the result by interpreting the decision in the context of the original claim.

CHAPTER THREE

LITERATURE REVIEW

3.0 Introduction

This section focuses on the review of previous studies related to remote sensing of urban land use/land cover using VHR images and LiDAR data with a focus on object-based image classification methods.

Urban landscapes are characterized by a complex spectral mixture of materials that are predominately made up of impervious surfaces, vegetation and soil. This heterogeneous composition of urban landscapes is difficult to map using traditional per pixel classification. Also due to the high internal variance of high resolution imagery, previous urban mapping efforts using the per-pixel method have often produced unsatisfactory results (Blaschke and Strobl, 2001; Blaschke, 2009). The new remote sensing technique such as object-oriented classification has further provided an opportunity for fast update of urban spatial classifications to match the dynamic transformations that characterize urban environments. This has also made it possible to use of high resolution satellite imagery and multispectral aerial photography have emerged as the most effective means of mapping large scale urban environments. This trend has increased dramatically in recent years due to availability of high-density laser scanner and high-resolution multi-spectral data.

The main drawback of per-pixel classification in a multi-dimensional feature space is that it doesn't make use of any spatial concept (Blaschke and Strobl, 2001). This affects the high resolution images because the neighboring pixels could belong to the same land

cover class due to spatial patterns of differing complexity or texture and this creates some uncertainty in the overall output. The object based image analysis method has overcome these difficulties by first segmenting the image into meaningful multi-pixel objects of various sizes, based on both spectral and spatial characteristics of groups of pixels. In general, it suffices to say that these pixel-based classification techniques improve classification accuracy with some limitations: 1) they have considerable difficulties dealing with the abundant information of HR data, 2) they produce a characteristic and inconsistent salt-and-pepper classification, 3) they are not capable of extracting objects of interest, and 4) they cannot update GIS database expediently (Baatz, M., et al., 2004). Thus, the pixel-based classification methods are no longer applicable for HR imagery.

VHR images and LiDAR data are common sources for object extraction. So many studies have been carried out by researchers in this area using different approaches and algorithms. In terms of utilizing LiDAR data in classification, particularly object-based approaches, a considerable amount of literature has been published in recent years and results show significant improvement in classification accuracy of impervious surface such as buildings, roads, and parking areas. Examples are Syed et al. (2005a), Syed et al. (2005b), Haitao et al. (2007), Sohn and Dowman (2007), Yongmin (2011), Dinis (2002) etc.

This review will aim to examine the various approaches in terms of data source, methodologies adopted, results and gaps to see where their approaches will be useful to the proposed study and possible chances of filling any gaps identified. Specifically this

review will be concerned with those of them that focused on the image analysis using the OBIA method, those that employed LiDAR data and VHR images. Currently, there are commercial systems (e.g. ENVI, ERDAS, e-Cognition, IDRISI, etc.), which use expert classification algorithms such as rule-based, object-oriented and fuzzy approaches.

3.1 Geometric Characteristics of Urban Features

The geometry of urban surface has an important impact in remote sensing. High resolution images (Spaceborne and Airborne) provide great possibility for achieving an efficient and effective extraction of cartographic features through automated extraction methods. However issues of shadow and image distortion can affect the accuracy of extraction and sometimes urban streets are misclassified as vegetation. For instance, Hodgson et al, (2003) found that the low reflectance from pixels under shadow frequently resulted to a misclassification into the water class. As a result, Tong et al, (2009) suggested that high resolution imagery must be accurately orthorectified by using the principle of photogrammetry before applying for mapping of urban land use.

LiDAR data has been a major focus in recent years because of its high resolution, short processing time and low cost. LiDAR data focus mainly on geometry rather than radiometry. Feature classification and extraction based on LiDAR data have been widely conducted (Lee et al 2008). Some researchers have used LiDAR in combination with optical remote sensing data in impervious surface estimation and mapping, Hodgson et al, (2003) for example used both digital aerial photographs and LiDAR data for urban impervious surface mapping and found that the combined dataset improves the result for

all classification approaches. The addition of LiDAR height information improved the coefficient of determination value.

The integration of high-resolution imagery and LiDAR data is well appreciated as it yields complementary benefits by providing a more complete scene description enriched with both spectral and 3-D surface information. This integration of both data sources has been exploited to increase the classification performance and to improve the accuracy and robustness in automatic building detection, reconstruction and change detection techniques (Awrangjeb et al., 2012, Li and Wu, 2013).

3.2 Related Studies Review

Effort has been made to group the related studies into three categories of extraction of General land cover features, Building extraction and Road extraction.

3.2.1 Automatic Classification and Extraction of General Land Cover Features.

Syed et al, (2005): Automatic Classification of Land Cover Features with High Resolution Imagery and Lidar Data: An Object-Oriented Approach

This automatic classification of land cover features was carried out in the small town of Mathoura in southern New South Wales. The study area is a part of Mathoura's central town and covers around 9600m². The area was part of a large data sets combine with aerial photographs and LiDAR data. The sample area is a good mixer of land cover features, which consists of rail line, storage sheds and silos, office building, vegetated areas and open space.

The software eCognition professional version 4.0 was used for the object based classification. This included multi-resolution segmentation and knowledge-based object

extraction. For comparison, ERDAS Imagine 8.7 was used for pixel-based maximum likelihood classification and image processing including image co-registration and resampling.

The OBIA began with the multi-resolution segmentation. In the segmentation process, for each image object a meaningful statistic is calculated in an increased uncorrelated feature space using shape, texture and topological features and this creates image object primitives. Finally, scale parameter of 15 was chosen to create local homogeneity and to keep global heterogeneity. Similarly, shape factor, compactness and smoothness were assigned 0.275, 0.3 and 0.7 respectively.

The next was the class hierarchy which creates the knowledge base for the classification. It was developed through inheritance hierarchy, which refers to the physical relations between the classes. Initially, vegetation and non-vegetation were the parent classes and they further divided into grass, tree and colour, non-colour classes as child classes and later, vegetation class became a parent class and grass and tree were the child classes as seen in Figure3.1.

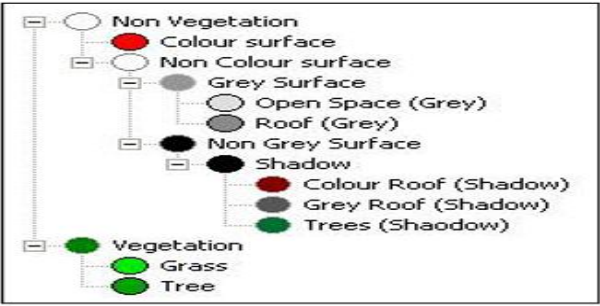


Figure 3.1: Feature classes, Source: Syed (2005)

The final stage calculated the classification based on spectral properties. Since the generated image objects hold more spectral information compared to pixels' digital

numbers, the object oriented classifier offers a huge variety of derivative spectral features (Hofmann, 2001). Brightness and spectral ratios of the image objects were calculated using all image layers. Textural features were calculated using standard deviations of layer values, spectral mean values of sub-objects, and average spectral differences of sub-objects. Contrast information were generated through spectral differences to neighbouring objects and super-objects. Colour Surface was the sub-class of non-vegetation class. This class was defined by the object's brightness and the ratio of the blue band.

The classification based on DEM properties was carried out with the understanding that it is the relative height and not the absolute. In eCognition this property can be modelled by describing the difference in elevation to neighbouring objects (Hofmann, 2001). An image object was represented as open space if its mean difference of nDSM was smaller or equal to 1.2m and the definition of roof was the opposite of the open space.

In this study, a shadow object is classified, as a grey roof shadow if its border to neighbour-object relation for grey object is larger or equal to 0.025m. A shadow object is classed as tree shadow if its border to vegetation neighbour-object is larger or equal to 0.02m.

For the pixel-based classification, statistics were generated for the high resolution image. After running the maximum likelihood classification scheme with equal prior probability, the classified image was generated with eight types of land cover features, the same as the number for the object-oriented classification.

The figures 3.2 a & b are the result from the pixel-based and object based classification methods. The main difference is the sharpness of the features, which look clearly better delineated in the object-oriented classification due to the combined use of the LiDAR derived DSM with multi-spectral image. The problem of the pixel based is clearly shown in the open space and roof classes as well as the shadow classes which were clearly defined using the object based because of the additional contextual information.

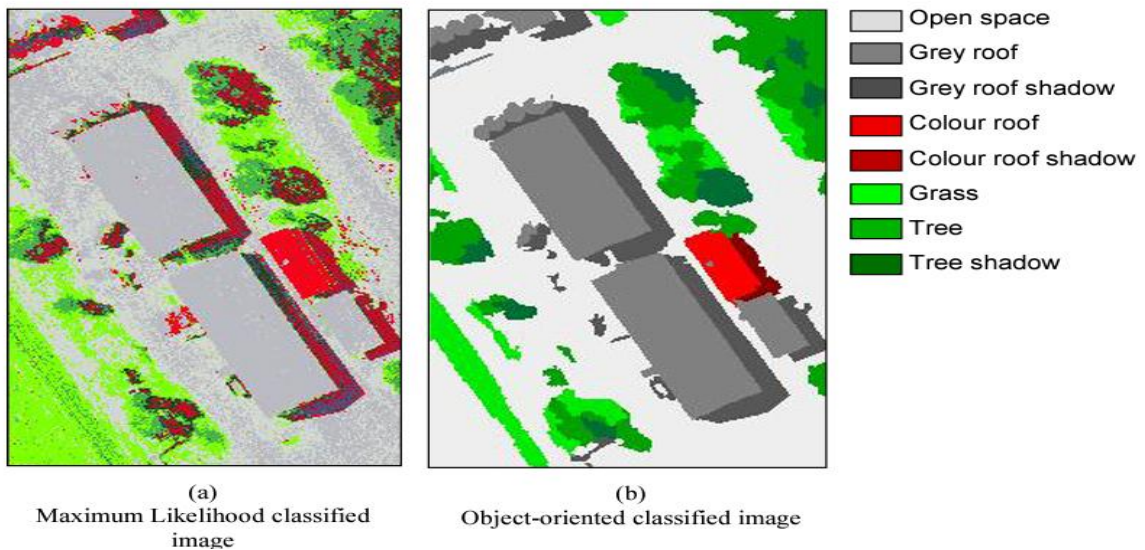


Figure 3.2a&b: Pixel based and object based classification respectively, Source: Syed (2005)

Yongmin (2011): Object-Based Classification of an Urban Area through a Combination of Aerial Image and Airborne Lidar Data

This study area is located in Chon-an, a city in South Korea and the study was carried out to classify an urban area through a combination of aerial image and airborne LiDAR data. The area was selected because it has various land covers and roof types making it difficult to classify using a single data. The aerial image and airborne LiDAR data were simultaneously acquired and used to solve this problem. The two data were registered and resampled to 0.25m spatial resolution.

Building extraction using LiDAR data is conducted through nDSM. The nDSM was used as not only the threshold for extraction of building information but also as an additional band in the process of pre-classification. The difference in height between last return and first return provides information about forest and non-forest cover. The input bands for classification included intensity and elevation information of LiDAR data, in addition to red, green, and blue bands of the aerial image and pre-classification was used to extract vegetation information. For the extraction of building objects, three conditions (see figure) were set out:

- i. $nDSM > 2 \text{ m}$
- ii. subtracted return information $\leq 1 \text{ m}$
- iii. \neq Vegetation area.

Initial segmentation is achieved by applying the modified SRG procedure, which integrates geometric structural and multispectral information to provide homogenous image regions with accurate and closed boundaries. The final segmentation result was obtained through a region adjacency graph (RAG)-based region-merging process, which merges the initial segments via a homogeneity cost measure that combines regional spectral and texture information. Post-processing operation was done using morphological filtering and filling the boundaries made during the segmentation process. A closing method is used in this step, and kernel size was 3×3 . There was elimination the objects that have areas smaller than 10 m^2 to minimize the errors in the aerial image. After this process, building objects are finally extracted as building shapes in the aerial image. The last step was the classification of the aerial image using an SVM (Support

Vector Machine). The SVM is an appropriate method of high-resolution multispectral image classification because it works well with small training data sets. The idea in this step is to conduct the SVM on the non-building areas of the aerial image. The bands used for classification

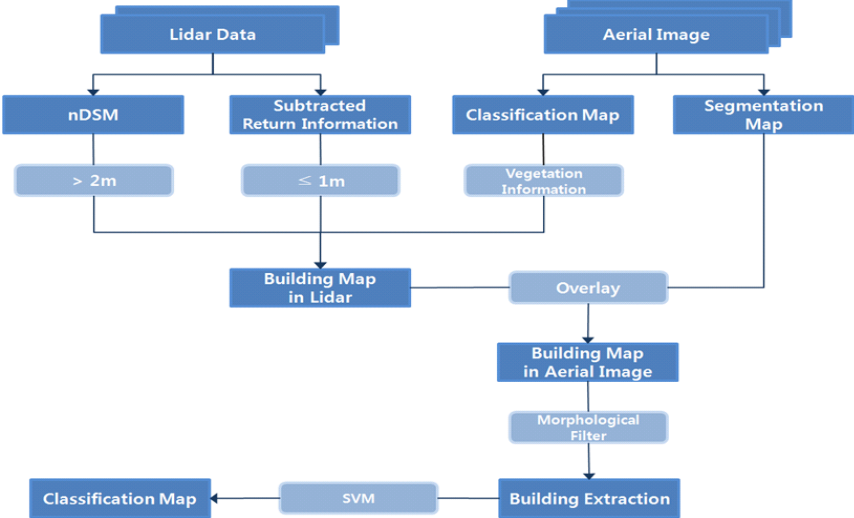


Figure 3.3: The flowchart for extraction of buildings. Source: Yongmin(2001)

The bands used for classification are the red, green, and blue bands of the aerial image and intensity and elevation information from the LiDAR data. The entire process involved the building objects extracted from LiDAR data through three thresholds, the segmentation of the aerial image, the extracted building objects of the aerial image derived by applying the definite rule after overlaying and the removal of small areas was applied to fill the boundaries and remove some errors.

The result showed that the method extracted well, buildings that are higher than 2m in study area by using an aerial image and LiDAR data, and the described classification process. Also building areas covered by shade were well extracted using the LiDAR data.

However, some vegetation areas were extracted as building class because they were not classified to vegetation class in the pre-classification step. This is due to the fact that the aerial image did not have Near Infrared band (NIR).

Bandyopadhyay, (2013):Classification and Extraction of Trees and Buildings from Urban Scenes Using Discrete Return LiDAR and Aerial Color Imagery

LiDAR point clouds and the aerial color (RGB) imagery of Downtown Rochester were collected during fall 2011. Two different regions of Downtown Rochester were selected to test the classification algorithm. Region 1 is a residential area of size 150x143 m, with smaller size buildings and many trees, whereas Region 2 consists of large commercial buildings and it covers an area of 360x 260 m.

The density of the LiDAR point cloud is approximately 10 -15 points/m². The LiDAR dataset contains the x, y, z location for each return, along with the return intensity;return number, number of returns, and vendor classification (ground, non-ground, or noise). The spatial resolution of color (RGB) imagery is 0.15m. The RGB imagery was orthorectified and processed into the same Universal Transverse Mercator (UTM) coordinate system as the LiDAR data. The LiDAR data was preprocessed. After preprocessing the LiDAR point clouds, the next step was to remove points below 1.5 m height. Thus the ground, roads, and small objects such as vehicles, shrubs, shades etc. were removed from the LiDAR data set and the remaining points consist of mainly buildings and/or vegetation points. Segmentation based on smoothness constraints was then applied to the remaining LiDAR points. Since building rooftops exhibit a regular pattern or flat surface compared to vegetation, this resulted in building regions that were

separated from the rest of the points. However parts of tree canopies sometimes were included in the segmentation result; these were eliminated using the NDVI map that is introduced later. Once building points were detected, they were removed from the point clouds. In the next step a vegetation mask was used to detect all the vegetation points. The figure below shows the workflow of the classification method.

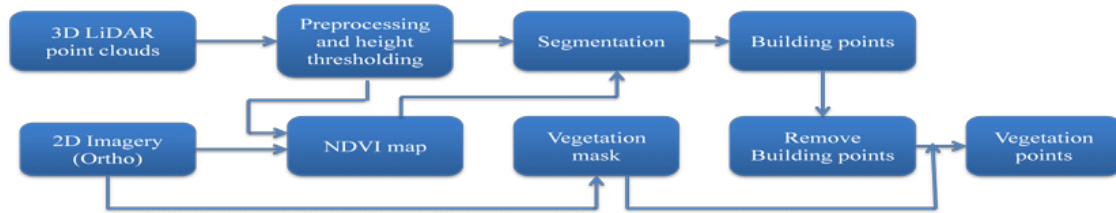


Figure 3.4: Workflow of classification method. Source: Bandyopadhyay, (2013)

NDVI map was produced from LiDAR point clouds and color (RGB) imagery. For each LiDAR point we found the closest pixel from the RGB image and assigned the red value to that LiDAR point, thus for each point we calculated the NDVI value using equation. Vegetation mask was also produced from RGB image. As a validation of the NDVI approach they have created another vegetation mask from the RGB image, utilizing the three bands from the color image and calculating two different indices. The table below shows the producers accuracy, users accuracy and the overall accuracy. From the table, we can observe that the classification accuracy for the building class is greater than 85%. But for vegetation class the Producer’s accuracy is comparatively low, near 81% for both regions.

Table 3.1: Prod. Accuracy, User Accuracy & Overall Accuracy,

	Region 1			Region 2		
	Building	Vegetation	Others	Building	Vegetation	Others
Producer's Accuracy (%)	89.63	81.18	93.01	92.95	81.42	96.08
User's Accuracy (%)	85.68	85.12	92.3	88.05	88.52	95.87
Overall Accuracy (%)	185149/205764 = 89.98			1937238/2061756 = 93.96		

Source: Bandyopadhyay, (2013)

The classification algorithm, based on the fusion of LiDAR point clouds and color RGB imagery resulted in a good classification result for both buildings and vegetation in an urban environment. On average the classification accuracy for both vegetation and buildings is greater than 85%, which can further be improved by correctly registering RGB imagery and LiDAR point clouds. An NDVI map, created by using the red channel of RGB and the intensity return of LiDAR proves to be very good indicator between vegetation and other classes.

Kokje, (2013): A simplified approach for classifying urban land cover using data fusion

This work demonstrates a simplified approach for classifying urban land cover using data fusion. The study area is Auckland city, specifically the core of the central business district (CBD).

The imagery was acquired from Worldview-2 (DigitalGlobe) multispectral imagery on 30th October 2010, covering approximately 25 km² of central Auckland is used as primary data source. 2005-06 LiDAR data was provided by New Zealand Aerial Mapping Ltd. (NZAM). The data supplied in LAS point cloud format comprising both

ground and above ground points at an average density of 1 point/m². is used as complementary datasets to satellite imagery.

An object-based feature identification approach, multi-resolution segmentation algorithm in eCognition environment is applied. nDSM data offering object elevation information is considered as main segmentation parameters supported by spectral information (NDVI, ZABUD and red spectral channel) applied to group various urban features based on homogeneity criteria. A hybrid supervised and Rule-set based parametric classification is performed on the intermediate (ground, and above-ground) classes identified, to obtain various land features (see figure). For data segmentation and classification, nDSM and slope derived from LiDAR data in conjunction with spectral components significantly improved the segmentation process, yielding better pixels grouping in spectrally complex impervious areas. Figure 3.5 shows the workflow.

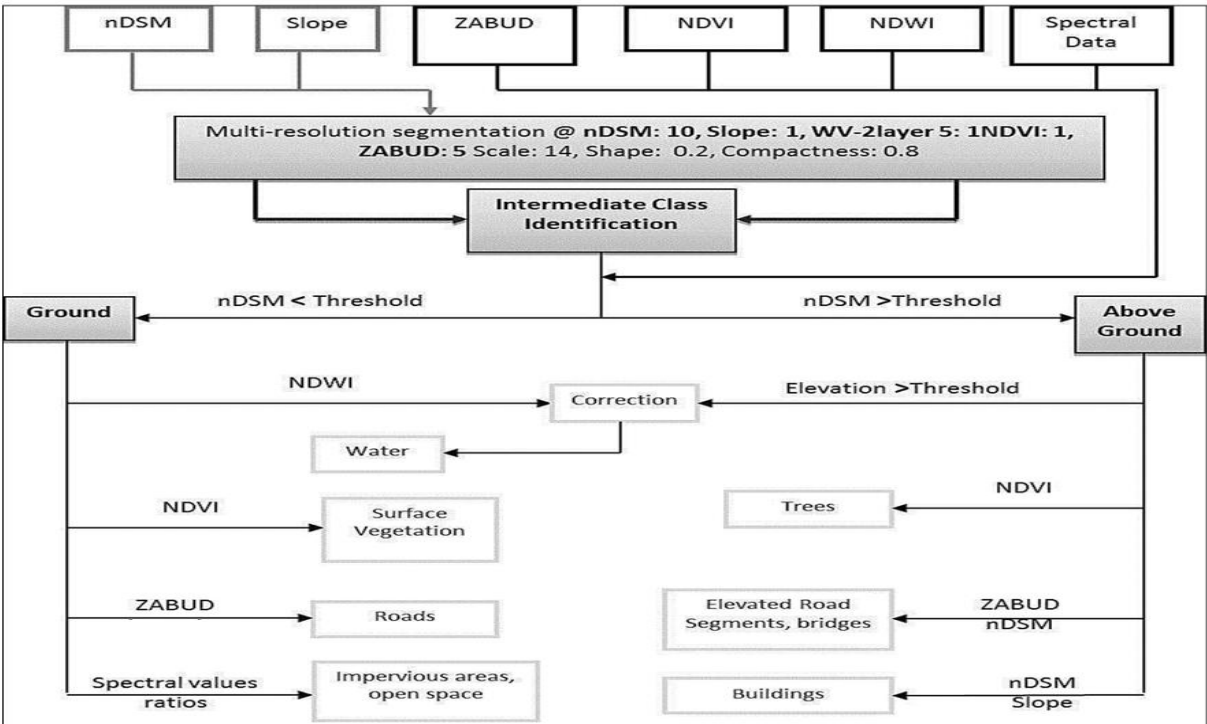


Figure 3.5: Methodology opted for the land feature identification. Source: Kokje, (2013)

Additionally, effect of shadows on segmentation region is reduced dramatically by applying active LiDAR nDSM data devoid of any shadows. Feature classification process was based on the proposition that the entire image objects (features) in a given area can be divided into ground and above-ground based on the elevation. Using this condition, intermediate classes (ground and above-ground) are derived from nDSM threshold.

In a stepwise classification approach, features categorised as ground are classified using sample based standard nearest neighbour (SNN) feature space optimisation. Due to spectral and spatial complexities associated with features in above-ground class, individual parametric rules are applied to extract trees and buildings (low, med and high rise)

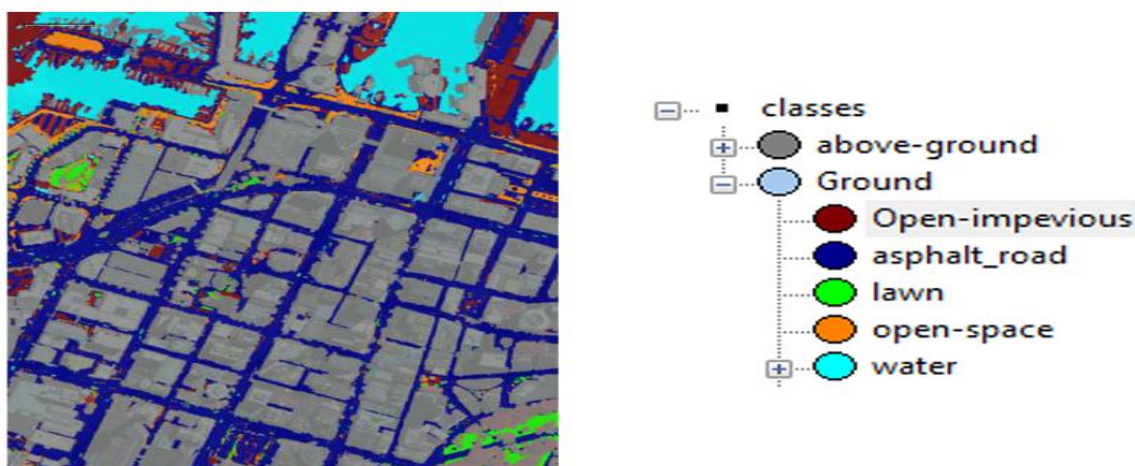


Figure 3.6: Various land features under intermediate class ‘ground’ is recognized.

Source: Kokje, (2013)

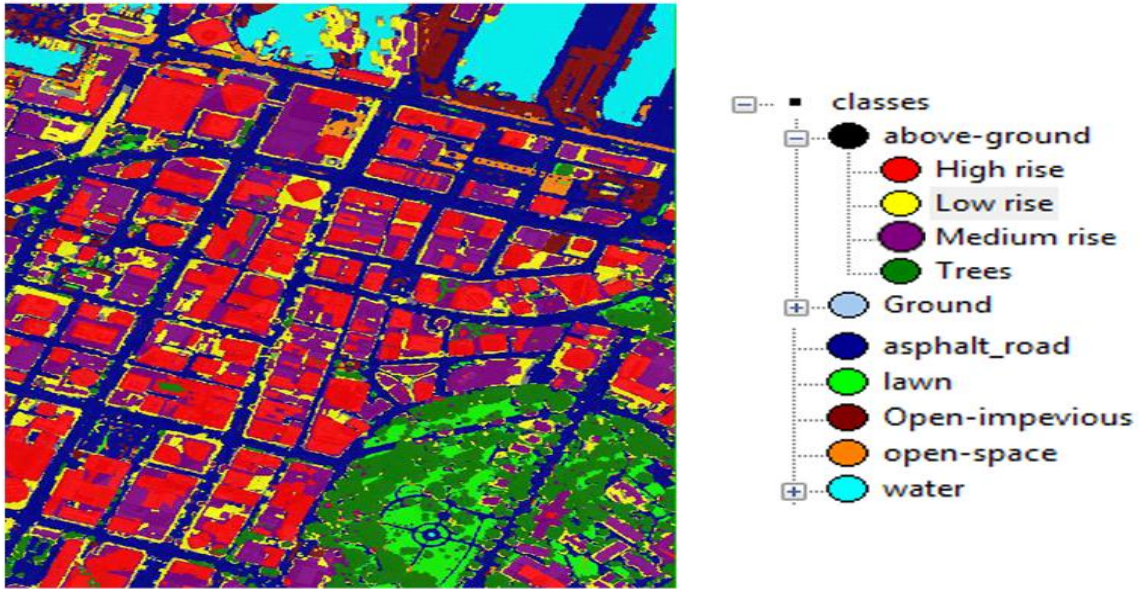


Figure 3.7: Sub classification of intermediate ground and above ground classes, yielding land features. Source: Kokje, (2013)

Initial analytical tests confirm accuracy of 93% for objects classified under transitional ground feature class.

Li, (2007): Fusion of VHR Imagery and LiDAR data for Object Oriented Urban Land Cover Classification Based on SVM

This study used lidar data and VHRimagery forland cover OBIA classification based on Support Vector Machine (SVM) and the study area is in Odense of Denmark.

The SVM method separates the classes with a hyperplane surface to maximize the margin among them (see figure 1), and m is the distance between 1 H and 2 H, and H is the optimum separation plane which is defined as: $w \cdot x + b = 0$, where x is a point on the hyperplane, 'w' is a n-dimensional vector perpendicular to the hyperplane, and 'b' is the distance of the closest point on the hyperplane to the origin. When multi-class SVM is concerned, three basic methods are available to solve the classification: One-Against-All (OAA), One-Against-One (OAO), and Directed-Acyclic-Graph (DAG).

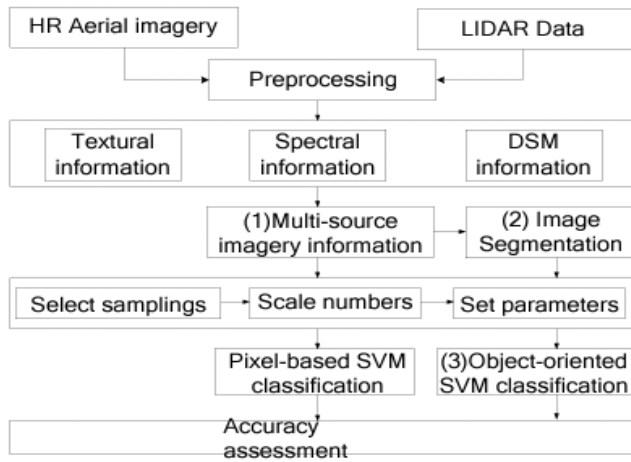


Figure 3.8: The flowchart of object-oriented classification based on SVM. Source: Li, (2007)

The LIDAR data and VHR aerial imagery had 0.4-m spatial resolution. The digital surface model was created from the first and last returns LIDAR data by applying height thresholds. Then the DSM image and VHR aerial image were geo-referenced to the same coordinate and projection with 376 by 339 pixels size. Seven land cover classes were identified for the study: 1 road, 2 building, 3 shadow of building, 4 tree, 5 shadow of tree, 6 grass, 7 bare land.

During the classification stage, a data preprocessing was carried out: the textural features (variance, contrast) of aerial imagery were calculated using Gray Level Co-occurrence Matrix (GLCM) filtering, and the texture and spectral information of HR aerial imagery were fused with the LIDAR derived DSM imagery to get multi-source image information.

The result showed that different shadow species are easier to distinguish when both aerial images and LIDAR data are used together. The results also show that the overall

accuracy of pixel-based SVM is 82.92%, whereas the overall accuracy of the object-oriented classification based on SVM is 95.97%. The overall accuracy is improved by 13.05%. The user's accuracy of each class using object-oriented classification is higher than the pixel-based SVM method. In particular, the land cover class, building and road, are obviously distinguished by the object-oriented classification method by fusing of DSM information of LIDAR data and spectral, textural information of aerial imagery.

In their conclusion they noted that SVM classification method could solve sparse sampling, non-linear, high dimensional data, and global optimum problems. The fusion of multi-source data could obtain more accurate information concerning features better than when a single data is used.

Jia, (2015):Object-based Land Cover Classification with Orthophoto and LIDAR Data

This used object-based land cover classification with orthophoto and LiDAR data. The study area is a subset area of city Örebro in Sweden. The two data were provided by the Swedish national mapping and DSM, DTM and intensity image derived from LiDAR data. The LiDAR data of this study area was generated in March 21st, 2012 with the spatial resolution in 1m and point density in 0.5 to 1 point per square meter. Orthophoto were produced from the aerial photograph that was collected by the camera Microsoft Vexcel UltraCam Eagle (UCE) in August 27th, 2012. The orthophoto image had four spectral bands, Red, Green, Blue (RGB) and Infrared (IR) with the resolution in 25cm.

From the orthophoto, seven surfaces aimed at discovering critical features in classification were derived. These were, DSM and NDSM, near-infrared (NIR) value,

Ratio Green, Ratio Vegetation Index (RVI), Normalized Difference Vegetation Index (NDVI), Normalized Difference Water Index (NDWI) and Land & Water Mask (LWM). DTM was produced from laser data. DSM was generated from linear array imaging by using image matching algorithm. NDSM as the normalized DSM was obtained by subtracting the DTM from the DSM.

Four surfaces were derived from LiDAR data, which were DTM, DSM, Fp-Lp image and intensity image. DTM was provided from the elevation model by extracting points on the ground surface from LiDAR point cloud. DSM was rasterized from LiDAR data by first return. Fp-Lp image was calculated by the difference of DSM between first pulse and last pulse, with spatial resolution in 1 meter. This has the capability to discriminate permeable objects e.g. vegetation. Consequently, the permeable objects always had the Fp-Lp value greater than zero which is useful to extract trees which have similar height with buildings from build-up area. In this study, only single and first pulse was used to obtain the intensity image, with a 2m resolution. This is because single and first pulse could reflect the land cover object surface on the surveyed area whereas the last pulse of multiple returns was useful for buildings delineate.

The software eCognition Developer 8.0 was used for the object-classification procedure of this study while Quantum GIS 2.0 (QGIS) was applied for design the layout and presenting the result image. Four land cover types were considered focusing on the essential land cover types in geographical database, forest (high vegetation), water, open land, and building. The rest of elements on the map were assigned to unclassified.

Firstly, surface derivation was implemented from provided orthophoto and LiDAR data. NDSM, Fp-Lp image and intensity image were generated for the classification process. Secondly, objects were created based on input dataset by using segmentation algorithm. Thirdly, spectral and spatial related features were experimented for each class i.e. forest, water, open land, building based on orthophoto, LiDAR and their surface derivation. Based on this, the features and the threshold to represent corresponding objects were found and rules for classifying object were decided. Classifications were performed based on orthophoto and lidar data, both alone and integrated, by following the rule set respectively. On the other hand, SVM classification algorithm was also performed based on the same data dataset as decision tree classification algorithm. Finally, corresponding samples in each class were selected for assessing the accuracy of classification results.

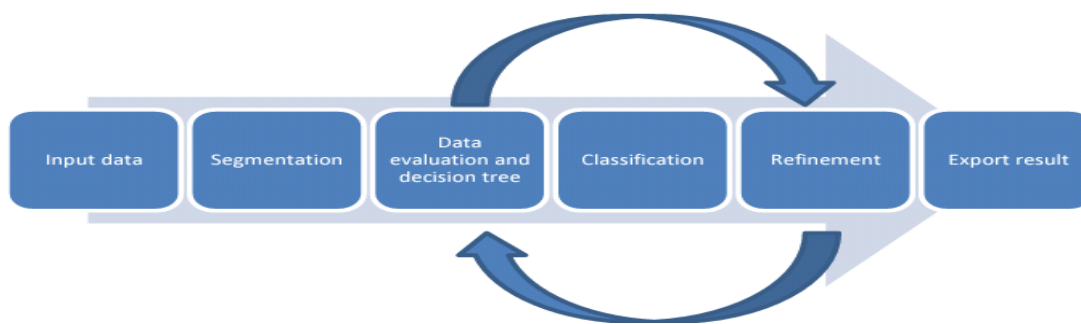


Figure 3.9: The workflow of object-based decision tree classification process. Source: Jia, (2015)

The results were generated in two different classification algorithms, i.e. decision tree and SVM. For orthophoto alone, the overall classification accuracy was 89.2%. Regarding producer's accuracies, forest achieves 95.5% classification accuracies, while the other classes get over 85% accuracies. Building is misclassified as forest and water. Of forest, the only source of omission error is from water. As for user's accuracies, all classes have

good results with accuracy over 90%. about 7.3% of open land are misclassified as water. 5.5% areas of building are misclassified as open land and water. These classification errors are caused by the similar spectral features of land cover types in orthophoto.

With regard to LiDAR classification dataset, the overall accuracy achieves 88.6%. Additionally, the four classes yielded over 88% average producer's accuracies. Water achieved the highest of 90.3% and building has the second of 89.2% and it is confused mainly with forest. Forest is 85.1% with misclassified areas mostly in open land which has a good accuracy in 88.6%. As for user's accuracies, building is classified with 99% accuracy with a few commission errors from forest. Water achieves a good accuracy as well (97.4%). Forest has the lowest user's accuracy due to commission errors from building and water basically. Open land reach 94.7% accuracy and some areas are confused with water. With the height value and intensity data, the LiDAR classification dataset achieved such optimal results without very high resolution.

Concerning of integration dataset, the classification results reach highest overall accuracy in 95.2% comparing with others producer's accuracies, building and open land achieve over 95% classification accuracies, while forest and water reach over 91% accuracy. Building is classified with 97.1%. Only small areas of open land and water are misclassified as building. On the side of user's accuracies, none of the four classes are down below 95%. Forest achieves the highest accuracy in 99%, while a small part of forest is misclassified as openland. Water has almost the same accuracy as forest, with the value of 98.9% accuracy.

The integration showed remarkable accuracy improvement. The overall accuracy improved expressively from 89.2% (orthophoto classification dataset) and 88.6% (lidar classification dataset) to 95.2%. Based on the study, the integration of orthophoto and lidar data could achieve satisfied classification results with very high agreement.

Dinis, (2009): Hierarchical Object-Based Classification of Dense Urban Areas by Integrating High Spatial Resolution Satellite Images and LiDAR Elevation Data

This is a hierarchical object-based classification of dense urban areas by integrating high spatial resolution satellite images and LiDAR elevation data. The study area, located within the Lisbon Municipality.

The satellite data consist of two pan-sharpened QuickBird images dated 13 April 2005 and 11 March 2007, with a spatial resolution of 0.6 m and 4 spectral bands. The sun azimuth and elevation of the 2005 image are $149^{\circ}.6$ and $57^{\circ}.3$, respectively, while for the 2007 image those values are $161^{\circ}.4$ and $46^{\circ}.0$, respectively.

All images have been orthorectified with sub-pixel accuracy, using Rational Polynomial Coefficients (RPCs) with 29 GCP's and validated with 22 checkpoints. For orthorectification, a Digital Terrain Model (DTM) was generated from the 1998 municipality vector cartographic map at scale 1:1000 with a spatial resolution of 0.5 m. A 2006 LiDAR Digital Surface Model (DSM) with a 1-meter spatial resolution was provided by LOGICA, covering only partially the extent of the municipality of Lisbon. Elevation and intensity of the first and last pulse returns from a TopoSys II 83 kHz LiDAR instrument, flown on a helicopter, were recorded for each laser pulse, with an average measurement density of 20 points per m². The provided DSM was produced

using only the last pulse returns, meaning that only data from the surface that was last hit by the laser pulse was considered. A surface cover height model (nDSM) was generated by subtracting the DTM from the DSM, to be used as ancillary data in the classification process.

Orthorectified photographs with 4 spectral bands were acquired on 16 August 2007 and provided by the Portuguese Geographical Institute (IGP) and used to collect the reference data used for the accuracy assessment of the map. All data was converted to the PT-TM06/ETRS89 coordinate system and the vertical datum of the DSM and the DTM is the maregraph of Cascais.

The Definiens Professional 5.0 software was used to conduct the object-oriented images analysis. Images orthorectification was undertaken in the PCI Geomatica V9.1 (OrthoEngine) since Definiens does not support those capabilities.

The methodology started with a hierarchical information extraction process involving three steps. First, the dark objects (water and shadows) and non-dark object were separated. Then, the non-dark objects were classified using the 2007 QuickBird image. Finally, shadows were classified using the 2005 QuickBird image. Vegetation and non-vegetation features are differentiated. Under the vegetation class, grass, shrubs and trees were extracted, while under the non-vegetation class, transport units, buildings and bare soil were discriminated and the common shadows between 2005 and 2007 were classified using contextual rules. The Definiens Professional 5.0 software was used for the segmentation which had two steps. The 2007 QuickBird image segmentation was applied, with a scale parameter of 75, a color parameter of 0.9 and a shape parameter of

0.1, whilst the 2005 QuickBird image was processed at a finer scale of 25, the weights for colour and shape were kept as 0.9 and 0.1, respectively. A threshold value of 180 was set to extract water and dark objects (water and shadow) and a Spectral Shape Index (SSI) was used to distinguish water from the black body mask.

Vegetation and non-vegetation features were separated using a NDVI. The NDVI was calculated based on the formula: $NDVI = (NIR-Red)/(NIR+Red)$ and the threshold was set to 0.36, through a pixel-based histogram analysis. Three different features, namely trees, shrubs and grass, were discriminated under the vegetation features. The non-vegetation features were further divided, using the nDSM, in high ($nDSM > 1.91$ m) and low ($nDSM \leq 1.91$ m) features. These high features were separated afterwards into buildings and high crossroads using a shape function. The hierarchical rule-based classification is better explained with the diagram below. For the classification of the shadowed areas, a new threshold was set using the spectral and spatial information of the 2005 satellite image. a shadow object with a relative border to a transportation unit ≥ 0.6 is classified as transportation unit; and a shadow object with a relative border to tree = 1 (i.e. totally surrounded) is classified as tree.

Overall accuracy: 87%; Kappa coefficient: 0.84 was achieved.

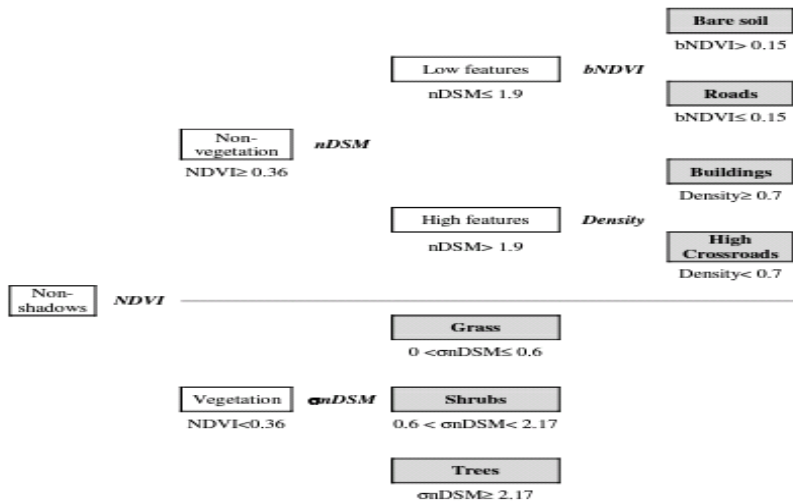


Figure 3.10: The hierarchical rule-based classification. Source: Dinis, (2002)

Dupuy, (2012): OBIA for Combining Lidar and Multispectral Data to Characterize Forested Areas and Land Cover in Tropical Region.

This research combined LiDAR data and multispectral data to characterize forested areas and land cover using OBIA classification method. The study area is Mayotte, an island of the Comoro Archipelago located at the entrance of the Mozambique Channel.

The data used are a Digital Surface model (DSM) and a Digital Terrain Model (DTM) built with a spatial resolution of 1m x 1m was produced by IGN (French Geographic Institute) using an adaptive triangulated irregular network algorithm from the software TerraScan (Terrasolid Ltd, Finland). Two types of multispectral images were acquired on the study zone: orthophotos (0.5 m pixels) required for precisely delimiting small objects and Spot 5 XS satellite images (10 m pixel) for better discriminating vegetation covers using both short wave and near infra-red information (Muller, 1997). All multispectral images were re-sampled to the same resolution of the DCM using the cubic convolution interpolation algorithm.

The methodology was based on an object-based procedure in three successive segmentation/classification levels implemented with the eCognition Developer 8 software using the multi-resolution segmentation algorithm. The workflow is presented below.

Table 3.2: Segmentation parameters for each OBIA level.

	Level 1	Level 2	Level 3
scale parameter	200	40	35
shape	0.9	0.7	0.1
compactness	0.5	0.4	0.5
spectral bands (weight)	not used	MNC (1) High pass filter (1) maxfilter (1)	Spot 5 (1) aerial photography (2)
Thematic vector data	used	not used	not used

Source: Dupuy, (2012)

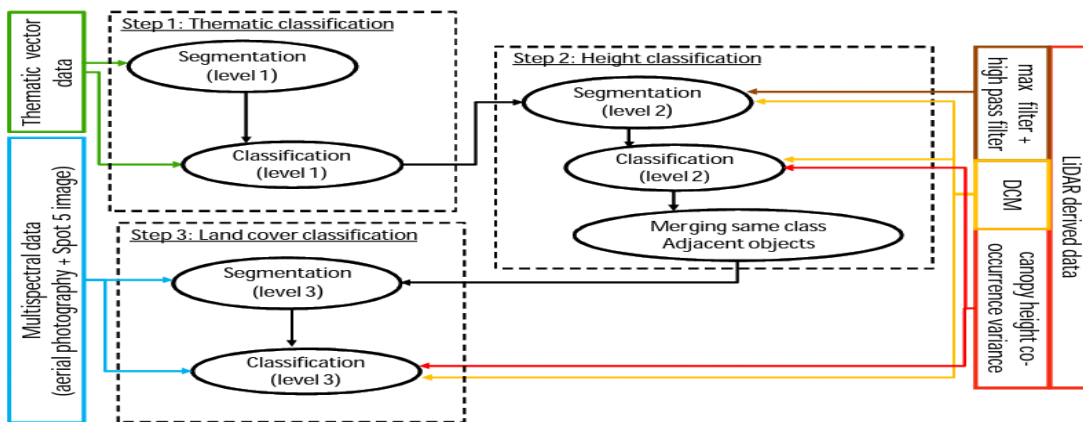


Figure 3.11: Workflow of the OBIA procedure. Source: Dupuy, (2012)

(i) Level 1: The first segmentation/classification step consists in masking and classifying the studied zone according to existing thematic data. The studied zone is thus segmented according to the limits of thematic data entities. Then, the resulting image objects are assigned – or not – to a thematic class using Boolean rules.

(ii) Level 2: Height classification - The second segmentation/classification step consists in classifying cover heights on non-thematic objects of level 1. Within the boundaries of the first segmentation level, a second segmentation level was based on the DCM and the Max and High Pass filters. The researcher obtained a quite good delineation between (i) the two forest stands observed in the field (forest area with low height canopy and high height canopy); and (ii) forest areas, shrub cover and low vegetation. The resulting image objects are first assigned according to 4 height classes (\bullet 1.5 m;] 1.5 – 5m;] 5 – 10m [; \bullet 10 m) using Boolean rules based on DCM values.

(iii) Level 3: Land cover classification: The third segmentation/classification level aim is two-fold: (i) to classify the different forested types objects discriminated at level 2 according to their composition (deciduous or evergreen); and (ii) to classify the two lowest height class objects discriminated at level 2 and the eroded area objects extracted at level 1 following the land cover categories defined in the research. Only one segmentation level, based on limits built in level 2 and multispectral information, was required to satisfy this double aim.

According to the confusion matrix, 84% of the control objects were correctly classified. This global accuracy is confirmed by the kappa index value of 80, which means that 80% of the objects would appear well classified according to any completely random validation process. Highly accurate results (\bullet 80%) were obtained for forest types (defined by the structure and heterogeneity), for shrub and low vegetation and fern eroded area classes. The poorest accuracy was for bare soil on eroded area (69%) and herbaceous on eroded area (58%) classes because of (i) confusion between these two

classes due to their similar spectral behavior; and (ii) radiometric heterogeneity of data source used for the discrimination of these classes (orthophotos).

In conclusion, acquisition of satellite data (with more radiometrically homogenous image) with higher spatial resolution (QuickBird 0.5 m pixels or Pleiades 0.5 m pixels for example) at suitable acquisition period (October) would be better for enhancing discrimination between evergreen and deciduous forest types.

Kiani, (2014): Urban Area Object-Based Classification by Fusion of Hyperspectral and Lidar Data

This is a research that investigated hyperspectral and LiDAR data fusion to generate accurate LC/LU maps with object based classification method. The dataset was co-registered and geo-referenced and was acquired over the University of Houston campus with its neighboring urban area.

The data used for this research were got from Data Fusion Technical Committee (DFTC) of the IEEE Geoscience and Remote Sensing Society (GRSS). They were two datasets – a hyperspectral image and a LiDAR derived Digital Surface Model (DSM), both at the same spatial resolution (2.5m). The hyperspectral imagery has 144 spectral bands in the 380 -1050 nm spectral region. Training and test samples provided by DFTC, include fifteen different classes as follows: healthy grass, stressed grass, synthetic grass, soil, water, tree, road, highway, railway, parking lot, car, tennis court, running track, residential and commercial buildings classes.

The first step in the methodology was to preprocess the data. Preprocessing of hyperspectral image include cloud shadow removal and dimension reduction and

extraction of nDSM from LiDAR data. Next step include image segmentation by applying a multi-resolution segmentation algorithm resulted in shadowed and no shadowed area separation. In this research Nonparametric Weighted Feature Extraction (NWFE) method was used which only ten features was applied. In this research a targeted segmentation strategy has been implemented that extracts each class by using data layer lead to highest separation with its neighboring objects of respective class. In addition to this strategy, various segmentation algorithms according to classes' geometric behavior, such as multi threshold, chessboard and multi-resolution segmentations, can be implemented to create meaningful objects. A suitable information layer for each class is obtained through first ten NWFE features spectra analysis.

An iterative classification process was used in this research. At first step, considering generated nDSM data, classes with highest spectral and elevation distinction and no specific geometric structure was extracted. For this data type classes such as vegetation, soil, water and synthetic grasses were classified. At second step, classes with similar spectral behavior but different and specified geometric features were extracted. Road, highway, railway, parking lot, car, tennis court, running track, residential and commercial buildings classes are categorized at this step. For extracting highway, road, railway and parking lot classes shape features include Length/Width, Area, Density and Compactness were used as well as spectral features. In addition to spectral features, for running track and tennis court classes respectively Ecliptic fit and Rectangular Fit features were used.

In order to separate commercial from residential classes, geometric features like Area, volume and class-related features such as Proximity, Distance between buildings, spatial distribution, Closeness and Distance to parking lot and also elevation features were utilized. Finally, for roof parking classification, geometric features, Rectangular Fit and Area in addition to extracted slope map for ramp identification were applied.

Results indicate an overall accuracy of about 97%. Classification results including producer’s accuracy, user’s accuracy, Kappa coefficient and overall accuracy is shown in the table below. Using LiDAR mitigate misclassification between roads and buildings and also healthy grass and trees. This classification method is performed at one level in an iterative Segmentation-Classification-Merging (SCM) process.

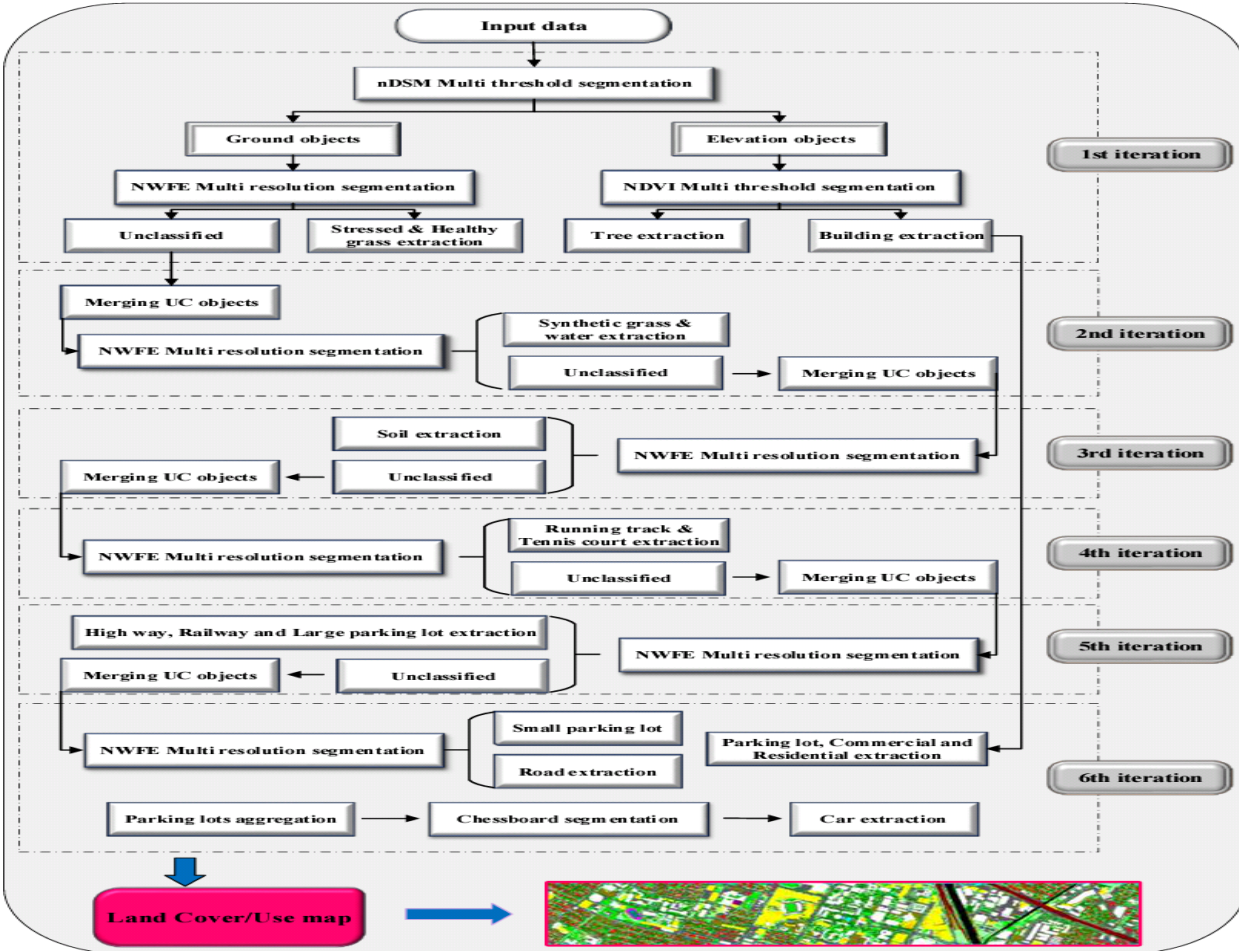


Figure 3.12: The iteration stages of the methodology. Source: Kiani, (2014)

This novel design takes advantage of classification at one level with keeping hierarchical model characteristics. Hierarchical model behavior retrieved by iterative procedure as in each iteration, one or two objects based on their spectral and geometric characteristics are classified. Applying segmentation and classification algorithms in accordance with behavior and condition of objects in image scene is one advantage of this method.

Zou, (2016): Object Based Image Analysis Combining High Spatial Resolution Imagery and Laser Point Clouds for Urban Land Cover

This is a study utilizing object based image analysis combining high spatial resolution imagery and laser point clouds for urban land cover. The study area is the photogrammetric test site Vaihingen/Enz of Institut für Photogrammetrie, Stuttgart University in Germany. eCognition Developer software (eCognition, 2014) to execute the image segmentation and image classification based on an OBIA approach.

For the datasets, the image consists of two state-of-the-art airborne image datasets, consisting of very high resolution colour-infrared TOP tiles and corresponding digital surface models (DSM). The DSM is generated via dense image matching with Trimble INPHO 5.3 software, and the TOP mosaic is generated with OrthoVista module in Trimble INPHO software (ISPRS Report, 2013). The TOPs are 8 bit TIFF World format with three bands: near infrared, green and red bands. The DSM is a TIFF World format with one band and the grey levels are encoded as 32 bit float values. The ground sampling distance (GSD) of both the TOP and the DSM is 9cm with the same grid.

The LiDAR data was captured with a Leica ALS50 system. Inside an individual strip the average point density is 4 points/m². The laser datasets are LAS 1.2 file format and each point with XYZ coordinate, intensity, elevation, number of returns, returns number, scan angle, class and source ID information. These laser datasets are made available as ancillary data for classification. The methodology can be seen in the workflow below as having 4 major steps.

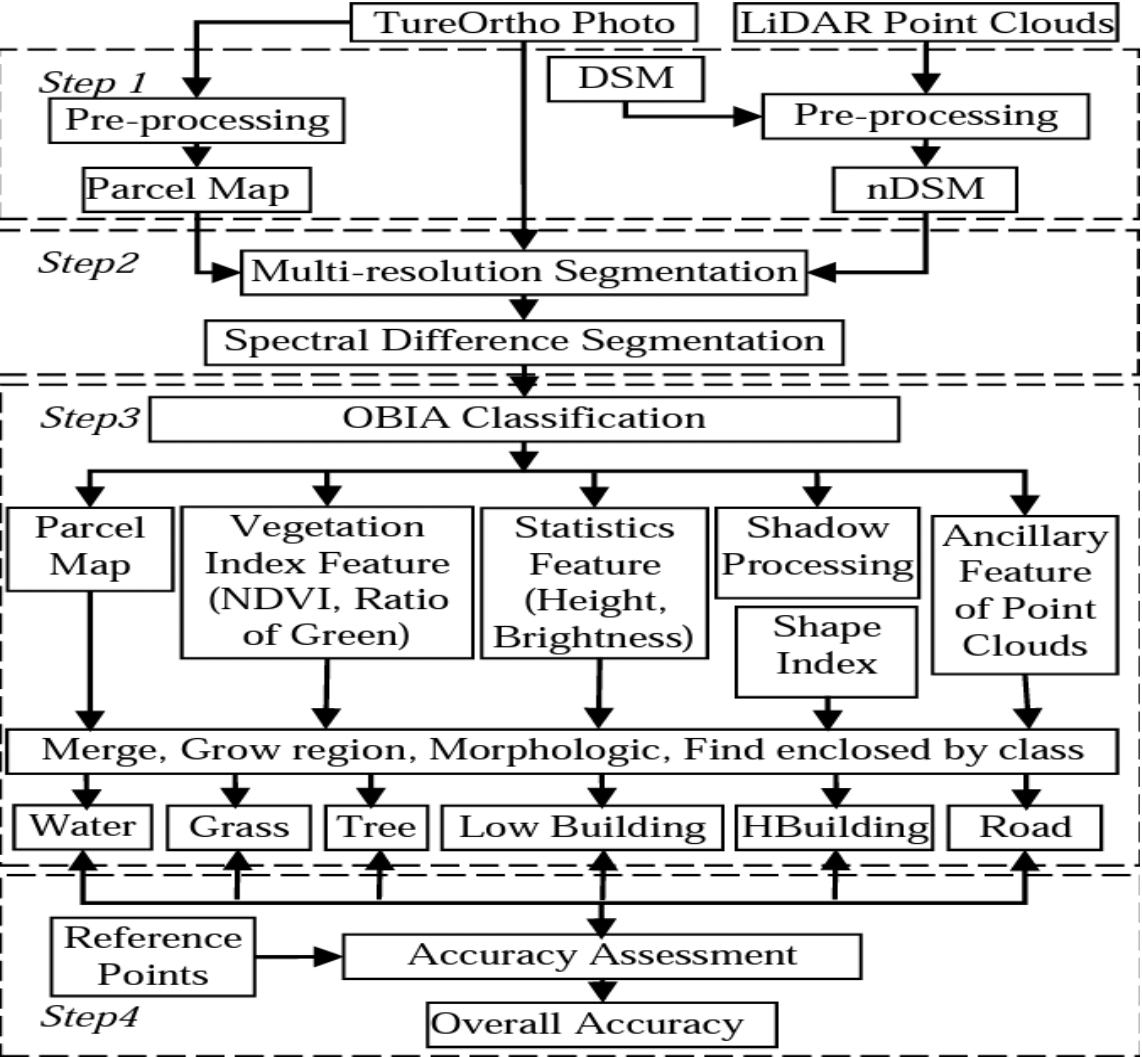


Figure 3.13: Workflow of OBIA classification with ancillary data. Source: Zou, (2016)

The first step is to pre-process in order to obtain parcel map of water bodies and to create a normalized digital surface model (nDSM) from the point clouds. The second

step is multi-resolution image segmentation. Image objects primitives are created via multi-resolution image segmentation integrating scale parameter, the colour and shape properties and compactness criterion. The third step is image objects classification. The image objects classes of interest typically discerned in urban classification are assigned to six different classes: water bodies, low vegetation/grass, tree, low building, high building and road. . A rule set of knowledge decision tree is created for classification with specific attributes e.g. vegetation index feature (NDVI, ratio of green), object shape feature (length/width, shape index, area), object statistics feature (difference in height, brightness) and ancillary feature of point clouds (intensity, class, elevation, number of returns, returns number).The forth step is to assess the validity of classification results. Accuracy assessment is performed by comparing randomly distributed sampled points with the classification results.

In summary, multi-resolution segmentation to create image objects primitives from image pixels. A group of parameters were selected, which scale parameter is equal to 30, shape parameter 0.3 and compactness parameter 0.5. The weighting of NIR image layer has been increased to 2, and the weightings of other image layers such as red, green are increased to 1. The thematic layer of water bodies with parcel boundary is used to be candidates for segmentation. The weighting of water body layer is increased to 1. The weighting of nDSM layer is increased to 1. Six categories in urban classification are defined as water bodies, low vegetation/grass, tree, low building, high building and road. A knowledge base of classification rules is constructed to classify each object into certain class. Objects characteristics such as NDVI, ratio of green, thematic attribute,

point cloud-related attribute, spatial relation and statistical measures are utilized to create the knowledge rules for classification. Ancillary data such as water bodies with parcel boundary and height information of building or tree derived from nDSM is also used to create the knowledge rules, forming process tree.

The accuracy assessment of the classification results for six classes is performed using a total number of 200 randomly distributed sampling point data. The overall accuracy (OA) of OBIA classification reaches 89.5% in the study area and the Kappa coefficient is recorded as 0.865. The research concluded that object based image analysis (OBIA) approach is proved to be an effective and convenient way to combine high spatial resolution imagery and LiDAR auxiliary data for classifying urban land cover. The use of LiDAR datasets and nDSM are very helpful for the separation of tree and low vegetation, building and road using the height information.

Hermosilla, (2012): Land-use Mapping of Valencia City Area from Aerial Images and LiDAR Data

This research was carried out for land-use mapping of Valencia city area from aerial Images and LiDAR data. Valencia is a compact city composed by a central historical area surrounded by buildings of different typologies,

Imagery and LiDAR data were acquired in the frame of the Spanish National Plan of Aerial Orthophotography (PNOA). The images were collected in August 2008 and they have 0.5 m/pixel spatial resolution, 8 bits radiometric resolution and four spectral bands: red, green, blue and near infrared. LiDAR data were acquired in September 2009 with a nominal density of 0.5 points/m² using a RIEGL LMS-Q680 laser scanner device. A

normalised digital surface model (nDSM), i.e., the difference between the digital surface model (DSM) and the digital terrain model (DTM), representing the physical heights of the elements present over the terrain, was generated from LiDAR data.

The methodology of the land use classification was carried out in five steps: class definition; sample selection; descriptive feature extraction; object classification; and evaluation.

Land-use class definition was performed based on the specifications of the Land Cover and Land Use Information System of Spain (SIOSE) database. The legend was composed of seventeen classes, discriminating between ten urban land use classes and seven agricultural classes. The urban classes and their sample plots defined were: historical buildings (264 samples), urban buildings (225), open urban buildings (142), semi-detached houses (90), detached houses (153), industrial/warehouse buildings (139), religious buildings (30), commercial buildings (24), public buildings (173), including schools, universities, sport facilities and civic and governmental buildings, and gardens and parks (57). The agricultural classes defined were: arable lands (92), citrus orchards (141), irrigated crops (81), carob-trees orchards (63), rice crops (74), forest (39) and greenhouses (43).

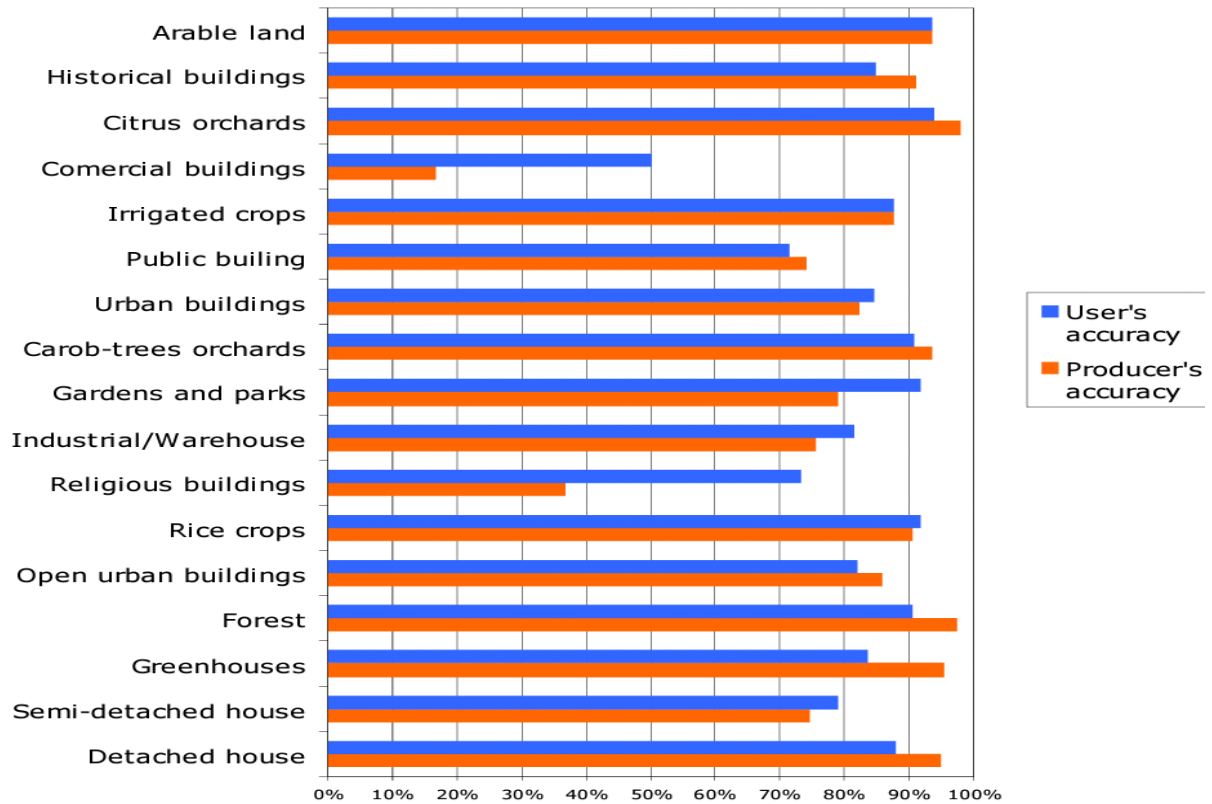


Figure 3.14: Legend of seventeen classes, Source: Hermosilla (2012)

For the feature extraction, object features were computed using the object based image analysis software FETEX 2.0. The computed features provided information regarding spectral, texture, structural, geometrical, three-dimensional and context based properties. Classification was performed using decision trees constructed with the C5.0 algorithm combined with the boosting technique. The overall accuracy of the classification was 84.8%, and the kappa coefficient 0.83. These were considered to be sound results, especially considering the large number of classes defined (17) and the structural similarities between some classes, e.g., semi-detached houses and detached houses.

Hamedianfar, (2014): Detailed Urban Object-based Classification from Worldview-2 Imagery and LiDAR data: Supervised vs Fuzzy Rule-based.

This paper investigates the comparative assessment of object-based classifications including fuzzy rule-based and supervised Support Vector Machine (SVM) to perform detailed characterization of urban classes. The study area is a part of Universiti Putra Malaysia (ranged from upper left longitude $3^{\circ}00'14.48''\text{N}$ and latitude $101^{\circ}42'14.71''\text{E}$, lower right longitude $3^{\circ}00'00.71''\text{N}$ and latitude $101^{\circ}42'44.12''\text{E}$, of WGS84 coordinate system).

The data used were Worldview-2 Imagery and LiDAR Data. Digital Elevation Model (DEM) was subtracted from Digital Surface Model (DSM) to create normalized Digital Surface Model (nDSM). Both WV-2 and nDSM are geometrically corrected to UTM projection, zone 47N and Kertau48. Pan-sharpening (Zhang 2002) of WV-2 image was performed to provide more de-tailed visualization about impervious features. To improve the accuracy of image classification, a multi-band file was generated including WV-2, nDSM, Normalized Difference Vegetation Index (NDVI).

The first classification was done using supervised object based by Support Vector Machine (SVM). SVM is popular in remote sensing data analysis due to its ability to deal with small training data sets. Supervised classification utilizes training data to allocate unknown objects to known classes. Radial Basis Function (RBF) was employed as a kernel for SVM. The cross validation determined the optimal parameter of $C = 0.5$ and $\gamma = 0.0078$ with 5-fold function rate = 99% (Hamedianfar and Shafri 2013).

The second part of the classification was done using rule based approach. Rule-based classification is a feature extraction approach that allows rule set creation to map particular features class based on its spectral, spatial and textural characteristics. Rules are created based on human knowledge and reasoning about specific land-cover types (ENVIZoom 2010). For example, dark building has a low NDVI, roads are elongated, buildings are rectangle in shape, water has a low mean value in NIR band, and vegetation has a high NDVI and trees are highly textured compared to grass. In this study, s-type membership function was employed to deal with fuzzy nature of urban environment (Jin & Paswaters 2007). Standard confusion matrix was used to perform the accuracy assessment of image classifications and ground truth data was collected by ground survey.

The result showed that SVM classifier achieved the overall accuracy and kappa coefficient of 85.02% and 0.82, respectively. Although feature height information was added to spectral, spatial and textural information; SVM classifier could not produce an accurate result from impervious surfaces. Utilization of height information was useful to separate the heterogeneous spectra of rooftops from roads and sidewalks. The classes of grass and trees were well extracted by the classifier by the use of textural, spectral, and elevation attributes. Pond was classified with high user and producer accuracies, but its misclassification can be seen with dark metal roofs showing that classifier could not make use of elevation information to separate these two classes effectively. The table below shows summary of the performance of the SVM classifier.

Table 3.3: Accuracy assessment of supervised SVM object-based classification,

class	Reference total	Classified total	Correct classified	Pa %	Ua %
Mr	80	58	58	72.50	100
Cr	58	57	47	81.03	82.46
Ar	24	40	24	100	60
R	61	43	41	67.21	95.35
S	10	24	10	100	41.67
G	52	52	51	98.08	98.08
T	72	83	71	98.61	85.54
P	33	38	33	100	86.84
Sp	5	5	5	100	100
Sh	39	34	29	74.36	85.29
Overall Accuracy = 85.02%			Kappa Coefficient = 0.82		

Note: Mr =metal, Cr: concrete tile roofs, Ar: asbestos roofs, R= roads, S=sidewalks, G=grass, T=trees,

P=pond, Sp= swimming pool, Sh=shadow, Pa= producer accuracy, and Ua= user accuracy

Source: Hamedianfar, (2014)

For the rule based classification, after performing segmentation and merging steps, fuzzy rule-based classifier with S type membership function was utilized to build the optimal rule-sets. The rule set is done in order to cope with the spatial and spectral diversity of the urban features. Fuzzy logic allows well approximation of human reasoning as well as the probabilities to assign image objects to their related feature classes. The overall accuracy and Kappa coefficient were reported to be 93.07% and 92%, respectively. Several attributes were used to differentiate metal roofs from other features. Firstly, nDSM applied to discriminate metal roofs from low elevated features such as roads and grass. Concrete tile roofs showed to be the most heterogeneous impervious surface. Different spatial, spectral, texture and elevation were used to extract these rooftops. There was an improvement made in mapping of concrete tile roofs compared to supervised SVM classifier result. NDVI was assisted in elimination of spectrally and spatially similar features as well as vegetated areas. Then, tx-entropy was applied to differentiate asbestos roofs from roads and this made it possible to overcome the mixed object of this class with concrete tile roofs and roads classes. In order to discriminate

roads, NDVI was used to remove the vegetation. Then, nDSM was applied to differentiate road from elevated features. After that, costal band was useful to get rid of spectrally similar features such as dark roof tops and water bodies. To extract sidewalks, different attributes were tested. Firstly, NDVI was used to remove building and vegetation. Then, NIR2 and mindir were used to differentiate sidewalks from dark rooftops and roads. The table below shows the performance of the rule based method.

Table 3.4: Accuracy assessment of rule-based object-based classification,

class	Reference total	Classified total	Correct classified	Pa %	Ua %
Mr	80	80	78	97.50	97.50
Cr	58	58	52	89.66	100
Ar	24	24	24	100	100
R	61	61	51	83.61	91.07
S	10	10	10	100	100
G	52	52	51	98.08	89.47
T	72	72	71	98.61	92.21
P	33	33	33	100	100
Sp	5	5	5	100	100
Sh	39	39	30	76.92	96.77
Overall Accuracy = 93.07%			Kappa Coefficient = 0.92		

Note: Mr =metal, Cr: concrete tile roofs, Ar: asbestos roofs, R= roads, S=sidewalks, G=grass, T=trees, P=pond, Sp= swimming pool, Sh=shadow, Pa= producer accuracy, and Ua= user accuracy

Source: Hamedianfar, (2014)

The supervised classification showed misclassification between impervious surfaces and this is because supervised classification cannot effectively differentiate the spatial and spectral diversity of roof types, roads and sidewalks. Developed object-based rule-sets produced better classified image compared to supervised SVM.

Aguilar, (2012):Optimizing Object-Based Classification in Urban Environments Using Very High Resolution Geoeye-1 Imagery

This is a study titled “Optimizing Object-Based Classification in Urban Environments using Very High Resolution Geoeye-1 Imagery”. The study area comprises the little village of Villaricos, Almería, Southern Spain, including an area of 17 ha. The working

area is centered on the WGS84 coordinates (Easting and Northing) of 609,007 m and 4,123,230 m.

For the data, over the study site an image of GeoEye-1 from the imagery archive of GeoEye was acquired. It was captured in reverse scan mode on 29 September 2010, recording the panchromatic (PAN) band and all four multispectral (MS) bands (i.e., R, G, B and NIR). The image products were resampled to 0.5 m and 2 m for the PAN and MS cases respectively. For these products, the pancharpened image with 0.5 m GSD and containing the four bands from MS image was attained using the PANSHARP module included in PCI Geomatica v. 10.3.2 (PCI Geomatics, Richmond Hill, Ontario, Canada). Finally, two orthoimages (PAN and pansharpened) were computed using the photogrammetric module of PCI Geomatica (OrthoEngine). Rational function model with a zero order transformation in image space, 7 DGPS ground control points and a very accurate LiDAR derived digital elevation models (which is going to be detailed later) were used for obtaining both orthoimages. In this work SAVI index was used. It was computed by SAVI algorithm from PCI Geomatica, and a new image was calculated from Red and NIR bands included in pansharpened orthoimage.

The LiDAR data was taken on August 28th, 2009, as a combined photogrammetric and LiDAR survey at a flying height above ground of approximately 1000m using a Leica ALS60 airborne laser scanner which derived DEM with a grid spacing of 1m. Normalized Digital Surface Model (nDSM) was generated by subtracting DEM from DSM as well as orthoimages with 15cm GSD were attained from this flight by Intergraph Z/I Imaging DMC (Digital Mapping Camera).

The methodology started with a multiresolution segmentation and object-based image analysis software used in this research was eCognition v. 8.0. The segmentation was always developed using the four equal-weighted bands from pansharpened orthoimage. Furthermore, the compactness was assigned a weight of 0.5 and the shape was fixed at 0.3. Following this way, 2723 image objects (IOs) were detected. Only 1894 IOs from the initial 2723 could be visually identified as meaningful objects (see Table 3.5). The hand-made or manual classification was developed into ArcGis v. 9.3 using the available datasets (orthoimages from GeoEye-1 and DMC, MDE, DSM, nDSM, SAVI). A subset of 945 well-distributed IOs were selected to carry out the training phase of the classifier used in this work (i.e., nearest neighbour) while the remaining 949 IOs, also well-distributed in the working area, were used for the validation or accuracy assessment phase. In this work, an object-based supervised classification has been used, being nearest neighbour the classifier chosen.

Table3.5: Image objects after the segmentation process.

Class	No. IOs	Subset IOs Validation	Subset IOs Training
Red buildings	298	149	149
White buildings	558	279	279
Grey buildings	68	34	34
Other buildings	55	28	27
Shadows	477	239	238
Vegetation	194	97	97
Bare soil	93	47	46
Roads	72	36	36
Streets	71	36	35
Swimming pools	8	4	4

Source: Aguilar, (2012)

For the feature extraction and selection, in addition to the four features (Red, Green, Blue and Infrared bands from pansharpened GeoEye-1 orthoimage) used for creating the IOs at the segmentation phase, other 43 features, were used for supervised classification.

The result and conclusion showed that:

1.- Using seven basic features of mean layer values such as Blue, Green, Red, Infrared, Pan, Brightness and Maximum difference, a vegetation index as the Soil Adjusted Vegetation Index (SAVI), and the normalized Digital Surface Model or Object Model (nDSM), the best overall accuracy (79.39 %) was reached. This result improved even those carried out using 45 features, being the last strategy much more time consuming in terms of CPU.

2. nDSM was the most important feature for detecting buildings, as it had already reported by many authors working with other sources of images, such as Ikonos, WorldView-2, or digital aerial images.

3. The inclusion of SAVI index was related with the detection of vegetation, and, together with NDBI, was a good strategy for the classification of roads

4. A percentage of 10% of training areas was enough for attaining good accuracies using object-based supervised classification with the nearest neighbour classifier.

Singh, (2015): Land Information Extraction with Boundary Preservation for High Resolution Satellite Image

This study was based on using high resolution satellite image to extract land information. The study area is located in Burghausen, Germany which is a Rapid Eye image with 5m resolution. This image contains various details such as buildings, roads, agricultural fields, forest area, river which we have to extract with their proper boundary.

The methodology started with edge detection which is the most important part of edge detection and it means to detect the pixel changing boundaries. Objects in satellite images do not have sharp edges and this gives problem to regular edge detection techniques so in order to get a better result in this study, the new edge detection algorithm which is written in MATLAB was used.

e-Cognition Developer 8.1 was used to define the land objects. The first step was to merge the edge detection result with the original image and then apply the multi resolution segmentation with a scale to define the objects boundary. After applying the above steps Rule Based Algorithms are written in e-Cognition which is based on the Feature Selection. The five classes of Forest, River, Roads, Agriculture Fields and Buildings have the following results.

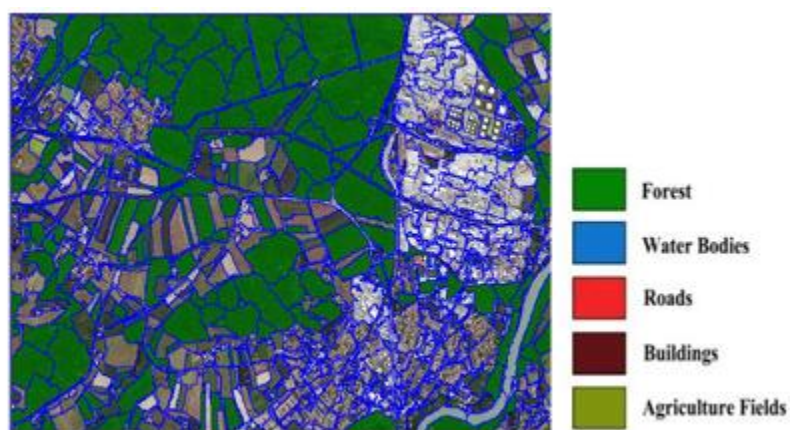


Figure 3.15a: Forest extraction - Object with Brightness<60, Assign Class=Forest

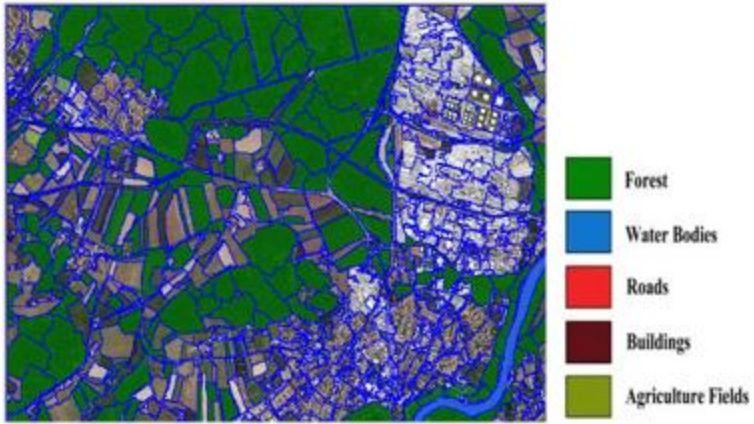


Figure 3.15b: River extraction - (a) Object with Brightness value- $132 < \text{Brightness} < 138$ Assign Class=River (b). River object with Standard Deviation (S.D) > 30 Marked Unclassified

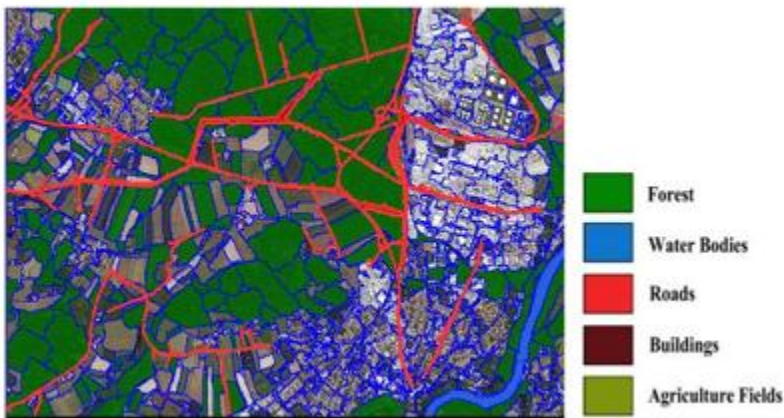


Figure 3.15c: Road extraction - (a) Object with Elliptical Fit < 0.1 Assign Class=Roads, (b). Merge Road Object and Road with area < 11000 Pixel Marked as Unclassified

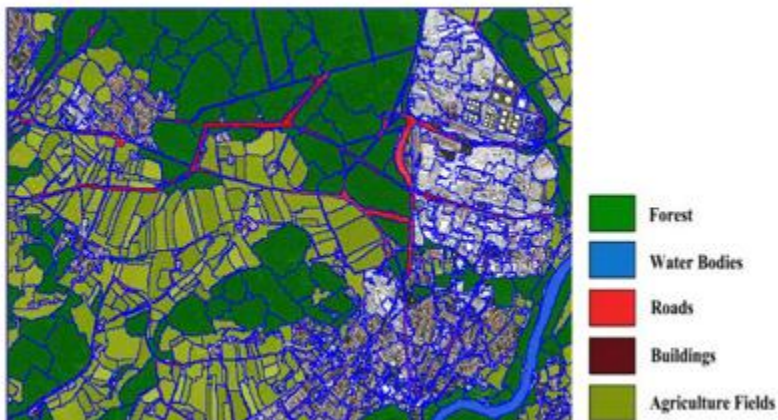


Figure 3.16d: Agricultural field extraction - (a). Unclassified Object with Brightness < 175 and S.D. < 30 Assign Class=Agriculture Fields, (b). Forest Object with Asymmetry > 0.89 Assign Class=Agriculture Fields

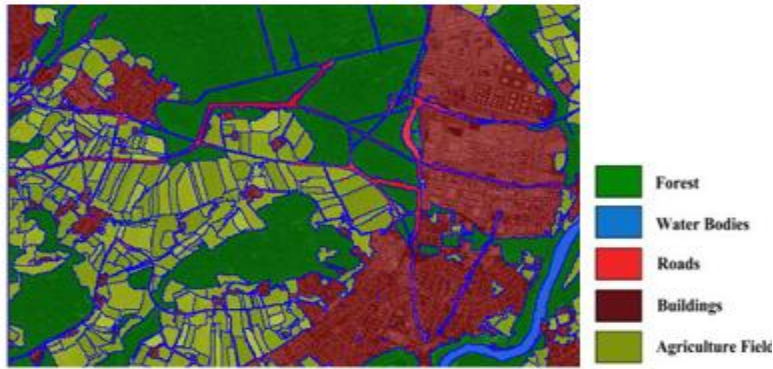


Figure 3.15e: Building extraction – (a) Feature Selection Assign Class=Buildings, (b). Merge Object assigned as Buildings and Forest. Source Fig 23a-23e: Singh, (2015)

The accuracy assessment was done with the error matrix and Overall Classification Accuracy of 94% and Kappa coefficient of 0.919 were realized.

Ronczyk, (2012): Object-based Classification of Urban Land Cover Extraction Using High Spatial Resolution Imagery

Object-based Classification of Urban Land Cover Extraction using High Spatial Resolution Imagery was carried out in Székesfehérvár, a city situated in central Hungary and one of the largest settlements in Transdanubia. The city and its surroundings were the most dynamically growing regions of Hungary in the 1990's.

The study used the following remote sensing data:

- WorldView2 satellite image (2011)
- Airborne photographs (2008, 2009)
- LIDAR data (2008)

Table3.6:Data details (WorldView2, Airborne photographs and LIDAR datasets),

Datasets	Spectral resolution	Other specification
<i>WorldView2 2011</i>	Multispectra (400-1040 nm) band 1 (coastal blue), band 2 (blue), band 3 (green), band 4 (yellow), band 5 (red), band 6 (red edge), band 7 (NIR 1), band 8 (NIR 2). Panchromatic	Spatial Resolution: PAN – 0,5 m MS – 2 m Quantization Level: 11 Bits
<i>Aiborne photographs 2008</i>	visible/infrared	Spatial Resolution: 0,5 m
<i>LIDAR 2008, Toposys</i>		LIDAR point cloud FE/LE Absolute accuracy: horizontal < ±0.50 m; height < ±0.15 m

Source: Ronczyk, (2012)

Other datasets used in addition are other data sources used for investigation: Field reference data (GPS), Vector data from Cadastre maps, Attribute data gained from the municipalities and other statistical data.

The main objective of this study was to develop a methodology to generate land cover classes of urban area from high spatial resolution satellite images through object-based classification. eCognition software was used not only the spectral information but also the shape, compactness and other parameters can be employed to extract objects. To extract buildings a combination of spectral (WorldView2) and LIDAR data contains elevation information were applied an object-oriented approach, which allowed context consideration during the classification process was used.

For the classification in this study only the two generalized first and second levels were used. The rule set (algorithm) was developed to identify land covers of urban area using the 2 m spatial resolution WorldView2 image. The process considered spectral value and spatial characteristics of objects and it is included the following steps:

i. Segmentation

- ii. Feature extraction
- iii. Object classification
- iv. Refinement of classification based on spectral value and spatial characteristics of objects
- v. Final identification of categories
- vi. Accuracy assessment

The algorithm spectral difference was used to refine existing segmentation results by merging spectrally similar image objects. The diagram 3.16 below is the segmentation scheme.

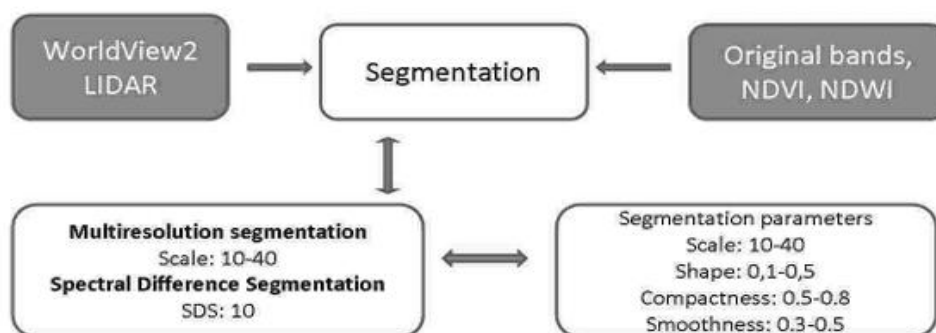


Figure 3.16: Segmentation scheme. Source: Ronczyk, (2012)

The following list of features was used during the classification process:

Table 3.7: List of features used

Class	Main features	The feature are used to clean up the classification
Vegetation (trees, brushy, grass, barren)	NDVI (Band8 – Band5)/(Band8 + Band5)	context: rel. Border to trees
Building	Height information	Spectral features, NDVI, context (Rel. Border to buliding), size information
Other man-made (road, other)	Spectral information (NDWI, NDVI)	size: area, length to width ratio
Parking place (big area)	Spectral information (NDVI, NDWI)	Shape: rectangular fit, shape index; size: area, length to width ratio, context: rel. Border to parking place)
Water*	Spectral information (NDWI)	
Shadows*	Spectral information (NDWI) (Band8 – Band1)/(Band8 + Band1)	

Source: Ronczyk, (2012)

The classification of urban areas was done in two levels. In the first one the main categories of land cover were determined by taking advantage of spectral properties of WorldView2 image. In the second level during the building extraction the elevation data was used as the most relevant characteristic of buildings. Additionally the spectral and context features were employed to clarify the classification (see table)

In the result, the outcome of our research confirms the original assumption that additional data like LIDAR can effectively improve the classification result of VHR data.

Table 3.8:Result of classification.

Class	WorldView2 and LIDAR based-classification area (m ²)	WorldView2 based classification area (m ²)
Building	107031	109077
Parking place	26116	23793
Road	65411	34191
Other man-made	55360	49477
Trees and bushy	61372	74438
Grass	35309	58976

Source: Ronczyk, (2012)

The accuracy assessment shows that over all accuracy for worldview2 based classification and worldview2 and LiDAR based classification were 71% and 82% respectively. Urban ecosystem presents a wide structural diversity and consequently spectral variability therefore the process of classification needs not only spectral information but other information like context or geometry as well.

Rampi, (2014): Wetland Mapping in the Upper Midwest United States: An Object Based Approach Integrating LiDAR and Imagery Data.

This study investigated the effectiveness of using high resolution data to map wetlands in three ecoregions in Minnesota. Two data sources were used to investigate the effectiveness of integrating multiple datasets to map wetlands in the three study areas. These sources included LiDAR data and orthorectified digital aerial photography (0.5 m). The half-meter orthorectified imagery used for Swan Lake and the Minnesota River while was collected in 2011 while another half meter orthorectified imagery collected in 2009 was used for the Thompson Reservoir St. Louis River watershed.

The wetlands were mapped by using an OBIA approach through the creation of rule sets for each study area. The software package Definiens eCognition Developer version 8.8.0 was used to develop the three rule sets. The first subsection of the methods used in this study describes the data preparation performed for each study area. The next subsection explains the design of the rule set created for each study area. Finally, the last subsection addresses the accuracy assessment procedures used to evaluate results in each study area. Before the creation of the three rule set, four data preparation we performed. For the LiDAR, the following raster layers were created: a digital surface model (DSM), a LiDAR intensity layer, the compound topographic index (CTI). These raster layers were chosen because of their topographic information, which is useful to differentiate wetland from other cover classes and were done for each study area.

Second, after calculating all the LiDAR layers, they used the MosaicPro tool from the ERDAS Image 2011 software to mosaic the orthorectified aerial imagery for each study

area. Third, once all the previous LiDAR and imagery layers were prepared, they used a watershed boundary shapefile layer for each study area to subset all the raster layers in ERDAS Image version 2011. Finally, the researcher produced a tile generation for each study area. The tile generation was carried out in ERDAS Image version 2011, using the Dice tool with the following parameters: tile size of 3,000 m × 3,000 m and an overlap of 300m between adjacent tiles on all four sides. Each study area had a tile stack of four LiDAR product layers (DEM, DSM, CTI, and Intensity) and four bands of imagery layers.

Each rule set consisted of four main components: (a) image processing, (b) segmentation and classification, (c) export operation, and (d) cleanup operation. In the image processing stage, nDSM was calculated as well as the computation of the Green Ratio Vegetation Index (GRVI) using the eCognition developer software tools for object features. In the segmentation and classification phase, preliminary objects were created using multi resolution segmentation algorithm. The following parameter values were created: scale 30, shape 0.3, and compactness 0.5. A weight value of 1 was given to the three visible optical bands and a weight value of 2 to the NIR band. The NIR band was given a higher weight value because of its ability to spectrally separate potential non-water objects from water objects. The second step was to refine those objects by applying a spectral difference segmentation algorithm, based on a maximum spectral difference value. The third step was to classify the preliminary objects into temporary classes, including wet versus dry, bright versus dark, and short versus tall. We used the following attributes of each dataset to create the temporary classes: min, max, and mean

threshold values of the CTI, nDSM, intensity, NIR band, imagery brightness, and GRVI. The following threshold values: $\text{NIR} \leq 45$, $\text{GRVI} \leq 0.9$, and $\text{CTI} \geq 10.78$ were used. These threshold parameters were determined through a series of trial-and error efforts in combination with photo-interpretation to determine whether different “wet classes” (potential wetland classes) across the three different ecoregions were sufficiently separated from dry classes (potential non-wetland classes).

The imagery brightness, intensity, and GRVI layer were used to classify bright versus dark objects using the spectral difference segmentation algorithm with a maximum spectral difference parameter of 12. The nDSM layer was used to separate short versus tall objects using the contrast split segmentation algorithm with the following parameters: a minimum threshold value of 2, a max threshold value of 5, and a step size of 1. Finally, they used contextual information from the different temporary classes to achieve the final desired classes and they included wetlands, agriculture, forest, and urban classes. The following accuracy assessment estimators were computed in ERDAS Imagine for each study area: overall accuracies, producer’s accuracy, user’s accuracy, and kappa coefficient.

Overall accuracy results for the OBIA classification were consistently high (90 to 93 percent), throughout the three study areas as can be seen in the following tables.

Table3.9a: OBIA classification error matrix for Minnesota river-headwater study area.

		Reference Data					
		Wetlands	Agriculture	Forest	Urban	Row Total	User's Accuracy
Map data	Wetlands	47	4	0	0	51	92%
	Agriculture	2	148	1	5	156	95%
	Forest	1	10	31	0	42	74%
	Urban	1	5	0	34	40	85%
	Column Total	51	167	32	39	289	Overall Accuracy
	Producer's Accuracy	92%	89%	97%	87%		90 %

Overall Kappa Statistic: 0.84

Source: Rampi, (2014)

Table 3.9b: OBIA classification error matrix for swan lake study area.

		Reference Data					
		Wetlands	Agriculture	Forest	Urban	Row Total	User's Accuracy
Map data	Wetlands	27	1	0	0	28	96%
	Agriculture	1	46	0	0	47	98%
	Forest	0	0	23	0	23	100%
	Urban	0	5	1	14	20	70%
	Column Total	28	52	24	14	118	Overall Accuracy
	Producer's Accuracy	96%	88%	96%	100%		93%

Overall Kappa Statistic: 0.90

Source: Rampi, (2014)

Table 3.9c:OBIA classification error matrix for Thompson reservoir St. Louis River study area.

		Reference Data					
		Wet-lands	Agriculture	Forest	Urban	Row Total	User's Accuracy
Map data	Wetlands	32	0	2	0	34	94
	Agriculture	1	20	3	0	24	83
	Forest	2	0	37	0	39	95
	Urban	0	2	1	17	20	85
	Column Total	35	22	43	17	117	Overall Accuracy
	Producer's Accuracy	91%	92%	86%	100%		91%

Overall Kappa Statistic: 0.87

Source: Rampi, (2014)

For Minnesota River-Headwater study area using the OBIA method the overall accuracy was 90 percent, with a kappa score of 0.84 and low errors of commission and omission.

For the Swan Lake study area the overall accuracy was 93 percent with a kappa score of 0.90, and with low errors of commission and omissions for the majority of the classes. For the Thompson Reservoir St. Louis River study area the overall accuracy was 91 percent with a kappa value of 0.87, and with low errors of commission and omissions for all the classes.

The results of this study reinforced previous findings regarding the value and importance of high resolution data to improve wetland classification accuracy. Previous studies have concluded that high resolution data including LiDAR, aerial, and satellite imagery are very advantageous to distinguish between wetlands and non-wetlands classes. This study demonstrated that an OBIA approach is more suitable than traditional pixel-based methods to take advantage of the high resolution data available to map wetlands (Dechka et al., 2002; Halabisky et al., 2011; Knight et al., 2013; Maxa and Bolstad, 2009). The OBIA approach used in this study incorporated contextual, spectral, and shape information that came from homogenous objects instead of pixel units.

Gilani, et al (2015): Fusion of Lidar Data and Multispectral Imagery for Effective Building Detection Based on Graph and Connected Component Analysis

The study is in Australia and the dataset covers two urban areas in Queensland, Australia: Aitkenvale (AV) and Hervey Bay (HB). The AV data set has a point density of 29 points/m² and comprises of a scene that covers an area of 214m x 159m. This scene contains 63 buildings, out of those four are between 4 to 5 m² and ten are between 5 to 10 m² in area. The HB data set has one scene and covers 108m x 104 m and contains 25 buildings.

The research present a graph based algorithm, which combines multispectral imagery and airborne LiDAR information to completely delineate the building boundaries in urban and densely vegetated area.

The methodology is described in six different steps as can be seen from the workflow below. The first step is a data preprocessing phase where they separate LiDAR points cloud, generate DEM, compute image entropy, NDVI and extract image line segments. The proposed method first divides the input LiDAR data into ground and non-ground points.

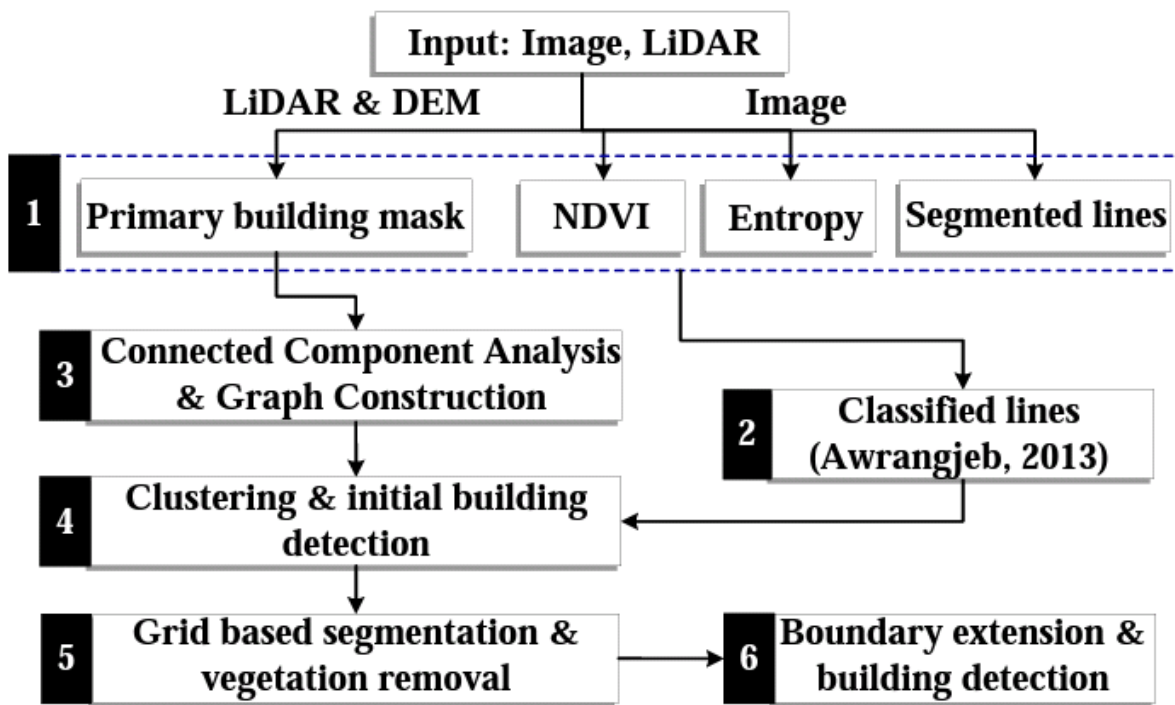


Figure 3.17: Work flow of proposed building detection technique. Source: Gilani, (2015)

The extracted image lines are classified into several classes e.g. ground, ridge, and edge. The line segments that belong to ‘edge‘ and ‘ridge‘ classes are of interest because these lines are either close or fall within the area of elevated objects. The second phase begins with the process of Connected Component Analysis (CCA) where the number of objects

present in the test scene is identified followed by initial boundary detection and labelling. Additionally, a graph from the connected components is generated, where each black pixel corresponds to a node. An edge of a unit distance is defined between a black pixel and a neighbouring black pixel, if any. An edge does not exist from a black pixel to a neighbouring white pixel, if any. This phenomenon produces a disconnected components graph, where each component represents a prospective building or dense vegetation (a contiguous block of black pixels from the primary mask). In the third phase, a clustering process clusters the segmented lines, extracted from multispectral imagery, around the graph components, if possible. In the fourth step, NDVI, image entropy, and LiDAR data are utilised to discriminate between vegetation, buildings, and isolated building's occluded parts. Finally, the initially extracted building boundary is extended pixel-wise using NDVI, entropy, and LiDAR data to completely delineate the building and to maximise the boundary reach towards building edges.

The proposed technique is evaluated using two Australian data sets: Aitkenvale and Hervey Bay, for object-based and pixel-based completeness, correctness, and quality. The automatic extraction of accurate building boundaries is important geo-spatial information that is indispensable for several applications. The most challenging factor confronted in boundary delineation is building shape variability and surrounding environment complexity. In order to deal with various building types, this research presents a new method for automatic building detection through an effective integration of LiDAR data and multispectral imagery. The technique used here detected buildings larger than 50m^2 and 10m^2 in the Aitkenvale site with 100% and 91% accuracy,

respectively, while in the Hervey Bay site it performs better with 100% for buildings larger than 10m² in area.

3.2.2 Application of VHR and LiDAR in Building Extraction

Lee (2015): Object-oriented Classification of Urban Areas Using Lidar and Aerial Images

In this paper, object-based classification of urban areas is used based on a combination of information from LiDAR and aerial images. The study area is Ocean City, located in the northern part of the coastal area of Maryland, U.S. This varied terrain is suitable for classification combining LiDAR and aerial imagery.

The dataset consists of stereo images and LiDAR data. An RC20 camera was used to acquire panchromatic aerial images; the camera model is UA9II 3043 and its calibrated focal length is 152.74 mm. The Airborne Topographic Mapper (ATM) laser system was used to acquire digital elevation data. The vertical accuracy of better than 10cm has been achieved.

The proposed method is based on integrating information from LiDAR and aerial images for object-oriented classification of urban areas. MATLAB was used for local maxima filtering and for the conversion from point data to images. ERDAS IMAGINE was used for the coordinate transformation and multiresolution segmentation to implement object-oriented classification. The method follows five major steps. First, LiDAR points on the building are extracted using the local maxima filter. Second, the building segmentation data from the LiDAR points are converted into images. Third, the

coordinate systems are unified. Fourth, multi-resolution segmentation and classification are implemented. The final step is accuracy assessment.

To provide information on the building location, LiDAR points on the building should be extracted from original LiDAR data. The local maxima filter extracts points over a threshold given by a minimum height plus a threshold value. In this paper, the threshold value was 6m, which is roughly equivalent to a two-story building or house. The size of the filter was 30m by 30m, since this exceeds the largest building and is an appropriate size for detecting only points on the building.

Figure shows the classification of an aerial image and building segmentation data from LiDAR in the residential area.

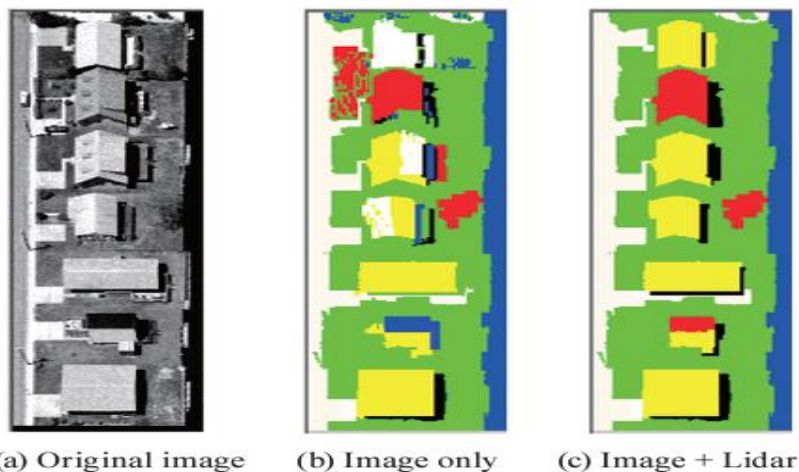


Figure3.18: Classification of an aerial image and building segmentation data from lidar in the residential area. Source: Won Hee (2015)

The overall accuracies reach 96.37% and 97.54% in the commercial and residential areas, respectively. The overall accuracies of the pixel based classification using only aerial imagery are 76.47% and 71.15% in the commercial and residential areas, respectively. Overall accuracy has been improved by combining aerial image with

LiDAR. LiDAR data provides supplementary data to the aerial image for the information about building areas. LiDAR offers accurate position and height information, but includes less information on the features' geometrical shapes. Thus, the extraction of building points was used to provide supplementary data on the features' geometrical shapes in this study.

Tee, (2004):Object-Based Building Detection from Lidar Data and High Resolution Satellite Imagery

This a study carried out for building detection using OBIA to classify LiDAR data and HR image. It was carried out in an area in Hsin-Chu Science-based Industrial Park of north Taiwan. LIDAR data acquired by Leica ALS 40 and QuickBird satellite images. The ground resolutions of QuickBird panchromatic and multispectral satellite image are 0.7m and 2.8m, respectively.

This work is composed of two major parts and these are Segmentation and Classification. The first step in the methodology was the data preprocessing which was carried out in two steps, which are interpolation of LIDAR data and space registration. The triangulated irregular network (TIN) approach was applied to rasterize the LiDAR data to DSM and DTM both with a pixel size of 0.5m. Space registration was done to establish the spatial relationship between the LIDAR data and the satellite images. Ground control points were used to reconstruct the mathematical model for space registration. This made the two data to be co-registered in the same georeferenced system.

For the building detection is to extract the building regions, two steps were employed – the region based segmentation and the object based classification as can be seen in the flowchart below.

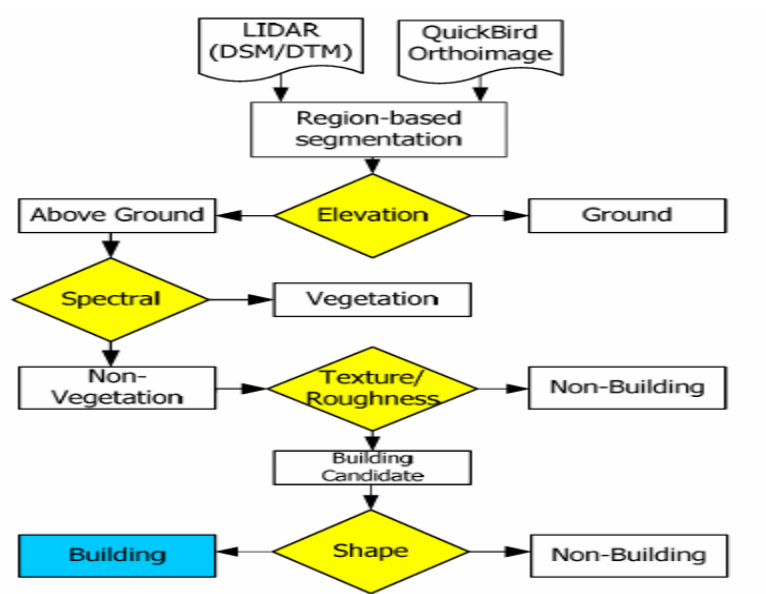


Figure 3.19: Flowchart of building detection. Source: Tee, (2004)

After the segmentation, the next step was object based classification. At this level, all regions separated during segmentation were candidates for classification. An object-based classification considering the characteristics of elevation, spectral, texture, roughness, and shape information is performed to detect the building regions.

i. The elevation was achieved by subtracting the DTM from the DSM to get nDSM (Normalised DSM) which describes the height information above ground. This enabled the researcher to set elevation threshold to separate objects (like trees and buildings) above ground from the ground.

ii. Spectral information comes from the multispectral data which includes blue, green, red, and near infrared bands. The NIR is useful in separating vegetation from non-vegetation using NDVI.

iii. Texture was used to separate the building and vegetation where the objects have similar spectral response. The Grey Level Co-occurrence Matrix (GLCM) for texture analysis. GLCM is a matrix of relative frequencies for pixel values occur in neighboring processing windows. The researcher selected the entropy and homogeneity to compute the co-occurrence probability.

iv. Roughness of the LiDAR was also used to classify the vegetation regions and non-vegetation ones because the surface roughness is similar to the texture information of spectral data (Mass, 1999).

v. Shape attribute includes size and length-to-width ratio so an area attribute was used to filter out those small objects.

The result showed that general land cover classification was 92% and when only building detection was considered, the accuracy result was 89%. The undetected buildings were small ones and that is because they are low and therefore have less texture information. The study recommended that further investigation of small buildings detection is needed.

Uzar, (2013):Automatic Building Extraction Using Lidar and Aerial Photographs

This is a study that presents an automatic building extraction approach using LiDAR data and aerial photographs from a multi-sensor system. It is a suburban neighborhood

located in the northwest of the city of San Bernardino, California, United States of America. The study area was chosen because the data set was collected simultaneously with the multi-sensor system onboard the same airplane and contained different types of land cover within a small area,

The input information consists of a DSM, an intensity image and a color infrared orthoimage of the study area generated with the data set obtained from LiDAR, GPS/IMU and a digital camera on the same platform. The NDVI, Slope and Hough images were used in the segmentation and classification steps. A gridded DSM with a 0.2-m-resolution intensity image with a ground sampling distance (GSD) of 0.2m and an orthoimage with a GSD of 0.2m was produced using the data set from the multi-sensor system. Table below shows a summary of the dataset.

Table 3.10: Dataset details

Sensor	System	Date of data collection	Specification
LiDAR	Optech ALTM 3100 LiDAR	25.May.2005	Point cloud (5 point/m ²) and intensity data
GPS/IMU	Novatel GPS and LN200 IMU	25.May.2005	Position and attitude information (200 Hz)
Digital Camera	Redlake MS 4100	25.May.2005	Color infrared image (0.2 m GSD)

Source: Uzar, (2013)

The object-oriented image analysis method used in this research has two major steps: segmentation and classification. The determined object primitives (such as spectral characteristics, scale parameter, shape, completeness, brightness, contrast difference and statistical parameters) in the segmentation were constantly altered in the analysis and classification steps until they became the target object class.

The segmentation, analysis and classification steps of the proposed object-oriented image analysis method included subsequent steps allowing the refinement or improvement of the segmentation locally for a specific class, such as building, ground or vegetation. The flow diagram below shows the segmentation being alternated iteratively between local segmentation modifications on the one hand and local object analysis and classification on the other hand. The rule-based classification was carried out because it offers the possibility to automate the entire classification process with decision rules based on determined object primitives combined with fuzzy logic operators at different levels of analysis. The entire object-oriented image analysis for automatic building extraction was performed in Definiens eCognition Developer 8.64 with defined rule sets.

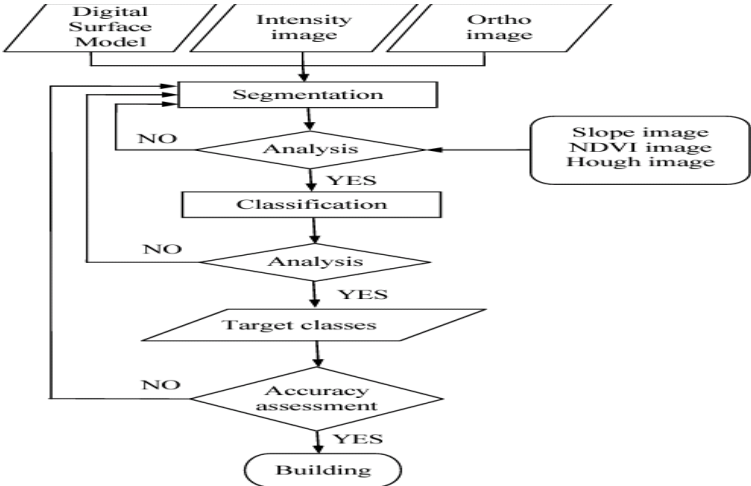


Figure 3.20: Flowchart for Methodology. Source: Uzar, (2013)

For the generation of classes, a hierarchical classification method was developed for the proposed automatic building extraction. Instead of focusing on building extraction at an early stage of the classification steps, a classification of the data in the following vegetation, ground and building classes was first performed. Building regions were then

derived from the classification results. Figure 3.21 is the hierarchical classification scheme.

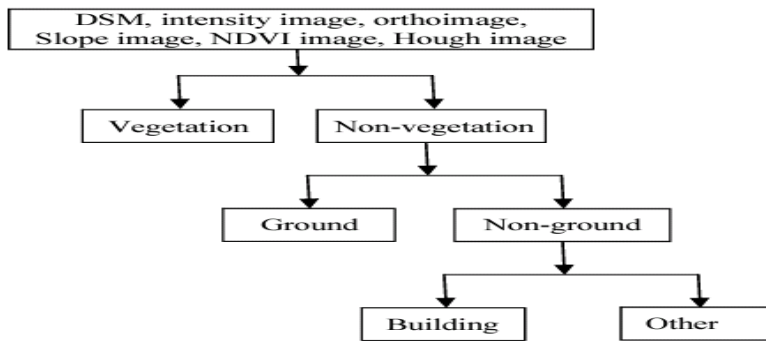


Figure 3.21: The hierarchical classification scheme, Uzar, (2013)

NDVI was used to differentiate vegetation with set out threshold, while the ground and non-ground classes were differentiated using the DSM of the study area, which contained the height information of the buildings and other objects elevated from the bare ground. The building extraction had five major steps:

- i. nDSM was created to exclude the influence of topography using the difference between the DSM of the non-ground class and the average point heights in the ground class.
- ii. Second, objects in the nDSM with heights above 1 m were classified as initial building 1
- iii. Third, the multi-resolution segmentation was performed using the initial building 1 class, the orthoimage and the generated Hough image. The parameters of scale, shape, compactness, smoothness and color were taken into consideration in multi-resolution segmentation.

iv. Fourth, the contrast split segmentation was utilized using the intensity image generated from the LiDAR data, and the initial building 3 class was generated as a result of the classification with the determined building intensity threshold.

v. Finally, the building class was acquired after morphological operations (opening and closing), and the non-building class was renamed as the other class.

The two performance accuracy methods used produced the following results: Error Matrix had an overall accuracy of 93% and Kappa values of 88% were obtained as a result of the performance evaluation. The second method was the completeness and correctness analyses of the automatic extracted buildings, which showed 95.02% completeness and 96.73% correctness.

Ramesh, (2009): High Resolution Satellite Images and Lidar Data for Small-Area Building Extraction and Population Estimation

This is a 2009 Master's thesis using high resolution satellite images and LiDAR data for small-area building extraction and population estimation. The study area is located in the eastern part of the city of Denton, Texas.

The IKONOS image data for this study was acquired on January 3rd 2000, including a 1-m resolution panchromatic band and four 4-m resolution multispectral bands. LiDAR data used for this study was acquired on September 4th, 2001. LiDAR Data was collected during leaf-on season and was post-processed to a point spacing of 3-5 meters. LiDAR data were used to create a DEM and a Digital Surface Model (DSM), which

allows for creation of a Normalized Digital Surface Model (nDSM) by subtracting DEM from DSM.

The six major steps involved in the process of estimating population are:

- (1) Preprocessing LiDAR data
- (2) Preprocessing IKONOS data
- (3) Object-based classification and extraction of residential buildings
- (4) Deriving population indicators, volume of the buildings, area of the buildings and the building count
- (5) Regression modeling and
- (6) Accuracy assessment

This can be seen in the methodology flowchart below.

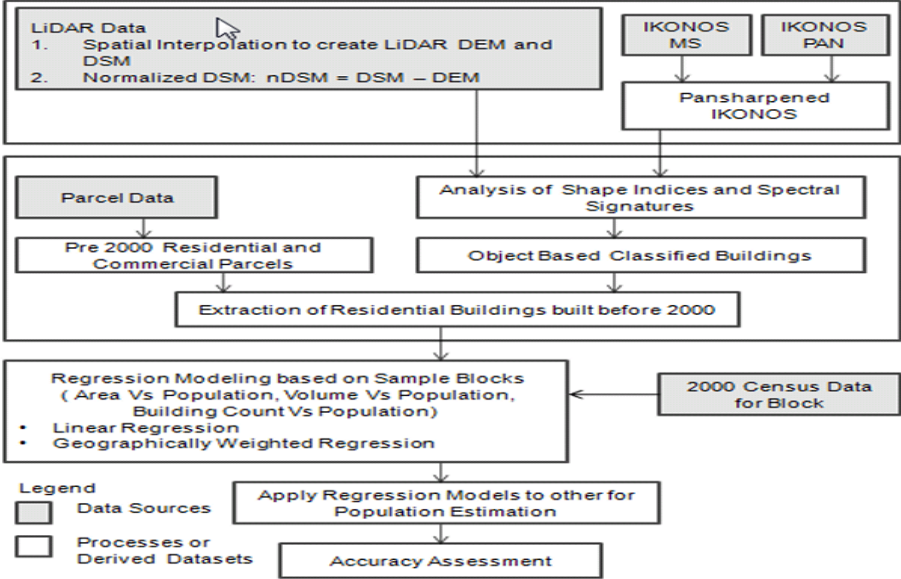


Figure3.22: Flowchart of Methodology. Source: Ramesh, (2009)

The pre-processing of the LiDAR data involved the generation of the DEM and the DSM from the acquired bare earth and reflected LiDAR points. The 29 tiles of LiDAR DEMs and DSMs covering the study area are imported to ArcGIS and a point shape file is created. Inverse Distance Weight (IDW) is used to interpolate the point shape file to create raster and all 29 individual tile raster are mosaicked to create respective DEM and DSM raster.

The acquired IKONOS multispectral data has 4- meter spatial resolution while the panchromatic image is a single band image with 1 meter spatial resolution. As a preliminary processing, IKONOS MS image is pan sharpened using IHS fusion technique using ESRI's ArcGIS software tool to produce MS image that has the resolution of PAN image.

eCognition software was employed in this study to classify high resolution multispectral data, IKONOS with LiDAR elevation data as an ancillary input. This research work aims at attaining higher classification accuracy thereby increasing the accuracy of population estimation model. Two classes, buildings and non-Buildings were identified using various shape indices mentioned below and general spectral characteristics.

Using multi-resolution segmentation, the image is divided into meaningful objects. Each object is then studied for its spectral and shape characteristics to distinguish between the two major classes - buildings and non-Buildings. Trees and other grasslands are removed by using its high vegetative index. Barren lands and other short shrubs are removed from its very low height property. Various shape indices are used to distinguish between building and non-building features. Building objects have certain unique characteristics which help us define such indicator parameters. The image objects for

residential buildings are extracted and exported to a vector shapefile. Using ESRI's ArcGIS software, 30 different building shapefiles obtained from eCognition are merged to a single polygon file that has the residential building information for the entire study area.

In this study, the whole study area is divided into 30 tiles to process the data faster and also to define more specific shape indices. As the study area has mixed topography from low to high density residences and vast farmlands, specifying local height thresholds and shape index thresholds enables to extract buildings more accurately.

Alhaddad, (2008): Satellite Imagery and Lidar Data for Efficiently Describing Structures and Densities in Residential Urban Land Uses Classification

This paper examines the utility of high-resolution remote sensing image and airborne laser altimetry data for mapping residential land uses within the spatial limits of Barcelona City Council (Spain). The chosen area is Barcelona, which is the regional capital of Catalonia, lying in the north-east of Spain. This study will examine in a simple way the relation between building site coverage ratio (BCR) and floor area ratio (FAR) to estimate building density of a city from two aspects, the buildings stretching on the surface and growing along the third dimension.

Two Remote sensing data sets were used for the study. One is subset of an SPOT5 scene, recorded on 2004. It is a fusion product of the four multispectral bands (10m spatial resolution) and the panchromatic band (2.5m spatial resolution), resulting in four multispectral bands with 2.5m spatial resolution. The multispectral bands cover blue, green, red and part of the near infrared of the electromagnetic spectrum. The second data

set is from an airborne laser scanner (ALS), acquired on 23rd July 2002, at flying height above ground of 1325m and average point density of 1 point/m². Two models were extracted from this – the first is digital surface model (nDSM), containing height information above ground and the other is a different model between first and last pulses (Δ HFL), which has a height of zero for sealed areas and height similar to that of the nDSM in green areas, thus aiding the identification of trees (Kressler, Steinnocher, 2006).

In the methodology, pixel-based approach as implemented in ENVI 4.2 was used for the classification of the satellite image. This was used to identify standing areas of buildings. The next was to use airborne laser scanner (ALS) to calculate the building heights. The results of the classification were eleven classes mapping the urban morphology – Residential, Industrial, Streets, Forest, Green Open, Irrigated fields, Dry Lands, Shallow water, Deep water and Shadow.

Here LiDAR provides the opportunity to identify land use types such as roads and buildings with high degree of accuracy. The nDSM information greatly improves the differentiation between roads and buildings. A correlation of LiDAR with corresponding building height is used to assess building height classes. Nine different height classes (1-3, 3-6... 15 and more floors) were derived.

Both the BCR and the FAR results in a local distribution of building density are shown in Figures 8 and 9. Diagram 1 presents the statistical results of the FAR and BCR based on the entire grid of all the cells in the selected study area. The results also indicate that the variation of BCR is more than that of FAR. The Diagram shows that 90% of all cells have FAR value less than 0.0062 ($H < 50$ m), while more than 76% of the cells are

between 0.6 and 1 (F between 60m2 and 100m2) for BCR. New development within existing and already developed urban areas of a city generally has a higher BCR and lower FAR.

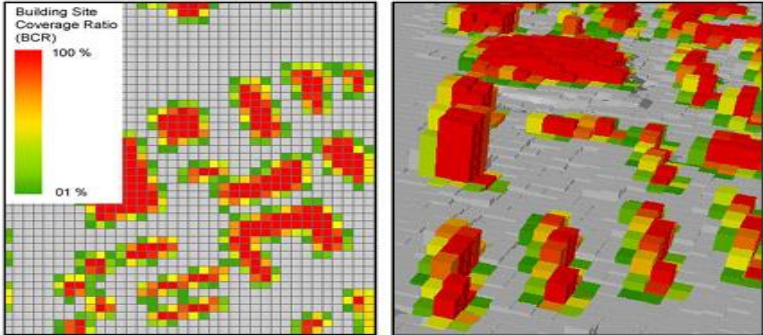


Figure3.23a: 3D simulation illustrates the frequency distributions for BCR for all cells grid inside the sample area. Source: Alhaddad, (2008)

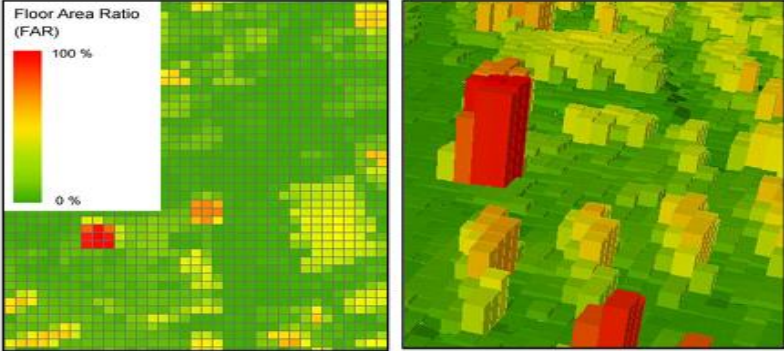


Figure3.23b: 3D simulation illustrates the frequency distributions for FAR for all cells grid inside the sample area. Source: Alhaddad, (2008)

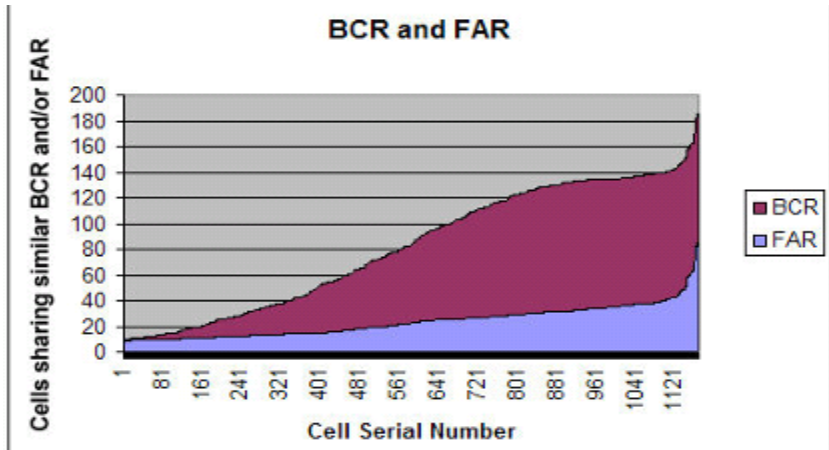


Figure 3.24: Cells gave unique serial number; the diagram presents BCR and FAR relation based on entire cells. Source: Alhaddad, (2008)

In conclusion, the use of LiDAR and pansharpened SPOT data sets allows an easy separation of the basic land cover types present in the study area. LiDAR data are especially beneficial for the separation of flat sealed areas from buildings, while optical data allows a good separation of vegetation and seal areas, then the integration of the classification results with the information provided by LiDAR to extract the building form to be adopted to obtain the BCR with high accuracy results.

Rahman, (2013): Extraction of Urban Building Heights from Lidar Data: An Integrated Remote Sensing and Gis Approach

In this paper, a combination of IKONOS and LiDAR data is used and processed through integrated remote sensing-GIS based method to extract individual building heights in the urban central part of Norman, Oklahoma. This area was chosen because it contains various types of commercial and residential buildings with variable heights and ages along with diverse features.

For this study, two separate data sets were used. First, a LiDAR data was obtained freely from the City of Norman's GIS Department. Using the dataset, a digital surface model (DSM) representing elevations of trees, buildings, and other surface features was created in ArcGIS v. 9.3 by using the inverse distance weight (IDW) interpolation technique with grid cell size of 0.3 m on the first return points received by the LiDAR sensor. Along with the LiDAR data, Norman's GIS Department also provided a digital elevation model (DEM). By calculating the differences between the DEM and DSM, a normalized digital surface model (nDSM) showing the heights of buildings and other features were

also created. Secondly, a high resolution IKONOS image provided by the GeoEye foundation was also used in the study. Table 3.11 below is the characteristics of the data.

Table3.11: Characteristics of the dataSource: Rahman, (2013)

LiDAR Data	IKONOS Imagery
Sensor: Leica Geosystems ALS50	Spectral Resolution: R, G, B, and NIR
Density: ~1 meter	Spatial Resolution: 1.0 m
Acquisition Date: February 27 th – March 3 rd , 2007	Acquisition Date: August 28, 2008

Source: Rahman, (2013)

Using the IKONOS image and the SPEAR Vegetation Delineation tool of ENVI v. 4.8 image processing software, the pixels containing trees and vegetation were first detected and separated. This was done to be able to extract the trees and their heights. The SPEAR Vegetation tool uses normalised difference vegetation index (NDVI) to find pixels containing trees and vegetation. Pixels containing healthy vegetation will result in high NDVI values closer to 1 while not healthy vegetation will yield lower NDVI values. Negative NDVI values will indicate no vegetation. In this study, pixels with NDVI values exceeding 0.249 were considered to contain trees and vegetation. These same areas/pixels in the nDSM data containing the vegetation were then subtracted from the nDSM resulting in the nDSM having only residential and commercial facilities.

The nDSM was then exported into an ArcGIS v. 9.3 shapefile containing polygon outlines of the buildings. Field survey showed that many buildings were more than 2m high and because many polygons which were not vegetation, residential or commercial buildings were created in the analysis, they needed to be separated and excluded from the analysis. The zonal statistics function of ArcGIS (to calculate the minimum and maximum heights of the polygons from the nDSM) was used and polygons with

maximum heights below 2m were eliminated. The areas of each polygon were also calculated and any polygon with an area below 21m² was eliminated from the analysis as well. This final step resulted in polygon outlines corresponding to individual houses and buildings along with their minimum, maximum, and average heights from the nDSM data set.

The accuracy of this methodology was assessed with a random sample of 100 buildings. Their heights were measured through field survey and compared with the results from the LiDAR data in order to assess the accuracy of heights obtained by the LiDAR data. A GIS shapefile created in 2012 with the building outlines were used as reference and they were compared with the outlines generated by the proposed building extraction method. The quality assessment result revealed that 75.32% of the buildings were detected and the areas of 68% of them were determined accurately. This moderate result can be attributed to the branches of trees surrounding the buildings and houses. The study area contains wide variety of urban trees and vegetation with different shapes and sizes. To overcome this issue and improve the detection of individual buildings in building blocks, this study recommends that future studies should be carried out using LiDAR data along with high resolution satellite imagery collected over the area during winter leaf-off condition.

Demir, (2012): Extraction of Buildings and Trees Using Images and Lidar Data

This work focuses on the 3D building roof modeling and the test site is in Vaihingen, Germany. The dataset include DMC digital images with NIR, R, G, B channels and raw LiDAR point cloud. DMC images have 8 cm GSD. LiDAR points have a density of

5pts/m². After generation of the DTM and subtracting it from the DSM, we get the normalized DSM (nDSM). Using the nDSM and a threshold of 1.5m, we get the above-ground objects.

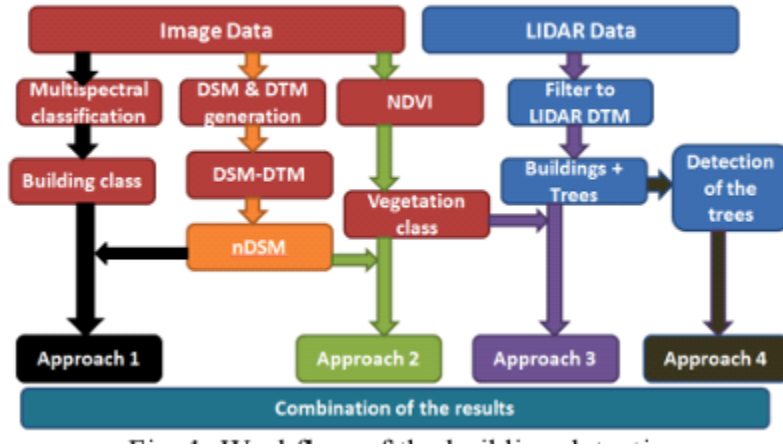


Figure 3.25: Flowchart of the building detection. Source: Demir, (2012)

In the first approach which is multispectral classification, a pixel-based supervised classification is used to detect buildings. The available channels are NIR (Near InfraRed), R (red), G (green), B (blue). The used classes are buildings, bare ground, roads, shadows, grass and trees. Principal components (PC), NDVI and saturation are added channels. NIR, R, PC1 (1st PC), NDVI, saturation are selected using divergence analysis to do a maximum likelihood classification using ERDAS software. Using the height information from the nDSM, the mixed building and ground class could be separated. There is a 94% correct classification in this method.

The second one uses blobs and NDVI for classification. ISODATA clustering of the NDVI image extracts the vegetation and no vegetation regions. Finally, the intersection of no vegetation regions and blobs extracts the buildings. The correctness of the buildings is calculated as 91%.

The third approach is the filtering of LiDAR point cloud and NDVI for the classification. The LiDAR DTM (non-interpolated) is used to detect the above-ground objects. The LiDAR DTM is derived from the raw LiDAR point cloud by using the SCOP++ LiDAR package. The buildings are voids and the trees have low density (< 2 points / m²) in the LiDAR DTM, thus buildings and trees are estimated. Using the vegetation class from the NDVI classification as a mask, removes trees, while the remaining objects (buildings) are deleted, if their area is smaller than 25m². The correctness of the buildings is 81 %.

The fourth approach detects trees from raw LiDAR point cloud. The detection of the trees is not always convenient when using image data, because roof surfaces may be covered by trees or may contain a green surface. Then, these surfaces are detected as vegetation using any image classification process. Usage of the LiDAR data avoids this kind of problems since the detection is based on the geometry of the objects. In the LiDAR data, the vertical point density is generally much higher at trees than at open terrain or buildings. We start from the above-ground objects, which were detected with the LiDAR data filtering of section in the last method. Then, the RANSAC method (Schnabel et al., 2007) is applied on all above-ground points to find planar surfaces, which belong to the buildings. This method has correctness of 80%. First, dilation is applied on the detected buildings to include most LiDAR points, which belong to buildings and the dilation threshold is set as 2m.

3.2.3 Application of VHR and LiDAR in Roads Extraction

Rahimi, (2015): Automatic Road Extraction Based on Integration of High Resolution Lidar and Aerial Imagery

This paper proposes a new unsupervised fully-automatic road extraction method, based on the integration of the high resolution LiDAR and aerial images of a scene using Principal Component Analysis (PCA). The researcher used images of an area in Zeebrugge, Belgium, which were acquired on March 13th, 2011. They used its high resolution LiDAR and RGB aerial images. The LiDAR image has a spatial resolution of 10 cm, while the aerial image's spatial resolution is 5 cm. Therefore, they down sampled the aerial image to have the same resolution as the LiDAR image.

This method discriminates the existing roads in a scene; and then precisely delineates them. Hough transform is then applied to the integrated information to extract straight lines; which are further used to segment the scene and discriminate the existing roads.

The flow chart below explains the method.

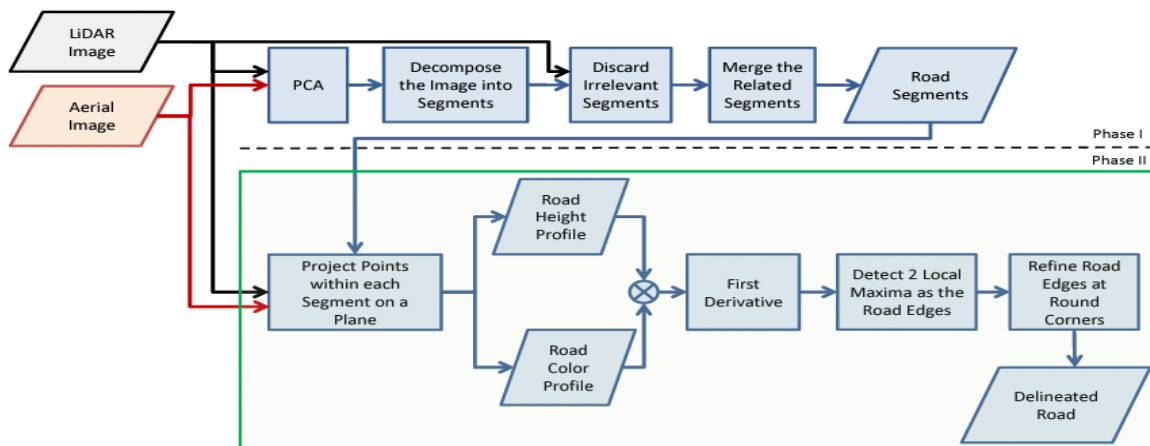


Figure3.26: The method showing the process within the green rectangle is repeated for every road segment. Source: Rahimi, (2015)

As a first step, in order to integrate the height and color information, we use the PCA (Pearson, 1901, Hotelling, 1933) method and convert the 4 information bands (i.e., R, G, B, height) into 4 principal components. Among the resulting components, we select the one which provides the largest distinction between the roads and their neighboring objects. In the next step, a Hough transform (Hough, 1962) is applied to the selected component in order to extract straight lines. The lines are then intersected to segment the scene into different regions. Using the LiDAR and the aerial images, we verify whether the segments contain road parts, and discard the ones which do not. Since the roads' color and height are usually more homogeneous than their surrounding objects (e.g. Buildings), we suppose that the pixel value deviation of the segments containing road parts is smaller than those of the other segments. Thus, we discard the segments with the pixel value deviations larger than a certain threshold. Additionally, using the LiDAR image, the segments with average height values larger than a certain threshold are removed.

After extracting the road segments, we merge the segments which belong to the same road. The points within each segment are then projected on a perpendicular plane to the segment's main orientation, so that the majority of the points are able to generate the road's profile. As a final step, the edges at the round corners, which usually occur at the road intersections, are refined.

As an integration technique, PCA is used on the 4 available information bands, namely R, G, B, and height. The most road discriminating principal component is then used in Hough transform to extract the possible locations of the roads as straight lines. Using

these lines, the scene is segmented into various regions. The segments containing a road part are then detected and merged to shape the road network in the scene. The roads are then delineated using a projection-based method, and their round corners are further refined. For a quantitative evaluation, the extracted roads are compared to ground truth data using RMS and angular displacement measures. Experimental results demonstrate that our proposed method detects and delineates the roads precisely in a given scene.

Hu, (2004):Automatic Road Extraction from Dense Urban Area by Integrated Processing of High Resolution Imagery and Lidar Data

This paper focuses on the integrated processing of high resolution imagery and LIDAR (Light Detection and Ranging) data for automatic extraction of grid structured urban road network. In early 2002, Optech International, Toronto completed a flight mission of acquiring the LiDAR data of Toronto urban area using its ATLM 3200. The LiDAR dataset provided is around downtown region.

The test data set is color ortho-imagery with 0.5 m resolution and LiDAR data of Toronto downtown area. The first and last returns LiDAR range and intensity data were collected. The dataset contains about 10.6 million points and has a density of about 1.1 points/m². The DTM was generated using the last-return LiDAR range data, and also obtain the height data by subtracting the DTM from the range data. The high resolution imagery is obtained from ortho-rectified aerial image of the same area. The image resolution is 0.5m. To do integrating processing, it is resampled into 1m resolution and is manually registered with the LiDAR data in geometry.

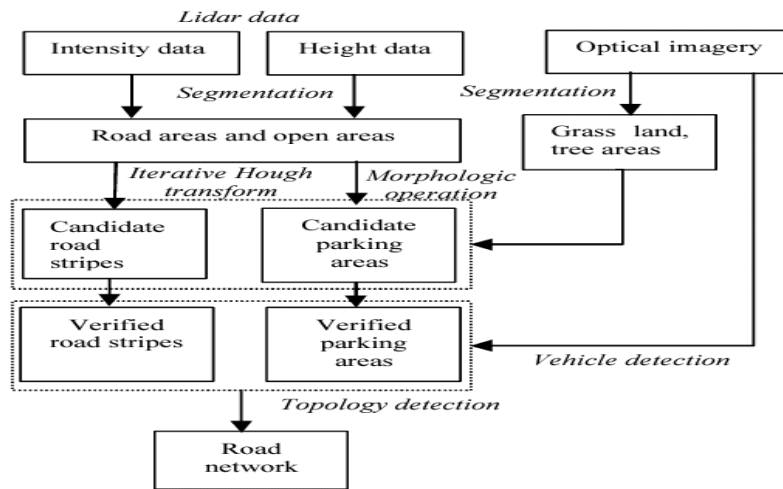


Figure 3.27: Workflow for the road extraction. Source: Hu, (2004)

Segmentation of LiDAR data and high resolution imagery: In reflectivity, the spectral signature of asphalt roads significantly differs from vegetation and most construction materials. The reflectivity rate of asphalt with pebbles is 17% for the infrared laser, and no other major materials have a close reflectivity rate. In height, pavements are attached to the bare surface and appear as smooth ribbons separating the street blocks in a city. Therefore, integrating intensity and height data may produce reliable road detection results. Using height information, the built-up areas with higher elevations than their surroundings will be safely removed; while using the (first-return) intensity information, the vegetated areas are easily removed. After segmentation of the LiDAR data, the possible road areas and other areas are converted to a binary image. Parking lots are kept because of same reflectance and low heights as roads, and bridges and viaducts are removed because of their large heights.

From the true colour high resolution imagery, the grass lands and tree areas can be separated from the open areas. First, because the roads and parking areas are covered and coated by concrete or rainproof asphalt, the saturation of the pixels of the areas is

low while in the grass lands and tree areas it is high and the hue tends to be ‘green’. So using a threshold the grass lands and tree areas can be separated from the low saturation areas. Subtracting the grass lands and tree areas, we can obtain the areas containing candidate road stripes and parking areas.

Extract Road Stripes by Iterative Hough Transform: Modified Hough transfer method is used to directly detect the candidate stripes of the streets from the segmented LiDAR data – the binary image. Hough transformation is frequently used for extracting straight lines.

Verification of road stripes and parking areas: The detected primary streets by Hough transform are possible streets and just straight line equations (parameters). To form a real street ‘grid’, we should identify the candidates and remove some wrong segments. The first step is to overlay the straight lines onto the binary image. To verify a parking area, we employ the vehicle clue to confirm the area. The vehicles are extracted by a pixel based classification method. Some samples of vehicles are provided by manual digitization, and they are used for learning the pixel intensity value of the vehicles. In the study, the open areas contain roads and parking lots. We assume a region with nearly squared shape and big area has high possibility of being parking lots. A morphologic operation is applied to the binary image to detect the big open areas. Combining the analysis result of shape and vehicle clue from LiDAR data and the optical imagery, we compute the ‘score’ of an open area of being a parking lot. The high score indicates the high possibility of being parking lot. By computing the length of the segment which goes through the parking area, the segments mostly lay in the parking areas are removed.

In conclusion, using LiDAR data, the difficulty of resolving the occlusion of roads in optical images is eliminated. It demonstrates the potential and power of using lidar data to extract information from complicated image scenes. To obtain more reliable results, image analysis (to detect contextual objects: grasslands, parking lots, vehicles etc.) for contextual information extraction is integrated into the whole procedure. It greatly improves the final results in correctness and accuracy. The work described in this paper clearly indicates that involving multiple source of information will definitely improve the extraction results in the complicated scene.

Ural, (2015): Road and Roadside Feature Extraction Using Imagery and Lidar Data for Transportation Operation

This study established a framework that used data from multiple sources, including one-foot resolution color infrared ortho-photos, airborne LiDAR point clouds, and existing spatially non-accurate ancillary road networks for road and roadside feature extraction. The study area selected for this work is the Union township, Clinton County, IN, USA.

The data employed include one-foot resolution CIR (Color Infrared) orthophotos, LiDAR point clouds, and the LiDAR derived DEMs (Digital Elevation Model, bare ground model) at a resolution of five feet. They also generated a DSM (Digital Surface Model) and an nDSM (normalized DSM) using the LiDAR point clouds of the study area. They used the existing road network dataset acquired from INDOT (Indiana Department of Transportation) database to generate an approximate buffer around the road lines.

The methodology is laid out in the following workflow. First, there is a preprocessing step for preparing the datasets to be analyzed. Then, these datasets are employed in feature extraction, paved surface classification, medial axis extraction, paved surface reconstruction, and cross section information extraction processes.

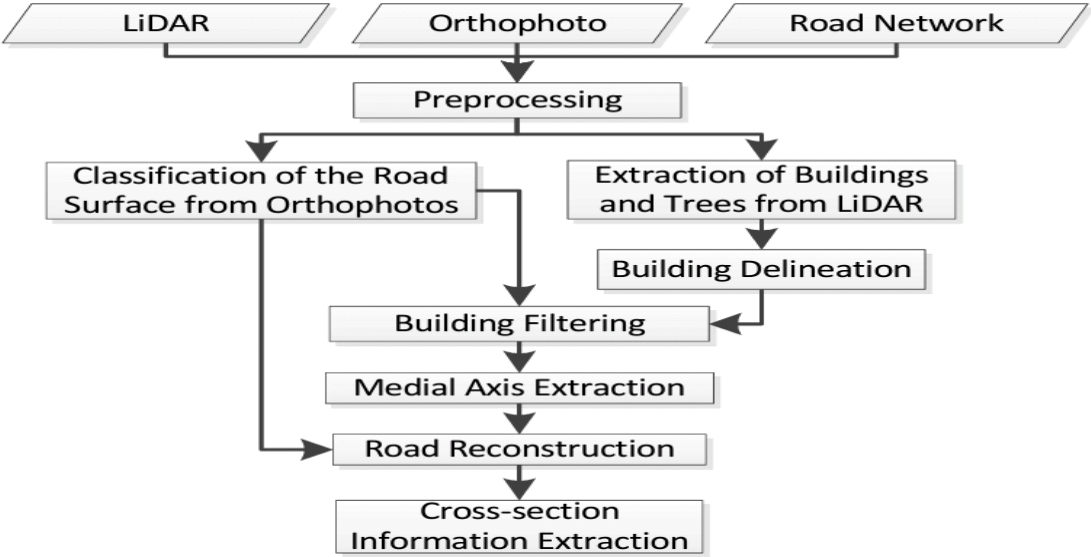


Figure 3.28: Flowchart of methodology. Source: Urala, (2015)

They applied SVM (Support Vector Machine) classifiers as part of a pixel based approach for the classification of the paved surface. SVM classification creates a maximum-margin hyper-plane in a transformed input space and splits the classes by maximizing the distance to the nearest clean split samples. A very common misclassification that occurs while extracting the paved road surface by classifying CIR orthophotos is the classification of some of the buildings contiguous to the roads due to their spectral similarity. A common alternative approach is to employ NDVI (Normalized Difference Vegetation Index) to mask the nDSM so that only high objects that are not vegetation remain to be used to filter the image classification results.

Classification results provide an irregularly shaped noisy raster sampling of the road surface. The road extent needs to be defined in order to determine the clear zones within which the features will be extracted; therefore the road has to be reconstructed. This was done through some morphological operations as well as cleaning and generalization. Cross-sections corresponding to the center of each center line segment based on the reconstructed paved road. The DEM was used to calculate the slope along the cross-section lines.

The first step in the filtering is the extraction of building and trees while the second filtering was for low points which were not considered as buildings. 3D airborne LiDAR point clouds were used to extract the features within clear zones and ground filtering was done. The final result shows that the method was able to extract 90% of the roads and complimentary information was extracted.

Hu et al (2014): Road Centerline Extraction in Complex Urban Scenes from LiDAR Data Based on Multiple Features

This paper proposes to use multiple features to detect road centerlines from the remaining ground points after filtering. The method consists of three major steps, i.e., spatial clustering based on multiple features using an adaptive mean shift to detect the center points of roads, stick tensor voting to enhance the salient linear features, and a weighted Hough transform to extract the arc primitives of the road centerlines.

Vaihingen and Toronto data were provided by the ISPRS Test Project on Urban Classification and 3-D Building Reconstruction. The LiDAR data for Vaihingen were captured by a Leica ALS50 system, and the point density is 4 points/m². The LiDAR

data for Toronto were acquired by Optech, Inc., and the point density is approximately 6 points/m². The workflow below shows the step by step method adopted in this work.

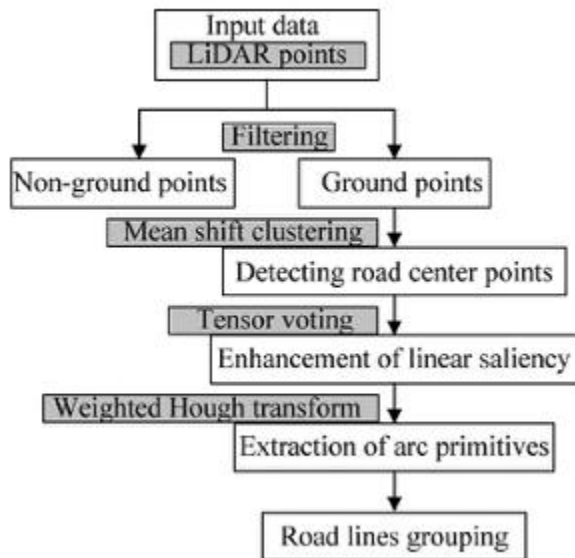


Figure 3.29: Workflow of methodology. Source: Hu (2014)

The initial step, i.e., filtering, is to classify the point clouds into ground and non-ground classes. They adopted the multidirectional ground filtering algorithm for this purpose. It combines the elevation differences and slopes of neighboring points in various directions to filter the ground points. The subsequent steps include: 1) spatial clustering using an adaptive mean shift to detect the center points of roads; 2) stick tensor voting to enhance the salient linear features; and 3) the Hough transform to detect the arc primitives of the road centerlines. In short and to reflect its key implementation steps, the proposed method is denoted by Mean shift, Tensor voting, Hough Transform (MTH). The final road networks are formed by connecting the extracted road primitives.

The completeness of the road network extraction on the Vaihingen data and the Toronto data are 81.7% and 72.3%, respectively, and the correctness are 88.4% and 89.2%,

respectively. This, in turn, implies that finding quality road primitives are an important prerequisite for a successful road network extractor, and the proposed method did contribute to this end.

3.2.4 Application of VHR and LiDAR for Vegetation Mapping

Machala, (2013): Forest Mapping Through Object-based Image Analysis of Multispectral and LiDAR Aerial Data

This study was carried out for forest mapping using LiDAR and multispectral data through OBIA. The study area is situated in the Czech Republic, in the region of South Moravia near the north-east edge of the City of Brno (Fig. 1). The research area covered 8 km² (i.e. 800 ha) of land and included a large part of the town of Bílovice nad Svitavou. 77 % of the area is covered by forest and the rest consists mainly of urban and agricultural areas. The forests in the research area consist of broadleaf as well as coniferous trees.

Image data were acquired by an aerial digital camera. The image is composed of four optical bands - Red, Green, Blue and Near-Infrared, with spatial resolution of 0.6 x 0.6 metres and radiometric resolution of 16 Bits. In addition, the Digital Terrain Model (DTM) and Digital Surface Model (DSM) with spatial resolutions of 1 x 1 meter and radiometric resolutions of 32 Bits were both derived from an airborne LiDAR scanner. The LiDAR device Leica ALS50-II has average point density of 2.5 points / m². Both, multispectral as well as LiDAR data were captured 13. 6. 2009 which is during the vegetation (leaf-on) season.

eCognition Developer 8.64 software was used for this study and the classification process was carried out on the basis of the three data sets – Multispectral image, DTM and DSM. Two classes, vegetation and non-vegetation were distinguished first, using a Normalised Difference Vegetation Index (NDVI). The multi-resolution segmentation was used to create the objects on the bases of these parameters:

1. Scale parameter – 40
2. Shape criterion – 0.15
3. Compactness criterion - 0.65

More than 80,000 individual objects were created with this segmentation following which non-vegetated areas were then classified into three further classes: water, clear-cuts (not all yet which were present in the whole area) and built-up areas. A new level of segmentation was created to classify the vegetated areas, and the results of both segmentations were synchronised at the end. The Image layer weights were tailored for the best differentiation of forested areas, with the emphasis being put mainly on the NIR band. The weight of DSM was multiplied too, because of the much smaller differences in its value range in comparison with the other bands while the weight of the DTM was set at zero as it would have no effect on the segmentation result. For this new level of segmentation, the scale parameter was set to 80, the shape criterion was set to 0.55 and the compactness criterion to 0.75. All those parameters were empirically found to ensure the best results for delineation of desired classes.

The vegetation class was re-classified into forest and non-forest (which included fields, meadows, gardens, solitary trees, etc.) before supervised Nearest Neighbour (NN)

classification was then used for a detailed classification of the forest areas which was the aim of the study. 73 customized arithmetic features were created and the correlations between customized features were computed by STATISTICA 9.0 software. Because the number of values in the eCognition file was enormous, the correlation result was not satisfactory so factor analysis was used to obtain the required information. Finally 26 arithmetic features were selected for defining the feature space. When the definition of feature space was complete and the training sites were selected for each particular class, the NN classification was performed under the following classes - broadleaf; coniferous; mixed (image objects containing broadleaf as well as coniferous trees in approximately equal number); young (for forest areas which had been recently deforested - these areas were either not yet re-afforested but covered by some kind of vegetation (e.g. grass or weeds), or were afforested but the young trees were too small to be identified); plantation (in one area the trees were planted strictly according to a square grid, with large distances between them); clear-cuts (the rest of the clear-cuts present in the research area, subsequently merged with those delineated already before); bare ground (referring to areas which were not fully covered by any type of vegetation, but were not clear-cuts); and shadow (a temporary class, later to be re-classified into one or other of the other classes). The classification flow chart is shown in figure below.

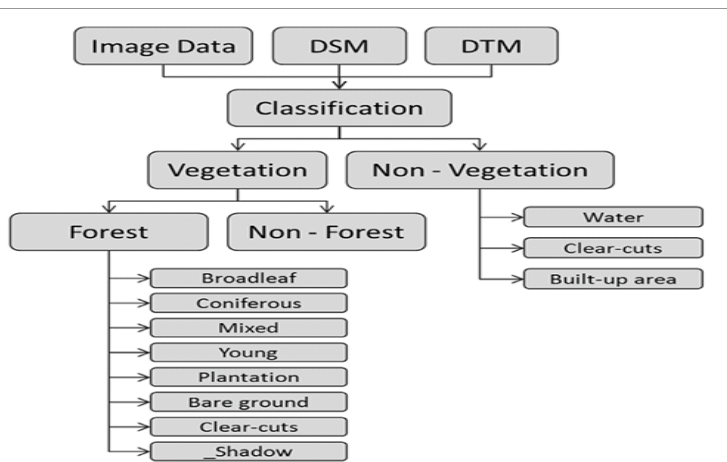


Figure3.30: Classification flow chart. Source: Machala, (2013)

For the result, two maps were produced. First map shows the results of assigning the forested areas to one of the following seven groups: Broadleaf, Coniferous, Mixed, Young, Plantation, Clear-cuts and Bare Ground. In addition, the non-forested areas were delimited and assigned to one of these classes: Water, Non-Forest and Built-up Areas.. Ground truth data was collected to verify the result. The overall accuracy of the forest NN classification was calculated to be nearly 90%. The value of the Kappa Index of Agreement (KIA) was calculated to more than 85% in this case.

Verlic, (2014): Tree Species Classification using WorldView-2 Satellite Images and Laser Scanning Data in a natural Urban Forest

An object-based image analysis of a combination of high-resolution WorldView-2 multi-spectral satellite imagery and airborne laser scanning (LiDAR) data was tested for classification of individual tree crowns of five different tree species. The study area is urban forests within the City of Ljubljana. The purpose of this study was to assess a straightforward method of object-based image analysis (OBIA) (Blaschke, 2010) with a combination of WV2 imagery and LiDAR data for successful classification of individual

crowns of five different tree species in the dominant layer of natural, mixed, heterogeneous urban forest in Ljubljana, Slovenia.

Aerial imagery and laser scanning data were recorded simultaneously on 24.3.2011 from a helicopter on a windless day to avoid errors in fused images due to moving tree crowns. Additional aerial images were taken in summer, when tree leaves were fully leafed-out and thus enabled a visual distinction among the tree species. The images were processed into a true orthophoto imagery which was used in the field work for detailed identification of individual trees, in the manual digitization of tree-crown polygons of trees selected in the field, as well as for the visual verification of the classification results.

The WorldView-2 (WV2) satellite image used in the study was acquired on August 1, 2010, in the peak of vegetation period. The satellite imagery consists of an 8-band multispectral image with resolution of approximately 2 meters and a panchromatic image with 0.5 m resolution. The panchromatic and multispectral images were first orthorectified using RPC and an accurate laser scanning digital surface model (with 1 m resolution). The orthoimages were generated only where the laser scanning digital surface model (DSM) was available. Then to maintain the high spatial resolution of the panchromatic images and the high spectral resolution of multispectral images, they were combined into a pansharpened image with a resolution of 1 m using the modified Intensity-Hue-Saturation (IHS) method. The pansharpened image was then used for the classification.

The tree data for tree species classification were obtained from a virtual network of circular 2000 m² plots in a 100 x 100 meter grid in the forest. On each of the 332 plots, a coniferous and a deciduous tree were recorded. A field manual for each plot was prepared for locating each plot in the field. It contained a section of the true orthophoto image, DCM and a digital model of terrain (DMT) derived from laser scanning data. DCM shows stand canopy model and DMT shows a detailed ground relief model. In total 608 trees of 15 different tree species were recorded. For further analysis 574 trees were selected – 304 coniferous trees and 270 deciduous trees of tree species whose sample consisted of more than 30 units (Baldeck and Asner, 2014), namely the Norway spruce, Scots pine, European beech, Sessile and Pedunculate oak and Sweet chestnut.

For the OBIA, Example-based Feature Extraction was performed in Exelis VIS ENVI 5 software applying support vector machine model (SVM). After a trial and error with various combinations, the optimal parameters of the segmentation were set. In addition to the original 8 bands, Red-Edge normalized difference vegetation index (Red-Edge NDVI) calculated from Red-Edge and Red band, and DMC layer were stacked into a 10-band image for the five tree species supervised classification. Confusion matrix was used to calculate the accuracy of the classification. In the first step of classification the area on the image was masked by laser scanning height data to include only areas with heights between 15 and 50 m to remove the lower (also ground) vegetation influence and reduce the abundance of data, In the second step, training samples of the five tree species were included as a reference.

The overall accuracy of the classification was 58 % and Kappa Coefficient was 0.431. The highest accuracy was for Norway spruce, where producer's accuracy was 80 % and user's accuracy was 69 %. Most S. chestnut crowns were misclassified as Oaks (73 %).

Table3.12: Classification accuracy assessment: Producers and users accuracy for the five trees.

Overall Accuracy = (7280/12608) 58 %				
Kappa Coefficient = 0.431				
Class	Prod. Acc. (Percent)	User Acc. (Percent)	Prod. Acc. (Pixels)	User Acc. (Pixels)
N. spruce	80	69	2716/3395	2716/3932
S. pine	50	57	793/1591	793/1401
E. beech	38	64	1330/3466	1330/2072
Oak	70	47	2437/3498	2437/5169
S. chestnut	0	12	4/658	4/34

Source: Verlic, (2014)

3.3 Discussion of the Reviews

A total of thirty (30) articles were reviewed and they conducted their studies using OBIA classification method which has proved to achieve better results when VHR images are used. eCognition software has also been found to be the most popular because it is a powerful development environment for OBIA. eCognition Developer can be applied for all common remote sensing tasks such as vegetation mapping, features extraction, change detection and object recognition. The object based approach facilitates analysis of all common data sources, such as medium to high resolution satellite data, high to very high resolution aerial photography, LiDAR, radar and hyperspectral data. Different techniques and algorithms have also been applied under a general principle depending on the feature class targeted. However it's important to state that the principles were based on the basic steps in general classification methodology. These are data preprocessing, segmentation, classification and accuracy evaluation.

LiDAR provides detailed information regarding geometries such as spatial distances, heights, and canopy penetration but lacks any information concerning details of the electromagnetic spectrum. Spectral provides highly detailed electromagnetic information to the point of material identification, but it is limited to two dimensions without spatial information in the 'z' or height dimension. These studies have taken advantage of their complementary qualities to carry out various feature extractions.

With the values LiDAR provides of elevation and intensity, classification is possible with the point cloud alone. In a study by the University of Cambridge and University of Wales, they created land cover type classification employing elevation, intensity, and also point distribution frequency. The classification method used a series of criteria based on height, intensity, and distribution which was then processed in the geographic information system ArcGIS and they achieved an accuracy of 95%. Integration of high-resolution image with LiDAR data gives a better description of earth surface and facilitates improved feature extraction. Researchers combined the multispectral data with LiDAR in object-based feature extraction and classification.

Yongmin et al, (2011) studied the effect of airborne elevation information on the classification of an aerial image in an urban area. This classification procedure used elevation and intensity information obtained from the LiDAR data, as well as the red, green, and blue bands obtained from the aerial image. As a result, a method using the combination of an aerial image and the airborne LiDAR data shows higher accuracy and improved classification, especially with regard to building objects, than results that rely solely on an aerial image.

Hu et al, (2004) conducted a study where he employed high resolution imagery and LIDAR (Light Detection and Ranging) data for automatic extraction of grid structured urban road network in Toronto down town area. The experimental results in the typical dense urban scene indicate it is able to extract the roads much more reliable and accurate by the integrated processing than by using imagery or LiDAR separately. It saliently exhibits advantages of the integrated processing of the multiple data sources for the road extraction from the complicated scenes. There are several recent algorithms available that makes the use of airborne LIDAR data for road feature extraction. Hu et al (2014) proposed a method which detects road center lines from airborne LIDAR data which consist of three steps spatial clustering based on multiple features using an adaptive mean shift method to detect center point of roads, Stick Tensor Voting to enhance salient linear features and weighted Hough Transform to extract the arc primitives of road center lines.

Another prominent issue which researchers had to contend with is the issue of shadow due to the high density of urban features but the study carried out by Haitao et al (2007) proved that object oriented SVM classification of high resolution image and LiDAR data has been effective in correctly identifying various kinds of shadows. Also, Dinis et al (2002) developed a methodology using multitemporal set of HR image and LiDAR data to separate shadowed areas. This was a simple approach, such as a bimodal histogram splitting, combined with a Spectral Shape Index provided an efficient way of separating shadows from non-shadows. Researchers combined the multispectral data with LiDAR in object-based feature extraction and classification.

Zuo et al, (2016) successfully conducted a research and proved that the use of LiDAR datasets and nDSM are very helpful for the separation of tree and low vegetation, building and road using the height information. The overall accuracy (OA) of OBIA classification reaches 89.5% in the study area and the Kappa coefficient is recorded as 0.865. In another study, Hermosilla,et al (2012) used aerial image and LiDAR to map Valencia city and achieved. They achieved overall accuracy of the classification was 84.8%, and the kappa coefficient 0.83. These were considered to be sound results, especially considering the large number of classes defined.

In Seyd et al (2005) study, the goal of the study was to automatically classify land cover features using high-resolution imagery and LiDAR derived DSM data, and the object-oriented approach did this effectively. Results indicate that object-oriented approaches have great potential for integration of LiDAR and high-resolution imagery for multi-sensor classification. Haitao et al, (2007) carried out his study using OBIA for the classification of LiDAR data and high resolution image and based it on Support Vector Machine (SVM). The result showed that different shadow species are easier to distinguish when both aerial images and LIDAR data are used together. The results also show that the overall accuracy of pixel-based SVM is 82.92%, whereas the overall accuracy of the object-oriented classification based on SVM is 95.97%. Tiwari et al (2009) explored an integrated approach to extract road automatically using airborne laser scanning altimetry and high resolution data in Amsterdam, Netherlands and achieved an accuracy of over 90%. Many methods have been developed to detect urban road network from high resolution images (Hu et al, 2007; Long & Zhao, 2005; Zhu et al, 2005). High

resolution allows more fine details to be seen, a better differentiation of road types and a more accurate geographic location.

These studies have successfully proved that High Resolution (HR) imagery has the advantage of high user interpretability, rich information content, sharpness, high image clarity, and integrity, which provides the unique tool for classification. It is also clear that it is no longer convenient to classify high resolution imagery with pixel-based classification method (e.g. Maximum Likelihood) because of its limitations and considerable difficulties dealing with the abundant information of HR data.

3.4 Gap Identified

As mentioned earlier the 30 studies reviewed conducted these studies with the standard protocol for classification of high resolution images and LiDAR data for feature extraction. The techniques and algorithms only change with respect to the feature class targeted. It can also be noted that none of the studies were done within Nigeria and a majority of them were concentrated within the urban and suburban setting. Urban areas in the developed world are known to have paved road surfaces but it is not unlikely that the suburban areas where some of these studies were carried out could have a few stretches of roads which are made of neither asphalt nor concrete or even paved in any form. None of the studies gave consideration to the mapping of such earth roads and it is not safe to assume that all the roads are paved.

This is an observed gap which the reviewer considers important especially in the context of Nigeria where the proposed study will be carried out. Roads have long been important for development and prosperity and are essential for many applications such as urban

and rural planning, transportation management, vehicle navigation, emergency response, security etc. This will help in no small measure to facilitate planning of various development and services for such rural areas which have most of the roads unpaved. Suffice to mention that it will also be a very helpful approach to solving security problems especially in these days of kidnapping and related crimes. The rural roads which are mostly unpaved are escape routes as well as access to hiding places as criminals hardly settle or hide in urban areas after committing crimes. The mapping of such earth roads will greatly assist the security coordination of various stake holders.

This review started with an introduction of the subject matter which is the general importance of regularly updating geospatial information especially those that provide landuse/landcover information, since they provide key information for land management and environmental planning. Traditionally, LULC databases have been updated by means of photo-interpretation of aerial and satellite images and by field visit. These techniques are lengthy, subjective and costly. Digital image processing has therefore provided a very convenient and cost effective means of solving this problem.

This review investigated the current methods of extracting information from high resolution remote sensing images. Thirty (30) related studies were reviewed in terms of their techniques and algorithm viz. the respective images and feature classes being processed. The review targeted high resolution images and LiDAR data which are complemented by each other in ensuring best classification results. The review also looked closely at object based image analysis as opposed to the pixel based classification. While pixel-based image analysis is based on the information in each

pixel, object-based image analysis is based on information from a set of similar pixels called objects or image objects. More specifically, image objects are groups of pixels that are similar to one another based on a measure of spectral properties (i.e., color), size, shape, and texture, as well as context from a neighborhood surrounding the pixels.

In conclusion, this review is able to confirm the significant potential of LiDAR and high resolution data to extract urban classes. LiDAR data assists in reduction of vertical and horizontal heterogeneities. Combining attributes of high resolution images with nDSM provided an effective separation of spectrally similar image objects. No doubt that the spatial resolution of remotely sensed data has improved, multispectral images are insufficient for urban classification due to confusion in discriminating between trees and grass, misclassification of buildings caused by diverse roof compositions and shadow effects, and difficulty in distinguishing cars on roads. However, the incorporation of LiDAR data, especially nDSM, significantly improves accuracy. Most of the studies show that LiDAR data in conjunction with hyperspectral imagery are not only capable of detecting individual trees and estimating their tree metrics, but also identifying their species types using the developed algorithms. The integration of these two data sources has great potential to take the place of traditional field surveys.

Finally this study identified a gap which has to do with non-consideration for the existence and classification of earth roads even in the suburban areas where the studies were carried out. The proposed study will attempt to fill the gap as it will be a major boost to planning of infrastructure and supply of various services including the coordination of security matters.

CHAPTER FOUR

METHODOLOGY

4.0 Introduction

This chapter discusses the methodology adopted in this research study. It specifically focuses on the data available for use, the software and hardware input, data processing and the various approaches adopted for the analyses tailored towards achieving the aim of the research through the already stated objectives and research questions.

4.1 Data Requirements

The data used for this study came from both primary and secondary sources as follows:

4.1.1 Primary data includes:-

- (i) DGPS coordinate positions of selected points in the study area (see Appendix 4)
- (ii) Handheld GPS points (appendix 5)

4.1.2 Secondary data include:-

- (1) Geoeye-1 image of the study area acquired 2012
- (ii) LiDAR data of the study area acquired 2012
- (iii) 1:125,000 base map of the study area
- (iv) Google image of study area (appendix 6)

4.2 Hardware and Software Requirements

The following hardware and software were used:

4.2.1 Hardware

- (i) HP laptop with configuration of 2GB RAM, 300GM Hard disk and 3.00GHZ microprocessor speedused for all computer/software manipulations.
- (ii) HP Designjet AO Scanner for conversion of paper maps into digital formats.

- (iii) HP Deskjet 3636 Series A4 Printer for printing of reports, maps and images.
- (iv) 500GB External Hard disk for storage of data and other information.
- (v) Garmin 78s Handheld GPS for capturing geographic location of points in the field.
- (vi) Digital Camera for taking pictures in the study area.

4.2.2 Software

- (i) eCognition 9 Developer Software (For execution of OBIA)
- (ii) ArcGIS 10.1 GIS Software Package (For execution of GIS processes)
- (iii) Erdas Imagine 9.2 software (For execution of Pixel Based Classification)
- (iv) Microsoft Excel 2013 (Used to display statistical information)
- (v) Microsoft Word 2007 (Used for preparing the report)
- (vi) Microsoft PowerPoint 2007 (Used for presentation)

4.3 Data Sources

4.3.1 Base Map

The base maps covering the study area wassourced from the Surveyor General's office Ministry of Lands & Survey, Port Harcourt, Rivers State, Nigeria.

4.3.2 GeoEye-1 Image

GeoEye-1 imagery was launched on 6th September 2008 from Vandenberg Airbase and is owned and operated by DigitalGlobe, It is one of the latest in a series of commercial very high spatial resolution EO satellites. GeoEye-1 collects four-band multispectral images (see table 4.1) at nadir, with 0.41 m panchromatic (black & white) and 1.65 m multispectral (colour) resolution and has a revisiting capability of 1-3days depending on latitude. The panchromatic band is resampled to 0.5 m, which is used with the

information from the multispectral image to produce the pan-sharpened imagery with the final full-colour image of 0.5 m resolution (Land info World Mapping, LLC 2013).

The 0.5m High Resolution Geoeye-1 multispectral image captured on 23rd December, 2012 was obtained from Shell Petroleum Development Company, Port Harcourt, Nigeria through an education support scheme. The Geoeye-1 image (figure 4.1) is four band multi-spectral image of the study area, with Blue (450-510nm), Green (510-580nm), Red (655-690nm) and NIR (780-920nm) bands.

Table 4.1: Characteristics of GeoEye-1 imagery

Bands	Resolution
Pan resolution at nadir	0.41 metres
Spectral range (pan)	450-800 nanometres
Multispectral resolution at nadir	1.65 metres GDS at nadir
Blue band	450-510 nanometres
Green band	510-580 nanometres
Red band	655-690 nanometres
Near Infrared band	780-920 nanometres

Source: DigitalGlobe Inc 2014

Prior to delivery the image was pre-processed and as a result no further geometric or radiometric adjustments were performed. The image is in UTM Projection Zone 32, defined using spheroid of Clarke 1880 and datum of Minna, Nigeria.

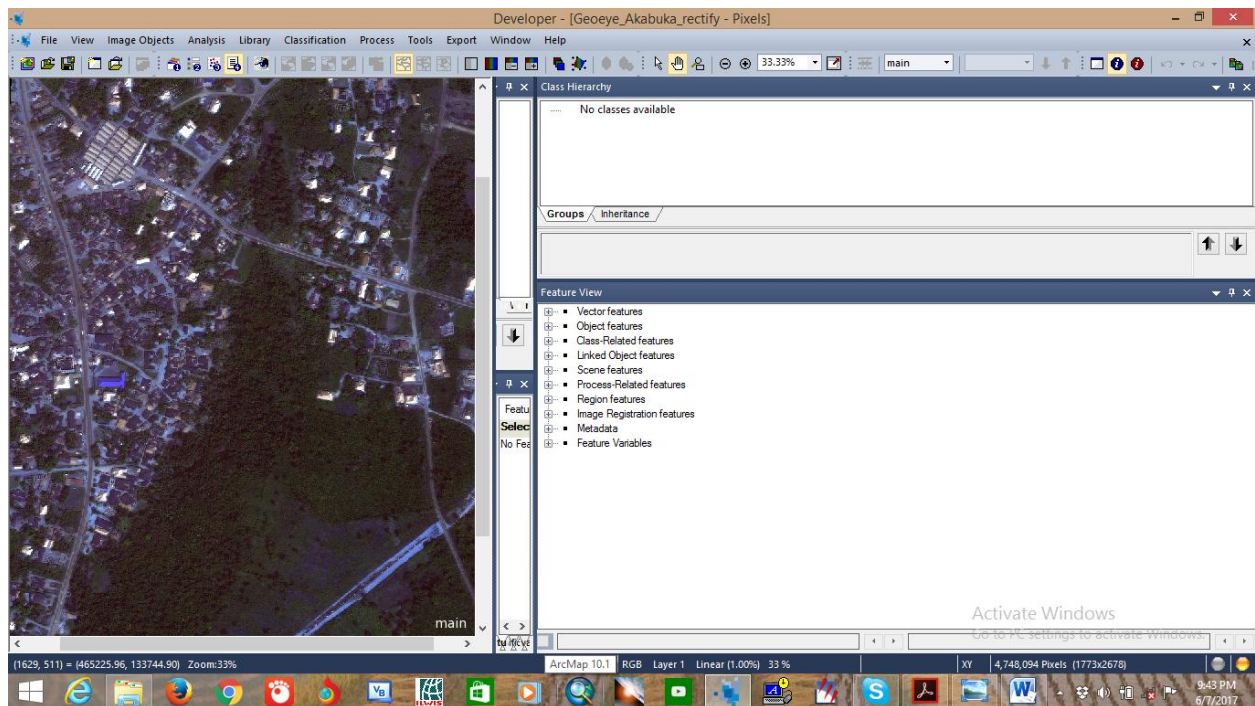


Figure 4.1: GeoEye-1 Image

4.3.3 LiDAR data

The LiDAR data (figure 4.2) was also obtained from Shell Petroleum Development Company Limited, Port Harcourt Nigeria and was captured in December 2012 with the raw data already processed to DSM and DTM from source. This meant that the usual process of generating the DTM and DSM had been performed from source. Consequently, there were no LiDAR intensity values or cloud points supplied with the LiDAR data. The DTM, DSM and GeoEye-1 image were already processed and georeferenced which meant the only data processing required was georectifying the GeoEye images using the LiDAR data and generating the Normalised Digital Surface Model (nDSM). The height value to be used in this research is the normalised DSM (nDSM) and this is an ideal value in image classification for isolating tall features like buildings and trees from surroundings. The $nDSM = DSM - DTM$ and this process was carried out within the ArcGIS environment. The nDSM was calculated by subtracting the DTM

from the DSM using Raster Calculator in ArcGIS. The nDSM represents the absolute heights of non-ground objects such as buildings and trees, above the ground.

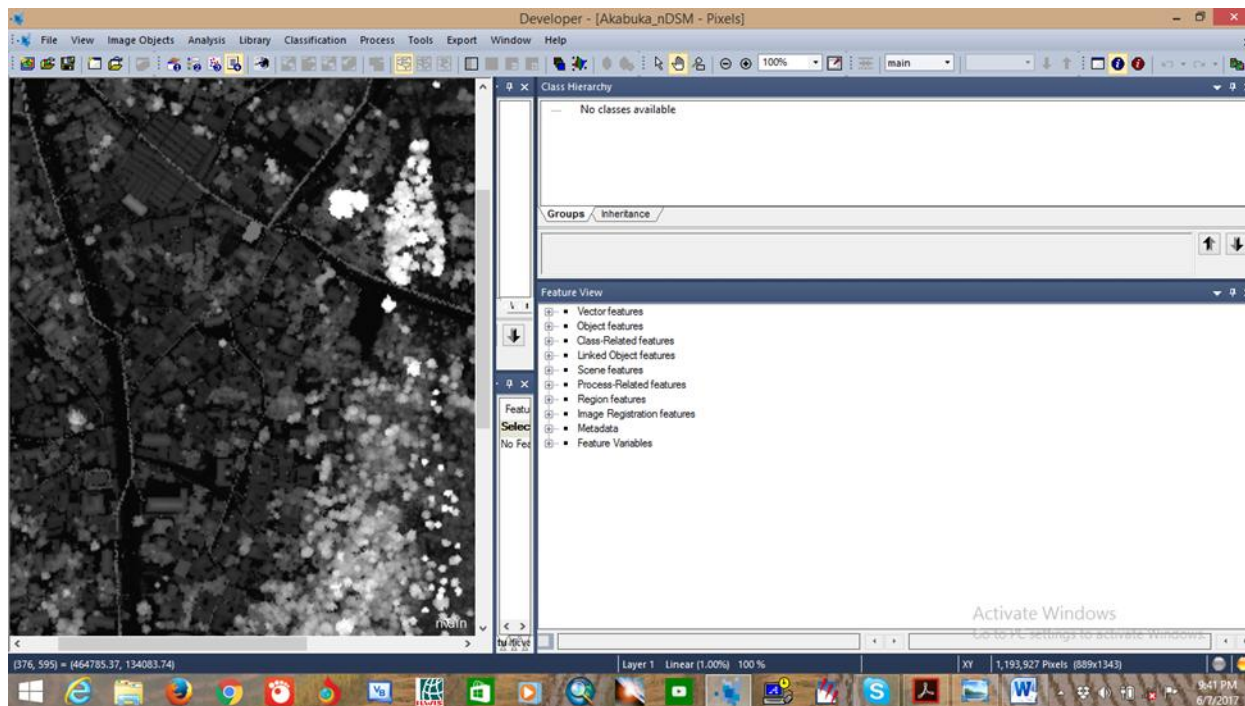


Figure 4.2: LiDAR data

4.4 Data Processing

Remotely sensed data are most often provided in their recorded raw form with various degrees of distortion (mostly radiometric and geometric) making them less valuable for classification processes (Varshney & Arora 2004). Consequently, an array of data processing procedures, called pre-processing are usually undertaken before land cover extraction process could proceed (Campbell & Vynne 2011). Campbell (2006) emphasized the role of pre-processing, in enhancing the quality of satellite imagery. Pre-processing includes georeferencing, mosaicking, sub-setting, and radiometric normalization. Geometric and radiometric corrections are mostly concerned with improving image quality (Chuvieco, Li & Yang 2010). Several studies have focused on optimizing preprocessing workflows to improve data quality and ensure good land cover

extraction. For example Leiss et al. (1995) reported that classification errors induced by insufficient radiometric and geometric precision can be reduced by appropriate geometric and radiometric correction.

Based on the images supplied, seven study sites were proposed within the image scene, each with varying levels of urbanization. In addition, areas not affected by cloud cover and those that coincided with the LiDAR data were key considerations in selecting these study sites. The image was also subset with the intention of having a good mix of real world shadows, urban sprawl with both small and tall buildings, water areas, vegetation, bare soil, and impervious surfaces. These study sites were subsequently clipped from the GeoEye-1 image and geo-rectified using the LiDAR data. This process of geo-rectification was performed using the georeferencing tool in ArcGIS 10.1 desktop software. Figure 4.3 presents the study sites and the geo-rectified GeoEye-I extracts.

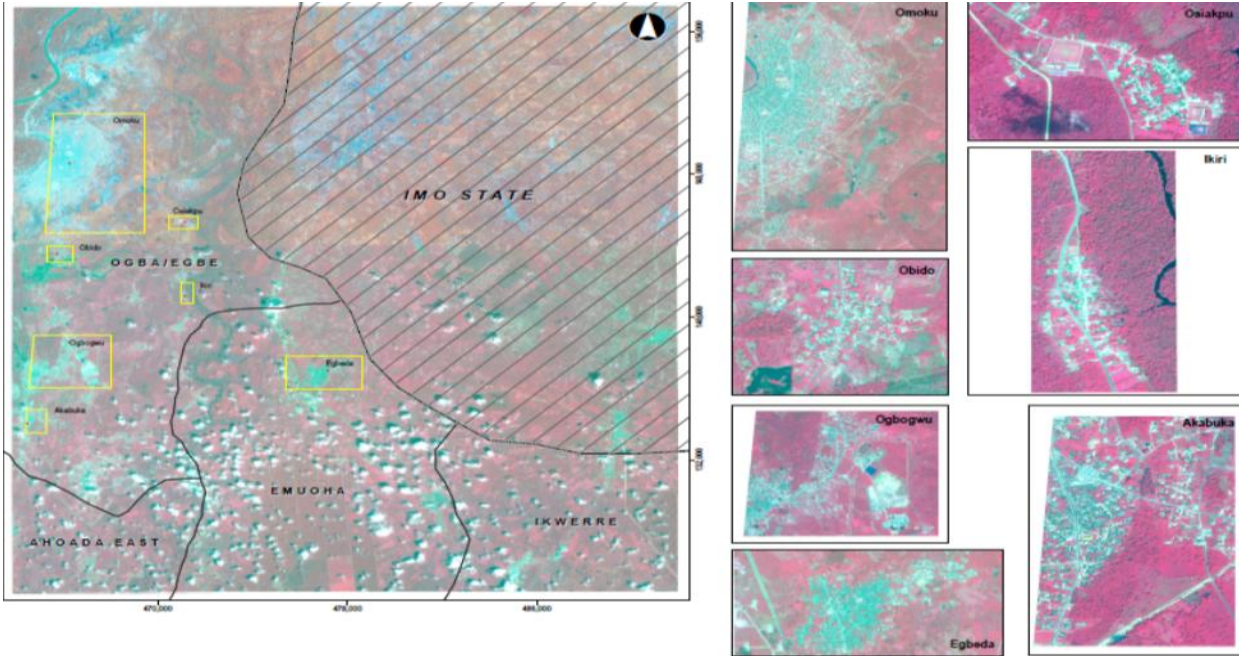


Figure 4.3: Study sites and the geo-rectified GeoEye-I extracts.

The aim of this research is to evaluate the object based classification over the traditional pixel based in classifying VHR and to access the advantage of the integration of nDSM data to Very High Resolution (VHR) image classification of urban features. Figure 4.4 is the flowchart used to achieve the objectives

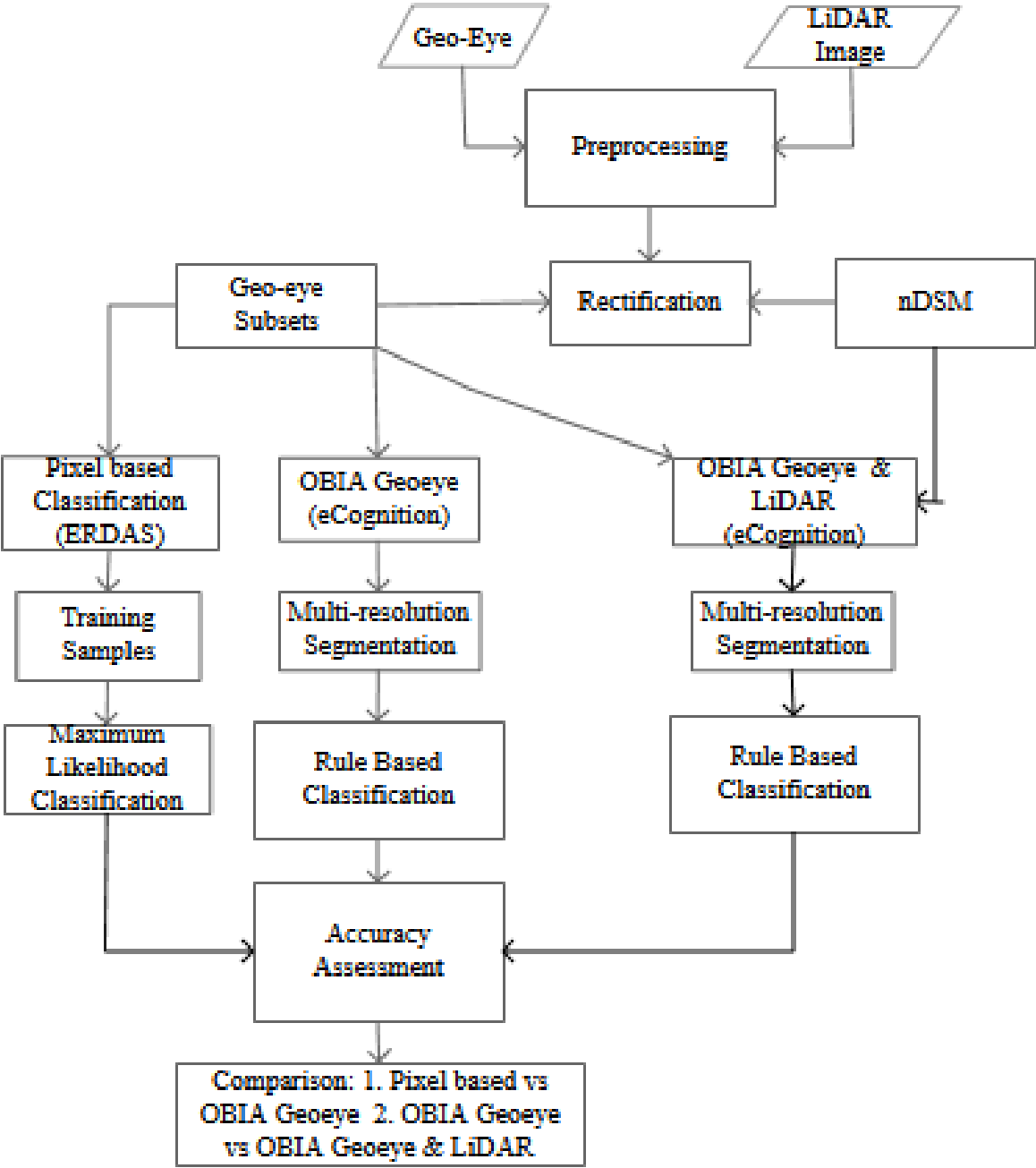


Figure 4.4: Flowchart of the Methodology

4.5 Procedure Adopted in Achieving Objective Number One.

4.5.1 Objective One: To carry out mapping of urban features within the study area using Pixel and Object based analysis techniques.

4.5.2 Research Question 1: Does object the based method of classification achieve higher accuracy than the pixel based method in land cover classification using VHR image?

The first step was to achieve a pixel based classification by carrying out a supervised classification of the VHR image using Eradas 9.2 software after which OBIA of the VHR image was carried out within the eCognition environment. This was done for all the seven study sites.

4.5.3 Part A of Objective One - Pixel Based Classification in Erdas Imagine

The supervised classification adopted at this stage was performed using ERDAS Imagine 9.2 processing software. Classification is the process of sorting out pixels into finite number of individual classes or categories, of data based on data file values. The choice of a supervised classification was because the process is more closely controlled by the researcher and also the researcher has a prior knowledge of the study areas of interest. In a supervised classification, the analyst selects and digitizes polygons (training areas) and places these polygons in an AOI (Area of Interest) layer from which to create the signature files. In Imagine, an individual training site is delineated as an "area of interest" and given a class name. The pixels within the training site are used to generate a "signature." This process is repeated to gather several training sites for each class.

The step by step procedure adopted in the supervised classification is as follows:

1. Open Erdas from the start menu and create a workshop folder, Start >Programs> Erdas imagine
2. Select File -> Open -> Raster Layer from the Viewer menu bar, or click the Open icon on the Viewer toolbar to display the image file to be classified.
3. In the Select Layer To Add dialog File name section (figure 4.5), select subset image, which is located in the <IMAGINE_HOME>/directory. This is the image file that is going to be classified.

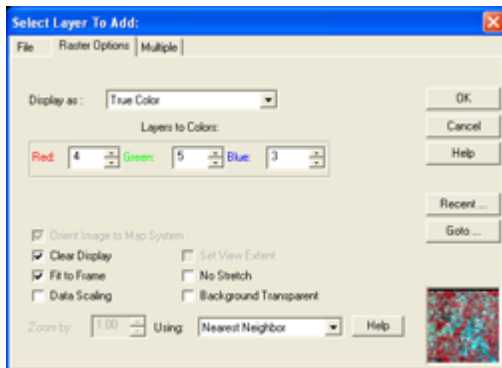


Figure 4.5: Select layer to add dialogue, Source: ERDAS IMAGINE Tour Guides (2008)

4. Click the Raster Options tab at the top of the dialog, and then set the Layers to Colors to 4, 5, and 3 (Red, Green, and Blue, respectively) – colour combination
5. Click the Fit to Frame option to enable it.
6. To open the signature editor, click the Classifier icon on the ERDAS IMAGINE icon panel, then the Classifier menu displays.

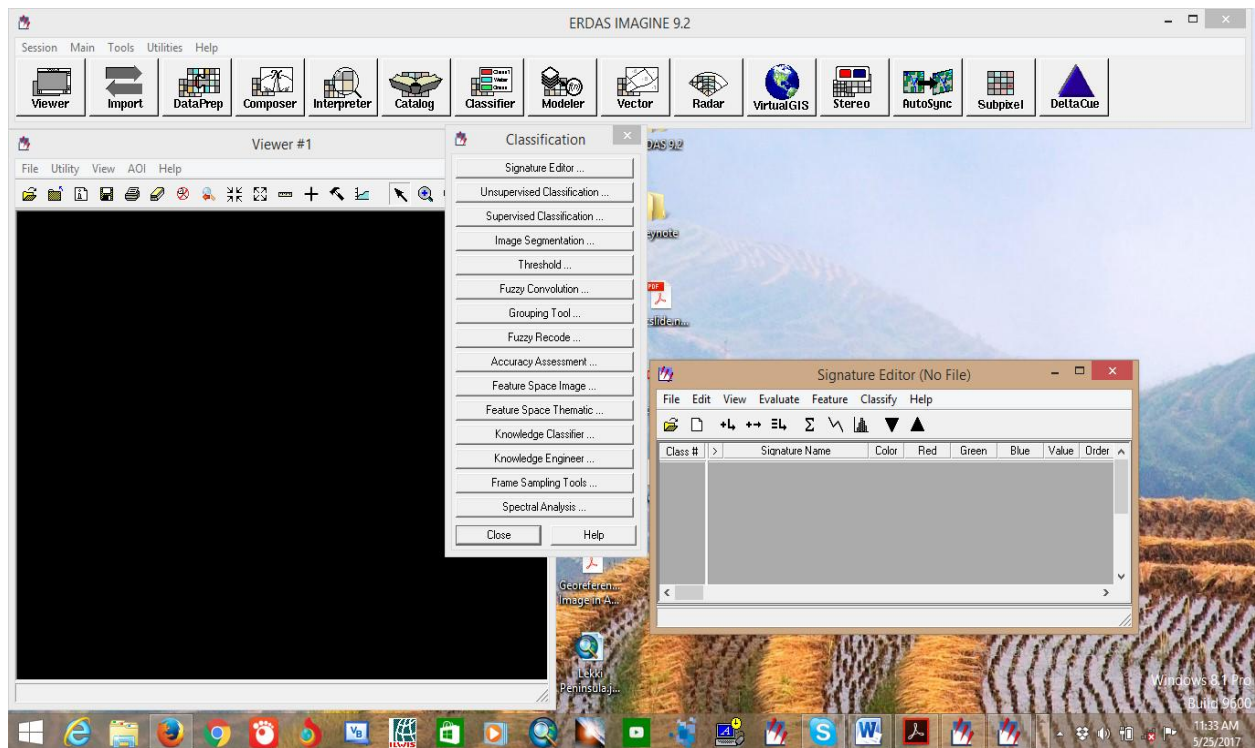


Figure 4.6: Viewer, Classifier menu and Signature editor of Erdas 9.2., Source: ERDAS IMAGINE Tour Guides (2008)

7. Select Signature Editor from the Classification menu to start the Signature Editor.

The AOI tools allow you to select the areas in an image to be used as signatures. These signatures are parametric because they have statistical information.

8. Select AOI -> Tools from the Viewer menu bar. The AOI tool palette displays, then click the polygon icon in the AOI tool palette.

9. In the Viewer, draw a polygon around the green area you just magnified. Click to draw the vertices of the polygon. Middle-click or double-click to close the polygon to show a bounding box surrounds the polygon, indicating that it is currently selected. Effort was made to select at not less than five signatures for each class which were later merged.

10. In the example below (Fig.4.7) the respective classes have been merged to 4 classes by selecting and holding the shift key and left clicking in the Class # column.

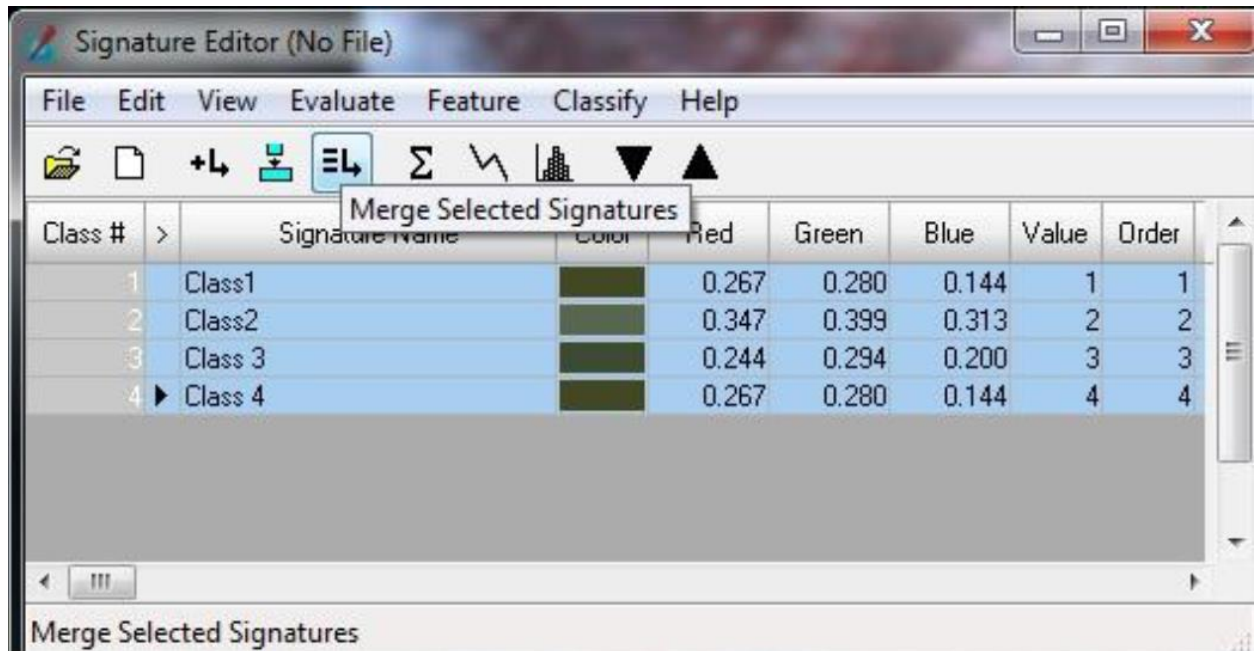


Figure4.7:Merged selected classes, Source: ERDAS IMAGINE Tour Guides (2008)

11. Register the spectral signature of the defined classes and save the file.

12. Apply the supervised classification and open the classified image in a new viewer.

13. Open another viewer to view the classified image.

13. Recode the classified image and display the recoded image, Interpreter>GIS analysis>Recode, and save.

14. Change the colour of the recoded image and save as classified image.

15. In remote sensing, accuracy assessment is mandatory (Matsakis et al. 2000, Foody 2002), and is important for providing information about the quality of the product of classification as well as furnishing the norms for comparing the performance of different classification methods. Therefore accuracy assessment was performed on the thematic

information. Accuracy assessment compares two sources of information; pixels or polygons from a classification map developed from remotely sensed data and ground reference test information (Jensen 2005). A confusion matrix or error matrix which consists of some rows and columns was used to check the relationship between the two sources in this research. A typical confusion matrix for the accuracy assessment is shown in table 4.2.

Table 4.2: Typical Confusion matrix

		Reference Data							
Class		Con A	Wetland	Con B	Water	Hardwood	Exposed Dirt	Sand	Row Total
Remote Sensing Classification	Con A	79	0	12	0	3	3	0	97
	Wetland	2	78	7	0	5	0	0	92
	Con B	13	3	64	0	23	4	1	108
	Water	0	0	0	99	0	0	0	99
	Hardwood	6	17	17	0	65	28	5	138
	Exposed Dirt	0	2	0	0	3	52	5	62
	Sand	0	0	0	1	1	13	89	104
	Column total	100	100	100	100	100	100	100	700

Overall Accuracy = 526/700 = 75.14%

Source: Jensen, 2005

4.5.4 Part B of Objective One - OBIA of VHR Image in eCognition

The software eCognition Developer version 9 was used for OBIA. The 64-bit software was used for the import and manipulation of the subset image, multi-resolution segmentation, development of a rule-based classification and accuracy assessment. eCognition software was also used to define the arithmetic expressions to calculate the NDWI and SSI used in the study. These indices are used to differentiate water and shadows respectively.

Object based analysis typically involves the segmentation of the image scene, classification of the object primitives into classes and accuracy assessment. During the sub-setting of the study area image, one major consideration was that normally, image

files that are large in size are difficult to process during segmentation. Therefore effort was made to reduce the subset images to sizes that would take less memory and time during segmentation.

The general OBIA procedure followed during the classification is as follows: The general procedure was in the following sequence, load and display raster data, perform image segmentation, create a simple class hierarchy, insert the nearest neighbor classifier into the class description, classify, and perform classification quality assessment. Image objects were created using multiresolution segmentation by first starting up with a single pixel and merges neighbouring segments until a heterogeneity threshold is reached (Benz et al., 2004). By specifying user-defined scale parameter, colour/shape and smoothness/compactness weights, the heterogeneity threshold is achieved. It is important to note that image segmentation is scale dependent. This to a great extent determines the overall classification accuracy (Zhang, 2014). Zhang and Feng (2005) noted that the final decision of selecting scale parameters is often based on the discretion of the operator's visual inspection of the image.

1. *To load image* - go the Windows Start menu and Click Start > All Programs > eCognition Developer 9 > eCognition Developer. Select rule set mode and click ok then the default eCognition display appears (figure 4.8).



Figure4.8: eCognition Start-up interface, (Source: eCognition reference book, 2011)

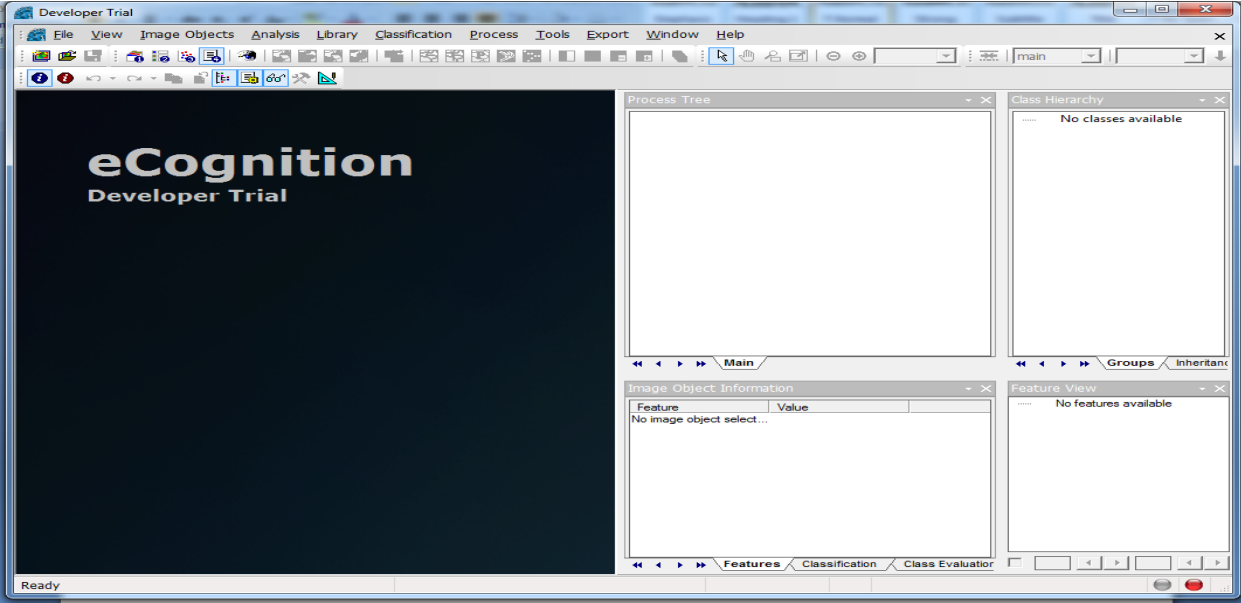


Figure4.9: Default eCognition display, (Source: eCognition reference book, 2011)

The next stage was to create a new project by choosing File > New Project on the main menu bar (figure 4.9). Navigate the folder containing the subsets, select Image.img > Open (the particular subset), then select from the appropriate file in the files type (figure 4.10).

Double-Click on Image Layer Alias and rename the all layers name - Double-Click on Layer Alias Rename the all the layers name Layer 1 (Blue), Layer 2 (Green), Layer 3 (Red), Layer 4 (Near IR) etc. and save the project.

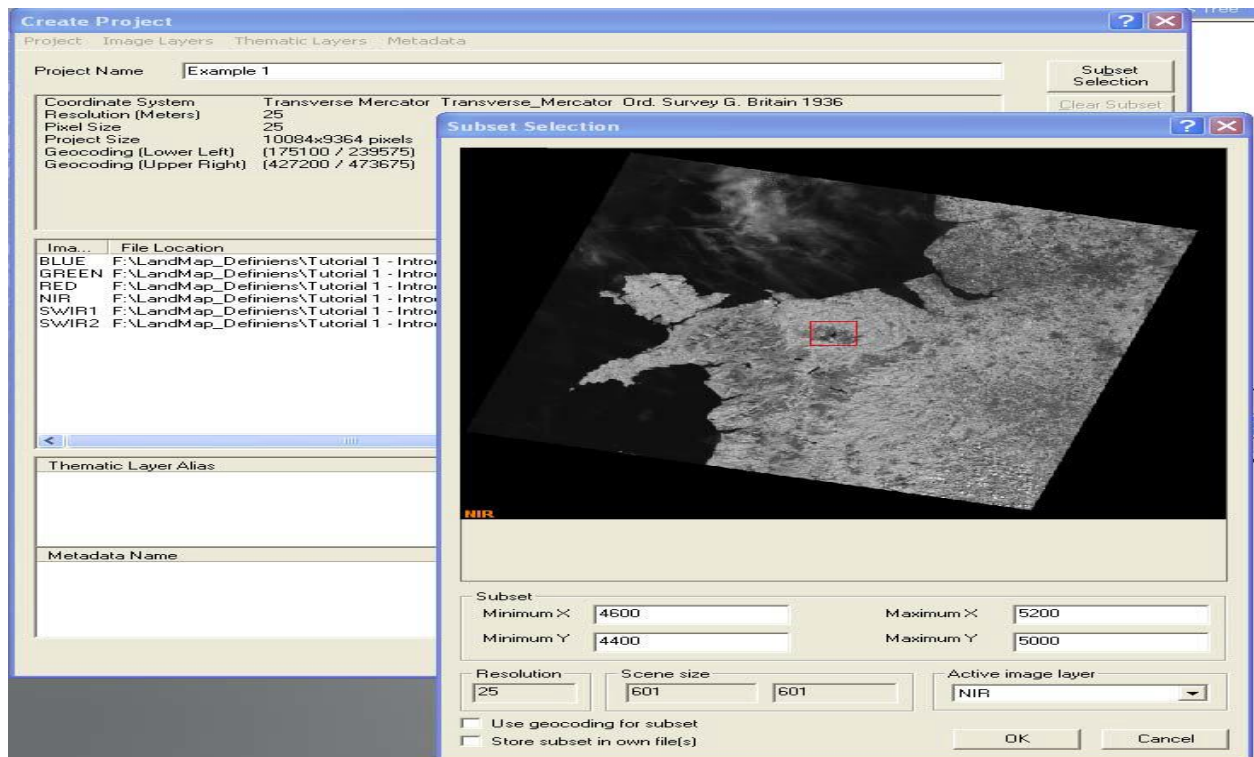


Figure 4.10: New project created, (Source: eCognition reference book, 2011)

Using the 'Layer Mixing' drop down menu the number of layers to be mixed in the display was selected. Edit the Image Layer Mixing is one kind of band combination process which makes it possible to have a better view of the image. To open the 'Edit Image Layer Mixing', do one of the following:

- From the View menu, select Image Layer Mixing
- Click View > Image Layer Mixing on the main menu bar, or Click on the Edit Image Layer Mixing button in the View Settings toolbar. Choose a layer mixing and click ok (Figure 4.11).

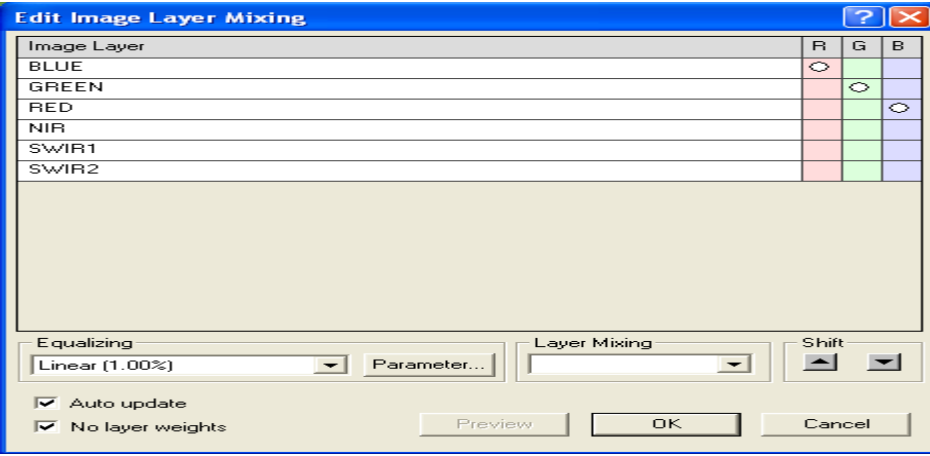


Figure 4 11: Edit Image Layer Mixing dialog box, (Source: eCognition reference book, 2011)

2. *Image segmentation.* The fundamental step of any eCognition image analysis is to do segmentation of a scene representing an image into image object primitives. A good classification result begins with a good segmentation. Segmentation begins by setting up a process tree which contains script you produce to control the processes (algorithms) which run and the order in which they are executed.

To insert a process, right-click within the process tree window and the process tree menu will appear. Select 'Append New' and the 'Edit Process dialog will appear, change the name to Process template and click ok (figure 4.12).

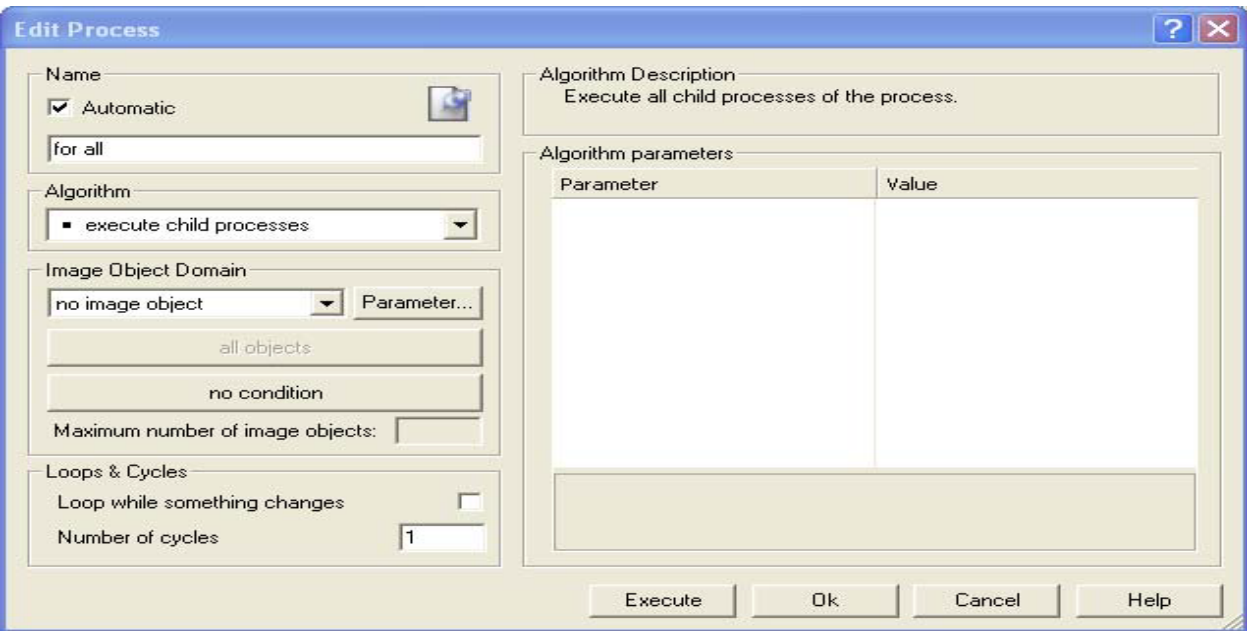


Figure 4.12: Edit process dialog, (Source: eCognition reference book, 2011)

(a) Insert a Segmentation Parent Process right-click' of the process you have just created and select 'Insert Child', this will create a new process under your previous process. Edit the name of the new process to be segmentation and click ok. To insert a Child Process (Multiresolution Segmentation), Select the inserted Segmentation Process and Right-Click on it and choose 'Insert Child' from the context menu. Click Algorithm > Select Multiresolution Segmentations and give it a name – Level 1. See Figure 4.12

(b) Change the image layer weights

(c) Trial and error process was employed to achieve the optimal segmentation parameters for each subset after which the 'execute' button was clicked to execute the segmentation (figure 4.13).

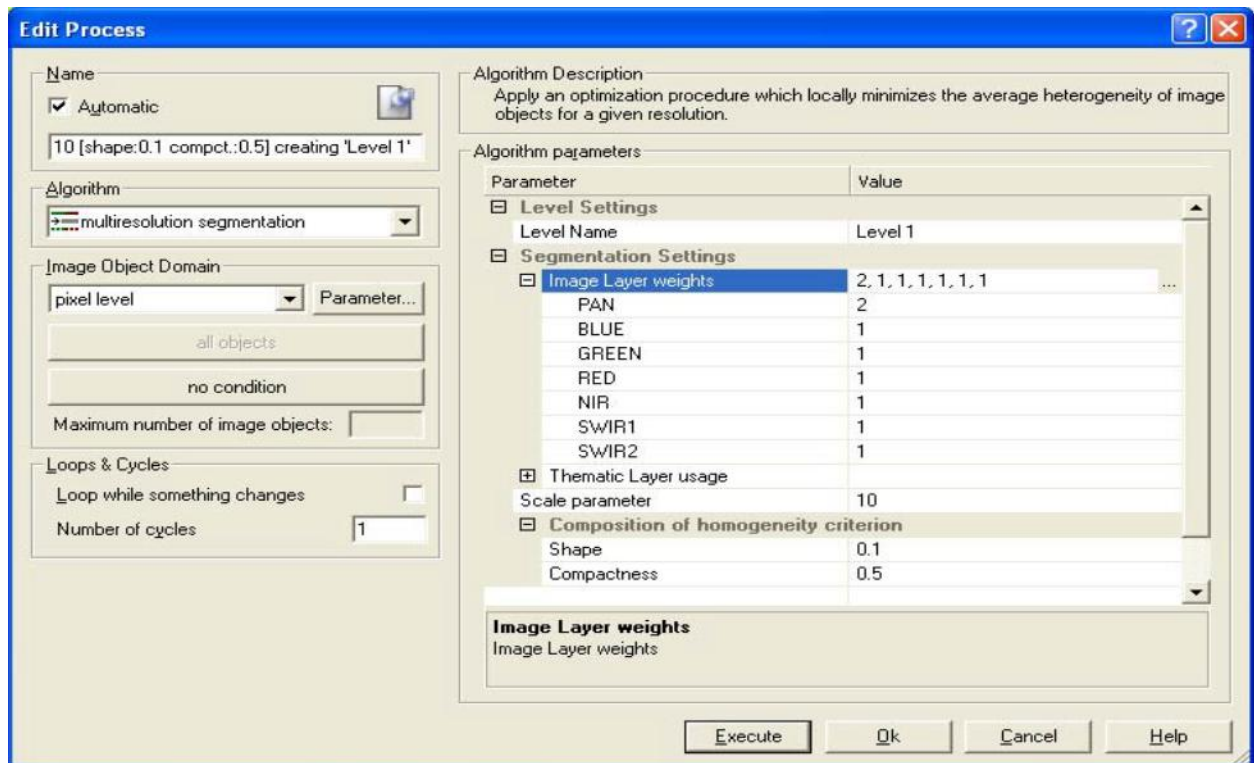


Figure 4.13: Segmentation dialog box showing parameters, (Source: eCognition reference book 2011)

3. Classification: The objective here was to classify the GeoEye image into land cover classes after segmentation. At this state a decision has been made on the land classes which include the following classes: Buildings, Forest, Open surface, Paved roads, Unpaved roads, Rangeland and Water bodies. The rule based method of classification was employed by using feature sets in a rule set including nDSM, NDVI, NDWI etc.

The next stage was to export the result. Usually the classification result is exported from Definiens into a GIS for further processing or the production of a map. To select the classes to export you again edit the Image Object Domain. The name of the outputted shapefile has been defined as 'Classification' while the features to be exported are the area (of the image object) and the class name. Area is found under Object Features > Shape > Generic while class name is found under Class-Related features > Relations to

Classification > Class name. An example of the rulebased process tree will look like figure 4.15.

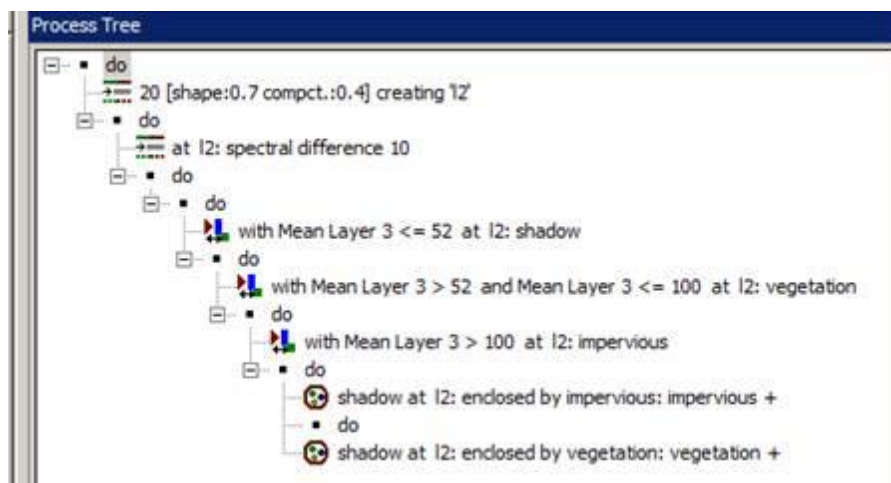


Figure 4.15: Process tree for segmentation, (Source: Kulkarni, 2012)

4.6 Procedure used to achieve Objective Two

4.6.1 Objective two: To statistically compare the results obtained from the two techniques and evaluate the capabilities of the nDSM to optimize the accuracy of urban features extraction.

4.6.2 Research Question2: Does the addition of nDSM from LiDAR datato the VHR image improve the classification accuracy of urban land cover?

The first step was to carry out a similar to OBIA operation in objective one but with the addition of nDSM. Consequently, the statistical evaluation was done byusing kappa statistics and overall accuracy andwhile test of the hypothesiswas used for validation.The kappa coefficient is an effective statistical tool for comparing and analysing two independent experiments. A confusion matrix (or error matrix) is usually used as the quantitative method of characterizing image classification accuracy. The

details of the comparison are shown in chapter five (sub-head 5.10 - 5.12) which contain the results.

Table 4.3: Sample of a Confusion Matrix. Source: Lillesand et al. (2004)

	Residential	Commercial	Wetland	Forest	Water	Row total
Residential	70	5	0	13	0	88
Commercial	3	55	0	0	0	58
Wetland	0	0	99	0	0	99
Forest	0	0	4	37	0	41
Water	0	0	0	0	121	121
Column total	73	60	103	50	121	407

Overall Accuracy = $382/407 = 93.86\%$

Producer's Accuracy (omission error)

Residential = $70/73 = 96\%$ 4% omission error
 Commercial = $55/60 = 92\%$ 8% omission error
 Wetland = $99/103 = 96\%$ 4% omission error
 Forest = $37/50 = 74\%$ 26% omission error
 Water = $20/22 = 100\%$ 0% omission error

User's Accuracy (commission error)

Residential = $70/88 = 80\%$ 20% commission error
 Commercial = $55/58 = 95\%$ 5% commission error
 Wetland = $99/99 = 100\%$ 0% commission error
 Forest = $37/41 = 90\%$ 10% commission error
 Water = $121/121 = 100\%$ 0% commission error

The second part of objective two was achieved by carrying out another OBIA on the VHR but the key difference between this procedure and the earlier OBIA procedure is the addition of nDSM. During rule set build up, nDSM was used to split the resulting image objects into elevated and non-elevated features using a threshold value. The addition of nDSM to the VHR image in the classification was to see the overall effect in the final accuracy.

The MRS was used given its ability to produce meaningful desired objects. The MRS algorithm starts with a single image object of one pixel and repeatedly merges it in several iterations, in pairs, to form larger units, as long as an upper threshold of homogeneity is not exceeded locally. The algorithm uses a scale factor to stop the object from getting too heterogeneous so that homogenous areas result in larger objects and

heterogeneous areas result in smaller objects. After the segmentation, sample classes were selected which were used to train the classifier. The rule set was used for classification into the land cover classes based on the land cover scheme of this research. The classified image was exported to GIS environment for further processing and for map production.

In the context of information extraction by image analysis, accuracy “measures the agreement between a standard assumed to be correct and a classified image of unknown quality.” (Campbell, 2007). Classification error occurs when a pixel (or feature) belonging to one category is assigned to another category. The following errors are put into consideration when carrying of accuracy assessment.

Therefore the accuracy assessment was calculated on the basis of the following measures:

1. Producer’s accuracy: How well a certain area can be classified (omission error)
2. User’s accuracy: Reliability, probability a pixel class on the map represents the category on the ground (commission error)
3. Overall accuracy: Dividing the total number of correct pixels (diagonal) by the total number of pixels in the error matrix.
4. Kappa: Measure of agreement between the classified map and the reference data. This agreement is based on the major diagonal of the error matrix and a chance agreement (row and column values). Strong agreement occurs if the 'k' is greater than 0.80.

Moderate agreement occurs when 'k' values fall between 0.4 and 0.8 and poor agreement occurs with 'k' values less than 0.40 (Jensen, 2005).

4.6.3 Procedure in Accuracy assessment

1. The Create Random Point, the Tool in the Data Management Tools of Arc Toolbox was used to generate random points using the classified images as Constraining Features. The result is a shape file of the location of points to be used for accuracy assessment
2. The generated points were overlaid on the VHR image and each point was assigned its true classification using visual analysis. The value was input into the attribute table of the generated points. The result is a shape file layer containing the True Land use of each point.
3. The Extract Value to Points tool in the Spatial Analyst Tools of Arc Toolbox was then used to extract the values classified for each point on the classified image. The result is a table containing the reference Value (Land use) vs Classified Value (Land use)
4. The Create Pivot Table was then used to convert the reference vs classified table into a matrix. The result is a matrix representation of reference value vs classified Value
5. The values in the matrix were entered into an Excel worksheet from which the various calculations of producer accuracy, user accuracy, overall accuracy and kappa statistics was done.

Summary of accuracy results are shown in section 5.10.1 while the error matrix tables and tables of quantitative values of the classified LC/LU are shown in Appendix 7 and Appendix 8 respectively.

4.7 Procedure Adopted in Achieving Objective Three

Objective Three: To combine the GeoEye-1 image and nDSM from LiDAR in the 3-D analysis of the study area.

4.7.1 Research Question 3: Does the addition of LiDAR derived nDSM to the VHR image effective in the 3-D analysis of features extracted?

3-D dimensional representation of geographic information in computers is known as Virtual Geographic Environment (VGE). To achieve the objective, the 3D visualization of the study area was done in the 3D environment of ArcScene. The Geoeye subset was added to the interface and subsequently the Layer properties were used to set the height value of the cells in the Geoeye subset from the elevations in the nDSM to define how the Geoeye subset will be displayed in 3D. In order to enhance the view, the vertical exaggeration, illumination azimuth and illumination elevation were adjusted. Results are presented as **figures 5.52b, 5.53-5.58 on pages 252 to 255.**

A similar operation was carried out for Akabuka subset but without the addition of the LiDAR derived nDSM so as to answer research question three. The result which is now displayed as 2-D representation, **figure 5.52a on page 252** together with the Akabuka 3-D result, showed a great difference in their VGE. 3-D models provide better ways to represent, understand, manage and communicate our natural world.

4.8 Procedure used in Achieving Objective Four

4.8.1 Objective Four: To develop a technique for the extraction of unpaved roads

After careful study of the rulesets developed for the extraction of various land cover types for the study area, there was need to refine the extracted unpaved roads. Consequently, an algorithm for the extraction of unpaved roads which has been successfully tested on all seven sites was developed as:

Unpaved Road = $\rho_{ndvi} < 0$ AND $\rho_{intensity} > 0.5$ AND $\rho_{asymmetry} > 0.85$ AND $\rho_{ndsm} < 2m$ AND $\rho_{nir} > 100$

Where;

ρ_{ndvi} is the mean normalized vegetation index of features on the imagery. Unpaved roads exhibit the characteristics of non-vegetated areas whose ndvi values are less than 0

$\rho_{intensity}$ is the Intensity Colour Space components of features on the imagery.

Unpaved roads comprise sand that appears bright in terms of colour.

$\rho_{asymmetry}$ is the degree of linearity of image features on a scale of 0-1. Unpaved roads are curvilinear manmade structures.

ρ_{ndsm} describes the relative surface height of features. Unpaved roads are low features.

ρ_{nir} is the mean reflectance of features on the imagery on a scale of 0-255. Sandy soils increase the radiance emergent from roads in the near infrared proportion of the electromagnetic spectrum.

The 5 parameters altogether form a spectral, spatial, colour and signature for detecting unpaved roads.

4.8.2 Procedure

In order to improve the accuracy of the extraction of unpaved roads, first the vegetation coverage in the images was masked out from the original VHR image through logical queries with the NDVI threshold of vegetation ($NDVI > 0$). The Extract by Attributes tool (see figure 4.18) and the Extract by Mask tool (see figure 4.19) in the Spatial Analyst Toolbox of ArcGIS 10.3 were used to achieve this. This was done in order to improve the segmentation process by reducing the homogeneity present in the image, and hence delimit better image objects shapes. The remaining pixels in the image correspond to the non-vegetated surface which contains unpaved roads. The research resorted to the use of ArcGIS for this operation because eCognition does not provide for a way to produce a new image layer from an existing image using a set of image properties. The respective steps are as follows:

4.8.1.1 Produce the NDVI image using the Raster Calculator Tool

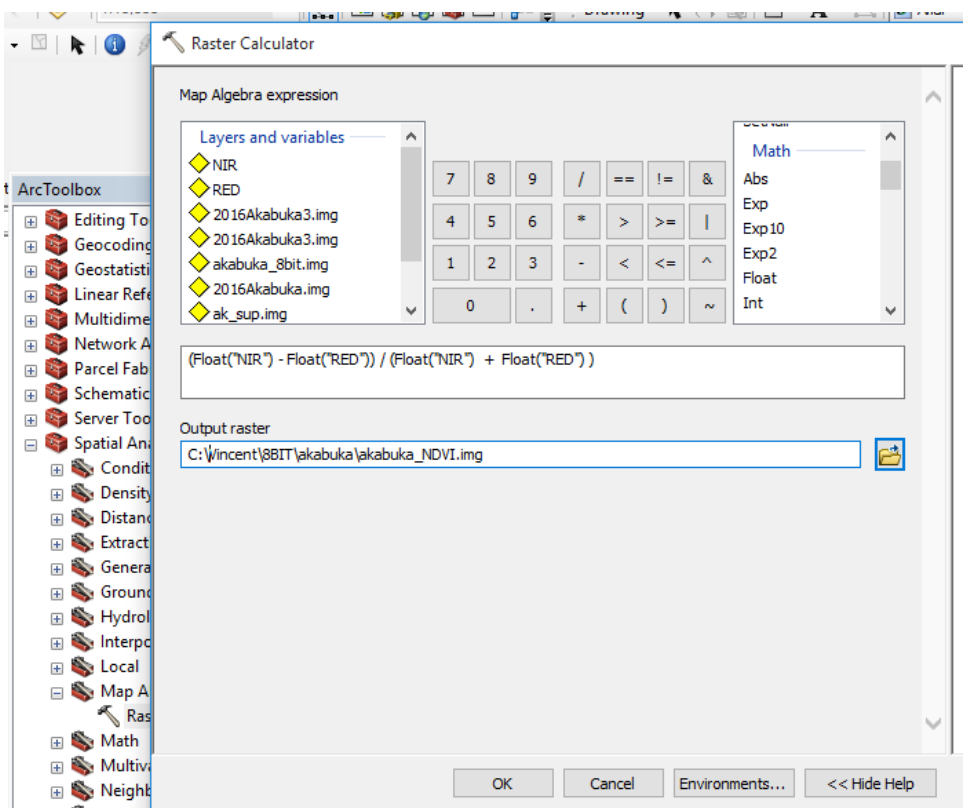


Figure 4.16: Raster Calculator Tool in ArcGIS

Similar operation was carried out for all seven subsets and figure 4.17 is for Akabuka subset where the resulting NDVI image was classified into -1 – 0 and 0 -1 indicating non-vegetated and vegetated areas.

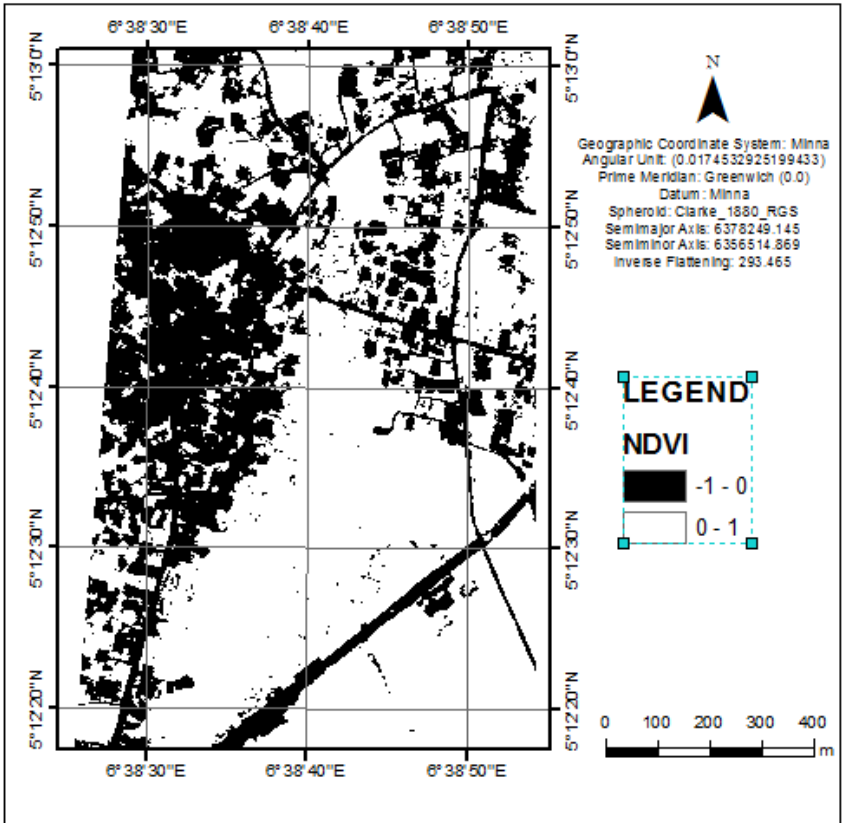


Figure 4.17: Akabuka NDVI Image

4.8.1.2. The extract by attribute tool

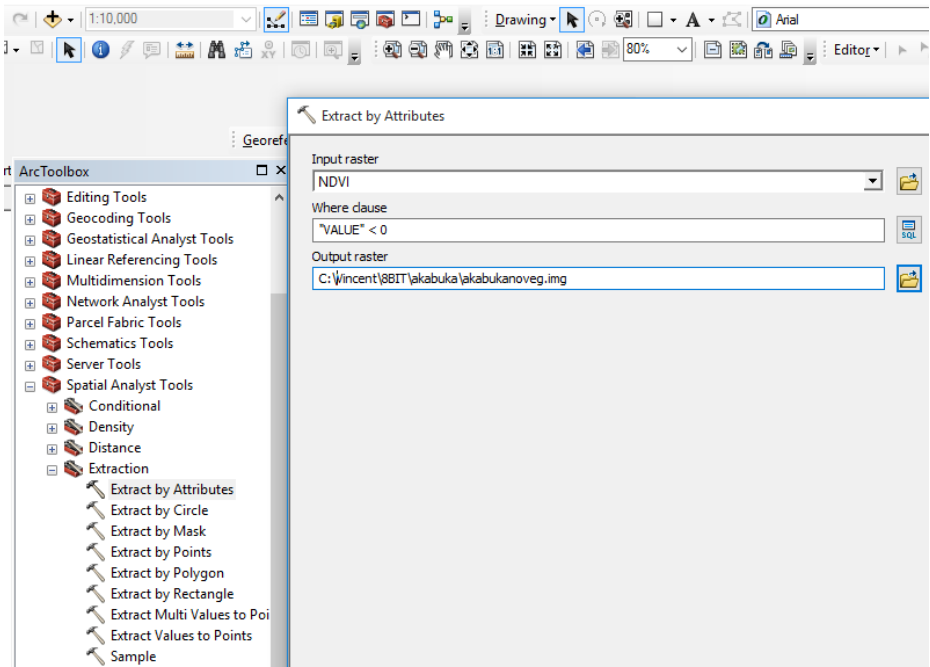


Figure 4.18: Extract by Attribute interface

4.8.1.3. The extract by mask tool

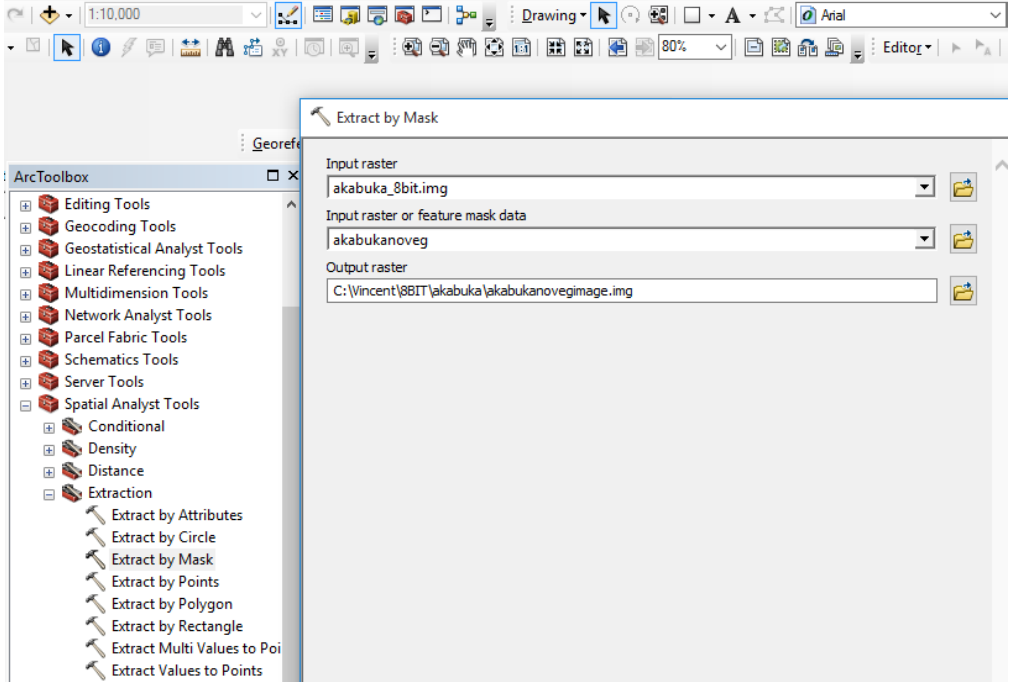


Figure 4.19: Extract by Mask Interface

4.8.1.4. The resulting image

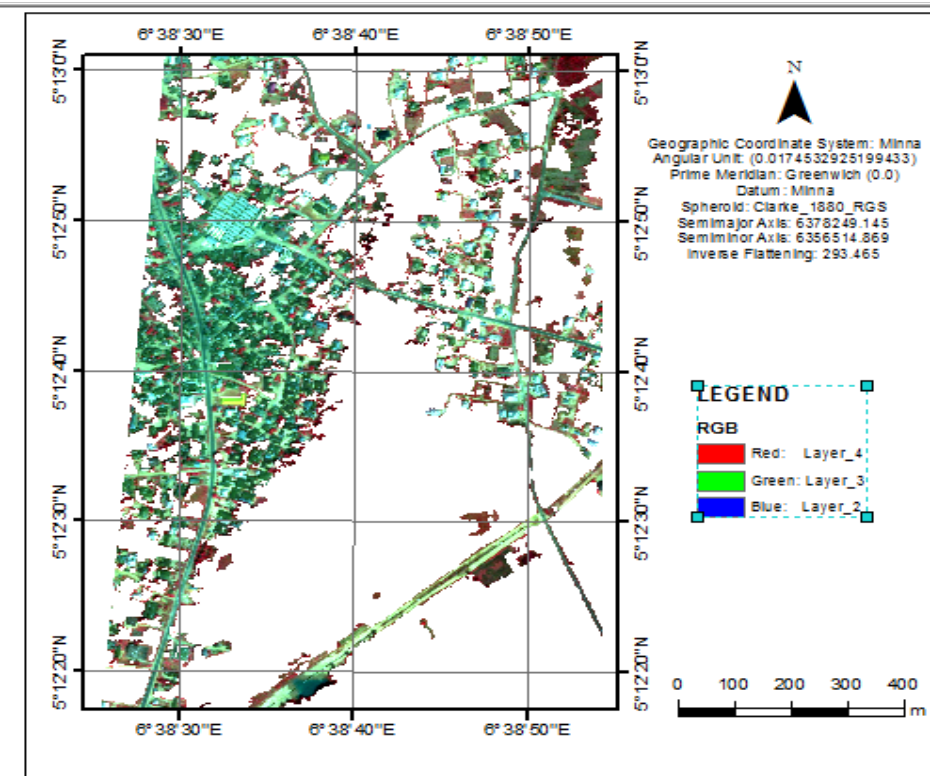


Figure 4.20: The resulting Image

4.8.1.5 Segmentation and Classification in eCognition

Afterwards, the resulting image was subjected to multi-resolution segmentation and the algorithm was implemented in the ruleset. A user defined segmentation parameters for optimal result was set as scale 20, shape 0.1 and compactness 0.8 (See figure 4.21). The segmentation process produced the segmented image in figure 4.22. This was classified using the new algorithm to produce the refined unpaved road maps presented as figures 5.44- 5.50 in the result section 5.6of chapter five(5).

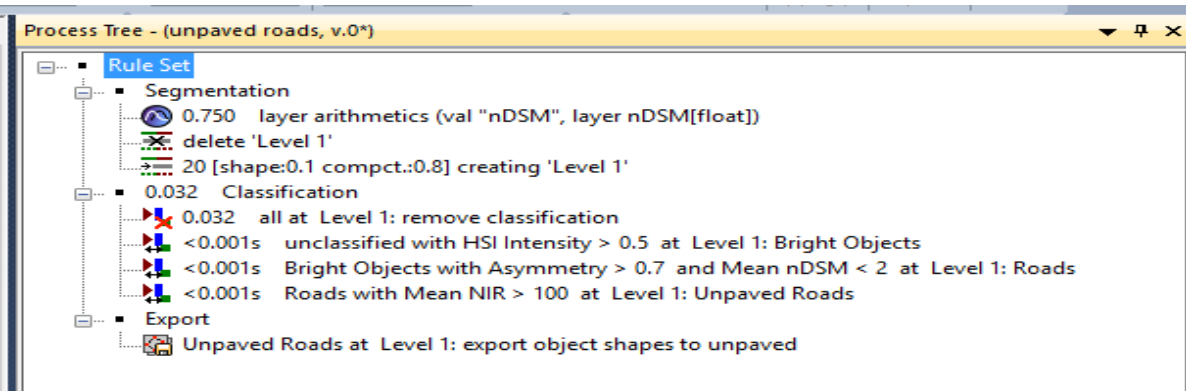


Figure 4.21: Unpaved roads Refinement Ruleset used for all subsets

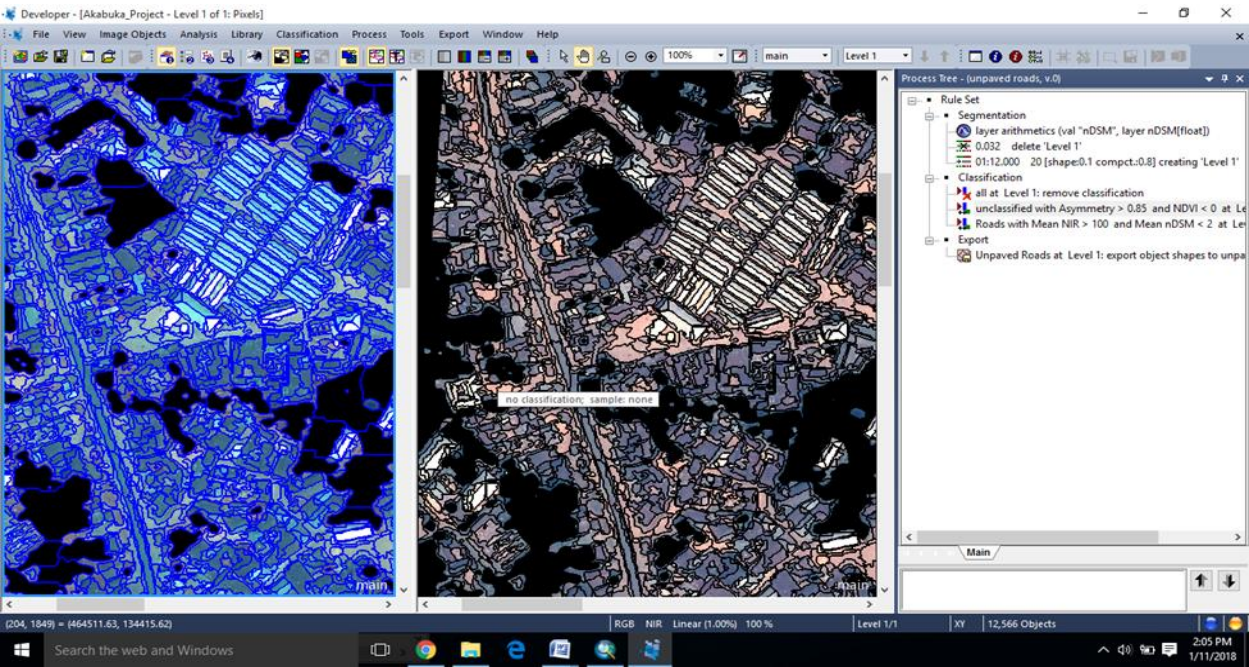


Figure 4.22: Akabuka Segmented Image

4.9 Procedure Used to Achieve Objective Five

Objective four: To produce an up-to-date map of the study sites.

Bearing in mind that the LiDAR and VHR image data available for this data date back to 2012, so there was need to update the map produced from the analyses so as to represent the current realities on ground as much as possible. Consequently, the latest satellite image available on Google map of the study area (see Appendix 6) and ground truth point data (see Appendix 5) collected from the study area were used to update the map.

A visit to the ministry of works and housing was useful in gathering some information for this purpose.

4.9.1 Procedure for Map Update using available satellite image on Google

1. The satellite imagery used for the update was saved as a JPEG Format from Google Earth.
2. The satellite imagery was then georeferenced using the 2012 Geoeye image through image-image georeferencing
3. The classified images exported as Vector Shapefiles from eCognition was loaded on ArcMap interface
4. The classified image was then compared with the Google Earth image to identify areas where there are changes.
5. Areas where there are changes were then digitized using the Editor Tool by placing markers around the newly identified features.
6. The following procedure was then followed using Microsoft Excel 2007 software to format the GPS coordinates of features collected from the field.
 - a. Formatting the GPS data into 4 columns namely: S/N, longitude, latitude and Description.
 - b. Saving the document to *.XLSX format
7. The field data was imported to ArcMap by following this procedure:

- a. Navigation to where the excel file was stored and adding it to the software interface.
 - b. Selection of the coordinate system of the field data.
 - c. Saving of the field data permanently as an ESRI Shapefile format
8. Markers were placed around the field data using the Editor Tool to digitize the surveyed features into the respective land use layer. The final updated map is presented on page 257 as figure 5.61a placed side by side with the old map shown as figure 5.61b.

4.10 Conclusion

Objective ‘one’ was carried out to verify the advantage of OBIA classification method over the traditional pixel method in classifying VHR images. The integration of the LiDAR derived nDSM into the classification was to evaluate its capability to optimize the classification accuracy. The idea as stated earlier is to evaluate the advantage gained by introducing the height component (nDSM) from the LiDAR data into the classification.

CHAPTER FIVE

DATA ANALYSIS, RESULTS AND DISCUSSION

5.0 Introduction

This section reports on the data analysis undertaken to achieve the objectives, the various results and the discussion following the results. For the key objective, three independent analyses were carried out. The first is the pixel based classification of VHR in Erdas Imagine 9.2, the Object based classification of VHR in the eCognition software

and finally the Object based classification of VHR with the addition of the nDSM as ancillary data from the LiDAR data. At the end the results were compared in other to answer the relevant research questions research questions. Seven subsets were mapped out from the study area for analysis and they include – Akabuka, Egbeda, Ikiri, Obido, Ogbogwu, Omoku and Osiakpu. The land cover types to classify were also consistently outlined for the three classification methods so that a basis for comparison could be created. The selected classes were Buildings, Forest, Rangeland, Paved roads, Unpaved roads, Water, Bare land and Shadow.

5.1 Pixel Based Supervised Classification in Erdas 9.2 Software

Supervised Maximum Likelihood Classifier (MLC) classification was carried out in all the subsets. The first stage in a supervised classification process is to collect reference training sites for each land cover type in order to generate training signatures. These signatures were generated using the Area of Interest (AOI) and Region Grow tools. These signature files were subsequently used as inputs to a MLC. If a pixel satisfies a certain set of criteria, then the pixel is assigned to the class that corresponds to those criteria.

The approach involved was in the following sequence. The seven subsets from the study area were in turn imported into ERDAS 9.2 colour composite operations were performed using red for near infra-red band, green for the red band and blue for the green band (RGB 4/3/2). The properties of the band are so described in the table below.

Table 5.1: Properties of Bands

Band	Properties
Band 2: 0.52 – 0.60µm (green)	This band corresponds to the green

	reflectance of healthy vegetation and it occupies the region between the blue and red chlorophyll absorption bands
Band 3: 0.63 – 0.69µm (red)	This red chlorophyll absorption band of healthy green vegetation is one of the most important bands for vegetation discrimination. In addition, it is useful for soil-boundary and geological boundary mapping.
Band 4: 0.76 – 0.90µm (near infrared)	This band is especially responsive to the amount of vegetation biomass present in a scene. It is useful for identification of vegetation types, and emphasizes soil-crop and land-water contrasts

Source: Jensen, (2004

This False Colour Composite (FCC) for all study sites was used to create the classified image. The Anderson et al. (1976) classification scheme was employed in this exercise to classify the GeoEye subsets into Buildings, Forest, Rangeland, Paved roads, Unpaved roads, Water, Bare land and Shadow.

Reference training sites were collected for each land cover type in order to generate training signatures by using the Area of Interest (AOI) and Region Grow tools. From the AOI tool palette, select the ‘create polygon AOI icon’. The cursor is used to digitize and create the sample of the particular class for the classifier. This procedure was used to collect as many samples as possible for each land cover class. This resulted in the dialog box which contained a cell Array of created signatures as can be seen for Akabuka subset in figure 5.1

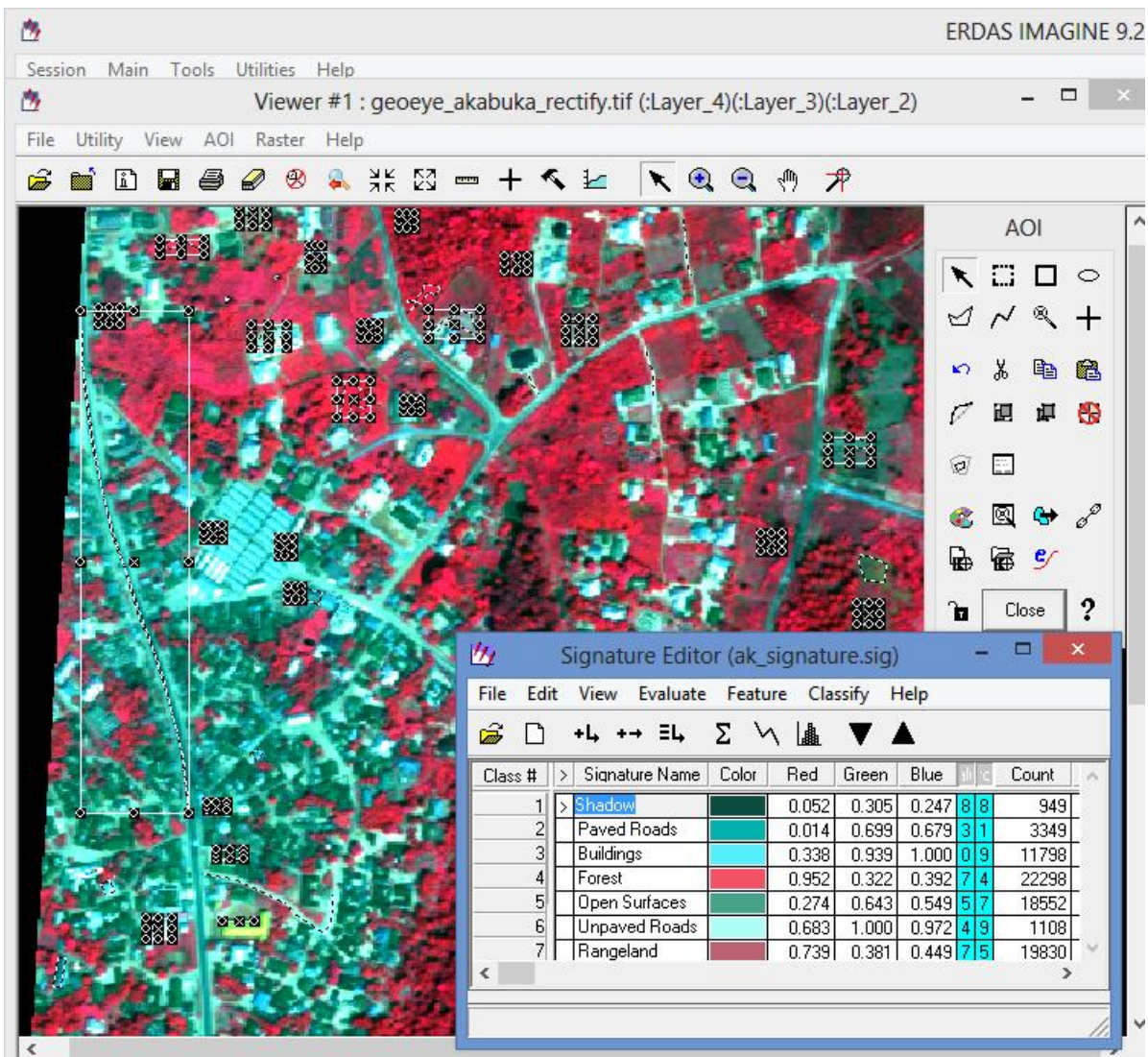


Figure 5.1: Akabuka created classes in signature editor.

After the creation of the samples for the various land classes, from the Signature Editor Menu Bar select File/Save, name the signature created (Akabuka.sig) and click ok.

From the Signature Editor Menu bar, select Classify/Supervised then enter the Input Raster File and the Input Signature File. For the Output Classified File, Akabuka_super.img was entered. Maximum likelihood algorithm was used as the classification technique. Select Maximum Likelihood and click ok and after the process, click ok again. To recode the new Akabuka_super.img image use Image Interpreter|GIS

Analysis|Recode. This process will combine same types of land use into a single one, for example, water 1 and water 2 should be combined to form water. This operation will create an output image in the viewer which appropriate colours were assigned. Finally, the classified images are converted to vector and exported to ArcGIS 10.3 for further processing.

5.2 Presentation of Supervised Classification Results

The results of the supervised classification of the respective seven subsets of the study area are presented below as figures 5.2 – 5.8 in the following order, Akabuka, Egbeda, Ikiri, Obido, Ogbogwu, Omoku and Osiakpu.

The accuracy assessment which has been calculated using error matrix is presented in section 5.7. Specifically, the accuracy assessment summary of pixel based method has been presented in table 5.11a on page 266.

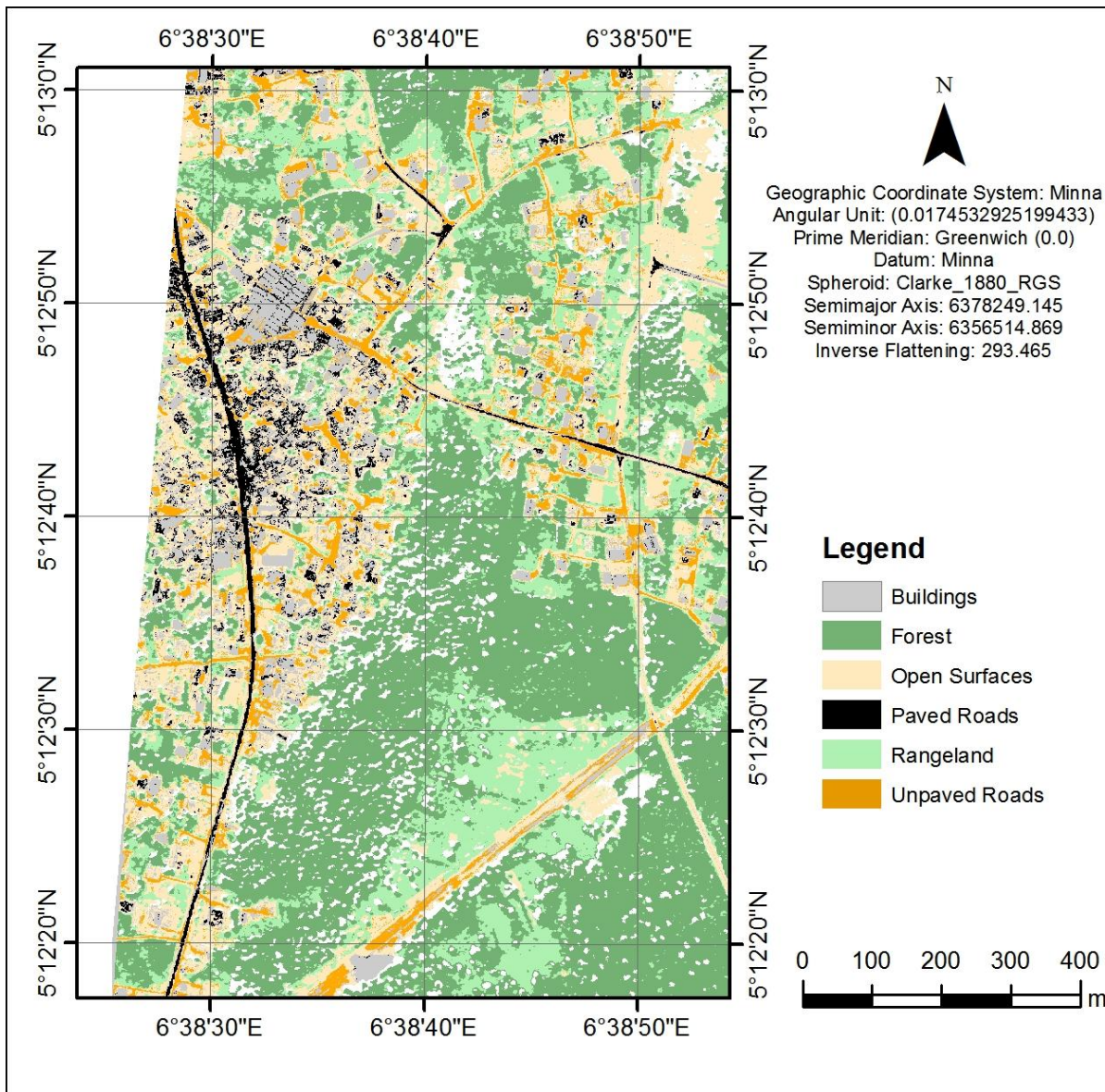


Figure5.2: Akabuka Supervised Classification Map

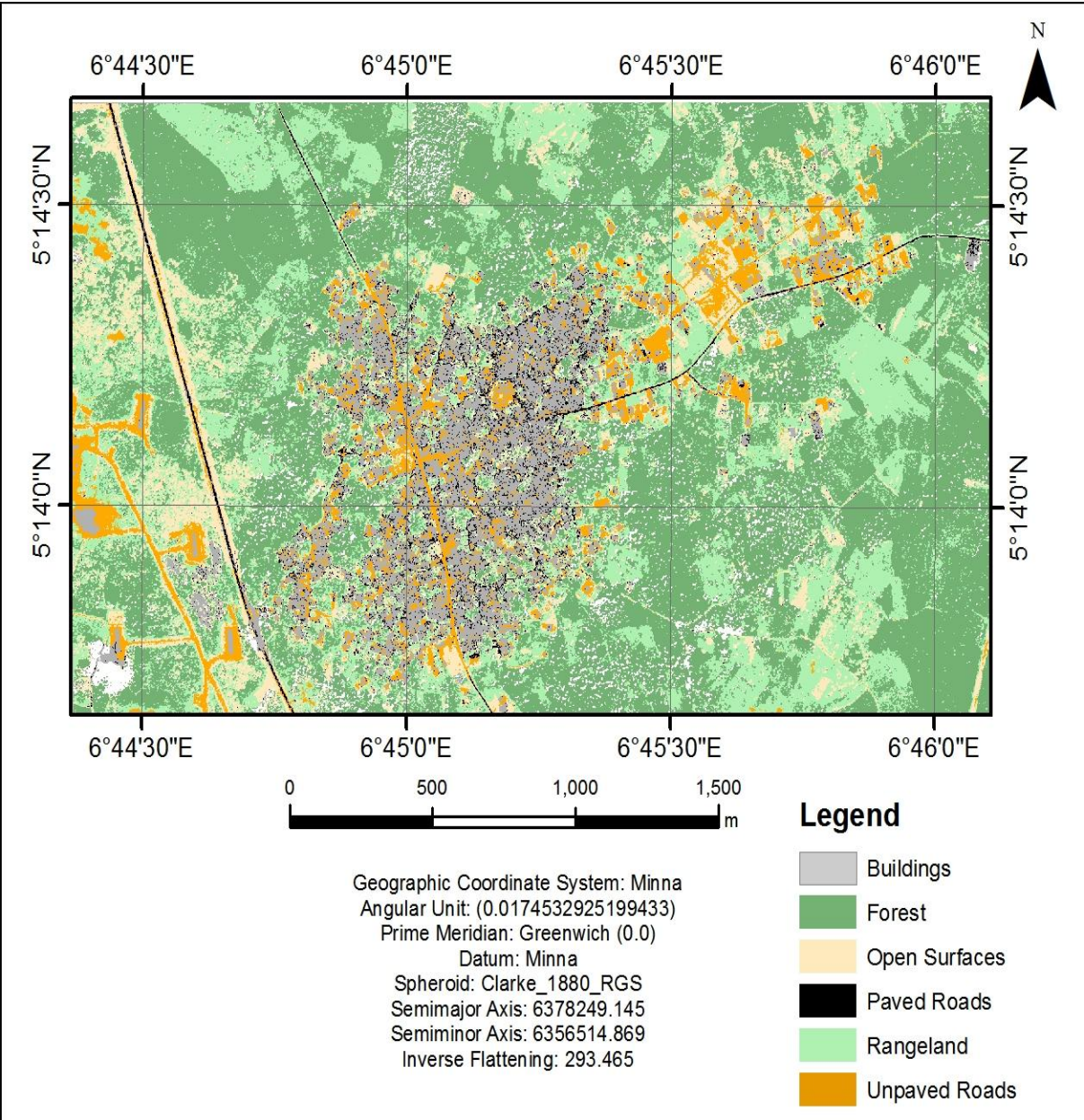


Figure 5.3: Egbeda Supervised Classification Map

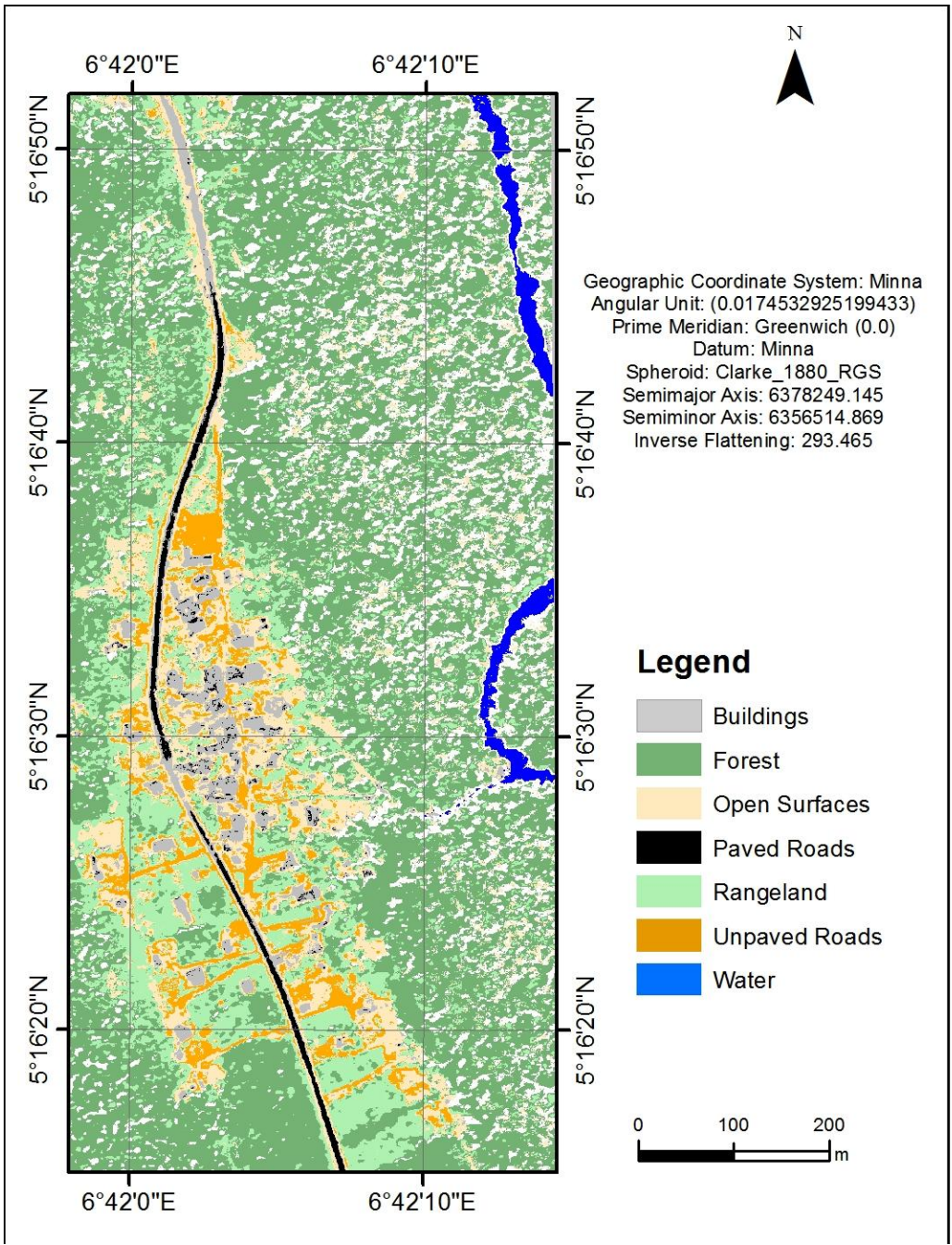


Figure 5.4: Ikiri Supervised Classification Map

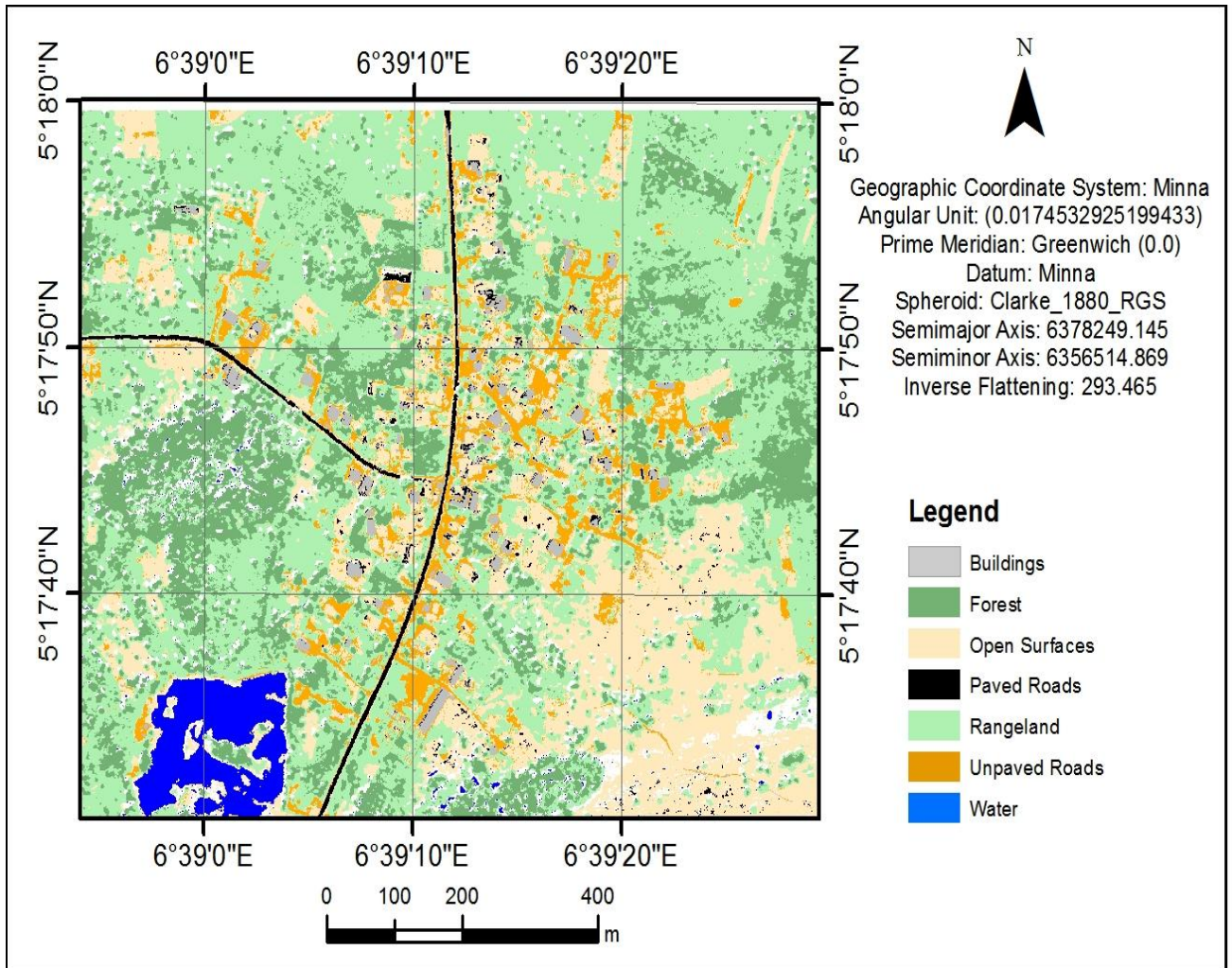


Figure 5.5: Obido Supervised Classification Map

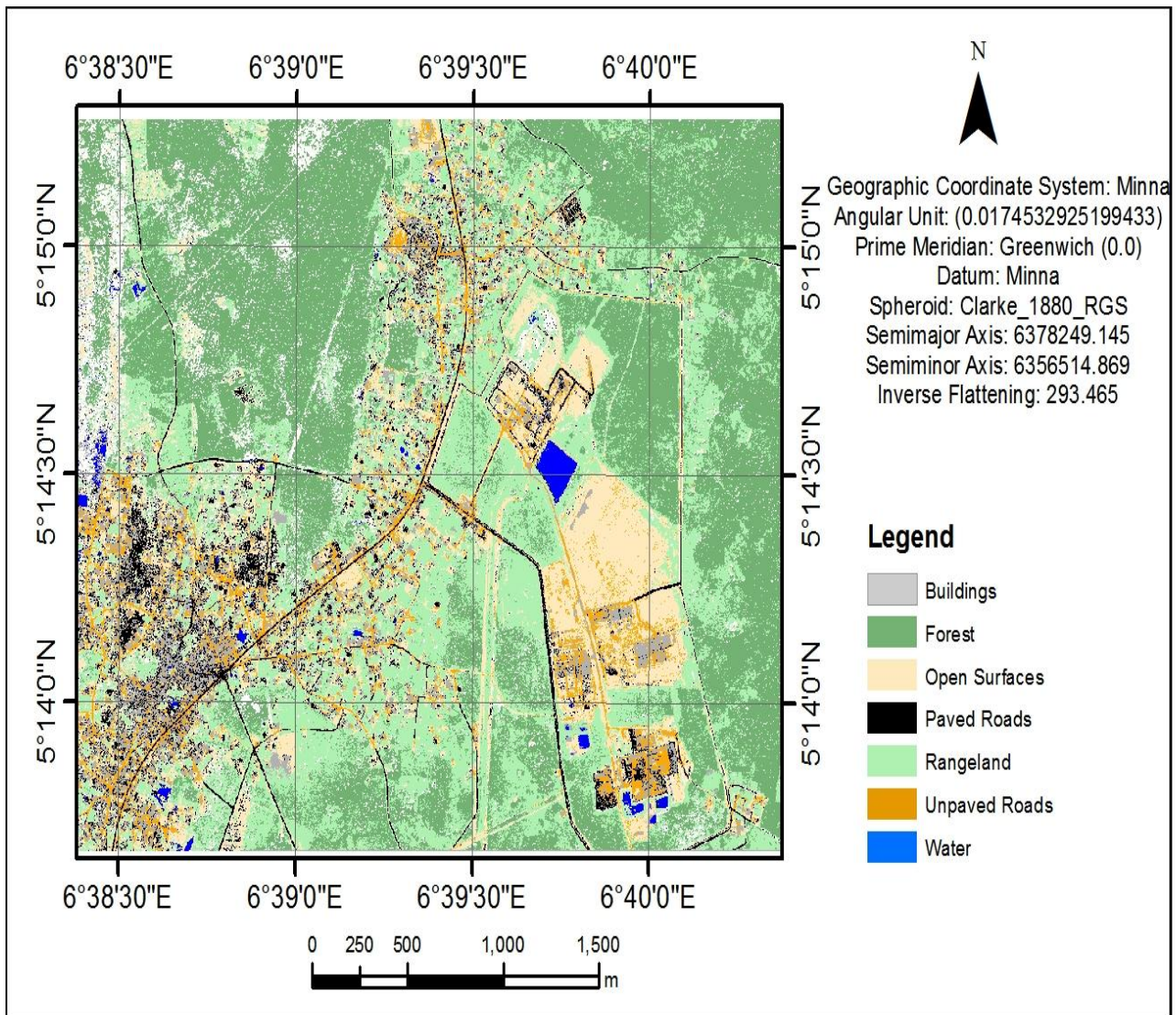


Figure 5.6: Ogbogwu Supervised Classification Map

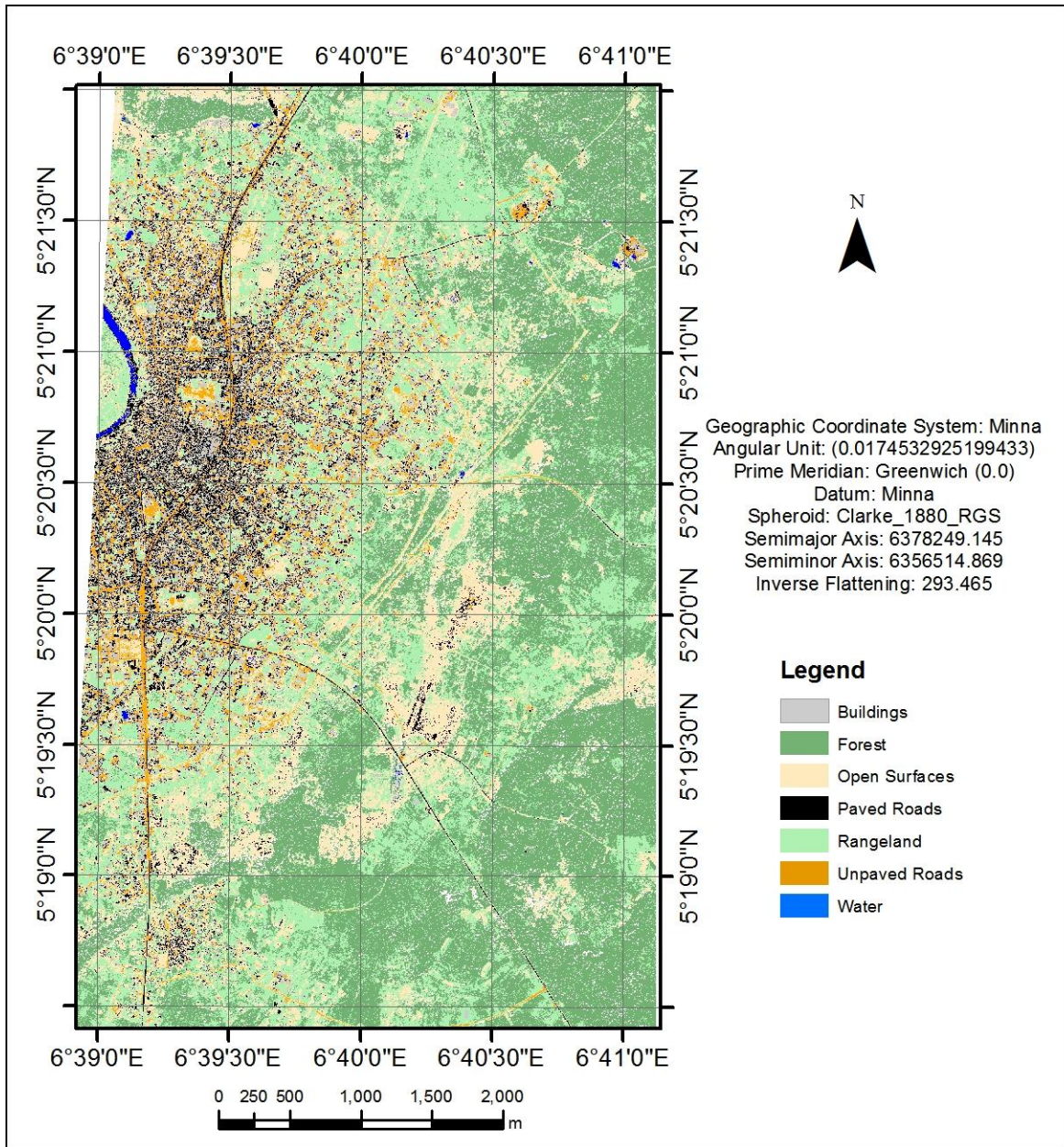


Figure 5.7: Omoku Supervised Classification Map

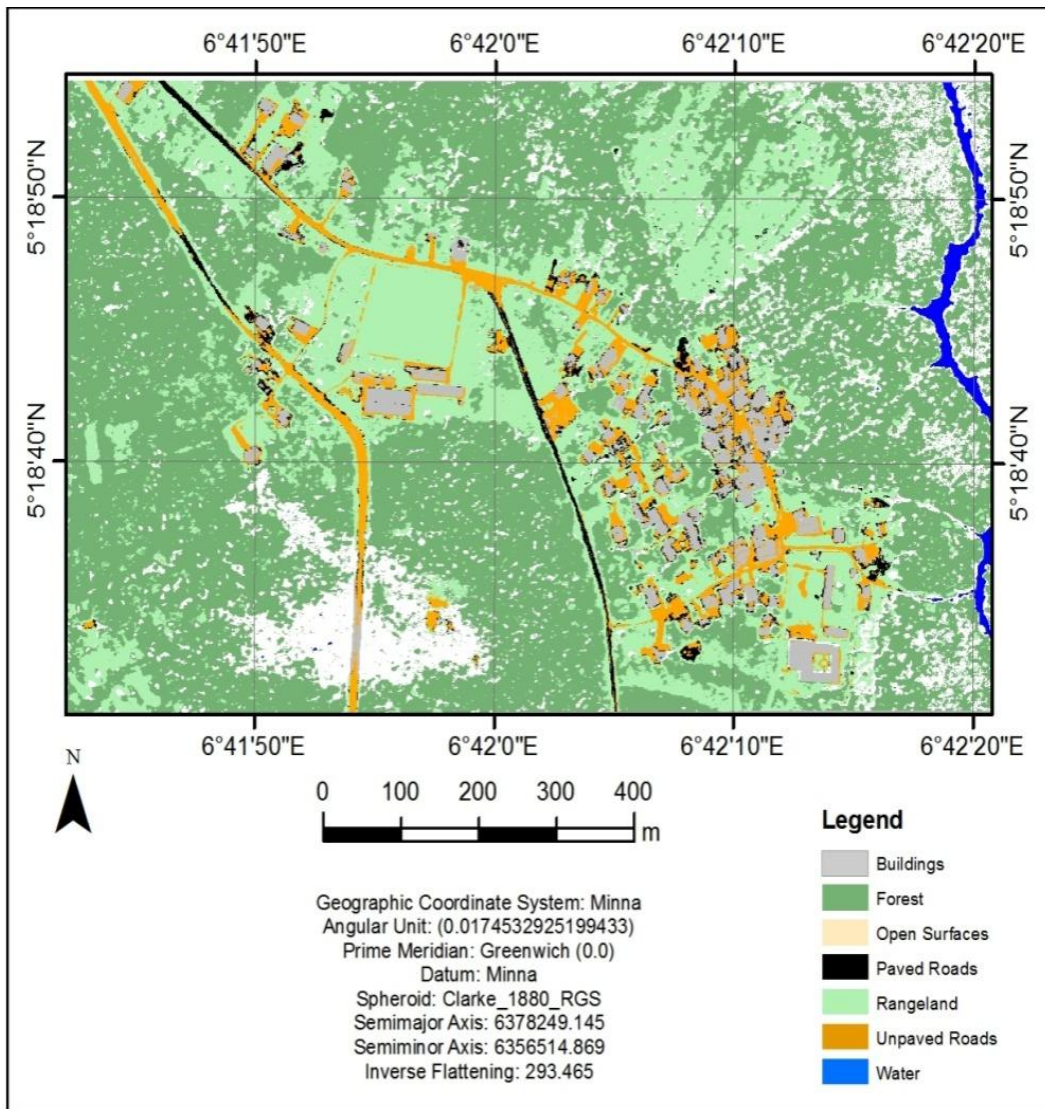


Figure 5.8: Osiakpu Supervised Classification in Erdas

5.3 OBIA of VHR in eCognition 9.0 Developer Software

The seven subsets from the study area were analyzed using the Object based method in eCognition environment on the basis of the same land cover scheme classified in supervised pixel based method. The general procedure involves generating image object primitives or segments using the spectral and contextual information to achieve optimal homogeneity of the segments. The Multiresolution segmentation as implemented in the eCognition software was used. This algorithm locally minimizes the average heterogeneity of image objects and maximizes their respective homogeneity for a given variance threshold of image objects (eCognition, 2014). This required the input of scale, shape and compactness parameters and the optimal values were achieved through trial and error and visual inspection, see table 5.2. The shape factor adjusts spectral homogeneity versus shape of objects, whereas the compactness factor balancing the compactness and smoothness determines the object shape between smooth boundaries and compact edges. The color/shape and the compactness/smoothness parameters are together known as homogeneity criterion (eCognition Reference Book, 2011). The scale parameter limits the maximum heterogeneity for combining adjoining image objects (eCognition Reference Book, 2011).

The scale parameter is an abstract value to determine the maximum possible change of heterogeneity caused by fusing several objects. It controls the object size to user's requirement and it's considered the most crucial parameter of image segmentation. "There is no consistent means to establish if a given segmentation is appropriate or more correct than another due to a lack of a formal and accepted conceptual foundation to support the belief that a segmentation-derived object is an understandable

representation of a structural or functional unit of the landscape’’ (Lein 2011: 11). This study therefore used the visual and subjective qualitative method to assess the specific arrangement of objects and how well they represent the target feature. Care was taken during the segmentation in order to avoid over segmentation or under segmentation. In implementing the ruleset, image feature descriptive characteristics of spectral, textural, structural and shape were used with threshold values for the classification. By visually interpreting different image segmentation results, scale parameters were chosen to create local homogeneity and to keep global heterogeneity. Similarly, a ratio of smoothness to compactness weight was defined for each of the subsets. Table 5.2 contains the various segmentation parameters used for the respective study sites.

The nDSM from LiDAR really helps in separating the tall features from the short features and the RGB values from the VHR image offer excellent visual and spectral analysis.

Table 5.2: Segmentation parameters

Study Sites	Scale	Shape	Compactness
Akabuka	50	0.1	0.8
Egbeda	50	0.1	0.8
Ikiri	50	0.1	0.8
Obido	35	0.1	0.8
Ogbogu	35	0.1	0.8
Omoku	80	0.1	0.8
Osiakpu	35	0.1	0.8

Table 5.3 contains a range of selected object features used in the rule set classification process. From the table it can be seen that the nDSM which is an ancillary data derived from LiDAR was not added to the first OBIA which used only the VHR image for the classification. LiDAR data was crucial to separate features with different elevation values, especially for the non-vegetated features.

Table 5.3: Feature sets used in the rule set classification

Land use	VHR only	VHR and nDSM
Built-up	NDVI < 0 and Rectangular Fit > 0.3	Height > 2, Rectangular Fit > 0.3 and NDVI < -0.5
Open Surface	NDVI < 0 and Asymetry < 0.6	Height < 2, Assymetry < 0.8 and NDVI < 0
Paved Roads	NDVI < 0, Mean NIR < 100 and Asymetry > 0.6	Height < 2, Assymetry > 0.8, NDVI < 0, NIR < 70
Unpaved Roads	NDVI < 0, Mean NIR > 100 and Asymetry > 0.6	Height < 2, Assymetry > 0.8, NDVI < 0, NIR > 70
Water	NDWI > 0.5 and NDVI < 0	Height < 2 and NDWI > 0.9
Rangeland	NDVI > 0 and < 0.3	Height < 2 and NDVI > 0 and < 0.5
Forest	NDVI > 0.3	Height > 2 and NDVI > 0.5
Shadow	Adjacent NIR = 1 and Mean BLUE/Image BLUE < 1	Adjacent NIR = 1 and Mean BLUE/Image BLUE < 1

eCognition contains one algorithm called the assign class algorithm, it is an algorithm of assigning classes using rules, giving conditions and unique values for each classes, somewhat making a decision tree or a rule-based feature separation. For example, NDVI was most important for differentiating trees from buildings. Similarly, brightness was used to classify shadow, whereas NDWI was used to differentiate water bodies and impervious surfaces. nDSM, was used to differentiate between high and low features. Additionally, the features length/width, border to, distance to, and texture were used. The respective thresholds applied are shown in the process trees.

In this research, shadows were classified by selecting objects whose Near Infrared Reflectance are the reverse of objects that share borders with it and objects whose Blue reflectance to the image scene are very low. The remaining objects were classified into vegetated objects and non-vegetated objects using NDVI threshold value. Non-vegetated objects with very high water index are classified as water using NDWI. Furthermore, non-vegetated objects with high linearity are classified as Roads objects, which were subsequently classified into Paved Roads that have very low Near Infra-Red reflectance compared to Unpaved Roads. Non-vegetated objects that have well defined boundaries are classified as Buildings while vegetated objects with very high vegetation index are classified as Forest. Finally, the rest of the non-vegetated objects that do not fall in the category Buildings, Roads and Water are classified as Open Surfaces while vegetated objects with lower vegetation index are classified as rangeland.

The segmentation and classification processes (see figures 5.9 – 5.22) from the OBIA technique eCognition screen using only VHR image are presented. Finally, the resulting classified maps for all seven subsets are also displayed as figures 5.23- 5.29.

The accuracy assessment which has been calculated using error matrix is presented in section 5.7. Specifically, the accuracy assessment summary of OBIA method using only the VHR image has been presented in Appendix 7.

5.3.1 Akabuka OBIA Classification Ruleset using VHRimage only.

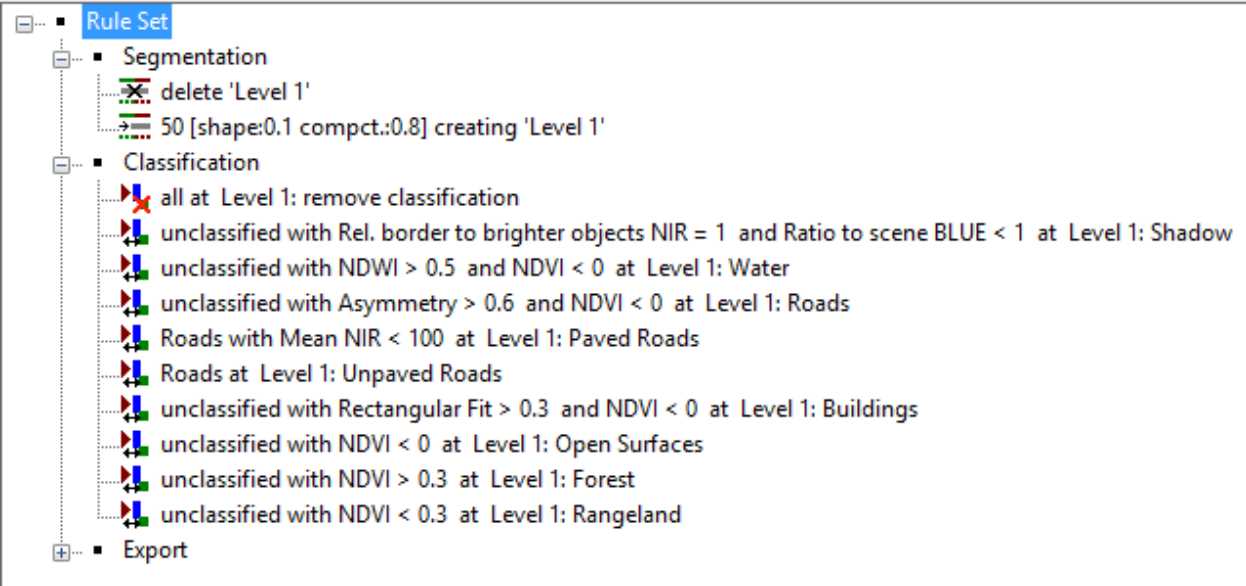


Figure 5.9: Akabuka segmentation parameter and classification ruleset



Figure 5.10 a: Akabuka VHR Image

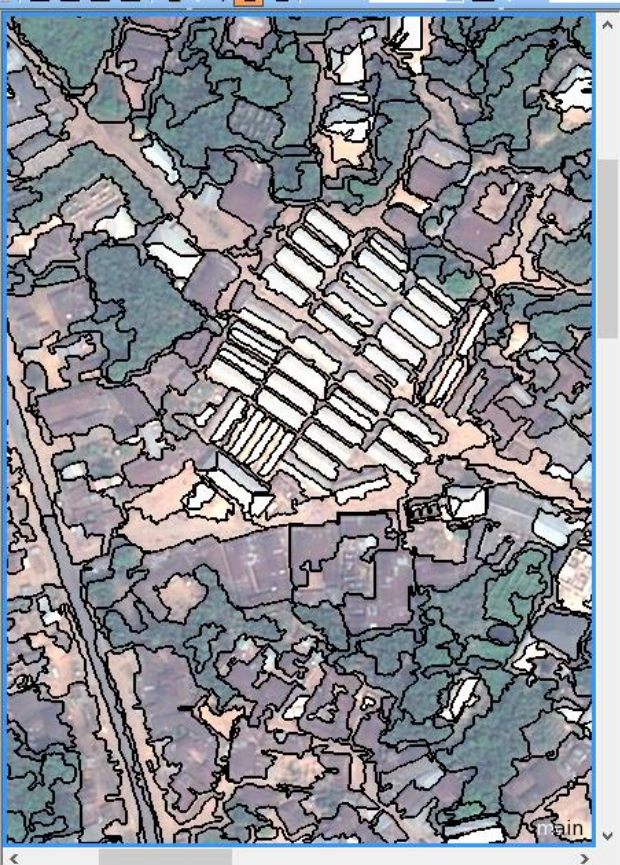


Figure5.10b: Akabuka Segmented Image

5.3.2 EgbedaOBIAClassification Rulesetusing VHR image only

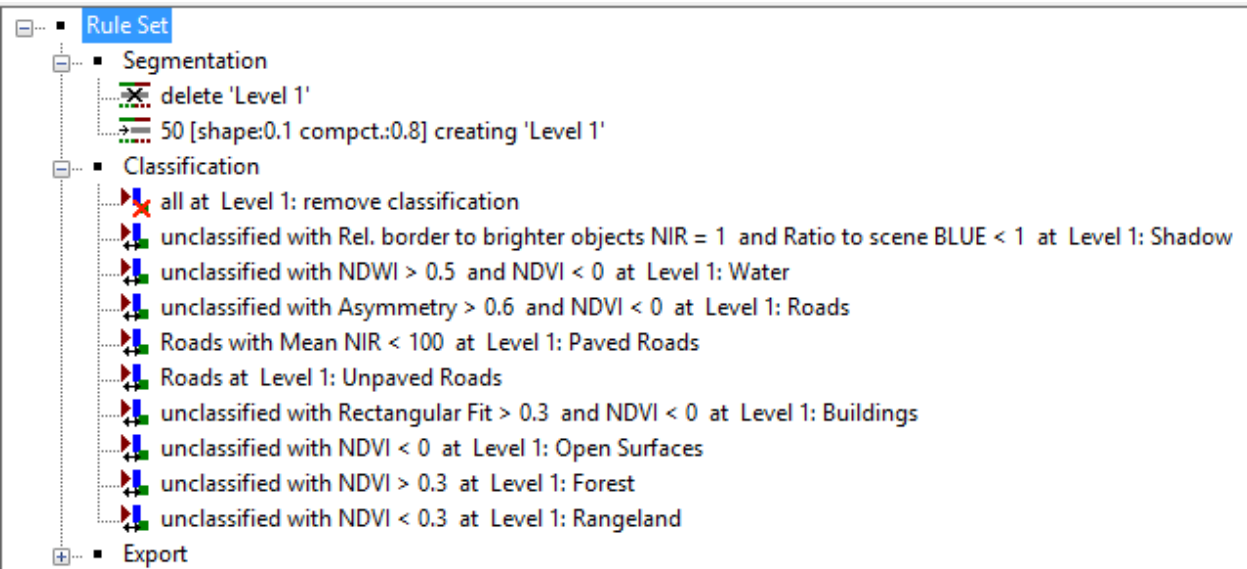


Figure 5.11: Egbedasegmentation parameter and classification ruleset



Figure 5.12 a: Egbeda image



Figure 5.12b: Egbeda segmented image

5.3.3 Ikiri OBIA Classification ruleset using VHR image only

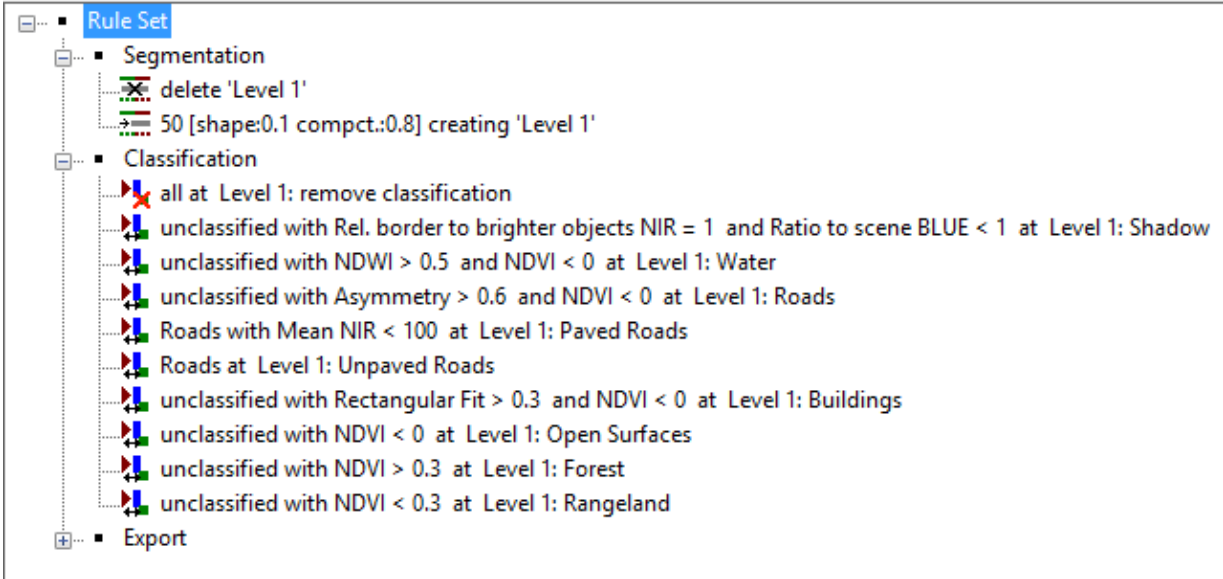


Figure 5.13: Ikiri segmentation parameter and classification ruleset



Figure 5.14 a: Ikiri subset image



Figure 5.14b: Ikiri Segmented image

5.3.4 Obido OBIA Classification Ruleset using VHR image only

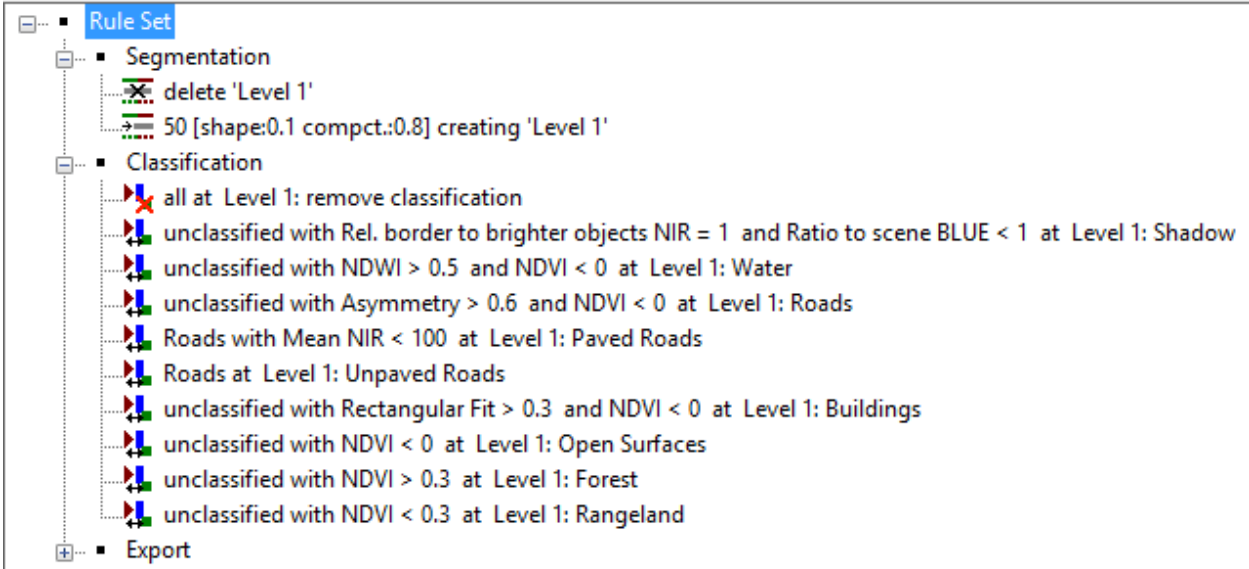


Figure 5.15: Obido segmentation parameter and classification ruleset



Figure 5.16 a: Obido subset image



Figure 5.16b: Obido Segmented image

5.3.5 Ogbogu OBIA Classification Ruleset using VHR image only

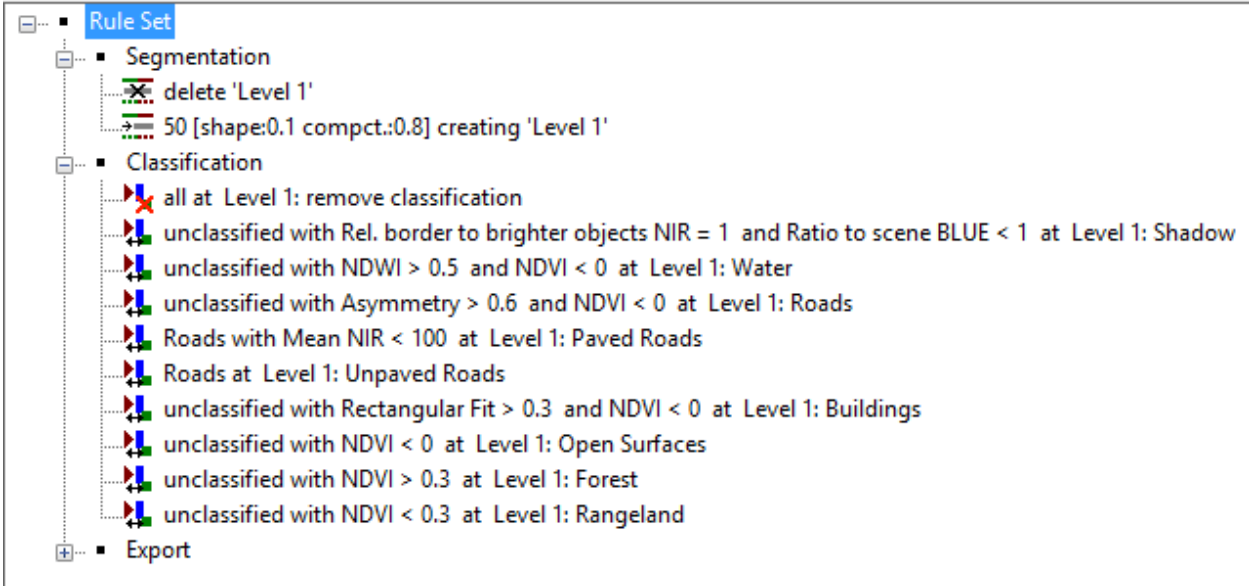


Figure 5.17: Ogbogu segmentation parameter and classification ruleset

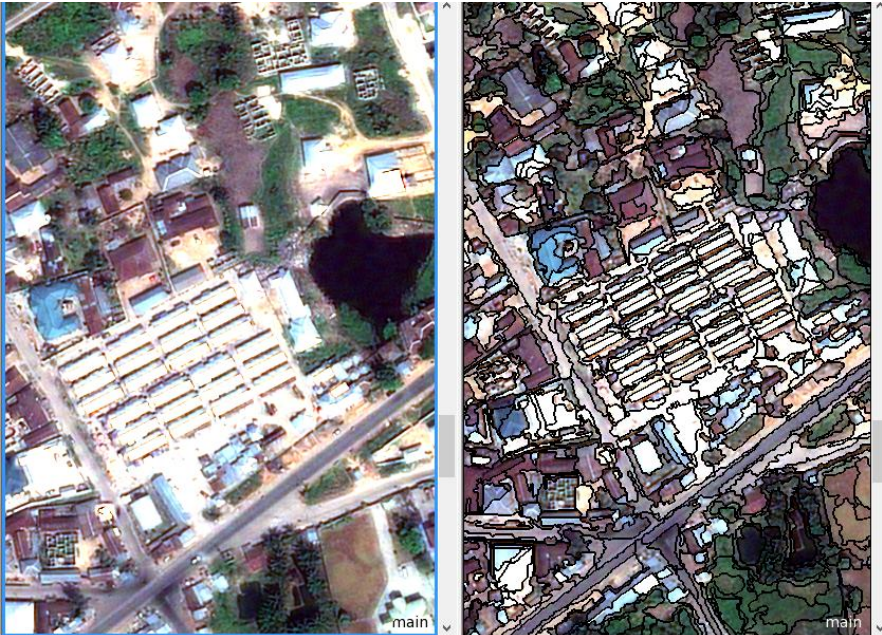


Figure 5. 18a: Ogbogu image Figure 5.18b: Ogbogu Segmented image

5.3.6 Omoku OBIA Classification Ruleset using VHR image only



Figure 5.19: Omoku segmentation parameter and classification ruleset



Figure 5.20a: Omoku subset image



Figure 5.20b: Omoku Segmentation image

5.3.7 Osiakpu OBIA Classification Ruleset using VHR image only

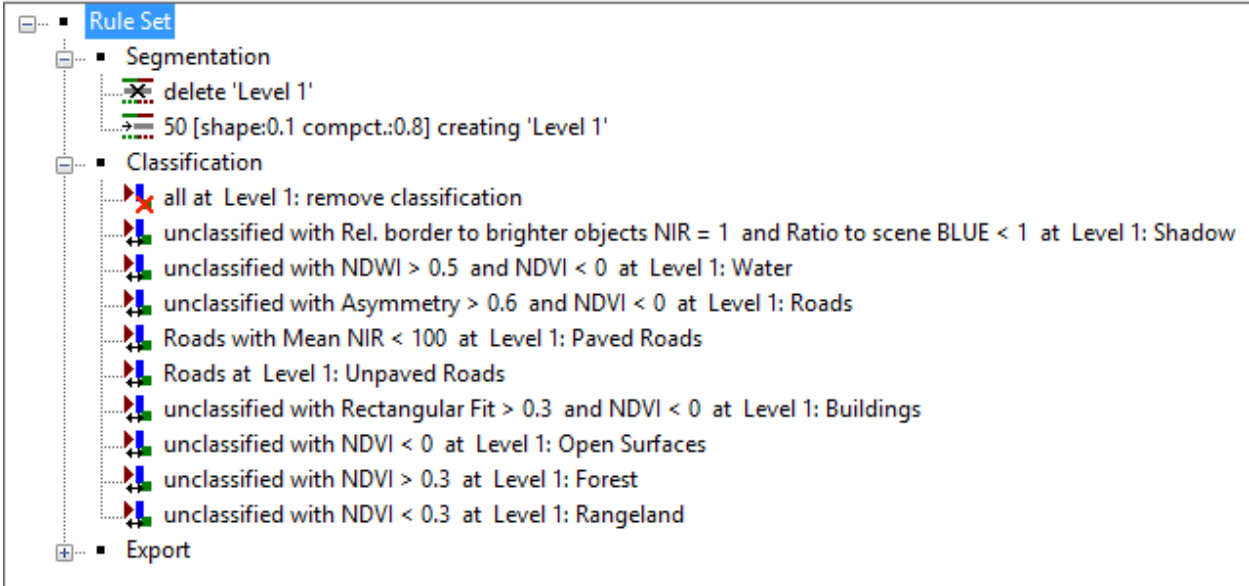


Figure 5.21: Osiakpu segmentation parameter and classification ruleset



Figure 5.22a: Osiakpu subset image



Figure 5.22b: Osiakpu Segmentation image

5.4 Result Presentation of OBIA Classification using VHR Image only

The resulting maps from the OBIA technique which used only the Geo-eye image are displayed in figures 5.23 – 5.29. The classification results were assessed qualitatively, through visual interpretation and quantitatively, using a confusion matrix. The accuracy assessment which has been calculated using error matrix is presented in section 5.7. Specifically, the accuracy assessment summary of OBIA method combining nDSM and VHR image has been presented in Appendix 7.

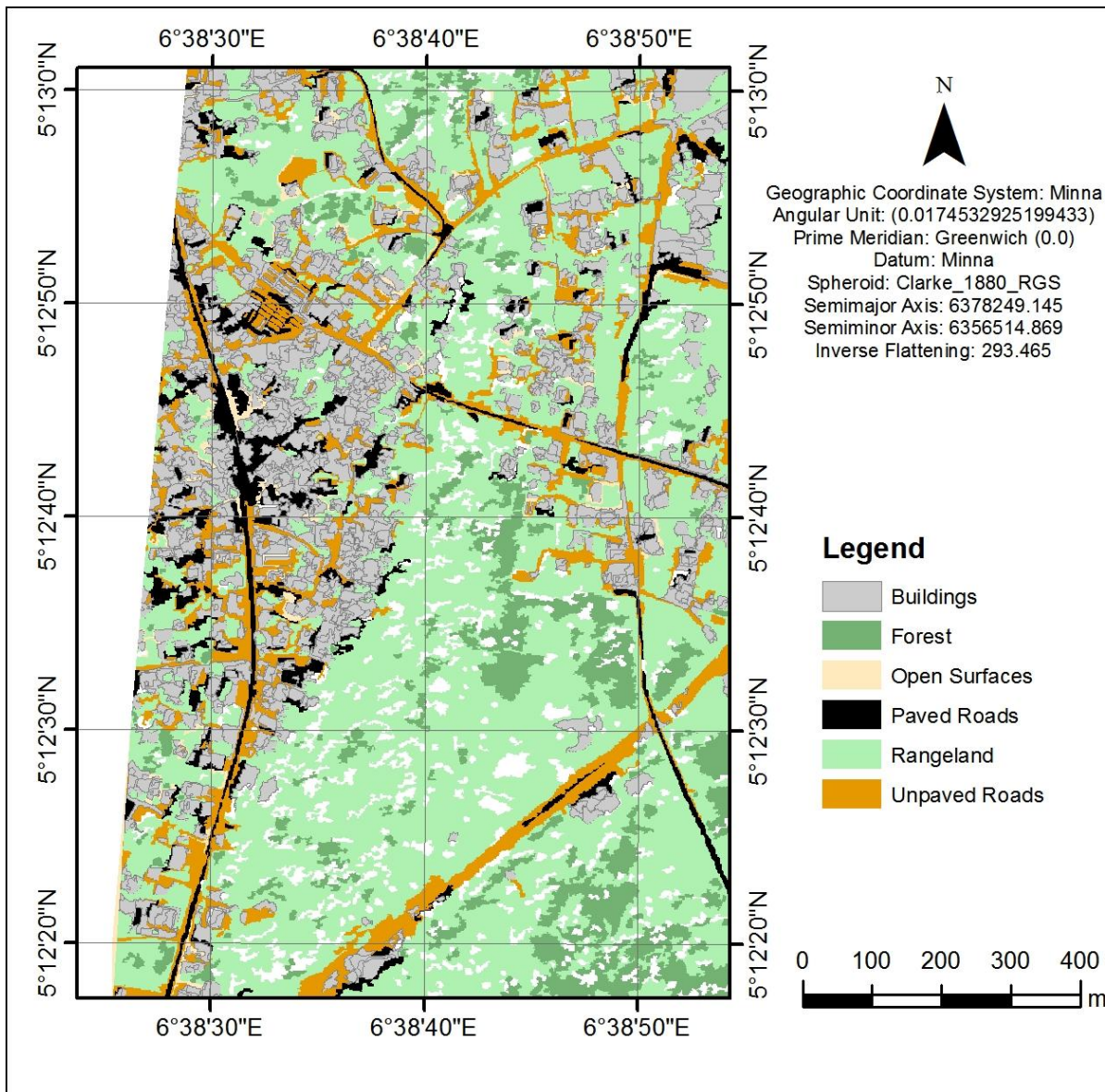


Figure 5.23: Resulting LU/LC map of Akabuka OBI using VHR image only

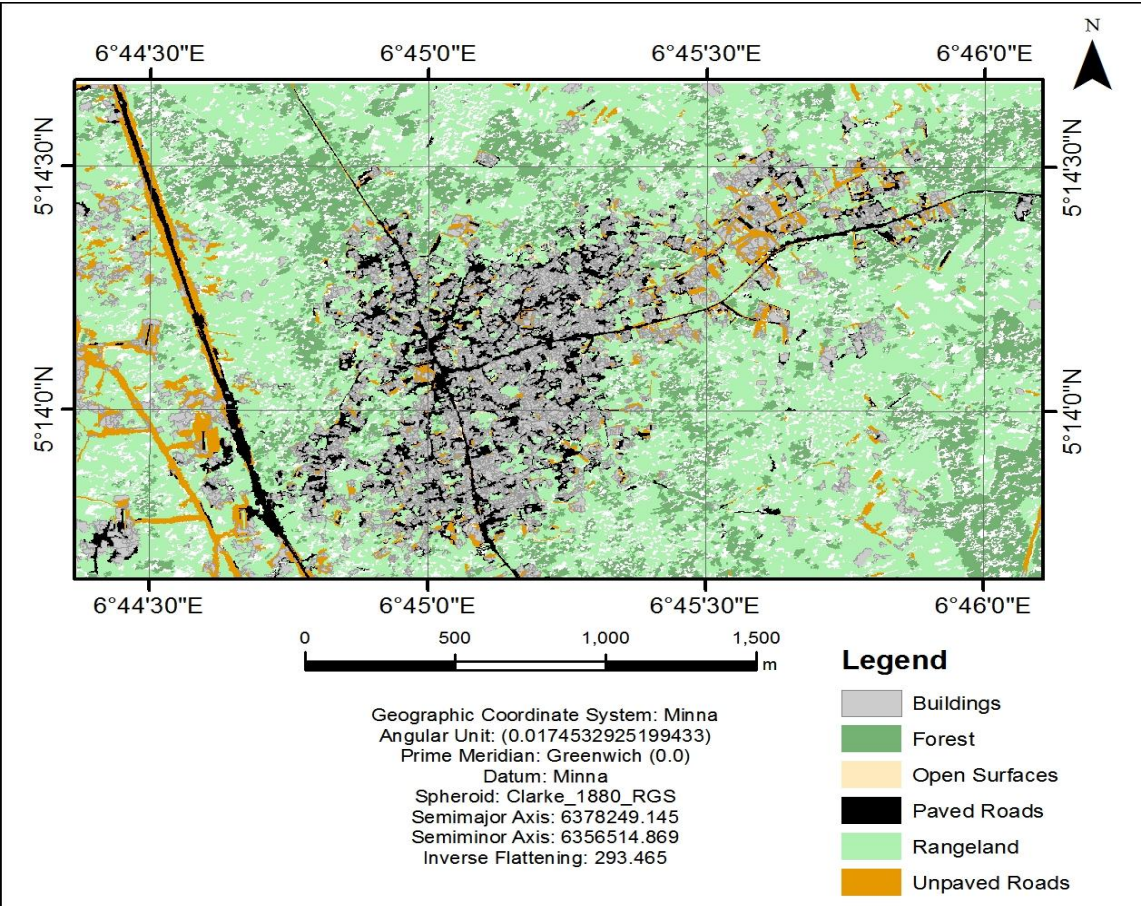


Figure 5.24: Resulting LU/LC map of Egbeda OBIA using VHRimage only

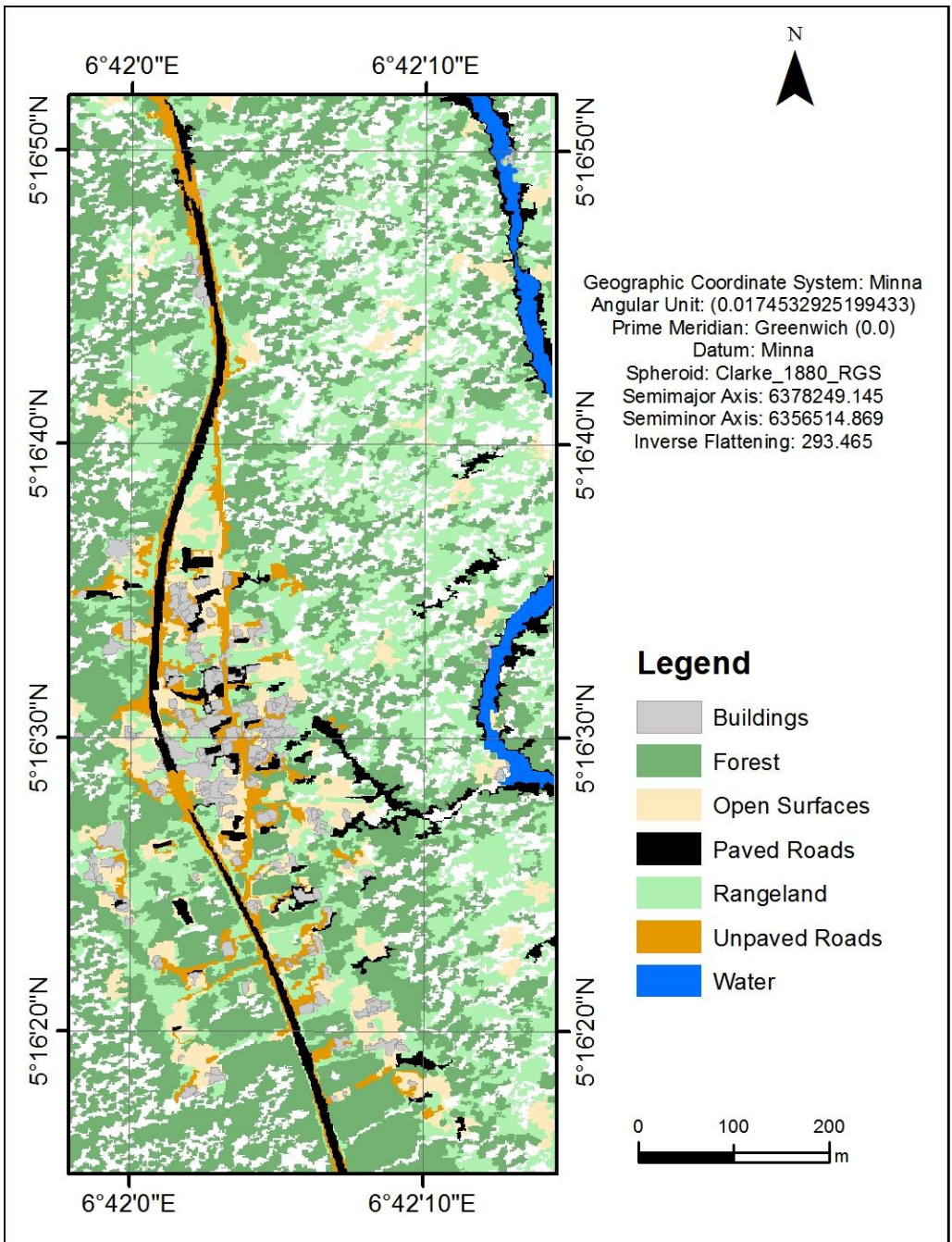


Figure 5.25: ResultingLU/LC map of Ikiri OBIA using VHR image only

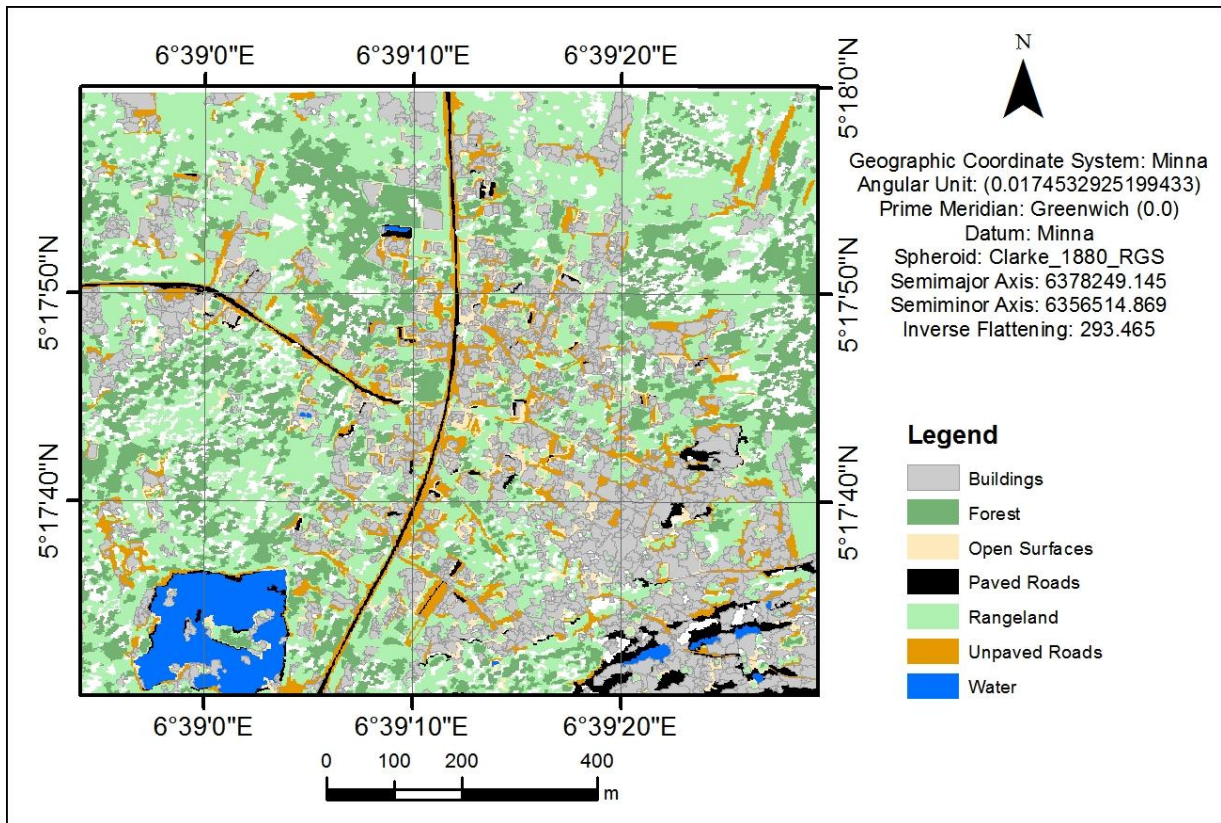


Figure 5.26: Resulting LU/LC map of Obido in OBIA using VHR image only

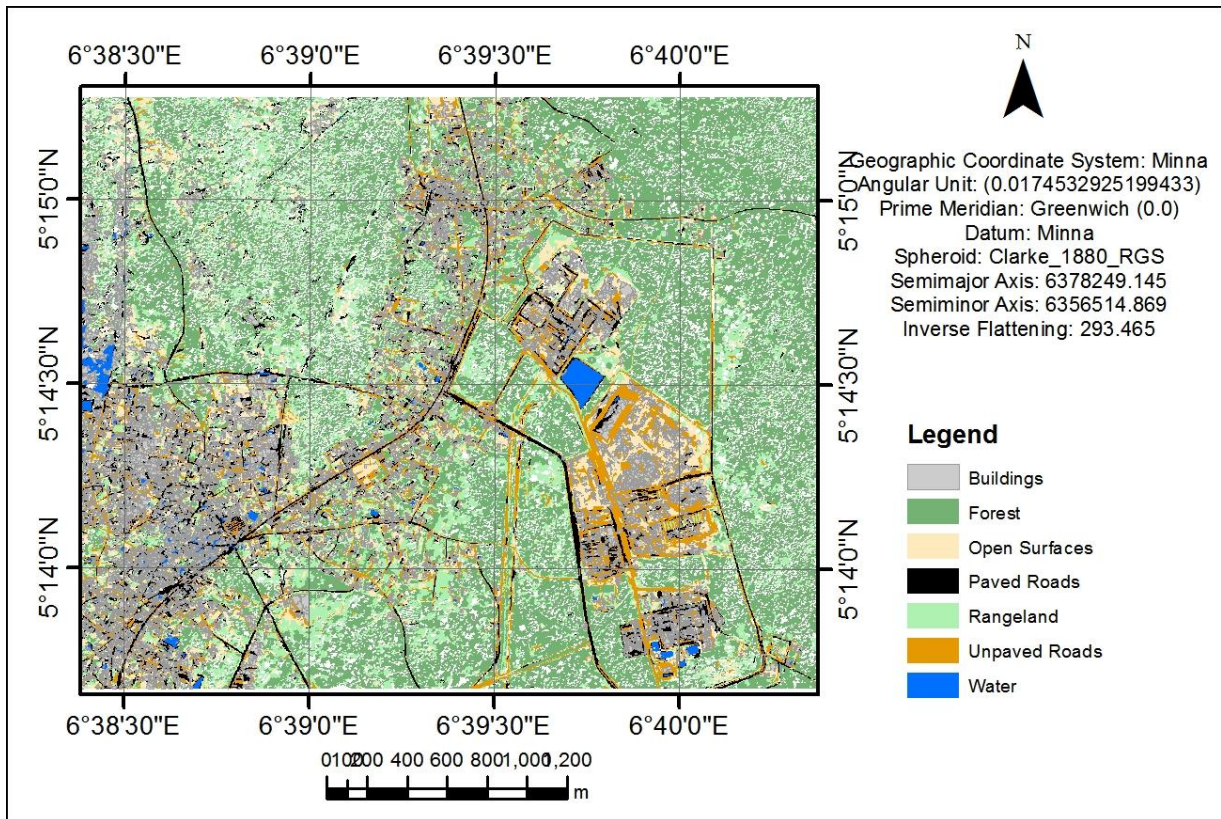


Figure 5.27: Resulting LU/LC map of Ogbogu OBIA using VHR image only

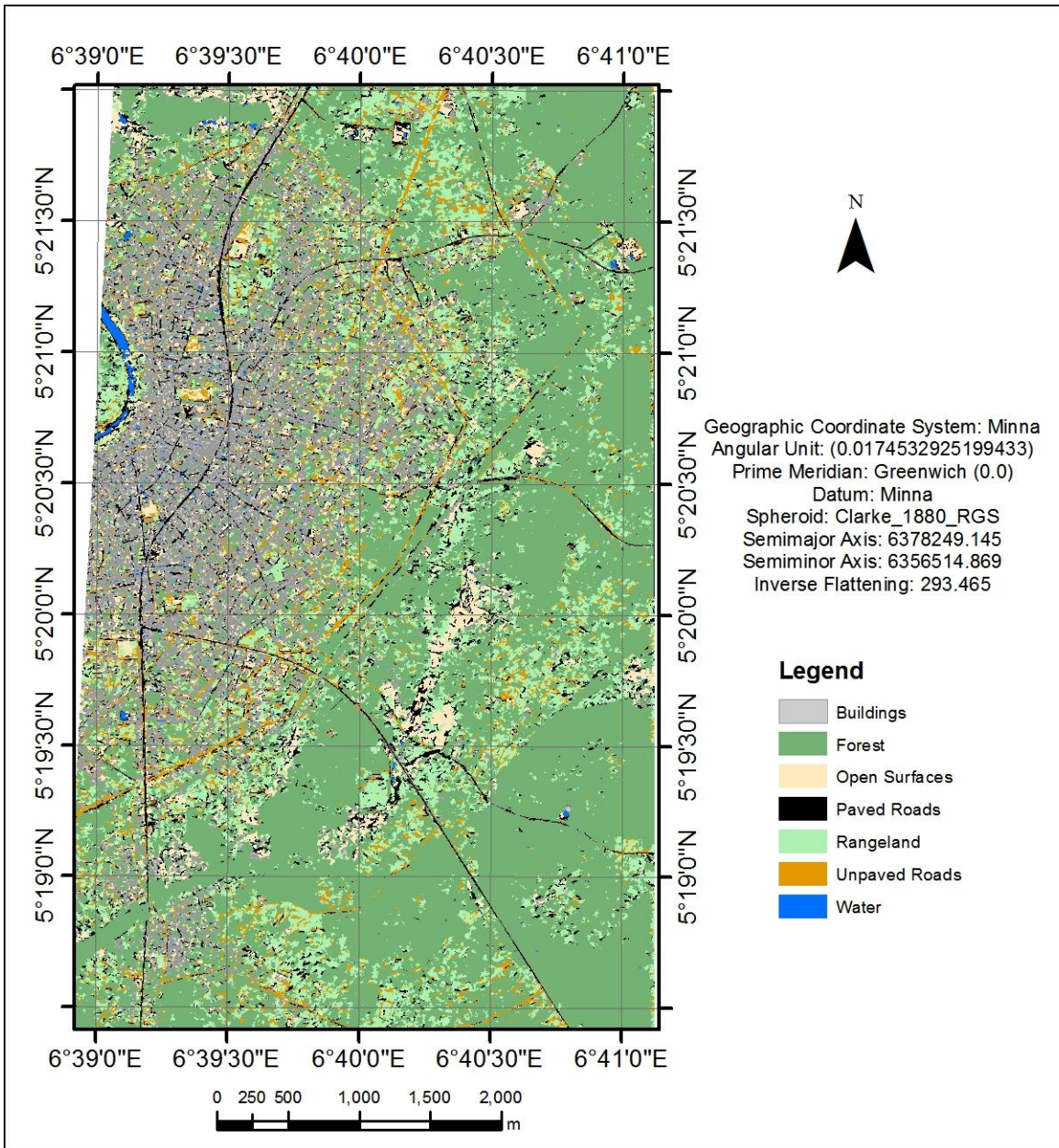


Figure 5.28: Resulting LU/LC map of Omoku OBIA using VHR image only

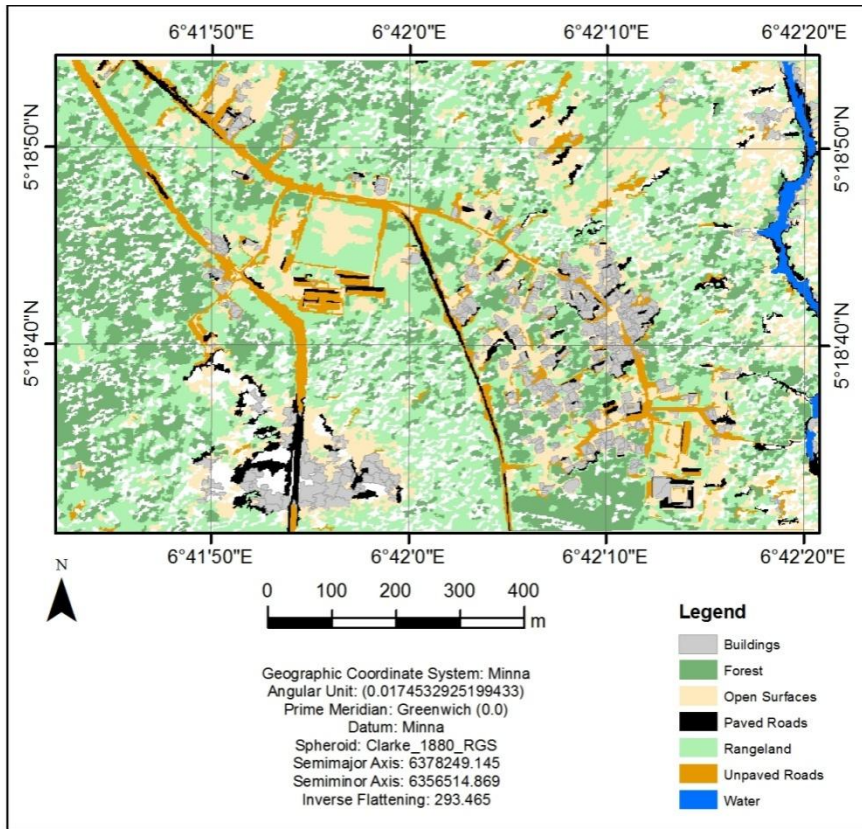


Figure 5.29: Resulting LU/LC map of Osiapku OBI using VHR only

5.5 OBIA combining VHR image and nDSM in eCognition 9.0 Software

The procedure adopted here is similar to the procedure adopted in sub head 5.3 except that Normalised Digital Surface Model derived from LiDAR was added in the rule set with a threshold value. (See Table 5.3). Normalized Digital Surface Model (nDSM) is used to model the height above the ground surface of structures and vegetation. This surface value is derived by subtracting the DSM from the DTM. In the multi-resolution segmentation process, the influence of the nDSM and the multi-spectral bands on object generation was controlled by layer weight, scale parameters, the amount of colour and shape factors. The segmented image was also classified using the classification rule set to extract the land cover classes.

5.5.1 Akabuka OBIA Classification Ruleset using VHR and nDSM

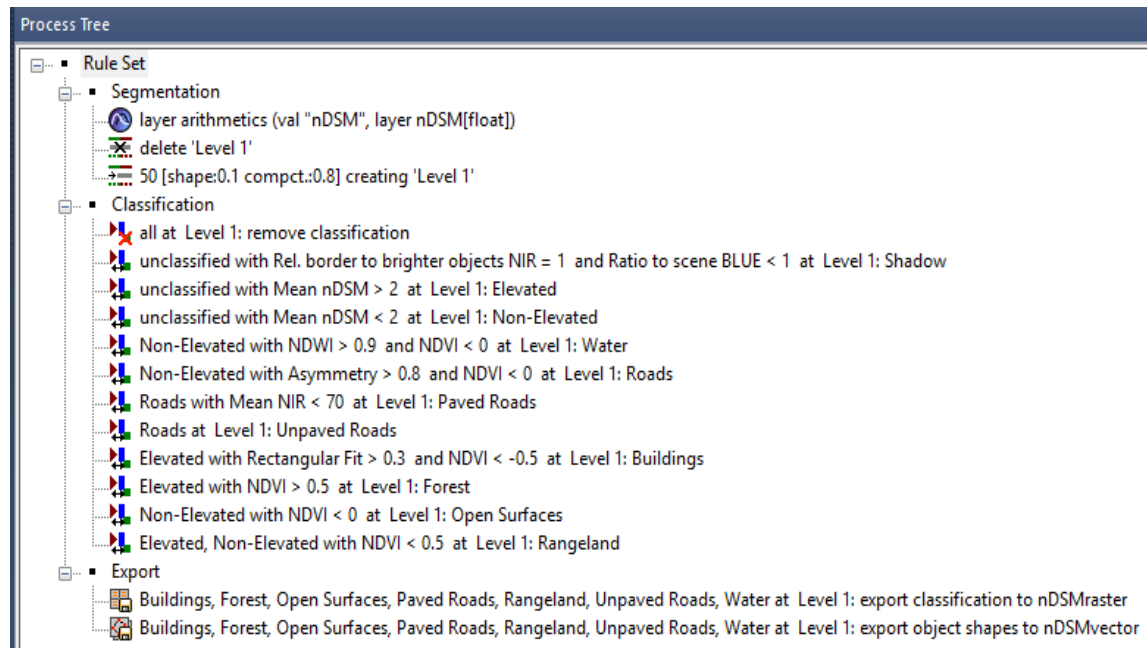


Figure 5.30: Akabuka segmentation parameter and classification ruleset with nDSM

5.5.2 Egbema OBIA Classification Ruleset using VHR and nDSM

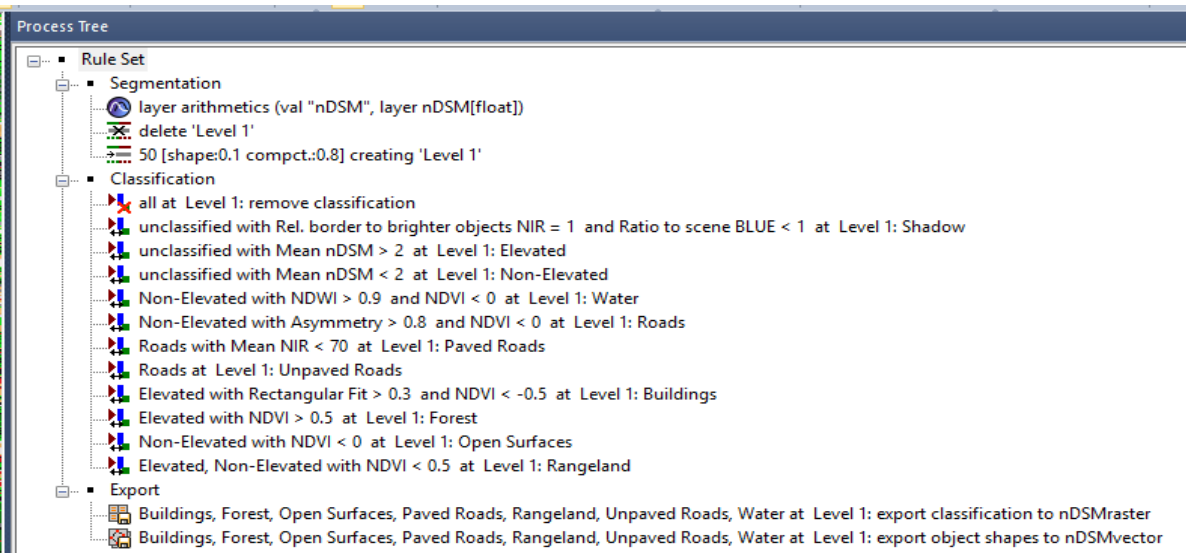


Figure 5.31: Egbema segmentation parameter and classification ruleset with nDSM

5.5.3 Ikiri OBIA Classification Ruleset using VHR and nDSM

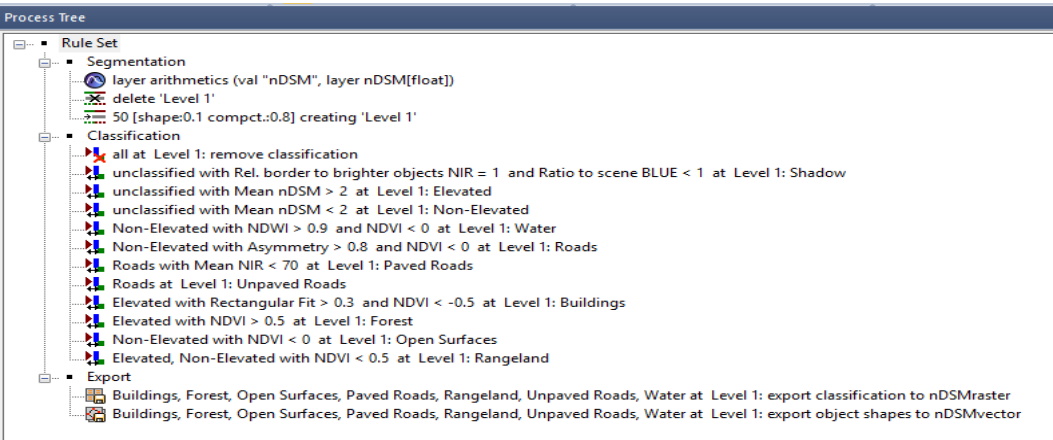


Figure 5.32: Ikiri segmentation parameter and classification ruleset with nDSM

5.5.4 Obido OBIA Classification Ruleset using VHR and nDSM

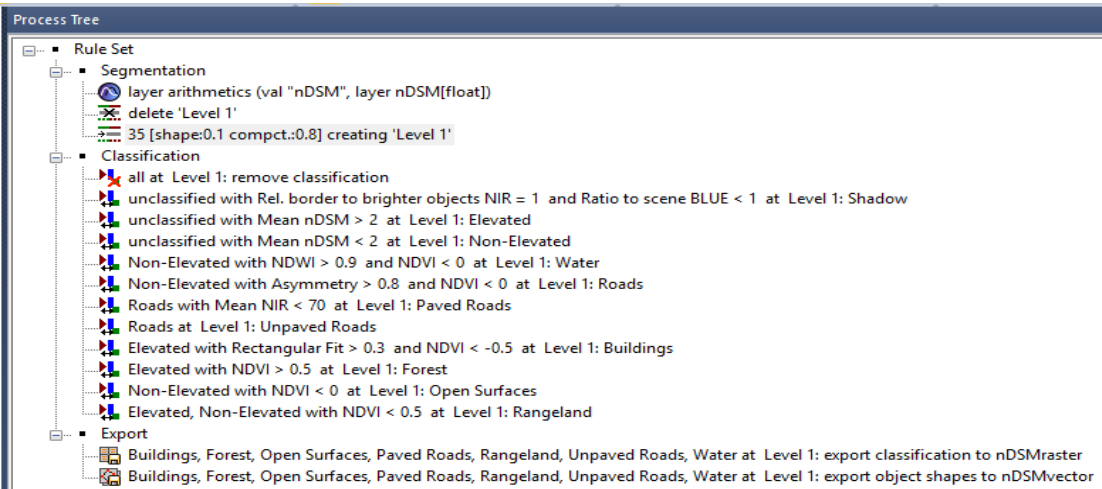


Figure 5.33: Obido segmentation parameter and classification ruleset with nDSM

5.5.5 Ogbogo OBIA Classification Ruleset using VHR and nDSM

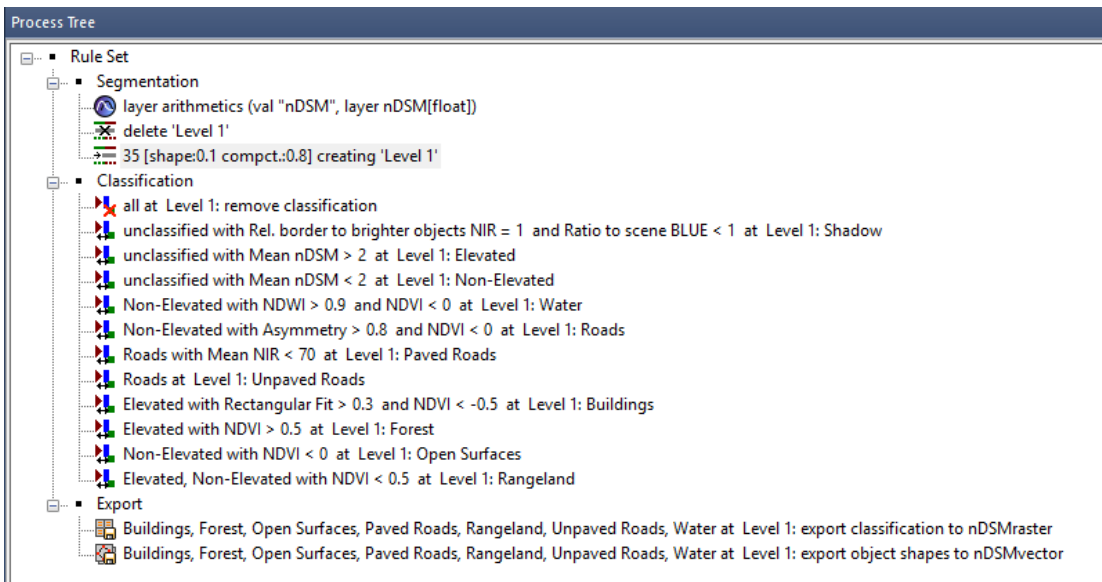


Figure 5.34: Ogbogo segmentation and classification ruleset with nDSM

5.5.6 Omoku OBIA Classification Ruleset using VHR and nDSM

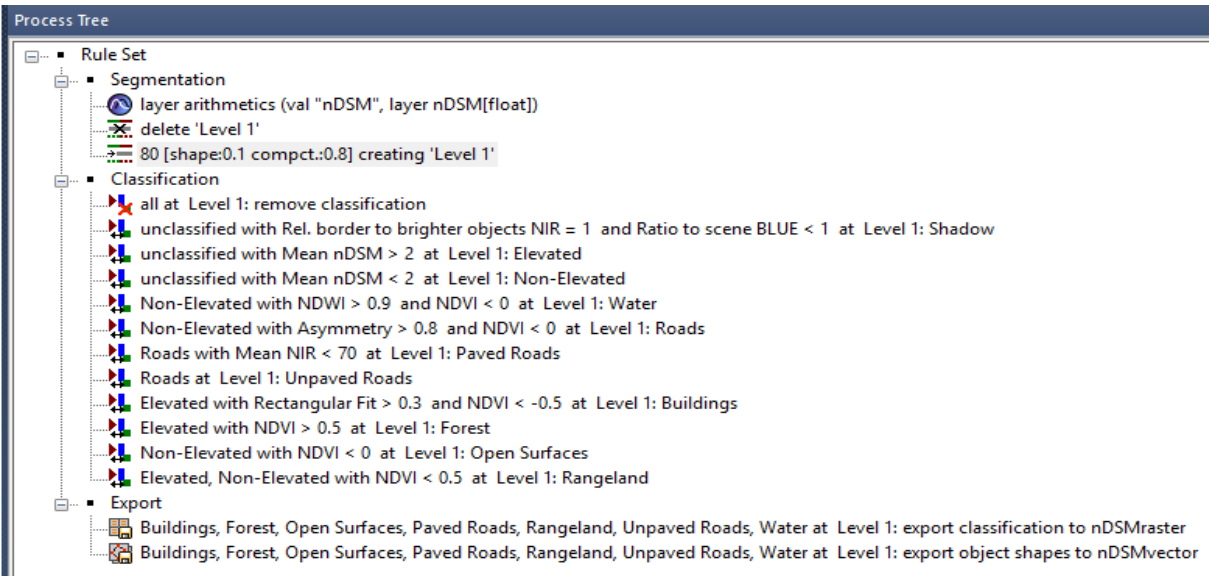


Figure 5.35: Omoku segmentation parameter and classification ruleset with nDSM

5.5.7 Osiakpu OBIA Classification Ruleset using VHR and nDSM

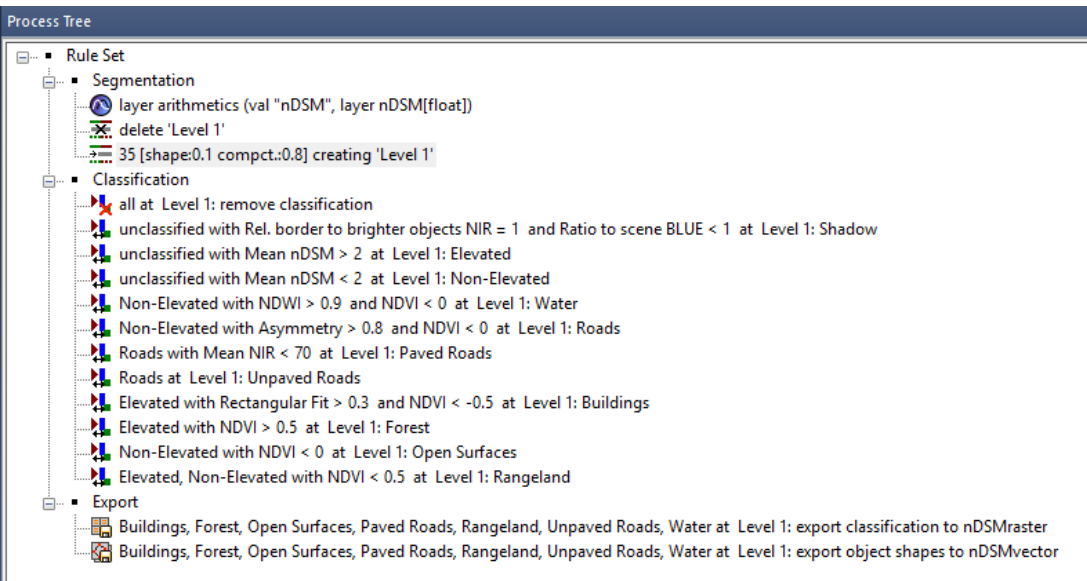


Figure 5.36: Osiakpu segmentation parameters and classification rule-set with nDSM

5.6 Result Presentation OBIA Combined nDSM and VHR Image

The resulting maps from the OBIA technique which used only the Geo-eye image are displayed in figures 5.37 – 5.43. The classification results were assessed both qualitatively, through visual interpretation of the classified images against results from other methods, and quantitatively, using a confusion matrix.

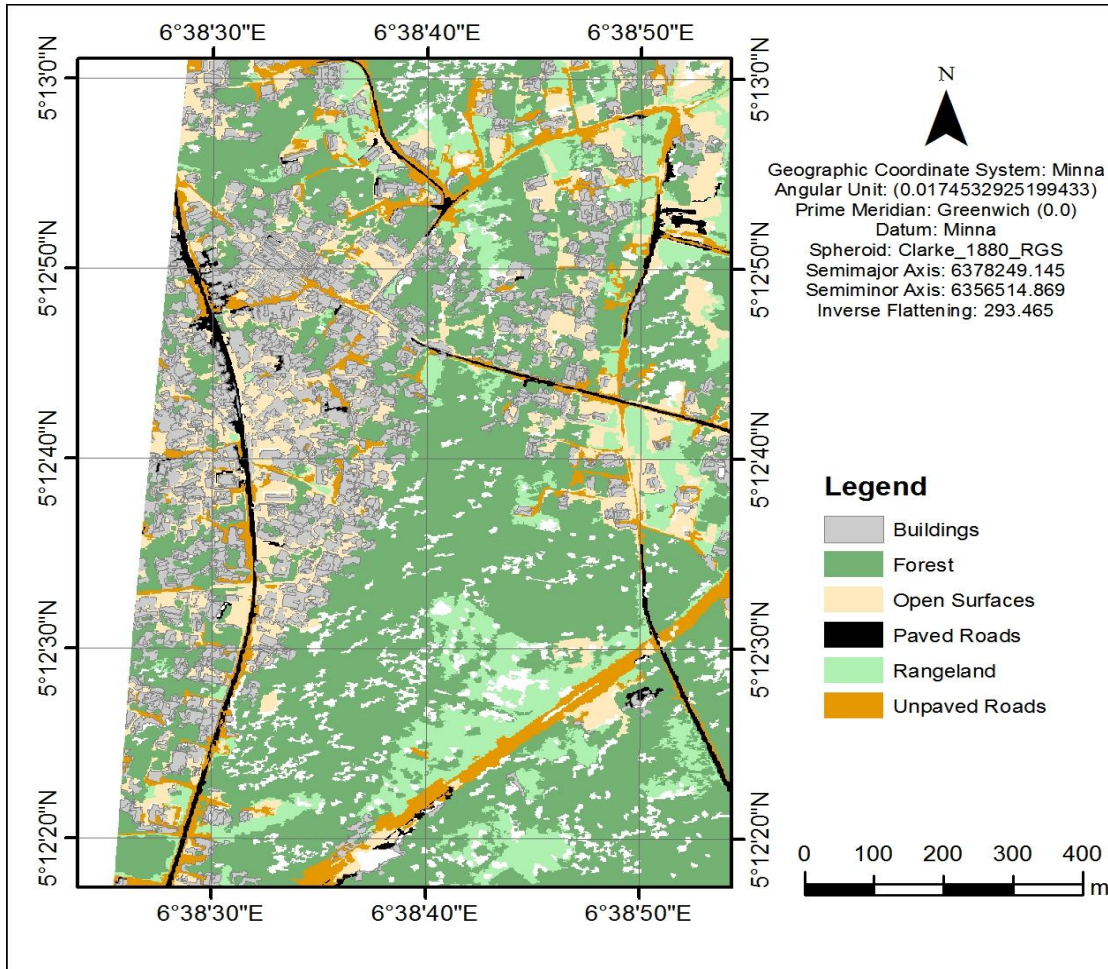


Figure 5.37: Resulting LU/LC map of Akabuka OBIA using VHR with nDSM

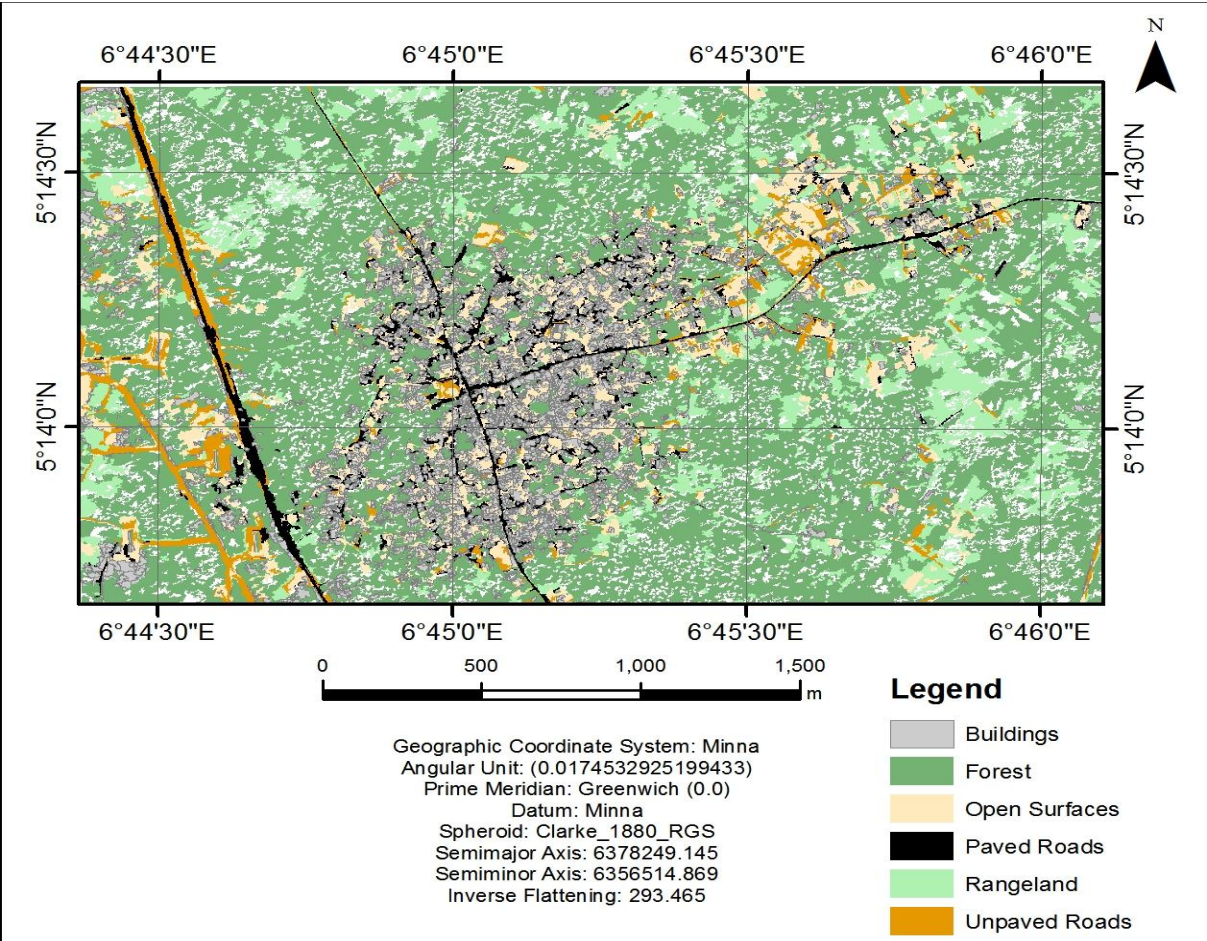


Figure5.38: LU/LC map of EgbedaOBIA using VHR with nDSM

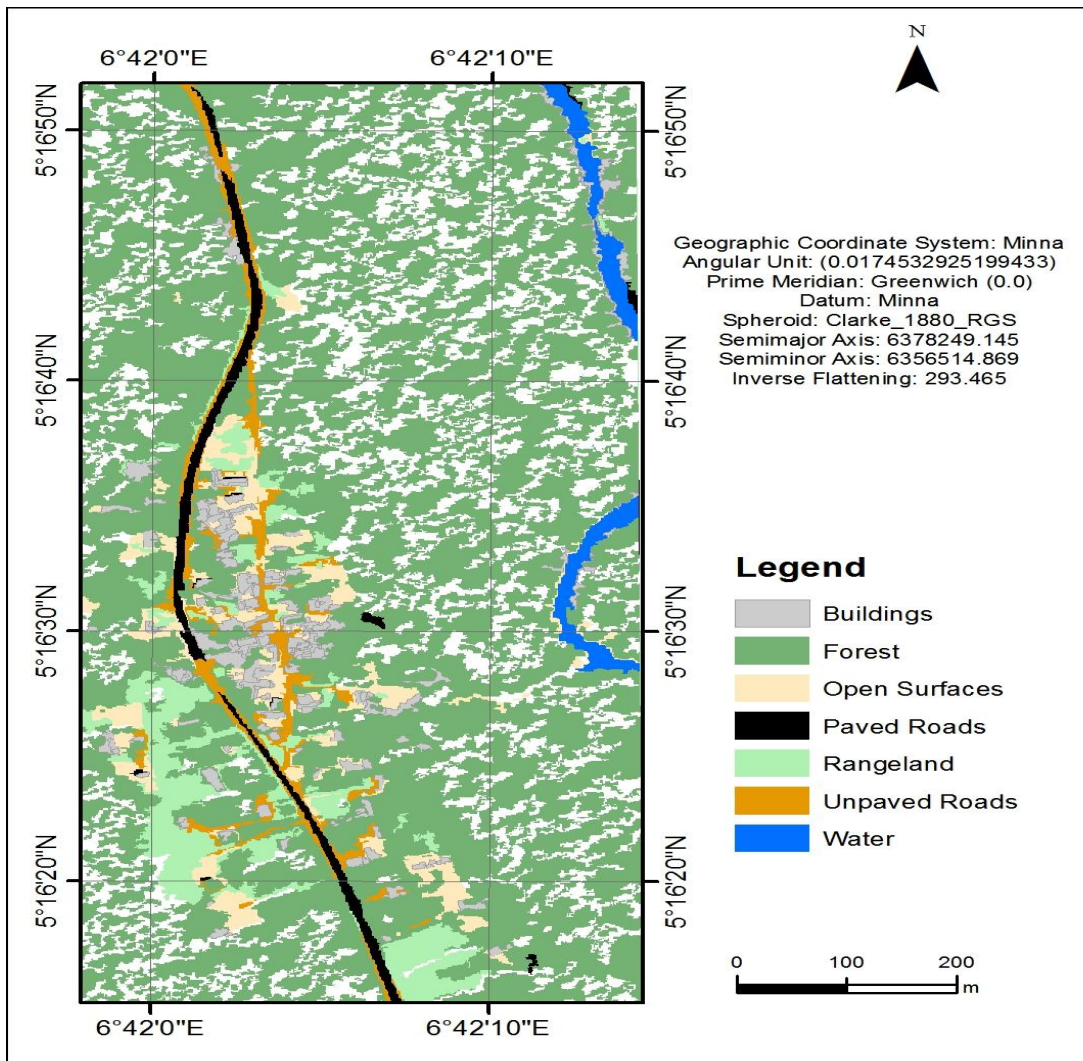


Figure5.39: LU/LC map of Ikiri OBIA using VHR with nDSM

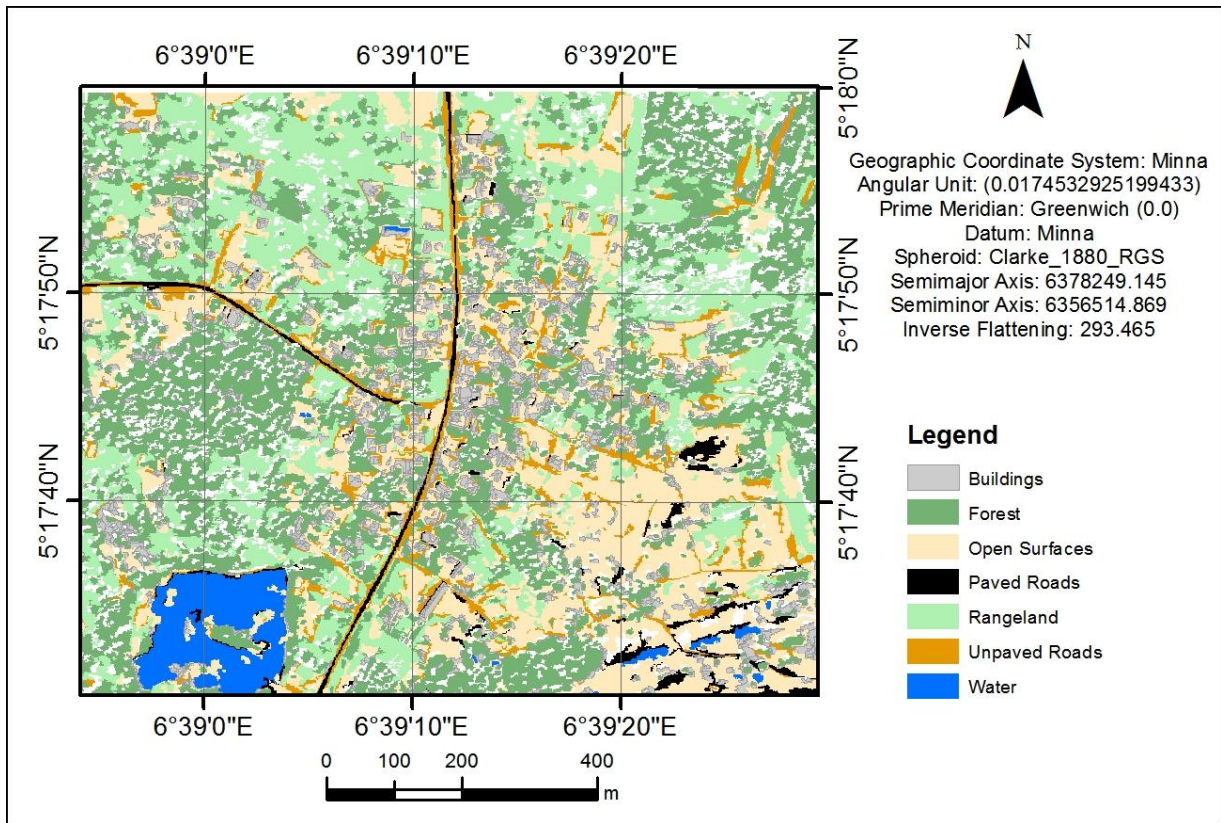


Figure 5.40: LU/LC map of ObidoOBIA using VHR with nDSM

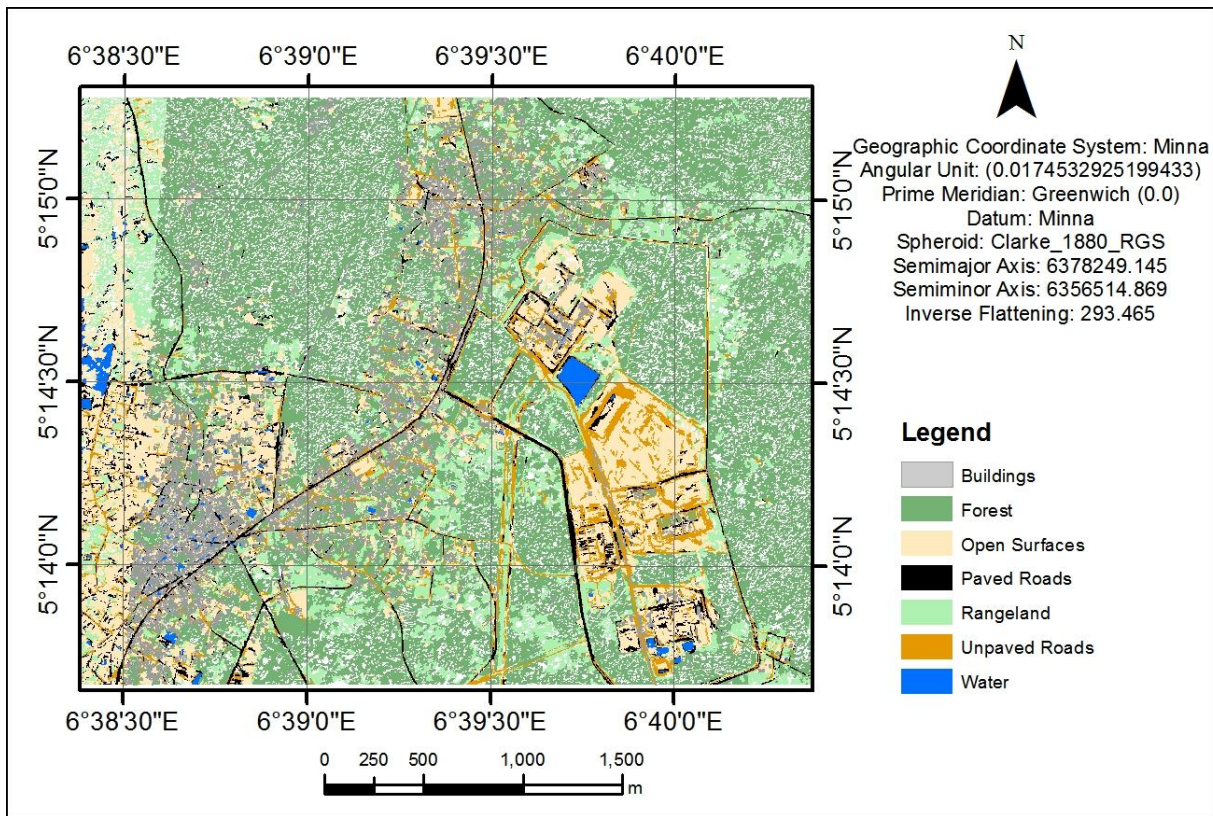


Figure 5.41: LU/LC map of OgboguOBIA using VHRand nDSM

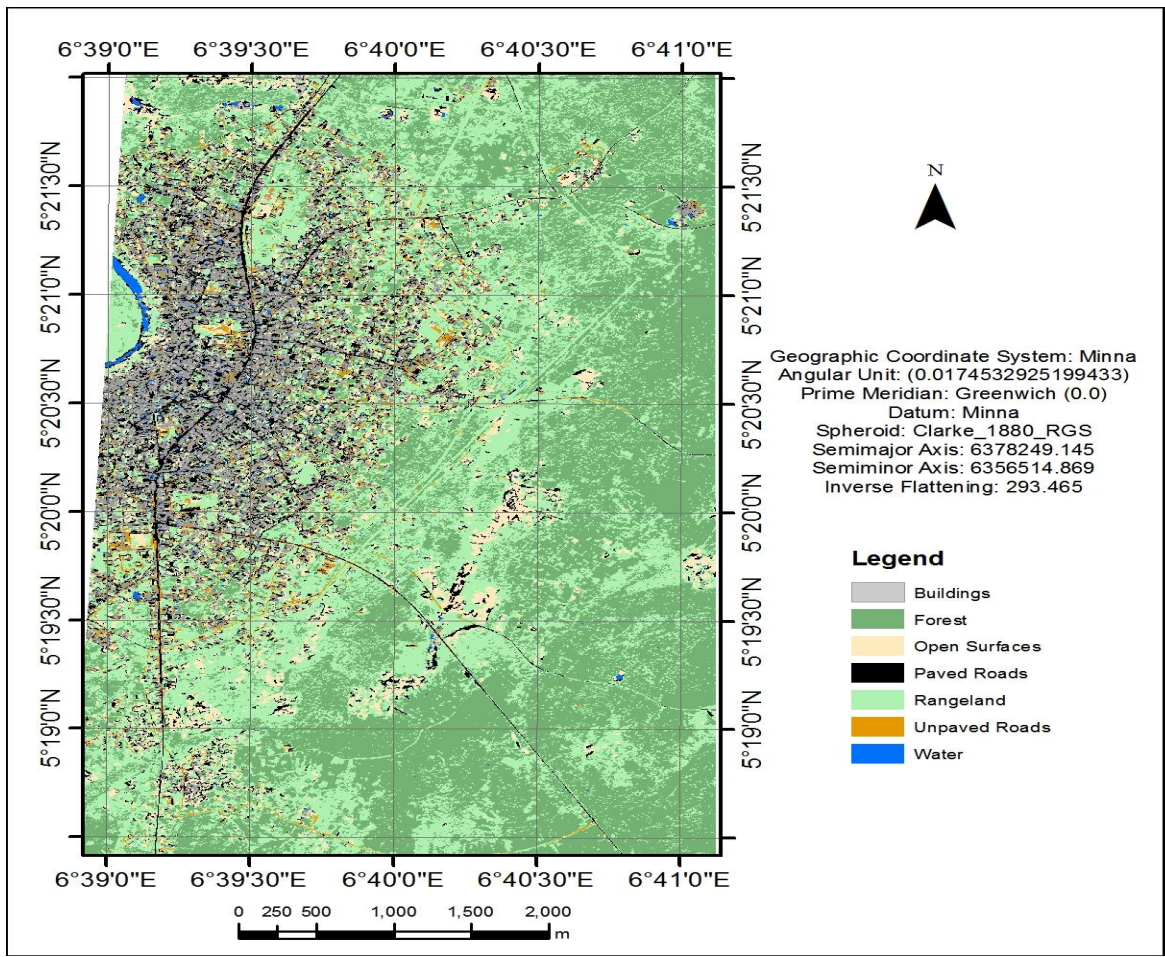


Figure 5.42: LU/LC map of OmokuOBIA using VHR with nDSM

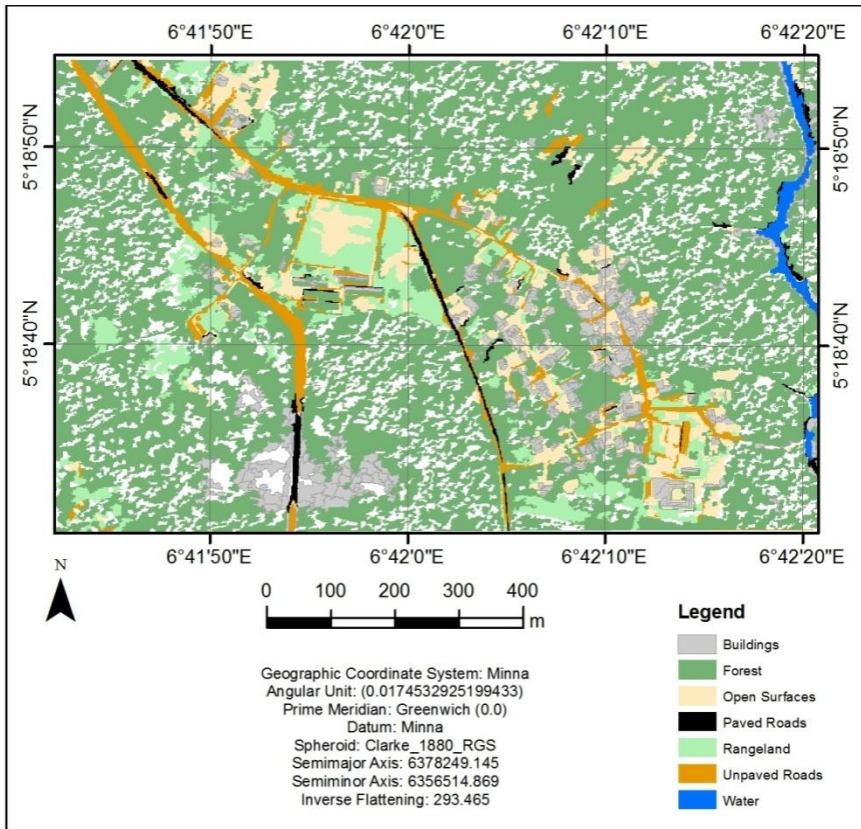


Figure 5.43: LU/LC map of OsiakpuOBIA using VHR with nDSM

5.7 The Refined unpaved roads Result

The final maps representing the refined unpaved roads using the developed algorithm in Objective three (3) have been presented below for the seven (7) subset study sites.

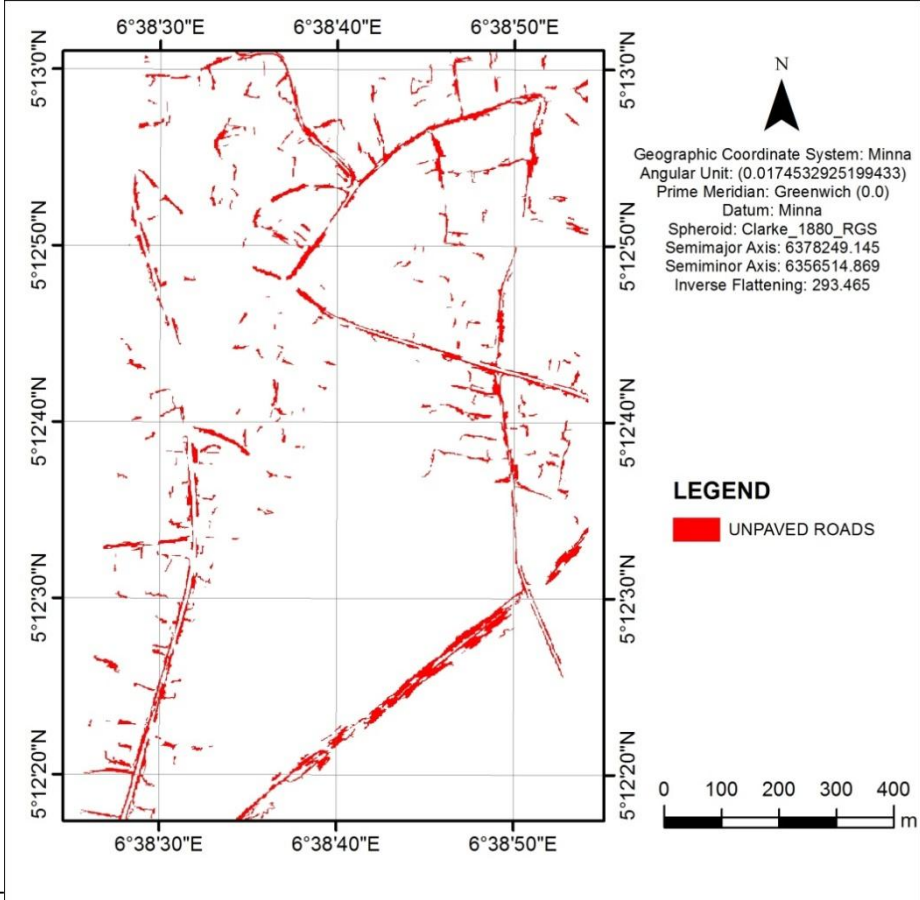


Figure 5.44: Refined Akabuka Unpaved Roads

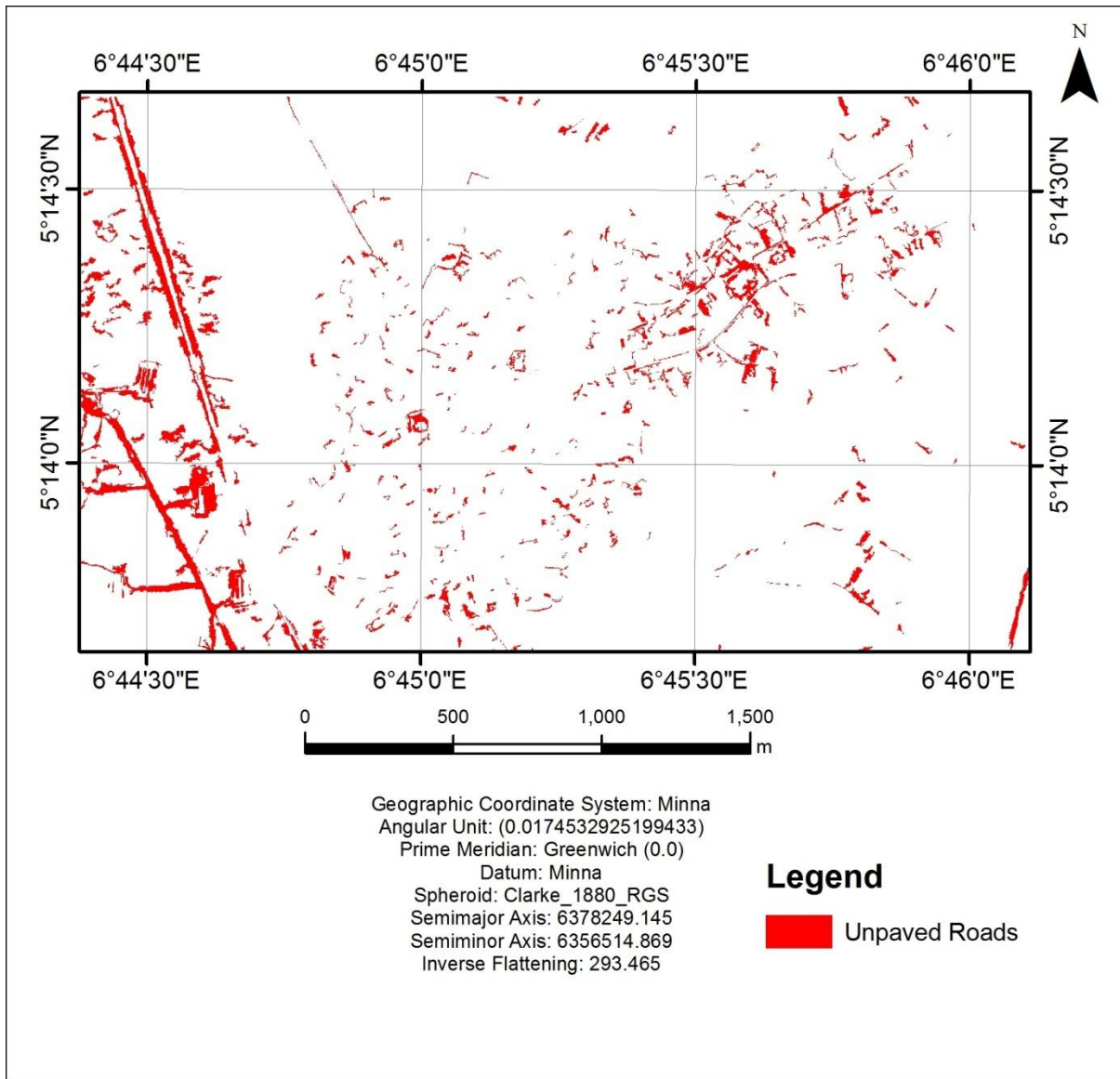


Figure 5.45: Refined Egbeda Unpaved Roads

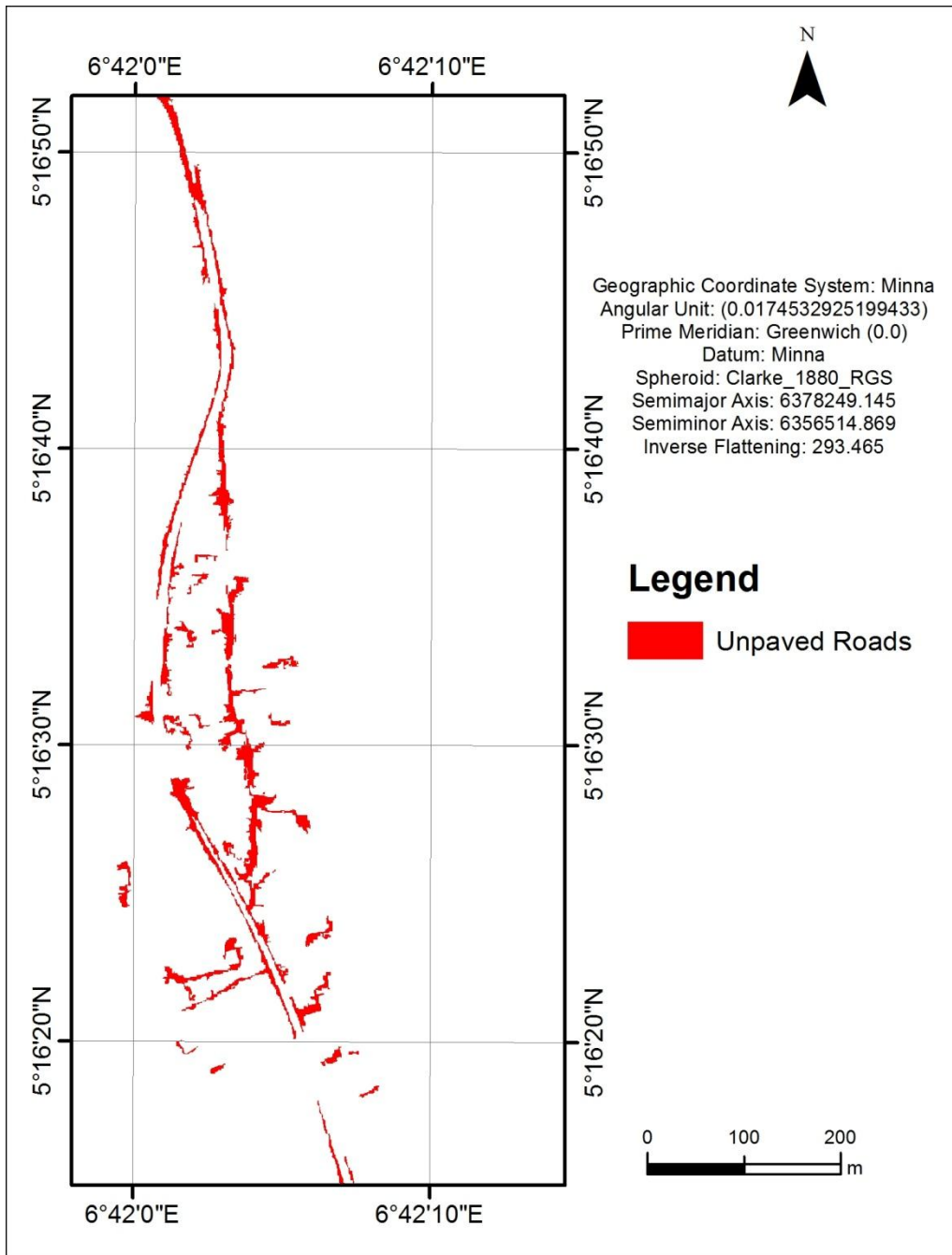


Figure 5.46: Refined Ikiri Unpaved Roads

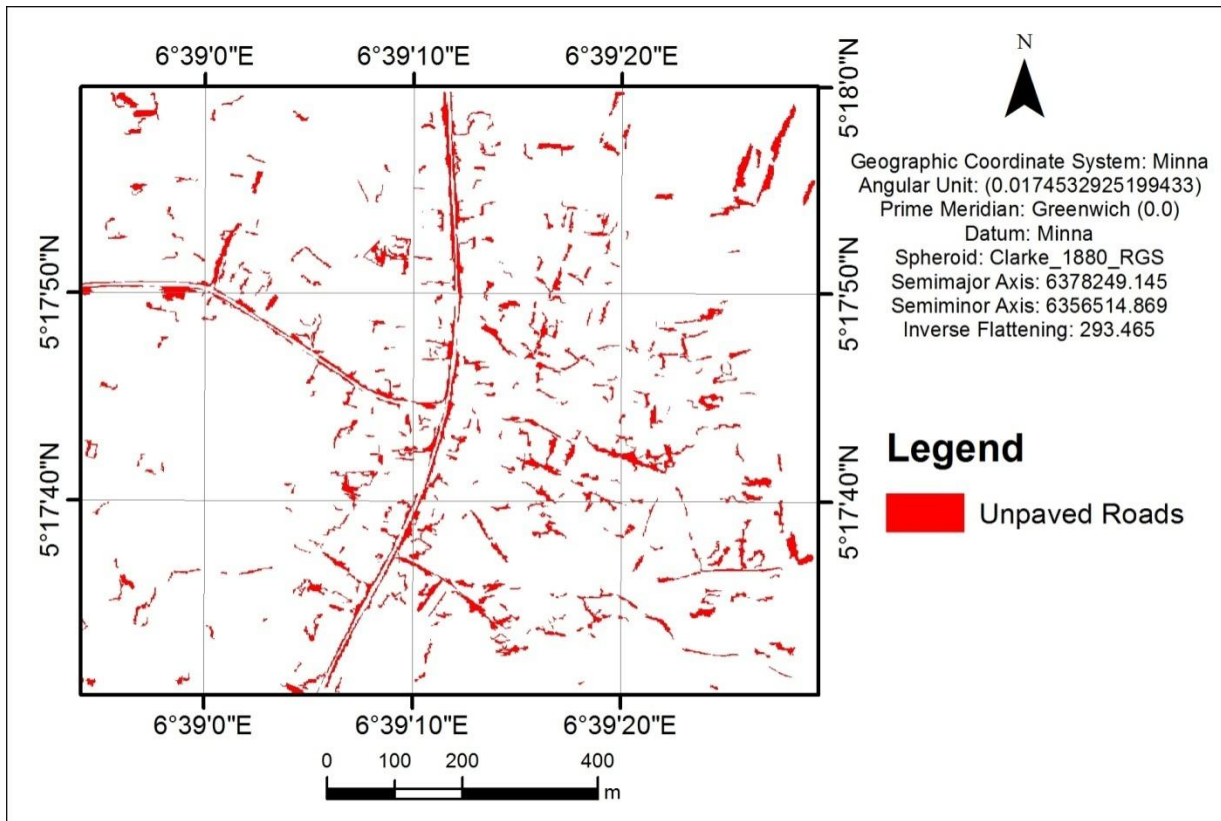


Figure 5.47: Refined Obido Unpaved Roads

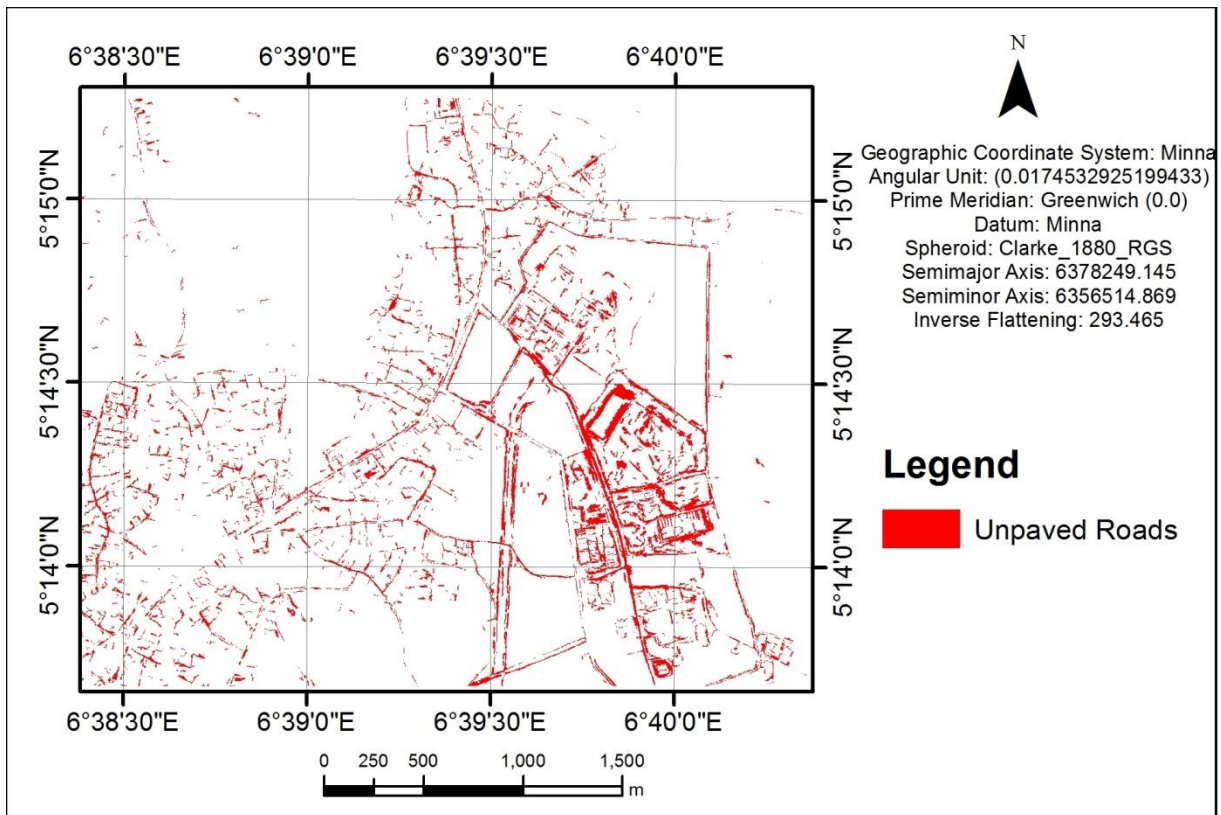


Figure 5.48: Refined Ogbogwu Unpaved Roads

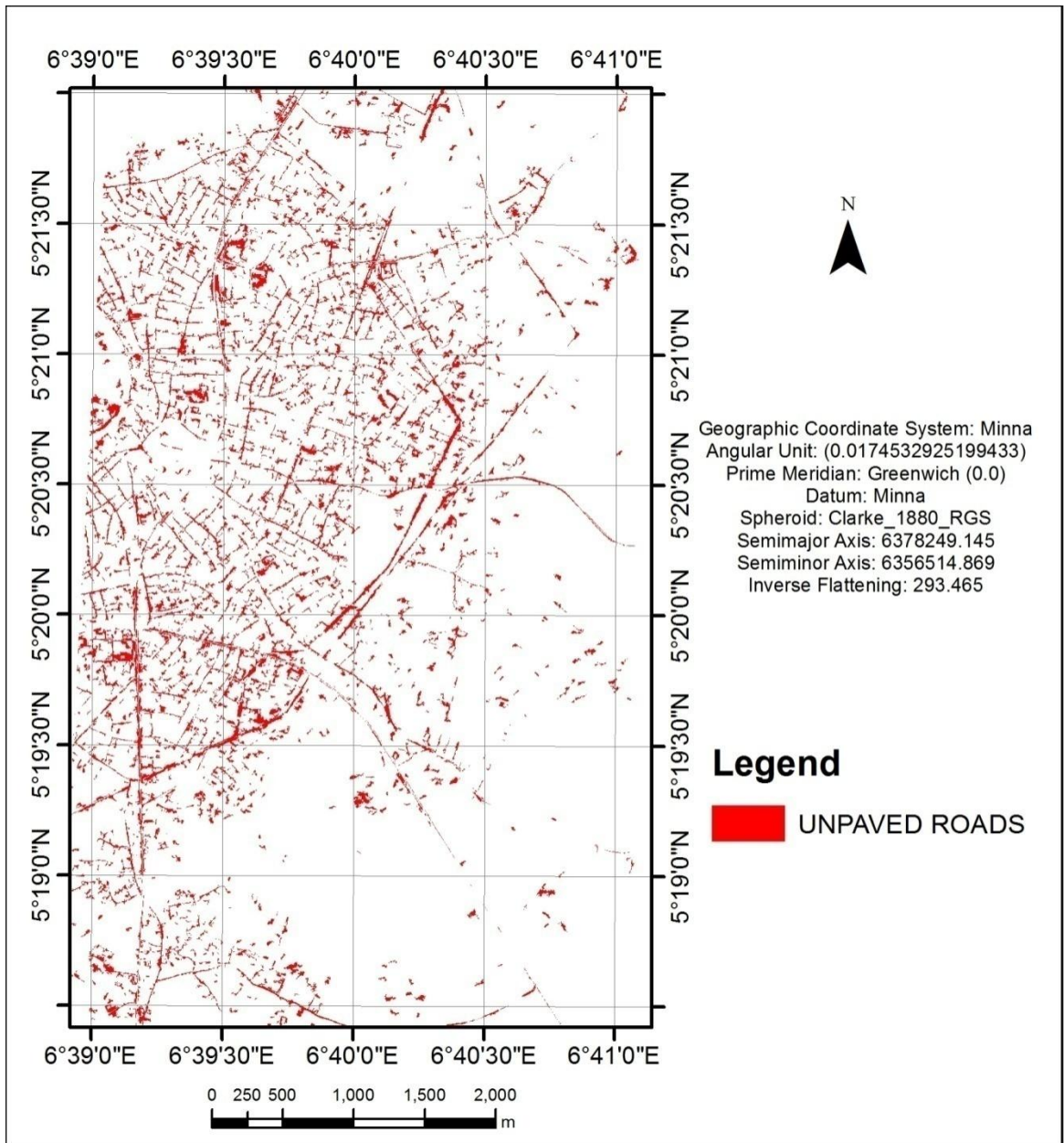


Figure 5.49: Refined Omokwu Unpaved Roads

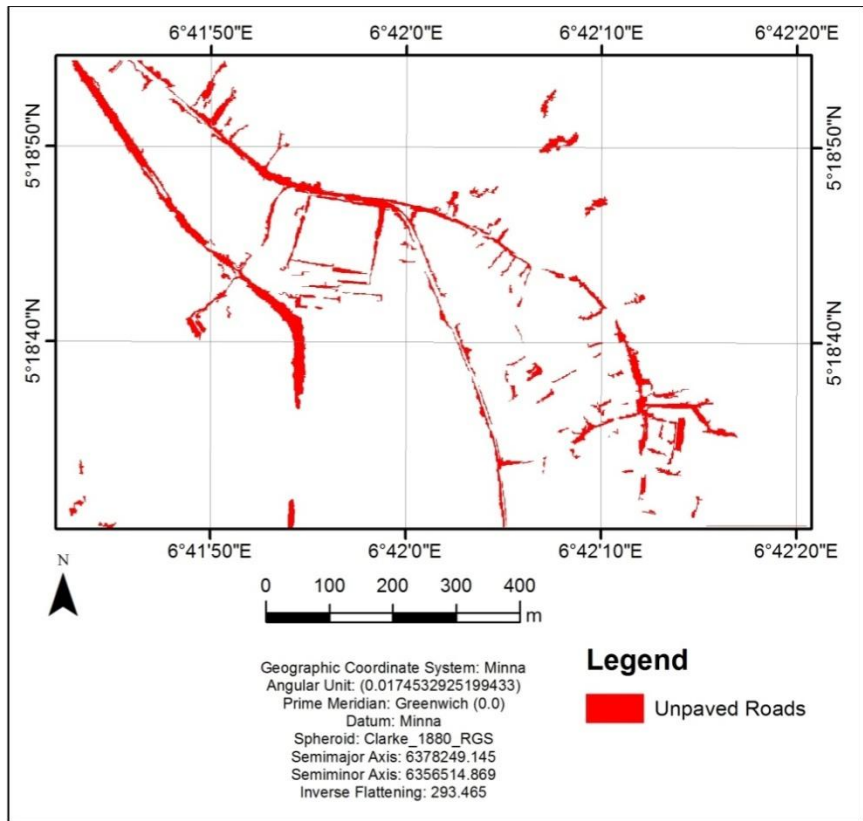


Figure 5.50: Refined Osiakpu Unpaved Roads

5.8 The 3D Representation Results

The 3D visualization of the study area was done in the 3D environment of ArcScene. The Geoeye subset was added to the interface and subsequently the Layer properties was used to set the height value of the cells in the Geoeye subset from the elevations in the nDSM to define how the Geoeye subset will be displayed in 3D. To enhance the 3D view, the vertical exaggeration was set to 1.5, illumination azimuth to 3150 (NW) and illumination elevation to 450 from the Scene properties (see diagram).

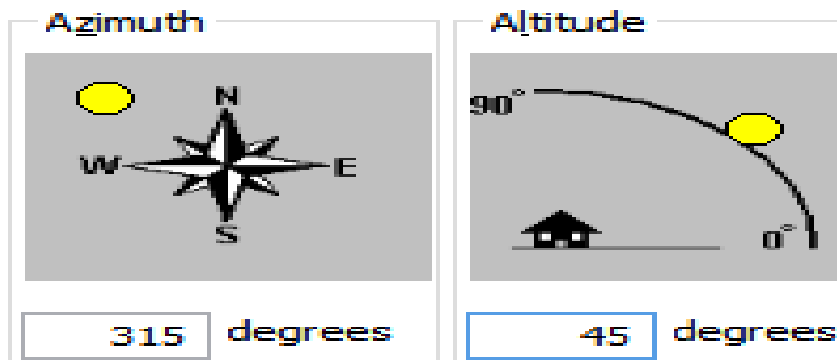


Figure 5.51: ArcScene settings to enhance illumination

The observer position was set to the south and the scene was captured to a JPEG format for presentation in this research.

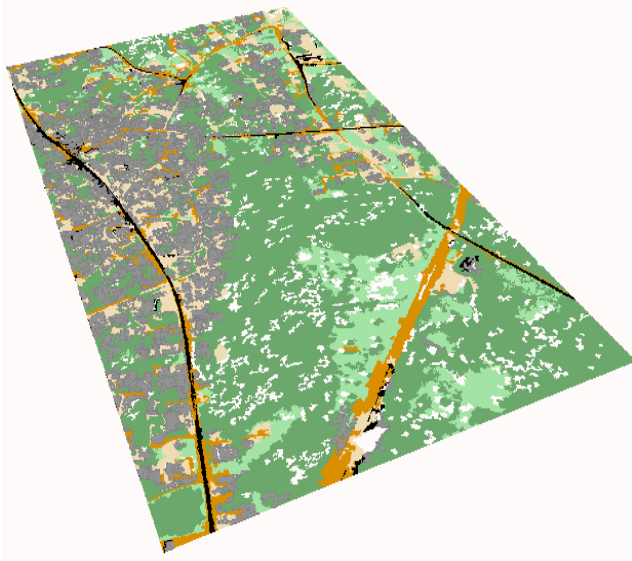


Figure 5.52a: Akabuka 2D representation

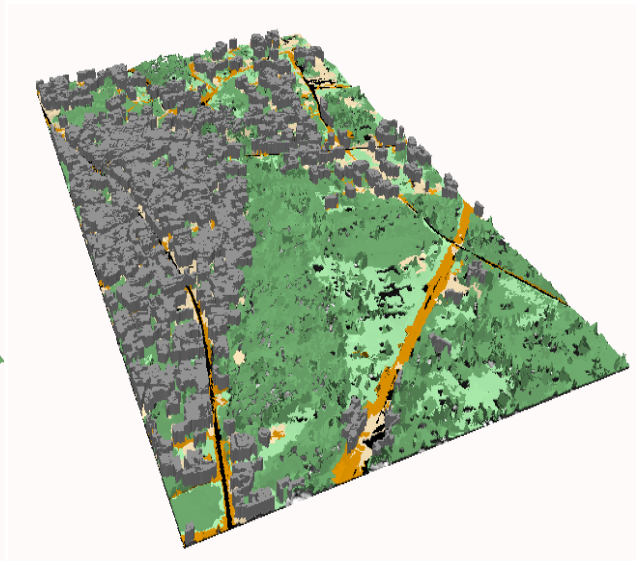


Figure 5.52b: Akabuka 3D representation

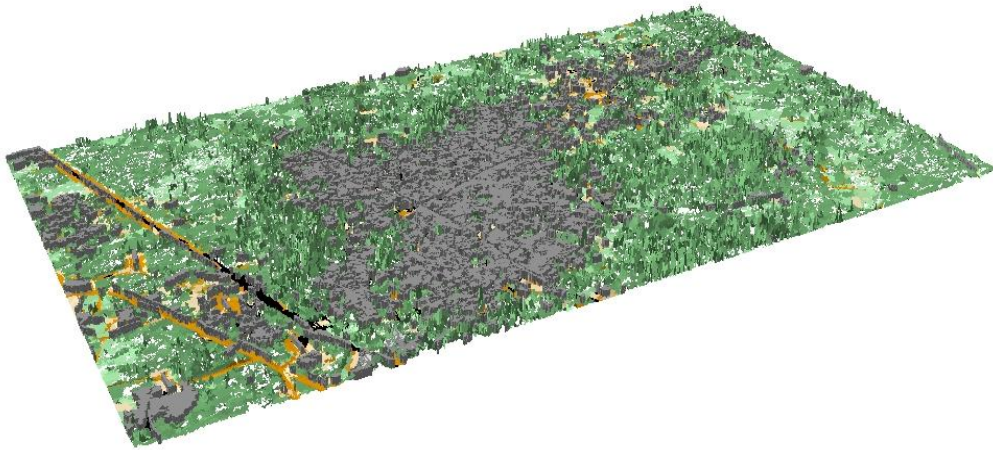


Figure 5.53: Egbeda 3D representation

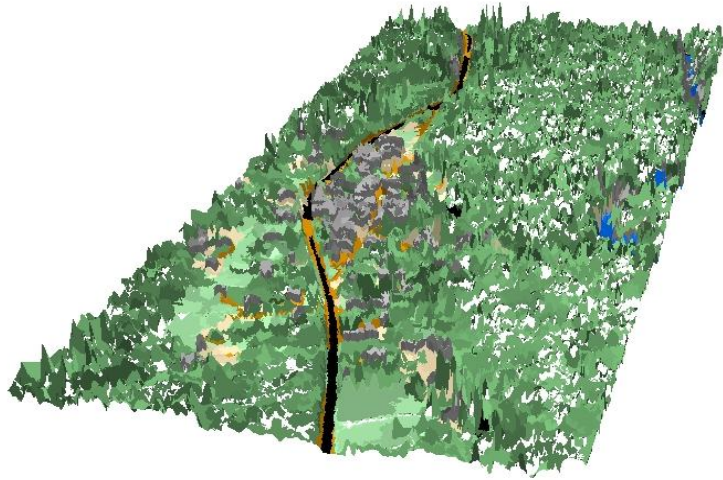


Figure 5.54: Ikiri 3D representation

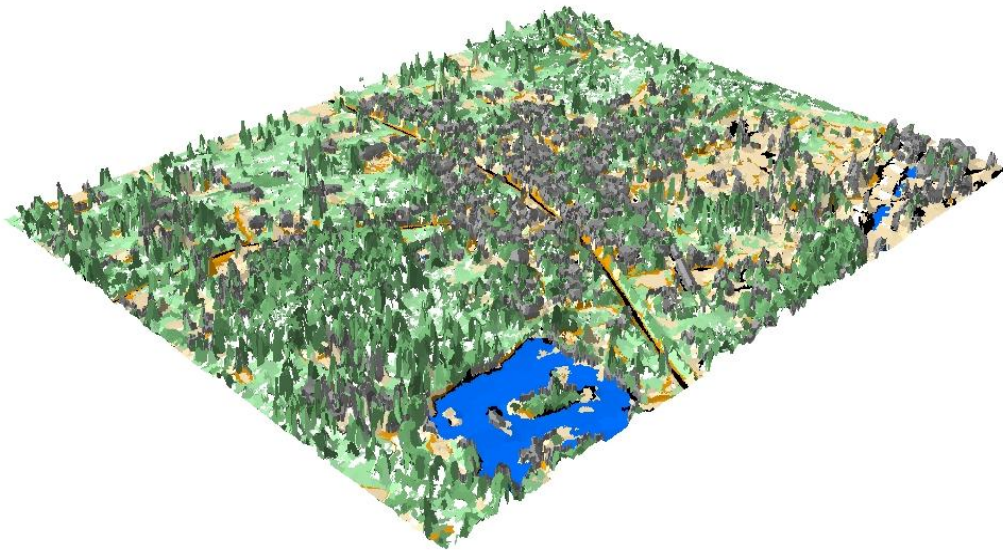


Figure 5.55: Obido 3D representation

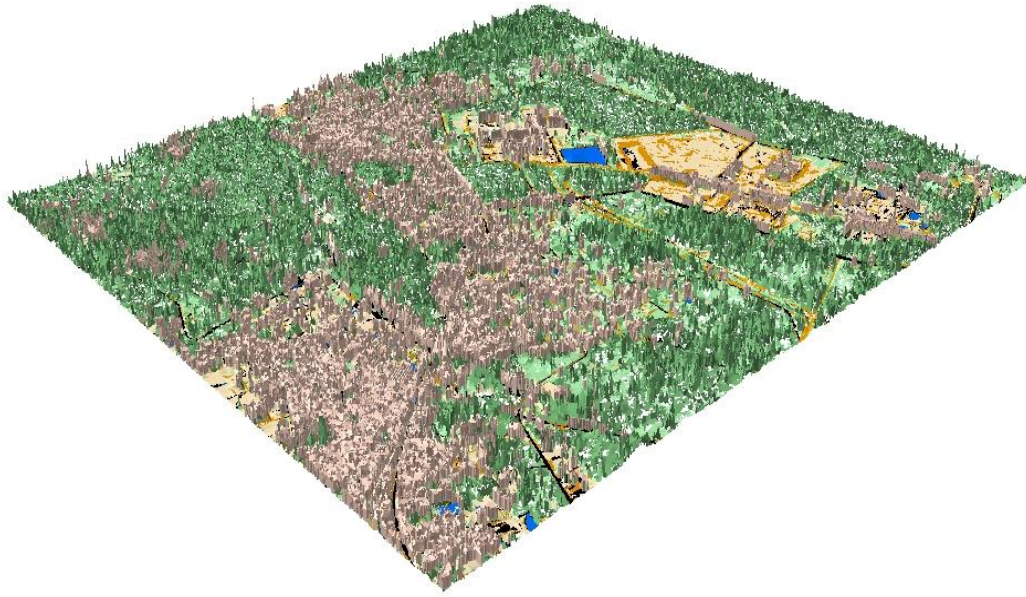


Figure 5.56: Ogbogu 3D representation

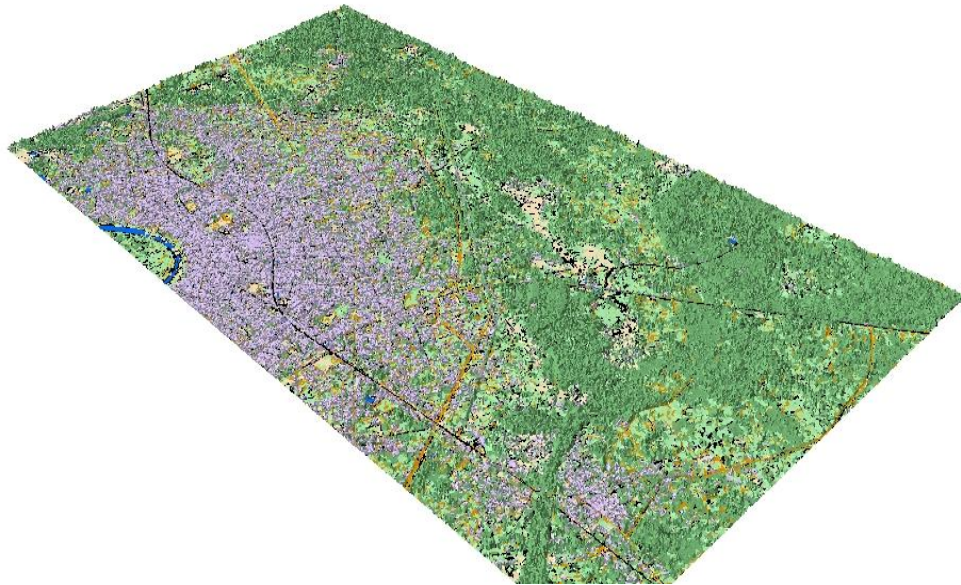


Figure 5.57: Omoku 3D representation

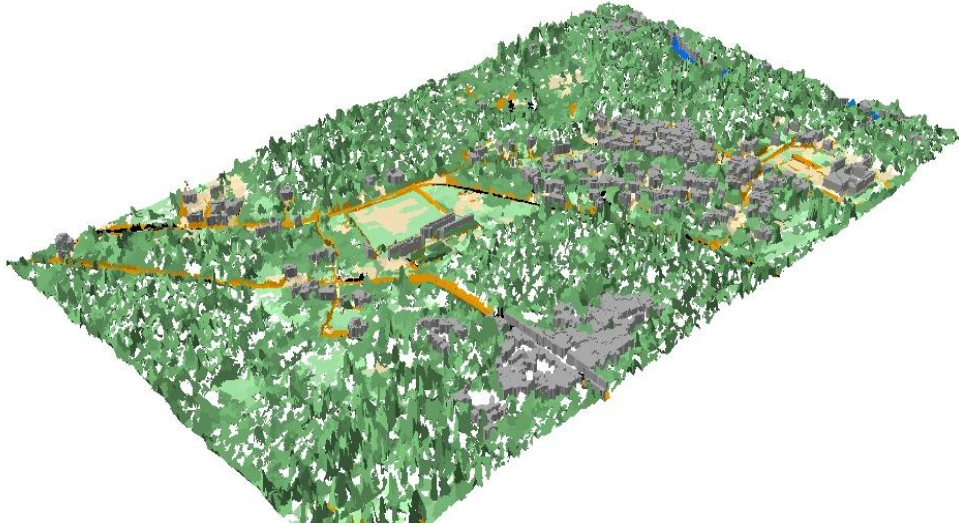


Figure 5.58: Osiakpu 3D representation

5.9 Updated Map of Study Area

In order to achieve objective four, the entire study area map was updated using the Google map image (see appendix 5) and some handheld GPS positions of selected points thought to have existed after the images were captured (see Appendix 4). However before this was done, an object based classification was carried out in the ecognition software environment. Several segmentation parameters were tested and objective visualization was employed for each result before achieving the optimal values which appeared to best reveal the real world features in the entire study area. The approved segmentation values were scale 150, shape 0.3 and compactness 0.8. The standard rule set for this research study was also inputted for the rule based classification. Figures 5.58 and 5.59 are the segmentation/classification rule set and the segmented image of the entire study area.

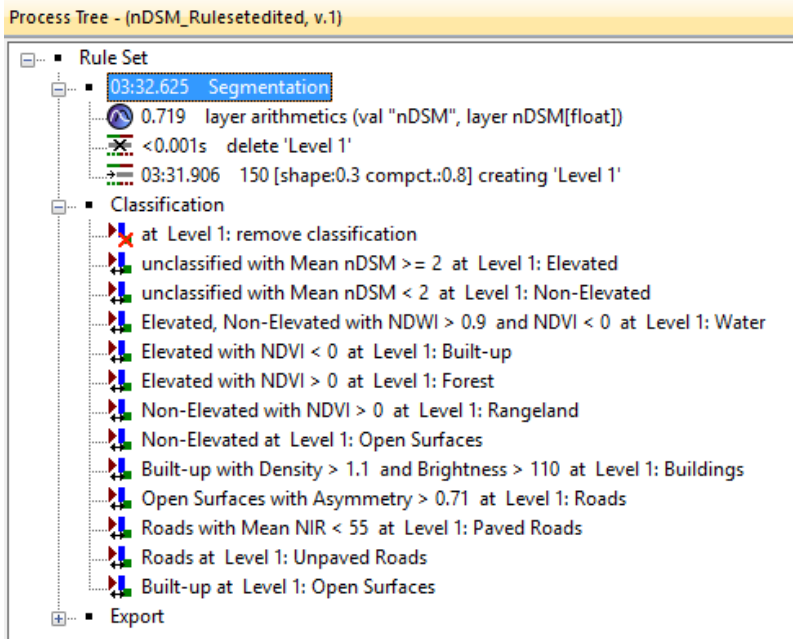


Figure 5.59: Segmentation parameters and classification rule set.

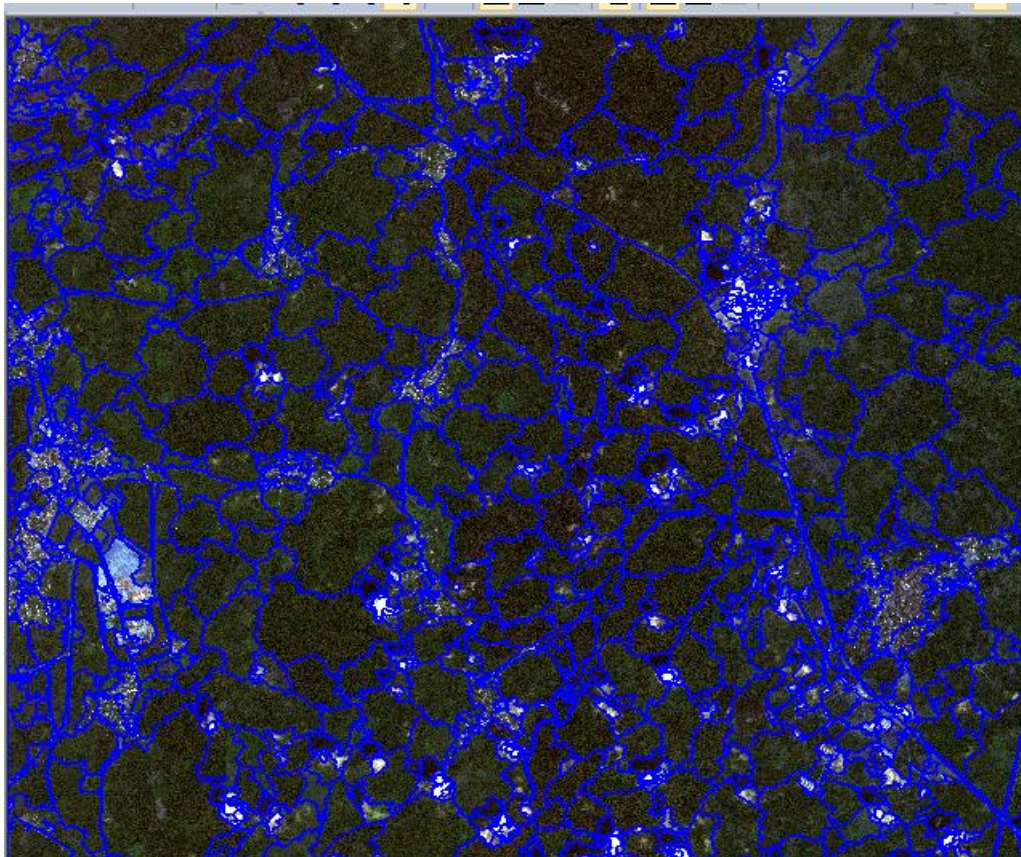


Figure 5.60: OBIA Segmented image of the study area.

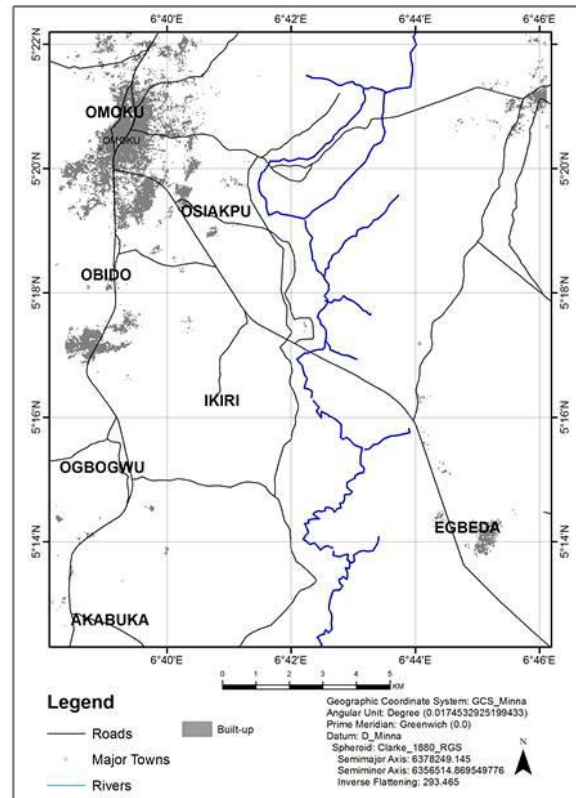
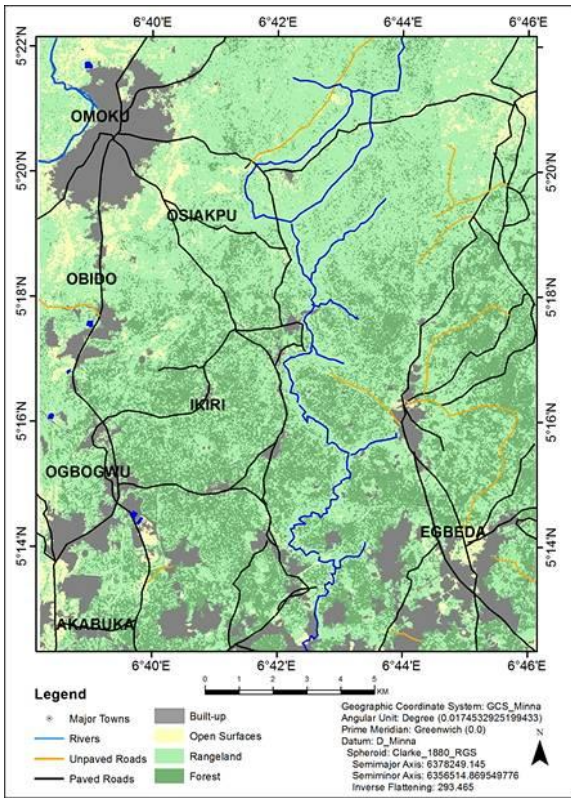


Figure 5.61a: Updated map of the study area Figure. 5.61b:Old map of the study area

5.10 Accuracy Assessment Results

There is no classification created from remote sensing data that can be completely accurate as errors originate from different sources including the classification algorithm itself (Steele et al. 1998, Smits et al. 1999). This makes it compelling that the user needs to know how accurate these products are by carrying out accuracy assessment of every remote sensing classification. One of the most common ways of representing accuracy assessment information is in the form of an error matrix, or contingency table (Congalton 1991, Congalton and Green 1998). Error matrix provides a detailed assessment of the how much the reference data and the classified data agree at specific locations. In addition to this assessment by error matrix, a number of descriptive and analytical statistical techniques, based on the error matrix, have been proposed (Okeke

and Karneli, 2006). These include the overall accuracy, user's and producer's accuracy, and various forms of kappa coefficients of agreement.

The tables in Appendix 7 (seven) contain the results of the accuracy assessment based on Producer's accuracy, User's accuracy, Overall accuracy and Kappa coefficient. Producer's accuracy and user's accuracy are related to commission and omission error, respectively. Commission error refers to misclassification that occurs because pixels of another class are labeled by the user as belonging to the class of interest. Omission error takes place when pixels belong to the ground truth class, but are assigned to a different class (Conchedda et al. 2008).

They are arranged correspondingly for the seven (7) study sites and the respective experiments of Pixel based OBIA with VHR and finally OBIA with VHR and LiDAR nDSM.

Figures 5.62 a-c and Tables 5.4 a-c in section 5.10.1 are the summaries of the overall accuracy and kappa (as bar chart and tables) for the three independent experiments for the seven study sites while figure 5.63 is a bar chart showing all three independent experiments for all the study sites. This representation was done in order to appreciate the consistency in the results.

All error matrix tables are displayed in Appendix 7 from tables AP7.1a,b&c – tables AP7.7a,b&c while Quantitative Values of the LU/LC classes achieved from different methods are displayed in Appendix 8 from tables AP8a – AP8g.

5.10.1 Summary of Overall Accuracy and Kappa Coefficient

Table 5.4 a: Summary of Pixel Method Overall Accuracy and Kappa Coefficient

PIXEL BASED		
STUDY SITES	OVERALL ACCURACY (%)	KAPPA
AKABUKA	71	0.654
EGBEDA	77	0.728
IKIRI	72	0.670
OBIDO	72	0.669
OGBOGU	74	0.692
OMOKU	71	0.659
OBIAKPU	70	0.647
Average	74.43%	0.674

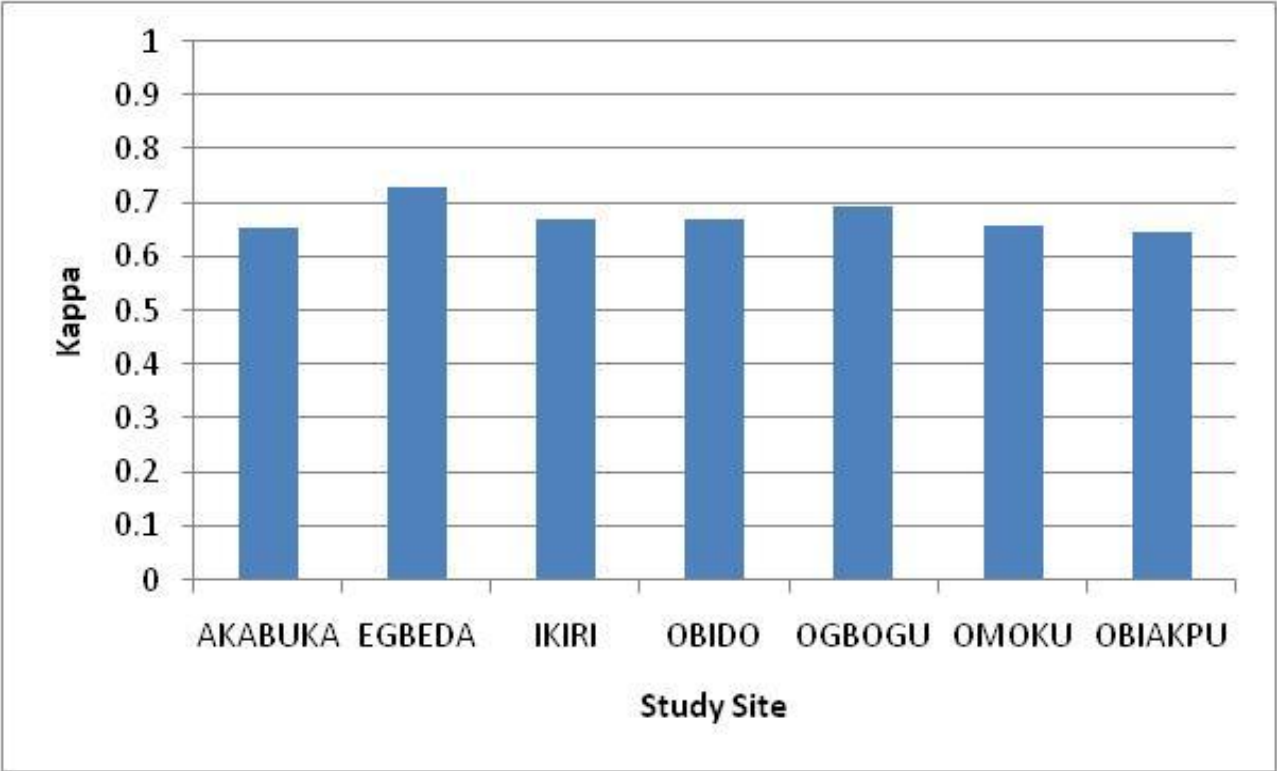


Figure 5.62 a: Bar chart for pixel based results.

Table 5.4 b: Summary of OBIA (VHR) Method Overall Accuracy and Kappa Coefficient

OBIA WITH VHR		
STUDY SITES	OVER-ALL % ACCURACY	KAPPA
AKABUKA	81	0.769
EGBEDA	87	0.839
IKIRI	81	0.776
OBIDO	81	0.776
OGBOGU	83	0.806
OMOKU	82	0.791
OBIAKPU	82	0.786
Average	82.43%	0.791

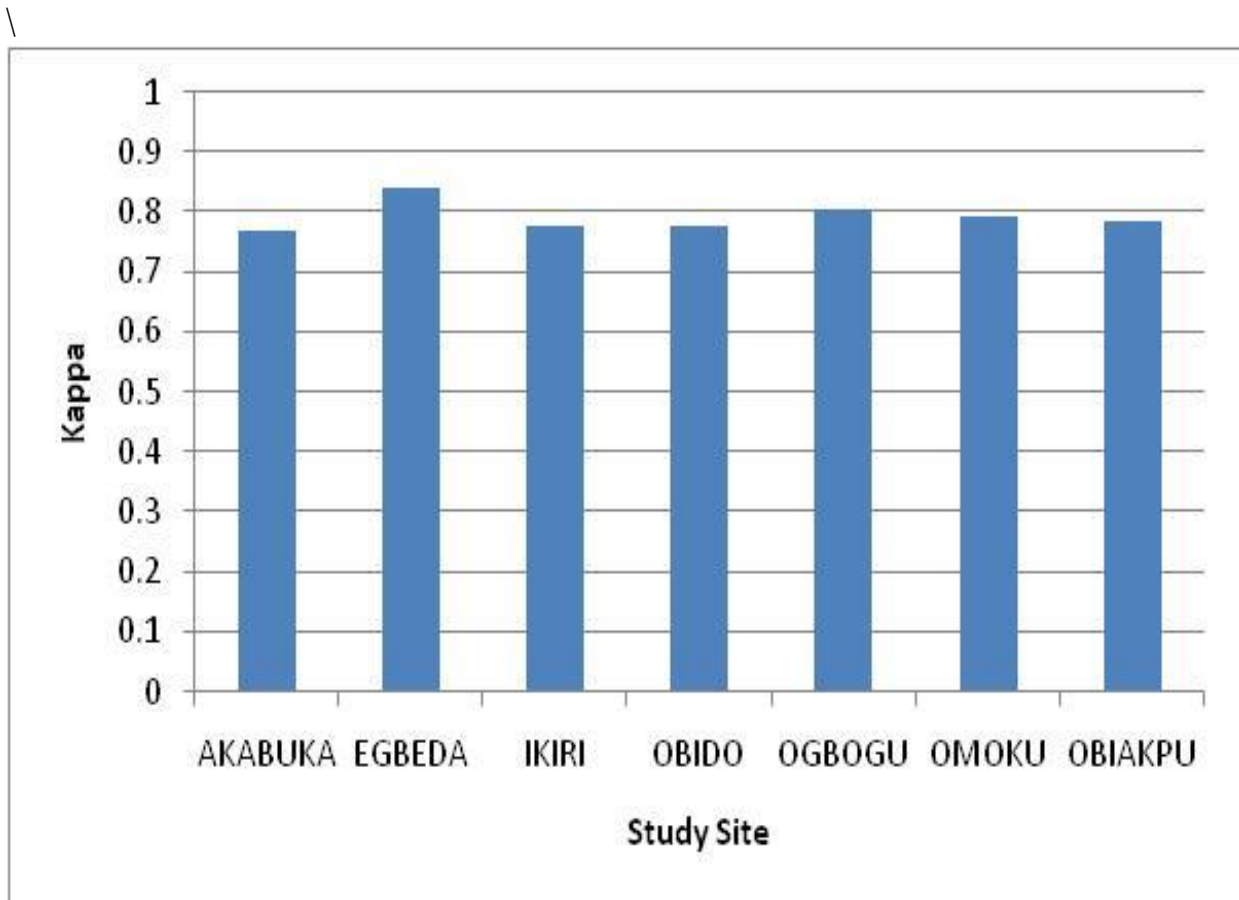


Figure 5.62 b: Bar chart for OBIA_{VHR} results

Table 5.4c: Summary of OBIA (VHR & nDSM) Method, Overall Accuracy and Kappa Coefficient

OBIA WITH VHR & NDSM		
STUDY SITES	OVER-ALL % ACCURACY	KAPPA
AKABUKA	92	0.899
EGBEDA	93	0.912
IKIRI	91	0.894
OBIDO	90	0.885
OGBOGU	94	0.927
OMOKU	93	0.916
OBIAKPU	92	0.903
Average	91.14%	0.905

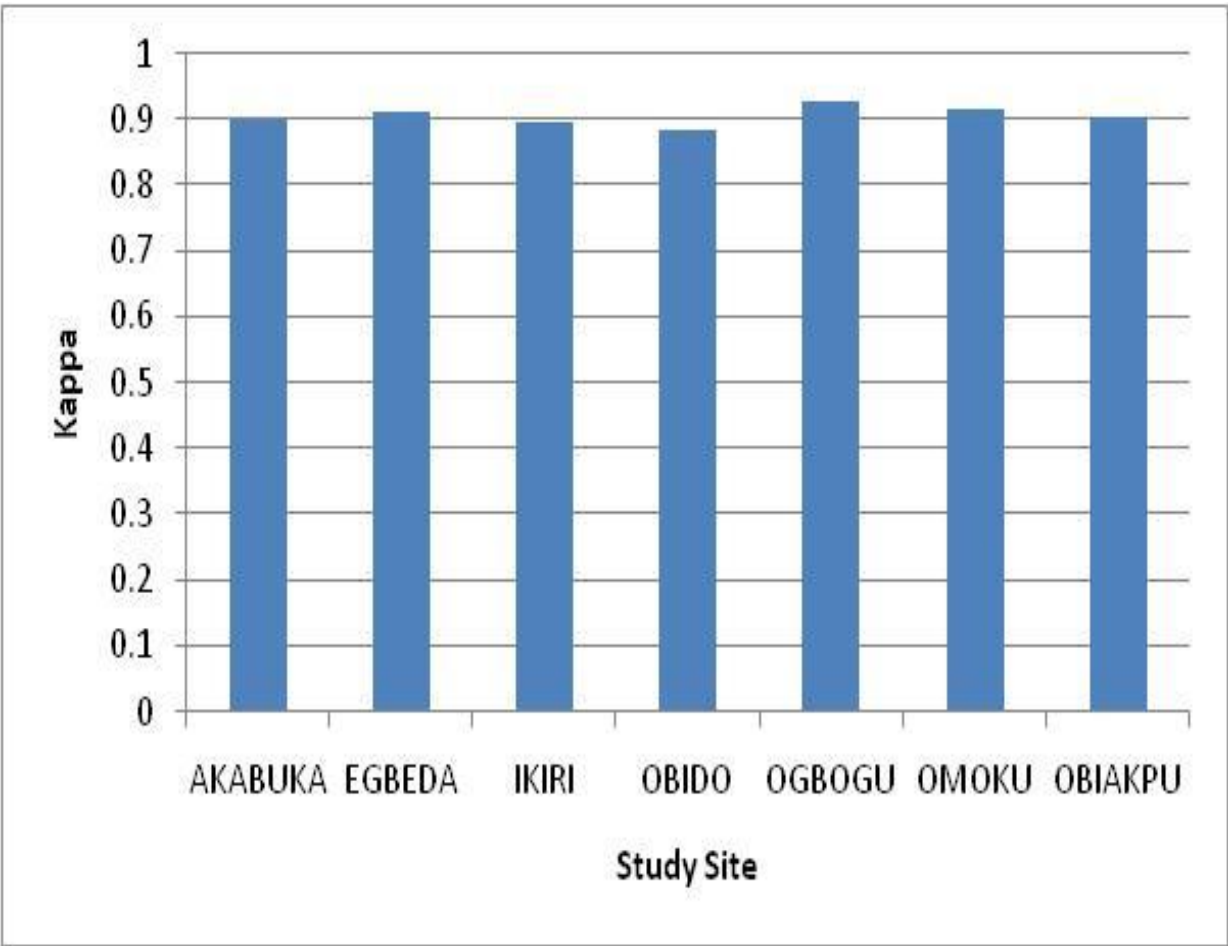


Figure 5.62 b: Bar chart for OBIA_{VHR} & n_{DSM} results

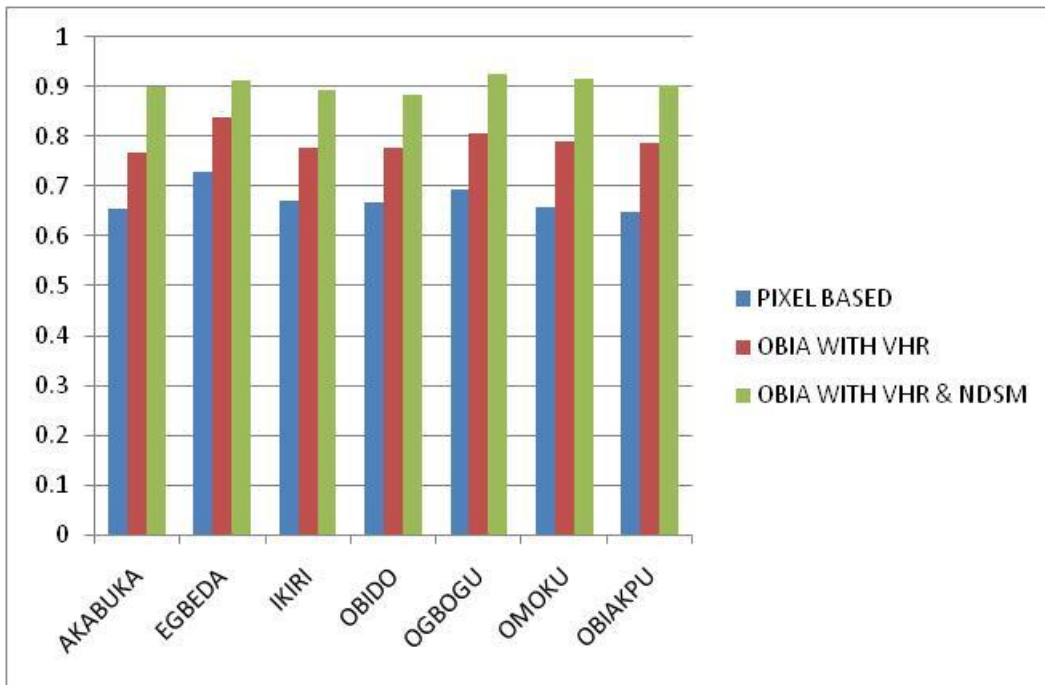


Figure 5.63: Bar Chart of Quantitative Values of the LU/LC classes achieved from different methods applied

5.11 Hypotheses Tests

One method of evaluating research questions in a quantitative research is through the process of hypothesis testing. A hypothesis test is a statistical test that is used to determine whether there is enough evidence in a sample of data to infer that a certain condition is true for the entire population. A hypothesis test examines two opposing hypotheses about a population: the null hypothesis and the alternative hypothesis. The null hypothesis is the statement being tested. Usually the null hypothesis is a statement of "no effect" or "no difference". The alternative hypothesis is the statement you want to be able to conclude is true. Two research questions have been set in this research and the hypothesis test will be used to evaluate them.

In this research, the T-test statistics has been selected for use. It is very likely that the T-test is most commonly used Statistical Data Analysis procedure for hypothesis testing since it is straightforward and easy to use. Additionally, it is flexible and adaptable to a broad range of circumstances.

The procedure used here is the independent sample T-test. This procedure is used when the population mean and standard deviation are unknown, and 2 separate groups are being compared. We therefore have to determine the sample mean and sample standard deviation or variance. To successfully achieve this, Efron and Tibshirani (1993) recommended between 25 and 200 random sample reference for the estimation of standard error so a total of 28 sample reference data were taken from each of the seven study sites for the three experiments (See Appendix 2):-

- i. Pixel based,
- ii. OBIA with VHR and

iii OBIA with VHR and nDSM.

5.11.1 T-Test for Two Independent Samples with Unknown Equal Population Variances

Let N_1 and N_2 represent two independent populations with means μ_1 and μ_2 respectively.

Also let their population variances be σ_1^2 and σ_2^2 such that $\sigma_1^2 = \sigma_2^2$.

Now let n_1 and n_2 denote samples of the two populations with sample mean \bar{x}_1 and \bar{x}_2 and sample variance s_1^2 and s_2^2 respectively.

Where $\bar{x}_i = \sum_{i=1}^n (x_i - \bar{x}) / n$ and

$$s_i^2 = \sum_{i=1}^n (x_i - \bar{x})^2 / n - 1 \quad \text{for } i = 1, 2$$

We can conduct a two tailed test of a null hypothesis:

$$H_0: \mu_1 = \mu_2 \text{ or } \mu_1 - \mu_2 = 0$$

Against an alternative hypothesis

$$H_1: \mu_1 \neq \mu_2 \text{ or } \mu_1 - \mu_2 \neq 0$$

A t-statistic assumed to be normally distributed is calculated using the formula.

$$t_{\text{cal}} = (\bar{x}_1 - \bar{x}_2) - (\mu_1 - \mu_2) / (s_1^2/n_1 + s_2^2/n_2)^{1/2} \quad (1)$$

Where $(\bar{x}_1 - \bar{x}_2)$ is the difference in sample means and

$(s_1^2/n_1 + s_2^2/n_2)^{1/2}$ is a pooled standard error

Since $\mu_1 - \mu_2 = 0$, equation 1 can be expressed as

$$t_{\text{cal}} = (\bar{x}_1 - \bar{x}_2) / (s_1^2/n_1 + s_2^2/n_2)^{1/2} \quad (2)$$

A critical t-value is read from the statistical table at α level of significance with degree of freedom equals $(n_1 + n_2 - 2)$. So that for a two-tailed critical t-value we may denote as

$t_{\text{cri}} = t_{(n_1+n_2-2); \alpha/2}$ We then compare absolute t_{cal} , ie, $|t_{\text{cal}}|$ and t_{cri} values to make a decision.

Decision rule is to reject the null hypothesis H_0 , and choose the alternative hypothesis H_1 if,

$$|t_{\text{cal}}| > t_{\text{cri}}$$

And conclude that the two population means μ_1 and μ_2 are not equal and statistically different.

Otherwise, we do not reject H_0 if

$$|t_{\text{cal}}| < t_{\text{cri}}$$

And conclude that the two populations have same mean and not statistically different from each other.

Also a 95% Confidence Interval (C.I.) of the null hypothesis can be constructed using:

95% C.I. = $(\bar{x}_S - \bar{x}_H) - \text{or} + 1.96(\text{S.E})$ where S.E. is the pooled standard error. We do not reject the null hypothesis if zero (0) lies in the constructed interval, otherwise we reject and conclude that there is a significant difference in the two means compared

5.11.2 Evaluation of Hypotheses

5.11.2.1 Null Hypothesis 1: There is no significant difference between the accuracies of object based and pixel based methods of classification using high spatial resolution imagery.

To evaluate the first null hypothesis stated for this study, consider the mean, variance and size of the sampling distribution of the Pixel Method denoted by \bar{x}_S, s^2_S and

n_S respectively. Also consider its counterpart OBIA Method with mean (\bar{x}_H), variance (s^2_H) and size (n_H).

From the study $n_S = n_H = 28$ and,

$$\bar{x}_S = \sum_{S=1}^{28} (x_S - \bar{x}_S) / n = 0.635 + 0.621 + \dots + 0.654 / 28$$

$$\bar{x}_S = 19.04 / 28 = 0.68.$$

$$\bar{x}_H = \sum_{H=1}^{28} (x_H - \bar{x}_H) / n = 0.769 + 0.741 + \dots + 0.815 / 28$$

$$\bar{x}_H = 22.12 / 28 = 0.79.$$

$$s^2_S = \sum_{S=1}^{28} (x_S - \bar{x}_S)^2 / n_S - 1$$

$$= (0.635 - 0.68)^2 + (0.621 - 0.68)^2 + \dots + (0.654 - 0.68)^2 / 28 - 1$$

$$= 0.051 / 27$$

$$s^2_S = 0.001875$$

$$s^2_H = \sum_{H=1}^{28} (x_H - \bar{x}_H)^2 / n_H - 1$$

$$= (0.769 - 0.79)^2 + (0.741 - 0.79)^2 + \dots + (0.815 - 0.79)^2 / 28 - 1$$

$$= 0.0303 / 27$$

$$s^2_H = 0.001124$$

Now for a two-tailed test of the null hypothesis

$$H_0: \mu_H = \mu_N \text{ or } \mu_H - \mu_N = 0$$

Against an alternative hypothesis

$$H_1: \mu_H \neq \mu_N \text{ or } \mu_H - \mu_N \neq 0$$

The two-tailed critical t-value at 5% (α) level of significance with $n_S + n_H - 2$ degrees of

freedom is given by

$$t_{cal} = (\bar{x}_S - \bar{x}_H) - (\mu_S - \mu_H) / (s^2_S / n_S + s^2_H / n_H)^{1/2}$$

$$= (0.68 - 0.79) - (0) / (0.001875 / 28 + 0.001124 / 28)^{1/2}$$

$$= -0.11 / (0.000067 + 0.00003)^{1/2}$$

$$= -0.11 / (0.000097)^{1/2}$$

$$= 0.11 / 0.0097$$

$$t_{cal} = -11.34$$

$$|t_{cal}| = 11.34$$

The two-tailed critical t-value at $\alpha = 5\%$ level of significance with D of F = $(n_S + n_H - 2)$

is given by

$$t_{cri} = t_{n_H + n_N - 2; \alpha/2} = t_{28+28-2; 0.05/2}$$

$$t_{cri} = t_{56-2; 0.025} = t_{54; 0.025}$$

$$t_{cri} = 2.0049 \text{ (from statistical tables see appendix 1)}$$

Hence $|t_{cal}| > t_{cri}$

$$11.34 > 2.0049$$

For the above hypothesis we construct

$$\text{C.I.} = (\bar{x}_S - \bar{x}_H) - \text{or} + 1.96(\text{S.E})$$

$$= (0.68 - 0.79) - \text{or} + 1.96(0.0097)$$

$$= -0.11 - \text{or} + 0.019$$

Since zero does not lie in the C.I., we reject H_0 .

Lastly, the probability that t is less than -11.34 is read from statistical tables and presented as:

$P(t \leq -11.34) = 6.5(10)^{-16}$ which is approximately zero, indicating a very high significant difference in the two averages compared.

5.11.2.2 Decision: Considering the t- test, C.I. and probability values, we reject the null hypothesis in favour of the alternative hypothesis and conclude that there is a significant

difference in the population means of the Pixel and OBIA methods. It implies that the Pixel method has mean (0.68) lower than OBIA mean (0.79). Thus OBIA yields a better outcome than the Pixel method.

5.11.2.3 Null Hypothesis 2: The addition of nDSM does not significantly improve the accuracy of high resolution image classification of urban area.

To evaluate the second hypothesis proposed by the study, we again consider the sample mean (\bar{x}_H), variance (s^2_H) and size (n_H) of OBIA method with those of its counterpart OBIA_{nDSM} with sample mean (\bar{x}_N), variance (s^2_N) and size (n_N).

Similarly, $n_H = n_N = 28$ from the study and

$\bar{x}_H = 0.79$; $s^2_H = 0.001124$ as earlier obtained.

But for OBIA_{nDSM} sample we have;

$$\bar{x}_N = \sum_{N=1}^{28} (x_N) / n$$

$$\bar{x}_N = \frac{0.903+0.88+\dots+0.903}{28}$$

$$\bar{x}_N = \frac{25.48}{28} = 0.91$$

$$s^2_N = \sum_{N=1}^{28} (x_N - \bar{x}_N)^2 / n_{N-1}$$

$$s^2_N = \frac{(0.903-0.91)^2 + (0.88-0.91)^2 + \dots + (0.903-0.91)^2}{28-1}$$

$$s^2_N = \frac{0.0129}{27} = 0.000477$$

A two-tailed test of the null hypothesis

$$H_0: \mu_H = \mu_N \text{ or } \mu_H - \mu_N = 0$$

Against an alternative hypothesis

$$H_1: \mu_H \neq \mu_N \text{ or } \mu_H - \mu_N \neq 0$$

$$t_{\text{cal}} = (\bar{x}_H - \bar{x}_N) - (\mu_H - \mu_N) / (s_H^2/n_H + s_N^2/n_N)^{1/2}$$

$$t_{\text{cal}} = \frac{(0.79-0.91)-(0)}{\sqrt{0.001124/28+(0.000477/28)}}$$

$$t_{\text{cal}} = \frac{-0.12}{\sqrt{0.00004+(0.000017)}}$$

$$t_{\text{cal}} = \frac{-0.12}{\sqrt{0.000057}}$$

$$t_{\text{cal}} = \frac{-0.12}{0.008} = -15$$

The two-tailed critical t-value at $\alpha = 5\%$ level of significance with D of F = $(n_H + n_N - 2)$ is given by

$$t_{\text{cri}} = t_{n_H + n_N - 2; \alpha/2} = t_{28+28-2; 0.05/2}$$

$$t_{\text{cri}} = t_{56-2; 0.025} = t_{54; 0.025}$$

$$t_{\text{cri}} = 2.0049 \quad (\text{from statistical tables see appendix 1})$$

Hence $|t_{\text{cal}}| > t_{\text{cri}}$

$$15 > 2.0049$$

Again for the above hypothesis 2 we construct

$$\text{C.I.} = (\bar{x}_S - \bar{x}_H) - \text{or} + 1.96(\text{S.E})$$

$$= (0.79 - 0.91) - \text{or} + 1.96 (0.008)$$

$$= (-0.11 - 0.016, -0.11 + 0.016)$$

$$\text{C.I.} = (-0.136, -0.104)$$

Since zero does not lie in the C.I., we reject H_0 .

The probability that t is less than -15 is read from statistical tables and presented as:

$P(t \leq -15) = 9.2(10)^{-21}$ which is approximately zero, indicating a very high significant difference in the two averages compared.

5.11.2.4 Decision: We therefore reject the null hypothesis of no significant difference in the kappa mean values of OBIA and OBIA_{nDSM} considering the t- test, C.I. and probability values. Thus we conclude that there is a significant difference in the average kappa values of OBIA and OBIA_{nDSM}. The implication is that OBIA_{nDSM} performed better since its average kappa value of 0.91 is significantly higher than that of OBIA with an average value of 0.79.

5.11.2.5 Null Hypothesis 3: Ho₂ the addition of LiDAR derived nDSM to the VHR image is not effective in the 3-D analysis of features extracted.

This hypothesis has been tested by visual inspection of the theVirtual Geographic Environment (VGE) experiment carried out in sub-head 4.7 and results displayed as figures 5.52a and 5.52b. The visual inspection clearly shows figure 5.52b as a 3-D display of Akabuka study site due to the addition of LiDAR derived nDSM while the figure 5.52a which had no nDSM showed a 2-D display of the site.

5.11.2.6 Decision: Since the addition of nDSM created a 3-D visualization of the site and the reverse was the case when excluded, we therefore reject the null hypothesis.

5.12 Comparison of Results

The summary of the results from the three experiments are displayed in tables a, b and c. for Pixel based, OBIA using VHR and OBIA using VHR and nDSM respectively. Each of the tables contain overall accuracy and kappa coefficient for each of the 7 (seven) study sites. The two OBIA achieved higher overall classification accuracies and higher individual LU/LC classes (“producer’s accuracy” and “user’s accuracy”) over the

Maximum Likelihood classifier of pixel-based approach. The details of the result from tables a, b and c show that the pixel based method has overall accuracy ranging from 70% to 77% and Kappa from 0.647 to 0.728, while OBIA using VHR image alone has overall accuracy ranging from 81% to 87% with Kappa 0.769 to 0.839 and finally, OBIA using VHR image and nDSM has overall accuracy ranging from 90% to 94% and Kappa from 0.885 to 0.927. Also from tables 5.11a, 5.11b and 5.11c, the average overall accuracy for the three independent experiments is 72.43% for the pixel based method, 82.43% for the OBIA using VHR image while 91.14% represents the average overall accuracy achieved in the OBIA using VHR and nDSM. Similarly, the average Kappa results are 0.674, 0.791 and 0.905 respectively for the three experiments. A careful look at the results will show a consistent increase in the overall accuracy as well as the Kappa coefficient from the pixel based method to the OBIA method using VHR and nDSM. A Kappa statistic of > 80% suggests a strong agreement, while 40% to 80% is a moderate agreement. Thus, strong agreements were achieved in OBIA methods, while a moderate agreement was observed in pixel-based method.

The pixel based method is only based on pixel value of spectral value whereas object based method is based on spectral value, shape, texture, and context information for processing images. OBIA has showed more capability to deal with the complexity of the VHR image. From visual inspection of the classification results from the two methods, you can judge by visual clarity which the OBIA maps have over the pixel based maps.

The comparison between the two object based processes which used VHR image alone and the other which used VHR in addition to nDSM also reveals a significant difference

in the results. The result showed 8.71% increase when nDSM was added to the process. Adding ancillary data to spectral bands of VHR imagery over urban areas is critical for classifying spectrally similar classes such as buildings and other tall features.

Tables from 5.12a-g contain values of the distribution of the land cover classes in the study sites. A careful look at the land cover classes distribution in the selected urban study sites the forest class has the highest coverage in all the seven study sites. In terms of relative distribution of the building class, Omoku has the highest with a corresponding high shadow content resulting from more urban structures than the other study sites. These results also show high accuracy for all vegetation extraction which indicates the very high potential of object-based classification of VHR imagery for extracting vegetation areas using the well-known index of NDVI. The selection of the threshold values for NDVI is critical in classifying vegetation areas.

The high accuracy values achieved in the general feature extraction for unpaved roads may have been as a result that most sections of the paved road have been covered by earth or top soil thereby giving such sections of the paved road to look more like unpaved road surfaces. This was clearly revealed during ground truthing. However, visual evaluation of results from the developed algorithm showed that the algorithm gave better performance. Future works shall focus more on the development of a filtering technique that can successfully differentiate unwanted patches from extracted unpaved road in the result.

CHAPTER SIX

SUMMARY, CONCLUSION AND RECOMMENDATION

6.1 Summary

The focus of this study was basically to examine the use of OBIA method in VHR and to evaluate the integration of LiDAR data derived nDSM in the optimization of the accuracy of extraction of urban land cover information from high resolution GeoEye-1. Seven study sites in Rivers State of Nigeria were subset from the available image and used for this study. Geoeye-1 image and LiDAR data of the study area acquired in 2012 were the only latest data available for the study. The aim of the study was to carry out a comprehensive mapping and analysis of internal urban features with a view to evaluating the supremacy of object-based analysis over pixel-based analysis techniques. Three independent classifications were carried out. The first was pixel-based supervised classification of the land cover features using the Geoeye-1 image in the Erdas imagine9.2 software, while second and third experiments were OBIA carried out within the eCognition developer software. The second experiment was conducted using the VHR image alone while the third had the addition of the LiDAR derived nDSM for optimization purpose. In eCognition this property can be modelled by describing the difference in elevation to neighbouring objects (Hofmann, 2001). The pixel based method and the object based methods used MLC and KNN classifiers respectively.

Object-based classification can fully utilize background user knowledge by readily applying spatial concepts to the classification approach (Benz et al. 2004). By including

contextual information, rather than only spectral information, object-based classification offers the opportunity to maximize accuracy and minimize the likelihood of producing results significantly affected by the “salt-and-pepper effect.” However, the initial segmentation of imagery into objects does not always prevent the “salt-and-pepper effect” (Blaschke 2010). If the user does not utilize the appropriate segmentation approach and apply suitable spatial information to the classification, spectral characteristics of image objects may produce the “salt-and-pepper effect” only at a larger minimum mapping unit (Matinfar et al. 2007). The use of spatial or contextual information from neighborhood pixels remains a major setback to pixel-based method. On the other hand, object-based methods allow integration of different object features, such as spectral values, shape, and texture. One of the strength of the object-based classification is the ability to combine spectral and spatial information for extracting target objects.

6.2 Conclusion

Most traditional classification approaches are based exclusively on the digital number of the pixel itself. Thereby only the spectral information is used for the classification. As a result, the use of spectral based classification methods has been repeatedly reported to create confusion among the classes. The concept is that important semantic information necessary to interpret an image is not represented in single pixels, but in meaningful image objects and their mutual relations. Only the spectral information is used for the classification. High spatial resolution sensors involve a general increase of spatial information and the accuracy of results may decrease on a per-pixel basis. In order to

realize the full potential of the VHR image data, object-oriented image analysis is implemented with the software eCognition. The two OBIA experiments showed better results than the pixel based method consistently for the seven study sites. The OBIA experiments (VHR only and VHR/nDSM) used spectral information that was not used in the pixel-based method. The visual appearances of the OBIA results clearly reveal its superiority over the pixel based classification method.

The impact of the nDSM on the classification process could be evaluated at approximately 9% increase in accuracy. The findings of this research indicate that the combination of the nDSM and GeoEye-1 satellite imagery constitutes an improved and effective approach for extracting detailed information of urban areas. Height information considerably increases the accuracy of land cover information. Therefore, producing land cover maps with an additional nDSM is more appropriate because it would optimize the accuracy. Consequently, this study and previous research studies have found that the addition of high resolution nDSM with VHR imagery always improved the accuracy of urban land cover feature extraction regardless of the site in question. Height information considerably increases the accuracy of land cover information. Therefore, producing land cover maps with an additional nDSM is more appropriate because it would optimise the accuracy, reduce the cost and the time.

The OBIA framework consists of multiresolution segmentation followed by hierarchical rule-based classification. The method offers a practical, fast, and easy to use (within eCognition) framework for classifying VHR imagery of urban areas. Despite the spectral and spatial complexity of land cover types, the method resulted in the overall accuracy

of up to an average of 82.43% when only VHR image was used and average of 91.14% when nDSM was added. This level of accuracy is very promising and the addition of nDSM shows the great potential of combining vector data, VHR imagery, and object-based image analysis for classification of urban areas.

The developed algorithm for the extraction of unpaved roads, on visual evaluation, can be seen to give a more refined map of the extracted unpaved roads (figure 5.44- 5.50) when compared with the unpaved road extracted during the general features extraction. However, future works shall focus more on the development of a filtering technique that can successfully differentiate unwanted patches from extracted unpaved road in the result.

6.3 Recommendations

Technological advances and increasing availability of high-resolution satellite imagery offer the potential for more accurate land cover classifications and analyses, which could greatly improve the detection and quantification of land cover/ land use changes, but these images are often expensive and difficult to acquire, which prohibits or reduces their use. However, effort must be made for easier access to low-cost, multiband, high-resolution satellite imagery as this would greatly facilitate conservation management and decision-making.

Object based images classification method has proved to be very effective in analyzing or extraction land cover features when using very high resolution images and ecognition software has also proved to one of the best software for OBIA. Therefore effort must also be made by research institutes and government to collaborate with software

provider companies towards making it available and affordable to researchers. For now it remains one of the most expensive software for analyzing high resolution remote sensing images.

A successful and accurate classification begins with a successful and accurate segmentation and a successful and accurate segmentation is determined by using the optimal segmentation parameters. Therefore I will strongly recommend that further studies should focus on developing an algorithm that will enable researchers automatically determine optimal segmentation parameters. The current popular method of trial and error cum visual inspection is subjective and leaves room for mistakes or inaccurate segmentation (over segmentation or under segmentation) which takes its toll on the final result or accuracy of classification.

Future studies will strive to develop more filtering technique that can successfully eliminate unwanted patches from extracted unpaved road in the result.

CHAPTER SEVEN

CONTRIBUTION TO KNOWLEDGE

This research further corroborates the results of previous studies (Dinis et al. 2009, Kongo 2015) that have combined satellite imagery with height information from LiDAR to extract urban land cover. It has developed and tested OBIA technique as well as the conventional pixel based approach to define and map LU/LC patterns in the study area of Rivers State, Nigeria. This work has emphasized that the OBIA approach has proved to be an advanced solution for image analysis, since the accuracies were improved at different study sites applied compared with those of pixel-based approach. The study pointed out that the OBIA yielded more accurate results than the classical per-pixel approach especially when analyst's expert knowledge is presented. Its also proved that a suitable segmentation parameter may not necessarily be suitable for use in another image even if its taken by same satellite due to factors like size of the site, sun elevation, topography, acquisition time, etc.

The experiments that combined the nDSM with the GeoEye-1 image as well as when only the GeoEye-1 image was used have confirmed the huge advantage in the integration of LiDAR derived nDSM to the classification of VHR image. This integration of nDSM improved the accuracy by about 9%. This was because the nDSM value was able to clearly discriminate or separate high and low features using feature thresholds thereby making it clear that height information considerably increases the accuracy of land cover information. Furthermore, it has also been successfully shown that rule based method of classification is a viable method and the rule set is transferable to other sites

as has been shown to work successfully in all seven study sites that make up the study area. The range and consistency of accuracy levels achieved in the respective OBIA for the subsets demonstrates the great potential of the transferability of the rule-set to other areas of the same VHR imagery. This study and previous research have found that combining the high resolution nDSM with RS imagery always improved the accuracy of urban land cover regardless of the site used for the experiment.

A good representative value to evaluate the classification accuracy performance is the Kappa statistic, which shows the measure of agreement between the classification result and the reference data, i.e. overall accuracy, and the chance agreement (Jensen, 2005). This research has also helped to verify statistically the reliability of the Kappa statistics as efficient accuracy parameters in validating remote sensing data over a given reference data. It also provides guidelines on the types of features (e.g., texture, shape, size, brightness) and ranges of thresholds which are suitable for classifying specific land cover types. The development of unpaved road refinement algorithm is a major step towards giving attention to the extraction of unpaved roads as a way to support security and surveillance in these times of kidnapping and insurgency.

The digital map of the study area remains a viable document for information in the understanding of the distribution of land cover classes within the study area and would be very helpful to planners and decision makers.

Reference

- Aguilar, M.A., Aguilar, F.J., Saldaña, M. M. and Fernández, I. (2012). Geopositioning accuracy assessment of GeoEye-1 Panchromatic and Multispectral imagery. *Photogrammetric Engineering and Remote Sensing*, 78(3), pp. 247-257.
- Alhaddad, B. I., Roca, J., Burns, M. C. and Garcia, J. (2008). Satellite Imagery and LiDAR Data for Efficiently Describing Structures and Densities In Residential Urban Land Uses Classification
- Anderson, J. R., Hardy, E. E., Roach, J. T. and Witmer, R. E. (2009). A Land Use and Land Cover Classification System for Use with remote Sensor Data.
- Antonarakis, A.S., Richards, K.S and Brasington, J (2008). Object-Based Land Cover Classification using Airborne Lidar. *Remote Sensing of Environment*, Pp. 2988-2998. *Approaches in Remote Sensing- Applied to Nuclear Facilities in Iran'*: Springer.
- Aplin, P. (2006). On Scales and Dynamics in Observing the Environment. *International Journal of Remote Sensing*, 27(11), 2123–2140.
- Awrangjeb, M., Zhang, C. and Fraser, C. S. (2012). Building Detection in Complex Scenes Thorough Effective Separation of Buildings from Trees. *Photogrammetric Engineering & Remote Sensing* 78(7), Pp. 729–745.
- Bandyopadhyay, M., Van Aardta, J. A. N. and Cawse-Nicholson, K. (2013), Classification and Extraction of Trees and Buildings from Urban Scenes Using Discrete Return LiDAR and Aerial Color Imagery
- Baatz, M., Benz, U., Dehghani, S., Heynen, M., Holtje, A., Hofmann, P., Lingenfelder, I., Mimler, M., Sohlbach, M., Weber, M and Willhauck, G (2004). eCognition User's Guide. <http://www2.definiens.com/central/default.asp> (the last accessed 07/March/2006).
- Baatz, M., Hoffmann, C. and Willhauck, G. (2008). Progressing from Object-based to Object-oriented Image Analysis. Pages 29-42, *Object-Based Image Analysis*. Springer.
- Baltsavias, P.E. and Gruen, A. (2003). A Comparison of Aerial Photos, Lidar And IKONOS For Monitoring Cities, *Remotely Sensed Cities* (V. Mesev, Editor), Taylor & Francis, New York, Pp. 47–84.
- Béland M, Widlowski, J. L. and Fournier, R. A. (2014). A model for deriving voxel-level tree leaf area density estimates from ground-based LiDAR. *Environmental Modelling & Software* 51: 184-189.
- Benz, U. C., Hofmann, P., Willhauck, G., Lingenfelder, I and Heynen, M. (2004). Multiresolution, Object-Oriented Fuzzy Analysis of Remote Sensing Data

for GIS-Ready Information. ISPRS Journal of Photogrammetry & Remote Sensing, 58, Pp. 239–258.

- Blaschke, T. and Strobl, J. (2001). 'What's Wrong with Pixels? Some Recent Developments Interfacing Remote Sensing And GIS', GIS _ Zeitschrift Für Geoinformationssysteme, 14(6), 12-17.
- Blaschke, T. (2009). 'Object Based Image Analysis for Remote Sensing', ISPRS Journal of Photogrammetry and Remote Sensing.
- Blaschke, T. (2010). Object Based Image Analysis for Remote Sensing. ISPRS J. Photogramm. Rem. Sens. 65 (1), 2–16.
- Brennan, R. and Webster, T. (2006). Object-Oriented Land Cover Classification of Lidar-Derived Surfaces. Can. J. Remote Sensing, Vol. 32, No. 2, Pp. 162-172.
- Brunn, A. and Weidner, U. (1997). Extracting Buildings from Digital Surface Models. International Archives of Photogrammetry and Remote Sensing 32, 3: 27-34.
- Campbell, J. B and Wynne, R. H (2011). Introduction to Remote Sensing. 5th ed. New York: Taylor & Francis
- Campbell, J. B. (2006). Introduction to Remote Sensing. 4th ed. New York: Taylor & Francis.
- Campbell, J.B. & Wynne, R.H. (2011) Introduction to Remote Sensing. 5th Edition. <http://www.guilford.com/books/Introduction-to-Remote-Sensing/Campbell-Wynne/9781609181765>
- Campbell, J.B. (1996). Introduction to Remote Sensing. 2nd Edition. New York, Guilford Press.
- Carleer, A.P. and Wolff, E. (2006). Urban Land Cover Multi-level Region-based Classification of VHR Data by Selecting Relevant Features, International Journal of Remote Sensing, Vol. 27, No. 5-6, pp. 1035-1051.
- Charlton, M. E., Large, A. R. G. and Fuller, I. C. (2003). Application of Airborne LIDAR in River Environments: The River COQUET, Northumberland, UK, Earth Surf. Process. Landforms, 28, 299– 306,
- Chen, Y., Su, W., Li, J. and Sun, Z. (2009). Hierarchical Object Oriented Classification Using Very High Resolution Imagery and LIDAR Data Over Urban Areas. Advances in Space Research, 43, Pp. 1101-1110.
- Chuvieco, E., Li, J. and Yang, X. (2010). Advance in Earth Observation of Global Change. London: Springer.
- Clode, S., Kootsookos, P. and Rottensteiner, F. (2004). The Automatic Extraction of Roads from LiDAR data. In Altan O (ed) ISPRS Archives-Volume XXXV Part

B7, 2004. Proceedings of International Congress held 12-23 July 2004, Istanbul, Turkey. Clode

- Conchedda, G., Durieux, L. and Mayaux, P. (2007). Object-based monitoring of land cover changes in mangrove ecosystems of Senegal. In Verhoest N, Bruneel S, Coppin P, Gabriëlle De Lannoy G, Verstraete W & Hoeben R (eds) 2007 International Workshop on the Analysis of Multi-temporal Remote Sensing Images, 1-6. Proceedings of a meeting held 18-20 July 2007, Leuven, Belgium.
- Conchedda, G., Durieux, L. and Mayaux, P.(2008).“An Object-Based Method for Mapping and Change Analysis in Mangrove Ecosystems.” ISPRS Journal of Photogrammetry and Remote Sensing 63: 578–89.
- Congalton R. and Green K. (2009). Assessing the Accuracy of Remotely Sensed Data: Principles and Practices. 2nd Ed. Boca Raton: Taylor & Francis.
- Congalton, R.G., Green, K. (1999). Assessing the Accuracy of Remotely Sensed Data: Principles and Practices. Lewis Publisher.
- Curran, P. J. (1985). Principles of Remote Sensing, Harlow: longman.
- Dare, P.M. (2005). Shadow analysis in high-resolution satellite imagery of urban areas. Photogrammetric Engineering & Remote Sensing, 71(2), 169–177.
- Debes, C., Merentitis, A., Heremans, R., Hahn, J., Frangiadakis, N., van Kasteren, T., Liao, W., Bellens, R., Pizurica, A., Gautama, S. and Philips, W., Prasad, S., Du, Q. and Pacific, F. (2014). Hyperspectral and LiDAR data fusion: Outcome of the 2013 GRSS Data Fusion Contest. IEEE Journal of Selected Topics in Applied Earth Observations and Remote Sensing.
- deKok, R., Schneider, T. and Ammer, U. (1999). Object Based Classification, Applications in the Alpine Forest Environment, International Archives of Photogrammetry And Remote Sensing, Vol. 32, No. 7-4-3 W6, 3-4 June, 1999.
- Demir, N. and Baltsavias, E. (2012). Automatic Modelling of 3D Building Roofs using Image and LiDAR Data.
- Devereux, B.J., Amable, G. S. and Posada, C. C. (2004). An Efficient Image Segmentation Algorithm for Landscape Analysis. International Journal of Applied Earth Observation And Geoinformation 6 (1), 47-61.
- Dinis, J., Navarro, A., Soares, F., Santosb, T., Freire, S., Fonseca, A., Afonso, N and Tenedório, J. (2009). Hierarchical Object-Based Classification of Dense Urban Areas by Integrating High Spatial Resolution Satellite Images and LiDAR Elevation Data
- Dupuy, S., Lainé, G. and Tormos, T. (2012). OBIA for Combining LiDAR and multispectral data to Characterize forested Areas

- Durieux, L., Lagabrielle, E. and Nelson, A. (2008). A Method For Monitoring Building Construction In Urban Sprawl Areas Using Object-Based Analysis Of SPOT 5 Images And Existing GIS Data. *ISPRS J. Photogramm.* 63, 399-408.
- eCognition Reference Book. (2011). Trimble eCognition, Developer 8.64.1 Reference Book.
- Efe, S.I (2003) 'Effects of Gas Flaring on Temperature and Adjacent Vegetation in Niger Delta Environment, international journal of environmental issues volume 1 number 1 2003 pp. 91-101
- Efron, B. and Tibshirani, R.J., (1993), *An Introduction to the Bootstrap* (New York: Chapman and Hall).
- Ellah, F. J. (1995). "Ali-Ogba: A History of Ogba People". www.africanbookscollective.com. Fourth Dimension Publishers. pp. 123–177. ISBN 9789781564000. Retrieved April 23, 2016.
- ERDAS IMAGINE Tour Guides (2006), Leica Geo-systems Geospatial Imaging.ESRI (2014), 3D Urban Mapping: From Pretty Pictures to 3D GIS
- Eurosense, (2011).Urban Green Monitoring [Online]. Available From [Http://Www.Eurosense.Com/Documents/Your-Application/Energy-Environment agriculture/Urban-Green-Monitoring.Xml?Lang=En-Gb](http://www.eurosense.com/Documents/Your-Application/Energy-Environment%20agriculture/Urban-Green-Monitoring.Xml?Lang=En-Gb) [Access 10 Mai 1012].
- Fauvel, M. (2007).Spectral and Spatial Method for Classification of Urban Remote Sensing Data, Ph.D thesis.
- Florinsky, I.V. (1998). Accuracy of local topographic variables derived from digital elevation models. *International Journal of Geographical Information Science* 12: 1, 47–61.
- Foley,J.A., Defries, R., Asner, G.P., Barford, C., Bonan, G., Carpenter, S and Syder, P.K., (2005).Global Consequences of Land Use. *Science*, 309, Pp. 570–574.
- Foody, G. M. (2004b). "Thematic Map Comparison: Evaluating the Statistical Significance of Differences in Classification Accuracy." *Photogrammetric Engineering & Remote Sensing* 70, no. 5 (2004b): 627-633.
- Foody, G.M., (2002).Status of land cover classification accuracy assessment. *Remote Sensing of Environment*, 80, pp. 185–201.
- Fraser C.S, Dial G. and Grodecki J. (2006). Sensor Orientation via Rpcs. *ISPRS Journal of Photogrammetry & Remote Sensing* 60, 3: 182-194.
- Gamanya, R., De Maeyer, P. and De Dapper, M. (2007). An Automated Satellite Image Classification Design Using Objectoriented Segmentation Algorithms: A Move towards Standardization. *Expert Systems with Applications*, 32(2), Pp. 616-624.

- Gamba, P. and Houshmand, B. (2000). Digital surface models and building extraction: A comparison of IFSAR and LiDAR data. *IEEE Transactions on Geoscience and Remote Sensing* 38, 4: 1959-1968.
- Gao, Y., Kerle, N., Mas, J. F., Navarrete, A. and Niemeyer, I. (2007). Optimized Image Segmentation and Its Effect on Classification Accuracy. Poster Session on 5th International Symposium on Spatial Data Quality, Enschede, the Netherlands
- Garcia-Feced, C., Temple, D. and Kelly M. (2011). Characterizing California spotted owl nest sites and their associated forest stands using Lidar data. *J Forest* 108:436–43.
- Gatziolis D. and Andersen H. E.(2008).A guide to LiDAR data acquisition and processing for the forests of the Pacific Northwest.US Department of Agriculture, Forest Service, Pacific Northwest Research Station.
- Gaulton, R and Malthus, T. J (2010). LiDAR Mapping of Canopy Gaps in Continuous Cover Forests: a Comparison of Canopy Height Model and Point Cloud Based Techniques. *International Journal of Remote Sensing* 31, 5: 1193-1211.
- Gilania, S. A. N., Awrangjebb, M. and Lu, G. (2015). Fusion of Lidar Data and Multispectral Imagery for Effective Building Detection Based on Graph and Connected Component Analysis
- Grimm, N.B., Faeth, S.H., Golubiewski, N.E., Redman, C.L., Wu, J., Bai, X and Briggs, J.M. (2008), *Global Change and The Ecology Of Cities*. *Science*, 319, Pp. 756–760.
- Habib, A., Ghanma, M., Morgan, M and Al-Ruzouq, R. (2005).Photogrammetric and LiDAR Data Registration using Linear Features. *Photogrammetric Engineering and Remote Sensing* 71, 6: 699-707.
- Hamedianfar, A., Shafri, H.Z.M., Mansor, S. and Ahmad, N. (2014). Improving detailed rulebased feature extraction of urban areas from WorldView-2 image and lidar data. *International Journal of Remote Sensing*, 5, pp. 1876-1899.
- Hay, G. J. and Castilla, G. (2006). Object-Based Image Analysis: Strengths, Weaknesses, Opportunities and Threats (Swot)
- Heistermann, M., Muller, C., and Ronneberger, K. (2006). Land in sight? Achievements, deficits and potentials of continental to global scale land-use modelling. *Agriculture, ecosystems and the environment* 114, p. 141-158, doi:10.1016/j.agee.2005.11.015.
- Hermosilla, T. L., Ruiz, J., Recio and Estornell, J. (2011).Evaluation of Automatic Building Detection Approaches Combining High Resolution Image and Lidar Data.*Remote Sensing*. 3: 1188-1210

- Hodgson, E.M., Jensen, J. R., Tullis, J. A., Riordan, K. D and Archer, C. M. (2003). Synergistic use of Lidar and Color Aerial Photography for Mapping Urban Parcel Imperviousness, *Photogrammetric Engineering & Remote Sensing*, 69(9):973–980.
- Hoffmann, A and Van der Vegt, J. (2001). New Sensor systems and New Classification Methods: Laser- and Digital Camera-Data meet Object-Oriented Strategies, *GIS*, Vol. 6. pp.18-23. (<http://www.definiens-imaging.com/documents/gis.htm>)
- Hu, X., Li, Y. and Shan, J. (2014). Road Centerline Extraction in Complex Urban Scenes from LiDAR Data Based on Multiple Features.
- Hu, X., Tao, C. V. and Hu, Y. (2004). Automatic road extraction from dense urban area by integrated processing of high resolution imagery and LIDAR data, *The International Archives of Photogrammetry, Remote Sensing and Spatial Information Science*, Vol. XXXV-B3, pp. 288–292.
- Igbokwe, J. I., Orisakwe, K. U., Akinyede J.O., Dang, B, and Alaga, T. (2009). Modeling Landslide susceptibility in parts of the southeastern Nigeria with Medium Resolution Remotely sensed images. *GIS Development*.
- Igbokwe J. I. (2010). Geospatial Information, Remote Sensing and Sustainable Development in Nigeria. 15TH Inaugural Lecture of Nnamdi Azikiwe University, Awka delivered on 19th May, 2010. EL ‘DEMARK Publishers, Enugu, Nigeria.
- Ioannidis, C., Psaltis, C and Potsiou, C. (2009). Towards a Strategy for Control of Suburban Informal Buildings through Automatic Change Detection. *Computer, Environment and Urban Systems* 33: 64-74.
- Iovan, C., Boldo, D and Cord, M. (2008). Detection, Characterization, and Modelling Vegetation in Urban Areas from High-Resolution Aerial Imagery. *Selected Topics in Applied Earth Observations and Remote Sensing* 1, 3: 206-213.
- Jensen, J. R. (1996). *Introductory Digital Image Processing: A Remote Sensing Perspective* (Second edition). Prentice Hall, Upper Saddle River, New Jersey 07458, USA, pp.247-252.
- Jensen, J. R. (2005). *Introductory digital image processing, a remote sensing perspective*, 3rd. edition, Upper Saddle River: Pearson Prentice Hall, 526.
- Jia, Y. (2015). Object-based Land Cover Classification with Orthophoto and LIDAR Data
- Jin, X. and Paswaters, S . (2007). A Fuzzy Rule Base System For Object-Based Feature Extraction and Classification. In: Kadar I, Editor. *Signal Processing, Sensor Fusion, and Target Recognition XVI*. Proceedings Of SPIE. Vol. 6567, Pp. 65671H1–65671H.

- Johansen, K., Tiede, D., Blaschke, T., Arroyo, L.A. and Phinn, S. (2011). Automatic geographic object based mapping of streambed and riparian zone extent from LiDAR data in a temperate rural urban environment, Australia. *Remote Sens.* 2011, 3, 1139-1156.
- Kiani, K., Mojaradi, B. and Esmaily, A. and Salehi, B. (2014). Urban Area Object-Based Classification by Fusion of Hyperspectral and Lidar Data
- Kim, J. and Muller, J. P. (2011). Trees and building Detection in Dense Urban Environments using Automated Processing of Ikonos Image and LiDAR Data. *International Journal of Remote Sensing* 32: 2245-2273.
- Koc, D. and Turker, M. (2005). Automatic building detection from high resolution satellite images. In Kurnaz S (ed), *Recent Advance in Space Technologies, Space in the Service of Society, RAST 2005*, 617-622. Proceedings of 2nd International Conference on Recent Advance in Space Technologies, held 9-11 June 2005, Istanbul, Turkey.
- Kokalj, Ž and Oštir, K. (2006). Ugotavljanje pokrovnosti Slovenije iz satelitskih posnetkov Landsat. *Geografski vestnik*, 2006, Vol. 78, No. 2.
- Kokje, A. A., and Jay G. (2013). "A Simplified Approach for Classifying Urban Land Cover using Data Fusion." In Proceedings of the SIRC NZ Conference.
- Konecny, G. and Schiewe, J. (1996). Mapping from Digital Image Data with Specific Reference to MOMS-02. *ISPRS Journal of Photogrammetry and Remote Sensing* 51, pp. 173–181.
- Kongo, U. P. E. (2015). Urban Land Cover Classification From High Resolution Geoeye-1 Imagery Using A Lidarbased Digital Surface Model
- Kost, K., Loddenkemper, M., and Petring, J. (1996). Airborne laserscanning, a new remote sensing method for mapping terrain. *Third EARSeL Workshop on LiDAR remote sensing of land and sea, Tallinne, Estonia, 17±19 July 1997* (pp. 89±96).
- Kraus, K (2003a): Laser Scan DTMs for Modeling Flood Risk Areas, *GIS (Geo-Information-Systems)* (invited), 12, 26–31,
- Kressler, F. and Steinnocher, K. (2008). Object-Based Image Analysis, Chapter 7 (Object-Oriented Analysis of Image and Lidar Data and its Potential for a Dasymetric Mapping Application), Springer Berlin Heidelberg, Pp: 611-624.
- Landis, J. R., and Koch. G. G. (1977). The measurement of observer agreement for categorical data. *Biometrics* 3 (1):159-174.
- Landmap Spatial Discovery (2014) : Characteristics of LiDAR
- Lee, W. H. (2015), Object-oriented Classification of Urban Areas Using LiDAR and Aerial Images

- Lein K. J., (2011). Environmental sensing: Analytical techniques for earth observation. New York: Springer.
- Leiss, I. A., Sandmeier S., Itten K. I. and Kellenberger, T. W. (1995). Improving land use classification in rugged terrain using radiometric corrections and a possibility based classification approach. In Stein TI (ed) IGARSS'95: Quantitative Remote Sensing for Science and Applications. Proceedings of Geoscience and Remote Sensing Symposium held 10-14 July 1995, Firenze, Italy. Quantitative Remote Sensing for Science and Applications.
- Li, J. and Jones, J.(2006). Classification using multiple and negative target rules. In Gabrys B, Howlett RJ & Jain LC (eds) Knowledge intelligent information and engineering systems. Proceedings of the 10 th International conference, KES 2006 held 9-11 October 2006, Bournemouth, UK.
- Li, S.and,Xue.Y. (1998). Positioning Accuracy of Airborne Laser Ranging And Multispectral Imaging Mapping System. Journal of Wuhan Technical University of Surveying and Mapping (WTUSM), WUHAN, CHIAN, Vol.12, Pp.341-344
- Lillesand, T. M. and Kiefer. R. W. (1994). Remote Sensing and Image Interpretation. 3rd Edition. John Wiley and Sons, Inc.
- Liu.J. and Zhang, X. (2005). Classification of Laser Scanning Altimetry Data Using Laser Intensity. Editorial Board of Geomatics and Information Science of Wuhan University, WUHAN, CHINA, Vol.30, pp.189-193.
- Lu, D.& Weng, Q. (2007). A Survey of Image Classification Methods and Techniques for Improving Classification Performance. International Journal of Remote Sensing, 28, 823-870. <http://dx.doi.org/10.1080/01431160600746456>
- Lu, D., Hetrick. S. and Moran, E (2010). Land Cover Classification in a Complex Urban-Rural Landscape with Quickbird Imagery. Photogrammetric Engineering and Remote Sensing 2010, 76(10), 1159-1168.
- Machala, M. and Zejdová, L. (2013). Forest Mapping Through Object-based Image Analysis of Multispectral and LiDAR Aerial Data
- Madhok, V. and Landgrebe, D. (1999). Supplementing Hyperspectral Data with Digital Elevation. In: IEEE Geoscience and Remote Sensing Symposium (IGARSS_99), Hamburg, Germany, June 1999, Vol. I, Pp. 59–61.
- Matinfar, H. R., Sarmadian, F., Alavi Panah, S. K. and Heck, R. J.(2007). “Comparisons of Object-Oriented and Pixel-Based Classification of Land Use/Land Cover Types Based on Landsat7, Etm+ Spectral Bands (Case Study : Arid Region of Iran).” American-Eurasian Journal of Agriculture and Environmental Science 2, no. 4: 448–56.
- Matsakis, P., Andrefouet, S. and Capolsini, P., (2000), Evaluation of fuzzy partitions. Remote Sensing of Environment, 74, pp. 516–533.

- Maune, D.F., Kopp, S.M., Crawford, C. A., and Zervas, C.E. (2001).Introduction. In Maune DF (ed). Digital Elevation Model Technologies and Applications: The DEM User's Manual (American Society for Photogrammetry and Remote Sensing: Bethesda, MD), 1–34.
- Mcfeters, S. K. (1996). The Use of Normalized Difference Water Index (NDWI)
- Mesiner, J. E. (2012). Urban Classification Techniques using the Fusion of LiDAR and Spectral Data
- Mhangara, P., Odindi, J., Kleyn, L and Remas, H. (2015).Mapping Urban Areas using Object Oriented Classification.
- Minho, K. (2012). “Object-based Spatial Classification of Forest Vegetation with IKONOS Imagery.” A Dissertation Submitted to the Graduate Faculty of the University of Georgia.
- Moffiet, T., Mengersen, K., Witte, C., King, R. and Denham, R., (2005). Airborne laser scanning: Exploratory data analysis indicates potential variables for classification of individual trees or forest stands according to species. *ISPRS Journal of Photogrammetry and Remote Sensing*, 59(5): 289-309.
- Navulur, K. (2007). Multi-Spectral Image Analysis Using the Object Oriented Paradigm. CRC Press, Taylor & Francis Group
- Netzband, M., Stefanov, W. L. and Redman, C. (2007). Applied Remote Sensing For Planning, Governance And Sustainability. Berlin: Springer-Verlag.
- Neubert,M., Herold, H. and Meinel, G. (2008).Assessing Image Segmentation Quality – Concepts, Methods and Application. In: Blaschke, T., Lang, S., Hay G.J (Eds.): Object-Based Image Analysis: Spatial Concepts for Knowledge Driven Remote Sensing Applications (Lecture Notes In Geoinformation And Cartography): 785-803.
- Niemeyer, J., Rottensteiner, F. and Soergel, U. (2014).Contextual Classification of LiDAR Data and Building Object Detection in Urban Areas. *ISPRS Journal of Photogrammetry and Remote Sensing* 87, 152-165.
- Norbert, H., and Claus, B. (1999).Extraction of Buildings and Trees in Urban Environments.*ISPRS Journal of Photogrammetry & Remote Sensing*, Vol. 54, pp. 130-137.
- Nussbaum, S. and Menz, G. (2008).'Object-Based Image Analysis and Treaty Verification. New Approaches in Remote Sensing- Applied to Nuclear Facilities in Iran', Springer.
- Okeke, F.I. and A. Karnieli (2006). Methods for fuzzy classification and accuracy assessment of historical aerial photographs for vegetation change analysis, part 1:

Algorithm, *International journal of Remote Sensing* 27(1-2), 153-176.(www.bgu.ac.il/phys/remote.papers/)(Assessed on 26/08/2015).

- Oštir, K. (2006). *Daljinsko zaznavanje (Remote Sensing)*. Ljubljana: Založba ZRC.
- Palmer, S. (1999). *Vision Science: From Photons to Phenomenology*. Cambridge, MA: MIT Press, 1999. P. Zygmunt, "Perception Viewed as an Inverse Problem," in *Vision Research*, vol. 24, p. 3145–3161, 2001.
- Patz, J.A., Campbell-Lendrum, D., Holloway, T. and Foley, J.A. (2005). Impact of Regional Climate Change on Human Health. *Nature*, 438, Pp. 310–317.
- Pereira, L. M. G. and Wicherson, R. J. (1999). Suitability of Laser Data for Deriving Geographical Information: A Case Study in the Context of Management of Fuvial Zones, *ISPRS Journal of Photogrammetry and Remote Sensing*, 54, 105–114,
- Potere, D and Schneider, A. (2007). A Critical Look at Representations of Urban Areas in Global Maps. *Geojournal*, 69, Pp. 55–80.
- Potsiou, C., Doytsher Y., Kelly, P., Khouri, R and McLaren, R (2010). Rapid Urbanization and Megacities: The Need For Spatial Information Management. In *FIG Congress 2010 Facing The Challenges - Building the Capacity*. Proceedings of the XXIV FIG International Congress Held 11-16 April 2010, Sydney, Australia.
- Powell, R.L., Matzke, N., DE Souza J.R, C., Clark, M., Numata, I., Hess, L.L. and Roberts, D.A., (2004). Sources of error in accuracy assessment of thematic landcover maps in the Brazilian Amazon. *Remote Sensing of Environment*, 90, pp. 221–234.
- Priestnall, G., Jaafar, J. and Duncan, A. (2000). Extracting Urban Features from LiDAR Digital Surface Models. *Computers, Environment and Urban Systems*, 24(2)., pp. 65-78.
- Prisley, S.P. and Smith, J.L. (1987). Using classification error matrices to improve the accuracy of weighted land-cover models. *Photogrammetric Engineering and Remote Sensing*, 53, pp. 1259–1263
- Rahimi, S., Arefia, H. and Bahmanyar, R. (2015). Automatic Road Extraction Based on Integration of High Resolution LiDAR And Aerial Imagery
- Rahman A. A., Boguslawski P., Gold C and Said M. I. (2013). *Developments in Multidimensional Spatial Data Models*. Heidelberg: Springs.
- Ramdani, F. (2013). Urban Vegetation Mapping from Fused Hyperspectral Image and LiDAR Data with Application to Monitor Urban Tree Heights. *Journal of Geographic Information System*, 5(4).

- Ramesh, S. and Dong, P. (2009), High Resolution Satellite Images and LiDAR Data for Small – Area Building Extraction and Population Estimation
- Rampi, L.P., Knight, J.F. and Pelletier, K.C. (2014). Wetland mapping in the Upper Midwest United States: An object-based approach integrating LiDAR and imagery data. *Photogramm. Eng. Remote Sens.*, 80, 439–448.
- Rego, F. and Koch, B. (2003). Automatic Classification of Land Cover with High Resolution Data of the Rio De Janeiro City Brazil Comparison Between Pixel And Object Classification. In: Proceedings of The International Archives Of The Photogrammetry, Remote Sensing and Spatial Information Sciences, Carstens, J. Ed., Regensburg, Germany, 27-29 June.
- Renslow M, Greenfield, P. and Guay T. (2000). Evaluation of Multi-Return LIDAR for Forestry Applications. RSAC- 2060/4810-LSP-0001-RPT1. USDA Forest Service – Engineering. Remote Sensing Applications Center.
- Ronczyk, L., (2012), Object-based Classification of Urban Land Cover Extraction Using High Spatial Resolution Imagery
- Rottensteiner, F. and Briese C., (2003). Automatic generation of building models from LiDAR data and the integration of aerial images. *ISPRS Vol. XXXIV*. Dresden 2003.
- Salehi, B, Zhang, Y. Zhong M. and Dey, V. (2012). Object-based classification of urban areas using VHR imagery and height points ancillary data. *Remote Sensing* 4, 8: 2256-2276.
- Saran S., Wate, P., Srivastav, S.K and Krishnamurthy, Y. V. N. (2015). CityGML at Semantic Level for Urban Energy Conservation Strategies, *Annals of GIS* 03/2015; 21(1). DOI: 10.1080/19475683.2014.992370.
- Schiewe, J. (2002). Segmentation of High-Resolution Remotely Sensed Data Concepts, Applications and Problems. In: *Symposium on Geospatial Theory, Processing and Applications*
- Schmugge, T. J., Kustas, W. P., Ritchie, J. C., Jackson, T. J and Rango, A (2002). Remote Sensing in Hydrology, *Advances in Water Resources*, 25, 1367–1385, 2002.
- Schöpfer, E., Lang, S. and Strobl, J. (2010): Segmentation and Object-Based Image Analysis. In: Rashed, T. – Jürgens, C. (Eds): *Remote Sensing of Urban and Suburban Areas*. Springer, Dordrecht. 181 – 192.
- Schowengerdt, R.A. (2007). *Remote Sensing. Models and Methods for Image Processing*. 3rd Edition. Academic Press, Elsevier Inc.
- Shackelford, A. K. and Davis, C.H. (2003). A Combined Fuzzy Pixel Based and Object-Based Approach for Classification of High Resolution Multispectral Data over

Urban Areas. *Geoscience and Remote Sensing, IEEE Transactions*, 41(10), Pp. 2354–2363.

- Shackelford, A.K. and Davis C.H. (2003). “A Hierarchical Fuzzy Classification Approach for High-Resolution Multispectral Data over Urban Areas,” *IEEE Transactions on Geoscience and Remote Sensing*, Vol. 41, Pp. 1920–1932.
- Siart, C., Bubenzer, O. and Eitel, B. (2009). Combining Digital Elevation Data (SRTM/ASTER), High Resolution Satellite Imagery (Quickbird) and GIS For Geomorphological Mapping: A Multi-Component Case Study On Mediterranean Karst In Central Crete. *Geomorphology* 112, 2: 106-121.
- Sima, J (2003). *Geoinformační Terminologie Pro Geodety A Kartografy*. [Geoinformatic Terminology for Surveyors and Cartographers]. Výzkumný Ústav Geodetický, Topografický A Kartografický (VÚGTK), Zdiby
- Singh, S., Suresh, M. and Jain, K. (2015). Land Information Extraction with Boundary Preservation for High Resolution Satellite Image
- Smith, G.M., Fuller, R.M., Hoffmann, A. and Wicks, T. (2000). Parcel-Based Approaches to Teh Analysis Of Remotely Sensed Data, *Proceedings of the Remote Sensing Society Conference*, Nottingham, UK.
- Smith, G.M., Morton and R. W. (2010). Real World Objects in GEOBIA through the Exploitation of Existing Digital Cartography and Image Segmentation. *Photogrammetric Engineering and Remote Sensing* 2010, 76(2), 163-170.
- Sohn, G.& Dowman, I (2007). Data Fusion of High-Resolution Satellite Imagery and Lidar Data for Automatic Building Extraction. *ISPRS Journal of Photogrammetry and Remote Sensing* 62 (1), 43-63.
- Soille, P. (2003). *Morphological Image Analysis: Principles and Applications* (2nd Edition), Springer, Berlin ; New York. 316 Pp.
- Song, J., Han, S., Yu.K and Kim, Y. (2002). Assessing the Possibility of Land-Cover Classification using Lidar Intensity Data. In *PCV'02: Photogrammetric Computer Vision*, ISPRS Commission III, 9-13 September, Graz, Austra.
- Steele, B.M., Winne, J.C. and Redmond, R. L., (1998). Estimation and mapping of misclassification probabilities for thematic land cover maps. *Remote Sensing of Environment*, 66, pp. 192–202.
- Sunitha, A. and Suresh, B. G,(2015). *Satellite Image Classification Methods and Techniques: A Review*
- Syed, S., Dare, P. and Jones, S. (2005a). Automatic Classification of Land Cover Features With High Resolution Imagery and Lidar Data: An Object-Oriented Approach. In: *Proceedings of SSC2005 Spatial Intelligence, Innovation And*

Praxis: The National Biennial Conference of the Spatial Sciences Institute, Melbourne, Australia.

- Syed, S., Dare, P. and Jones, S. (2005b). Semi-Automatic 3D Building Model Generation from LIDAR and High Resolution Imagery, In: Proceedings Of SSC2005 Spatial Intelligence, Innovation and Praxis: The National Biennial Conference of the Spatial Sciences Institute, Melbourne, Australia.
- Tao, G. and Yasuoka, Y. (2002), Combining High Resolution Satellite Imagery And Airborne Laser Scanning Data for Generating Bareland DEM in Urban Areas, Proceedings of International Workshop on Visualization and Animation of Landscape, International Archives of Photogrammetry, Remote Sensing and Spatial Information Science, Kunming, China, 26 - 28 February 2002.
- Taubenböck, H., Esch, T. and Roth, A. (2006). An Urban Classification Approach Based On an Object– Oriented Analysis of High Resolution Satellite Imagery for a Spatial Structuring Within Urban Areas
- Tee, A. T. and Liang, C. C. (2004). Object-Based Building Detection from LiDAR Data and High Resolution Satellite Imagery
- Tiwari, P.S., Pande, H. and Pandey, A.K. (2009).Automatic Urban Road Extraction Using Airborne Laser Scanning/Altimetry and High Resolution Satellite Data. Journal of the Indian Society of Remote Sensing (37), Pp 223-231.
- Tiwari, P. S. and Pande, H. (2011). LIDAR Remote Sensing Applications in Automated Urban Feature Extraction, Laser Scanning, Theory and Applications
- Tong, X., Liu, S and Weng, Q. (2009).Geometric Processing Of Quickbird Stereo Imagery For Urban Land Use Mapping — A Case Study in Shanghai, China. IEEE Journal of Selected Topics in Applied Earth Observations & Remote Sensing, 2(2), 61–66.
- Tormos, T., Durrieu, S., Kosuth, P., Dupuy, S., Villeneuve, B and Wasson, J.G. (2011). Object Based Image Analysis for Operational Fine-Scale Regional Mapping of Land Cover within River Corridors from Multispectral Imagery and Thematic Data. Int. J. Remote Sens., In Press.
- Tse, R. O. C., Gold, C. and Kidner, D. (2008). 3D City Modelling from LIDAR Data, Advances in 3D Geoinformation Systems, Lecture Notes in Geoinformation and Cartography 2008, 161-175
- United Nations (2008). World Urbanization Prospects: The 2007 Revision (Department of Economic and Social Affairs, Population Division). Available online at <http://esa.un.org/unup/> (accessed 28 February 2009).
- Urala,S., Shana, J., Romeroa, M., and Tarkoa, A. (2015), Road and Road Side Feature Extraction using Imagery and LiDAR Data for Transportation Operation.ISPRS

- Uzar, M. and Yastikli, N. (2013), Automatic Building Extraction Using Lidar and Aerial Photographs
- Van der Sande, C.J., de Jong, S.M and de Roo, A.P.J. (2003). A Segmentation and Classification Approach of IKONOS-2 Imagery For Land Cover Mapping to Assist Flood Risk And Flood Damage Assessment. *International Journal of Applied Earth Observation and Geoinformation*, 4, Pp. 217-229.
- Varshney, P. K. and Arora, M. K. (2004). *Advance Image Processing for Remotely Sensed Hyperspectral Data*. Berlin: Springer.
- Veljanovski, T., Lamovec, P., Pehani, P. and Oštir, K. (2011a). Comparison of Three Techniques for Detection of Flooded Areas on ENVISAT and RADARSAT-2 Satellite Images. In: *Geoinformation for Disaster Management: Gi4DM 2011*, 3.-8. May 2011, Antalya, Turkey.
- Verlič, A., Đurić, N., Kokalj, Z., Marsetič, A, Simončič, P and Oštir, K. (2014). Tree Specie Classification using Worldview-2 Satellite Images and Laser Scanning Data in a Natural Urban Forest.
- Vosselman, G. V. and Maas, H. G. (2010). *Airborne and Terrestrial Laser Scanning*. Whittles
- Vu, T.T., Matsuoka, M and Yamazaki, F. (2004). LIDAR-Based Change Detection of Buildings in Dense Urban Areas. In: *Proceedings of the International Geoscience and Remote Sensing Symposium, IEEE, CD-ROM*, 4pp.
- Wang O., Lodha, S.K. and Helmbold, D. P. (2006). A Bayesian Approach to Building Footprint Extraction From Aerial LiDAR Data. In Pollefeys M, Danilidis K (eds) *2006 3rd International Symposium on 3D Data Processing Visualization and Transmission, 192-1993. Proceedings of a Meeting held 14-16 June 2006, Chapel Hill, North Carolina*. Piscataway: Institute of Electrical and Electronics Engineers.
- Weidner, U. (1997). Digital surface models for building extraction. In Gruen A, Baltsavias EP & Henricsson O (eds) *Automatic Extraction of Man-made Objects from Aerial and Space Images 193-202*. Berlin: Birkhauser.
- Weng, Q. and Quattrochi, D. A.(2006). *Urban remote sensing*. Boca Raton: Taylor & Francis Group.
- Yongmin K., Youkyung H., Younggi B., Jaewan C., Dongyeob H. and Yongil K., (2011). Object-Based Classification of An Urban Area Through A Combination of Aerial Image and Airborne LiDAR Data

- Yu, H., Cheng, G., Ge, X and Lu, X (2011). Object oriented land cover classification using ALS and GeoEye imagery over mining area. *Transaction of Nonferrous Metals Society of China* 21: s733-s737.
- Yu, X.J and Ng, C.N. (2007). Spatial and temporal dynamics of urban sprawl along two urban-rural transects: A case study of Guangzhou, China. *Landscape and Urban Planning*, 79(1), 96–109.
- Yuan, F. B. and Bauer, M.E. (2006). Mapping Impervious Surface Area Using High Resolution Imagery: A Comparison of Object-Oriented Classification to Per-Pixel Classification. In: *Proceedings of American Society of Photogrammetry and Remote Sensing Annual Conference*, May 1–5, 2006, Reno, NV, CD-ROM.
- Zakka, K., (2016). *A Complete Guide to K-Nearest-Neighbors with Applications in Python and R*
- Zhang, C., (2014). Combining hyperspectral and LiDAR data for vegetation mapping in the Florida Everglades. *Photogramm. Engin. Remote Sens.* 80, 733–743.
- Zhang, X., Feng, X.(2005). Detecting urban vegetation from IKONOS data using an object-oriented approach. *Int. Geosci. Remote Sens. Symp.*, p1475.
- Zhou, W. (2013). An Object-Based Approach for Urban Land Cover Classification: Integrating Lidar Height And Intensity Data. *IEEE Geosci. Rem. Sens. Lett.* 10 (4), 928–931.
- Zhou, W. and Troy, A. (2008). 'An Object-Oriented Approach for Analysing And Characterizing Urban Landscape at the Parcel Level', *International Journal of Remote Sensing* 29(11), 3119-3135.
- Zhou, W., Huang, G., Troy, A and Cadenasso, M.L. (2009). Object Based Land Cover Classification Of Shaded Areas In High Spatial Resolution Imagery of Urban Areas: A Comparison Study. *Journal of Remote Sensing of the Environment*, 113, Pp. 1769-1777.
- Zou, X., Zhao, G., LI, J., Yang, Y. and Fang, Y. (2016). Object Based Image Analysis Combining High Spatial Resolution Imagery and Laser Point Clouds for Urban Land Cover

Appendix 1: T-Distribution Table

<i>One Sided</i>	75%	80%	85%	90%	95%	97.5%	99%	99.5%	99.75%	99.9%	99.95%
<i>Two Sided</i>	50%	60%	70%	80%	90%	95%	98%	99%	99.5%	99.8%	99.9%
1	1.000	1.376	1.963	3.078	6.314	12.71	31.82	63.66	127.3	318.3	636.6
2	0.816	1.080	1.386	1.886	2.920	4.303	6.965	9.925	14.09	22.33	31.60
3	0.765	0.978	1.250	1.638	2.353	3.182	4.541	5.841	7.453	10.21	12.92
4	0.741	0.941	1.190	1.533	2.132	2.776	3.747	4.604	5.598	7.173	8.610
5	0.727	0.920	1.156	1.476	2.015	2.571	3.365	4.032	4.773	5.893	6.869
6	0.718	0.906	1.134	1.440	1.943	2.447	3.143	3.707	4.317	5.208	5.959
7	0.711	0.896	1.119	1.415	1.895	2.365	2.998	3.499	4.029	4.785	5.408
8	0.706	0.889	1.108	1.397	1.860	2.306	2.896	3.355	3.833	4.501	5.041
9	0.703	0.883	1.100	1.383	1.833	2.262	2.821	3.250	3.690	4.297	4.781
10	0.700	0.879	1.093	1.372	1.812	2.228	2.764	3.169	3.581	4.144	4.587
11	0.697	0.876	1.088	1.363	1.796	2.201	2.718	3.106	3.497	4.025	4.437
12	0.695	0.873	1.083	1.356	1.782	2.179	2.681	3.055	3.428	3.930	4.318
13	0.694	0.870	1.079	1.350	1.771	2.160	2.650	3.012	3.372	3.852	4.221
14	0.692	0.868	1.076	1.345	1.761	2.145	2.624	2.977	3.326	3.787	4.140
15	0.691	0.866	1.074	1.341	1.753	2.131	2.602	2.947	3.286	3.733	4.073
16	0.690	0.865	1.071	1.337	1.746	2.120	2.583	2.921	3.252	3.686	4.015
17	0.689	0.863	1.069	1.333	1.740	2.110	2.567	2.898	3.222	3.646	3.965
18	0.688	0.862	1.067	1.330	1.734	2.101	2.552	2.878	3.197	3.610	3.922
19	0.688	0.861	1.066	1.328	1.729	2.093	2.539	2.861	3.174	3.579	3.883
20	0.687	0.860	1.064	1.325	1.725	2.086	2.528	2.845	3.153	3.552	3.850
21	0.686	0.859	1.063	1.323	1.721	2.080	2.518	2.831	3.135	3.527	3.819
22	0.686	0.858	1.061	1.321	1.717	2.074	2.508	2.819	3.119	3.505	3.792
23	0.685	0.858	1.060	1.319	1.714	2.069	2.500	2.807	3.104	3.485	3.767
24	0.685	0.857	1.059	1.318	1.711	2.064	2.492	2.797	3.091	3.467	3.745
25	0.684	0.856	1.058	1.316	1.708	2.060	2.485	2.787	3.078	3.450	3.725
26	0.684	0.856	1.058	1.315	1.706	2.056	2.479	2.779	3.067	3.435	3.707
27	0.684	0.855	1.057	1.314	1.703	2.052	2.473	2.771	3.057	3.421	3.690
28	0.683	0.855	1.056	1.313	1.701	2.048	2.467	2.763	3.047	3.408	3.674
29	0.683	0.854	1.055	1.311	1.699	2.045	2.462	2.756	3.038	3.396	3.659
30	0.683	0.854	1.055	1.310	1.697	2.042	2.457	2.750	3.030	3.385	3.646
40	0.681	0.851	1.050	1.303	1.684	2.021	2.423	2.704	2.971	3.307	3.551
50	0.679	0.849	1.047	1.299	1.676	2.009	2.403	2.678	2.937	3.261	3.496
60	0.679	0.848	1.045	1.296	1.671	2.000	2.390	2.660	2.915	3.232	3.460
80	0.678	0.846	1.043	1.292	1.664	1.990	2.374	2.639	2.887	3.195	3.416
100	0.677	0.845	1.042	1.290	1.660	1.984	2.364	2.626	2.871	3.174	3.390
120	0.677	0.845	1.041	1.289	1.658	1.980	2.358	2.617	2.860	3.160	3.373
∞	0.674	0.842	1.036	1.282	1.645	1.960	2.326	2.576	2.807	3.090	3.291

Appendix 2: Summary of Kappa Values used for Hypotheses Test.

Subsets	Pixel	VHR	VHR/nDSM
Akabuka	0.635	0.769	0.903
Akabuka	0.621	0.741	0.880
Akabuka	0.693	0.789	0.904
Akabuka	0.668	0.778	0.909
Mean	0.654	0.769	0.899
Egbeda	0.690	0.845	0.917
Egbeda	0.758	0.853	0.916
Egbeda	0.731	0.835	0.927
Egbeda	0.731	0.824	0.886
Mean	0.728	0.839	0.912
Ikiri	0.676	0.781	0.878
Ikiri	0.666	0.801	0.920
Ikiri	0.738	0.810	0.918
Ikiri	0.611	0.718	0.863
Mean	0.673	0.778	0.895
Obido	0.648	0.731	0.878
Obido	0.692	0.800	0.858
Obido	0.721	0.799	0.913
Obido	0.622	0.776	0.892
Mean	0.671	0.777	0.885
Ogbogwu	0.724	0.819	0.946
Ogbogwu	0.608	0.759	0.902
Ogbogwu	0.710	0.831	0.944
Ogbogwu	0.734	0.820	0.915
Mean	0.694	0.807	0.927
Omoku	0.661	0.779	0.913
Omoku	0.655	0.794	0.941
Omoku	0.669	0.807	0.908
Omoku	0.650	0.783	0.900
Mean	0.659	0.791	0.916
Osiakpu	0.617	0.759	0.894
Osiakpu	0.636	0.762	0.896
Osiakpu	0.684	0.812	0.917
Osiakpu	0.654	0.815	0.903
Mean	0.648	0.795	0.894
Mean of Mean	0.675	0.794	0.905

Appendix 3: GPS

OBSERVATIONS USED TO VALIDATE THE ALREADY GEOREFERENCED DATA

ADJUSTMENT REPORT

1 Coordinate System

1.1 Name of Coord. System

NIG MID BELT

1.2 Base Parameter

Major Semi-axis	a	6378249.1450
Flattening	f	1/293.46500000

1.3 Projection Parameter

M0=0.99975000 Projection Ratio
H =0.0000 Projection Height
Bm=0 Average long. on Projection plane
B0 =04:00:00 Origin long.
L0 =08:30:00 Central Meridian
N0 =0.0000 Northern Addition
E0 =670553.9840 Eastern Addition

[Go to top](#)

2 3D Non-constraint Adjustment

2.1 Adjustment Parameter

Base	WGS-84
Alternate amount	2
X square check (a=95%)	Pass
Free	0

2.2 Free adjustment coordinate

Station	lat. /RMS		long. /RMS		Height/RMS		RMS
	(Degree:Minute:Second)	(m)	(Degree:Minute:Second)	(m)	(m)		(m)
RON 124	5:17:38.29969 N	0.0000	6.42:49.02268 E	0.0000	155.2435	0.0000	0.0000
VUN 1	5:17:48.67782 N	0.0000	6:38:37.61656 E	0.0000	180.9806	0.0000	0.0000
VUN 2	5:14:41.37944 N	0.0000	6:37:46.42431 E	0.0000	170.9909	0.0000	0.0000
VUN 3	5:12:46.92391 N	0.0000	6:40:10.91417 E	0.0000	191.0375	0.0000	0.0000
VUN 4	5:13:07.86869 N	0.0000	6:43:26.75669 E	0.0000	165.0087	0.0000	0.0000
VUN 5	5:11:24.67844 N	0.0000	6:46:55.88316 E	0.0000	182.4478	0.0000	0.0000
VUN 6	5:07:43.94442 N	0.0000	6:45:35.16682 E	0.0000	176.2576	0.0000	0.0000

[Go to top](#)

3 2D Constraint Adjustment


3.1 Adjustment Parameter

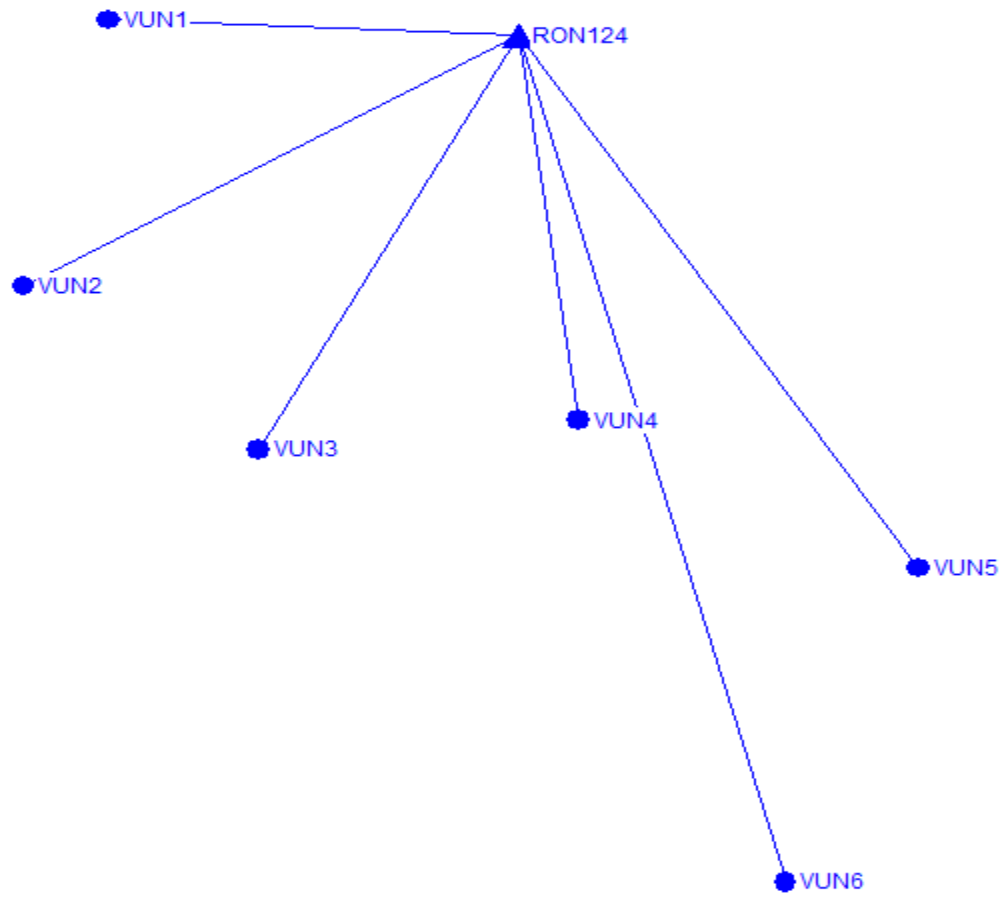
Alternate amount	3
Reference factor	
x(north)Move(Offset)	2.6391m
y(east)Move(Offset)	-6.4374 m
Scale	0.0000ppm
Rotate	0.0000 s

3.2 2D Adjustment Distance

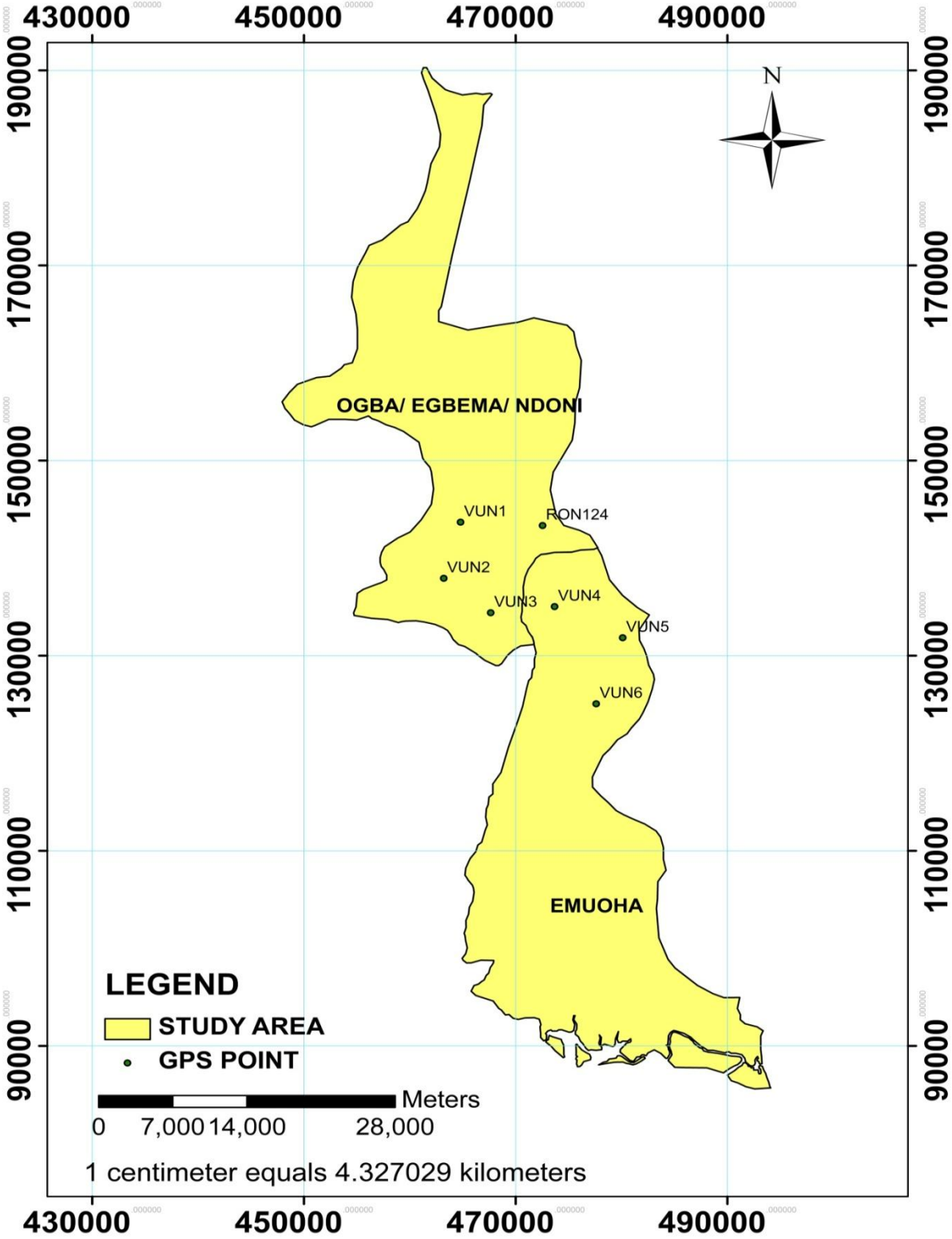
Start point	End Point	North(x)/RMS		East(y)/RMS		2D Distance	RMS	Relative error
		(m)		(m)		(m)	(m)	
RON 124	VUN 1	341.567	0.00 0	-7742.183	0.000	7749.714	0.000	1: 0
	VUN 2	-5408.143	0.00 0	-9336.162	0.000	10789.436	0.000	1: 0
	VUN 3	-8937.668	0.00 0	-4895.792	0.000	10190.716	0.000	1: 0
	VUN 4	-8311.462	0.00 0	1138.557	0.000	8389.083	0.000	1: 0
	VUN 5	-11499.420		7571.400	0.000	13768.179	0.000	1: 0
	VUN 6	-18273.830	0.00 0	5066.576	0.000	18963.203	0.000	1: 0

3.3 2D Coordinate

Station	North(x)/RMS (m)		East(y)/RMS (m)		RMS (m)	Error Ellipse		
	E(m)	F(m)	ET(Degree: Minute:Second)					
RON 124	143325.569	*****	472551.573	*****				
VUN1	143667.136	0.000	464809.390	0.000	0.000	0.000	0.000	0:00:00
VUN2	137917.426	0.000	463215.411	0.000	0.000	0.000	0.000	0:00:00
VUN3	134387.901	0.000	467655.781	0.000	0.000	0.000	0.000	0:00:00
VUN4	135014.107	0.000	473690.130	0.000	0.000	0.000	0.000	0:00:00
VUN5	131826.149	0.000	480122.973	0.000	0.000	0.000	0.000	0:00:00
VUN6	125051.739	0.000	477618.149	0.000	0.000	0.000	0.000	0:00:00



Appendix 4: GPS Established Stations

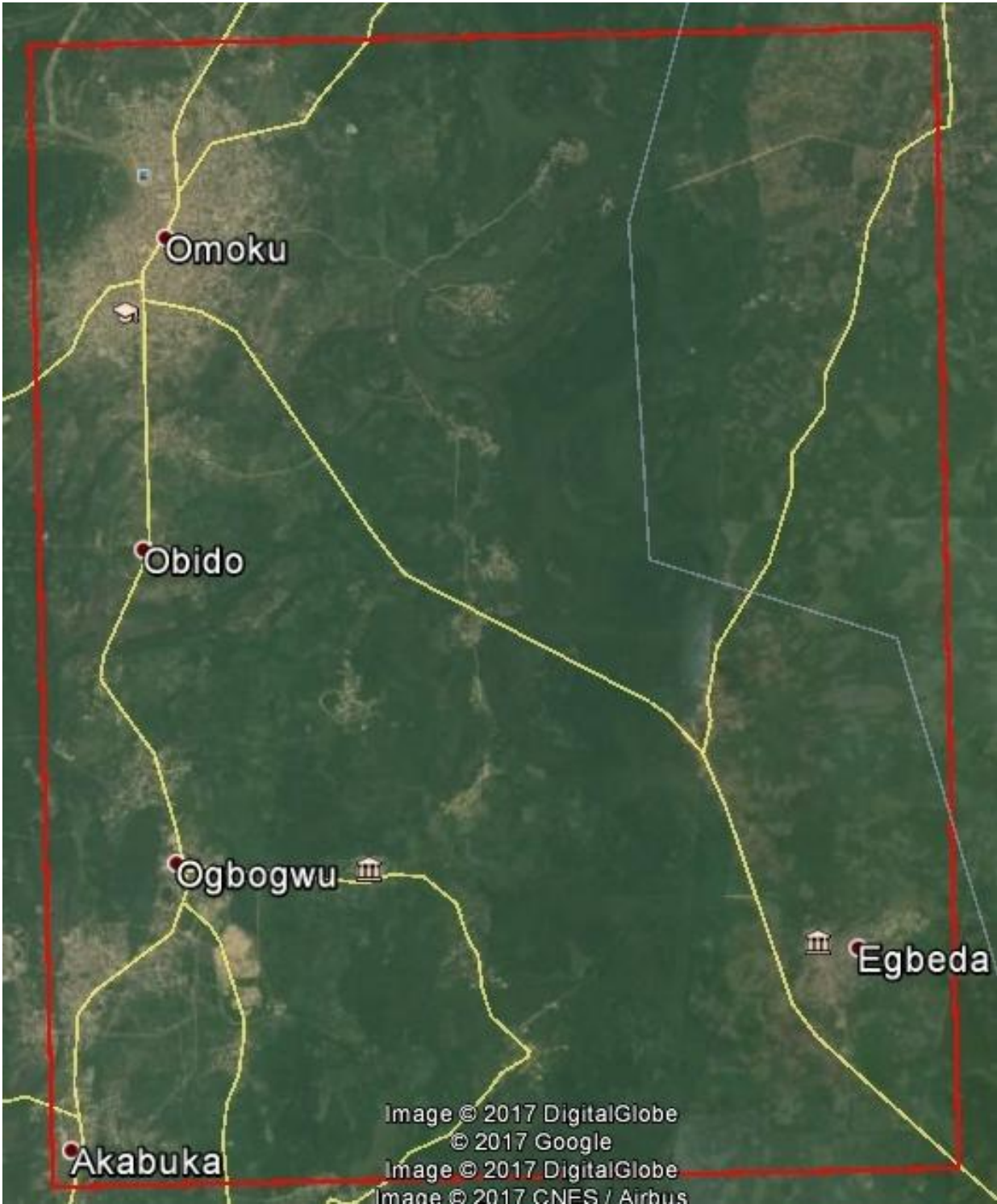


Appendix 5: Coordinates of Ground truth Features

LAT	LONG	Description
5.354923764	6.765995317	New classroom block.
5.354921663	6.765986874	New school building.
5.354924426	6.765983052	New primary school building.
5.350562459	6.761664779	Excavated area
5.352046875	6.762405485	New market square.
5.231845315	6.750994664	Tarred road at village sq in Egbeda
5.232059201	6.748878264	Unpaved road hall in Egbeda
5.233630674	6.746739043	Obugwor
5.235125586	6.750715435	Structure at village sq in Egbeda
5.237303068	6.753543869	town hall in imenyi Egbeda
5.239083365	6.753379611	Ebakwu hall
5.238560054	6.754651518	Omuikega
5.238822922	6.747920662	Ngbuoturu
5.267427538	6.733030576	New road in Ubimini
5.271579104	6.733917047	links new residential houses
5.273471670	6.734283906	large open space in Ubimini
5.349522586	6.652424522	Umualinwa street Omoku
5.351124759	6.652087505	The play Ground along Creek road
5.353112383	6.651488598	Creek road
5.348125401	6.653335062	Akor street Omoku
5.351438560	6.654562733	Okpoli Lane Omoku
5.350907719	6.653684283	Abua street Omoku
5.354202301	6.652899357	Toby Street Umuegbu
5.348634981	6.652966097	Osakwe street Omoku
5.349498407	6.652915548	Akor street Omoku
5.352095372	6.653343712	Oboburu street Omoku
5.354245014	6.654899072	Osere street Omoku
5.350886266	6.654492410	Abua street Omoku
5.347456014	6.653504742	Akor street Omoku
5.348666311	6.653799292	Osakwe street omoku
5.347154849	6.654270720	Court road Near Ezeali Palace
5.346298155	6.653134447	Ukposi Lane Omoku
5.351031915	6.654385781	Abua street Omoku
5.347143570	6.653176211	Ukpesi street Omoku
5.352420177	6.661232606	Albert Akogu's
5.347737103	6.653074574	Umuodogwu Lane Omoku
5.343359188	6.651989427	Iheukwu street Omoku
5.343562804	6.651520171	Cemetary road Omoku
5.344016961	6.651188691	Oba road
5.342363452	6.651451000	Okolo Close off Cemetry road
5.343088157	6.652531665	Iheukwu street Omoku

5.343962280	6.652837319	Church road
5.345052078	6.651316722	Adah Lane
5.343724723	6.650354725	Agburu street Omoku
5.338495251	6.648384140	Eze Obohias Palace Omoku
5.333281743	6.652169486	Safari Guest House along Ahodda road
5.359405261	6.677126493	Old Comm. Hall Ebogoro, along Ebogoro/Omoku road
5.333833792	6.702610479	Egbida Health Centre
5.310323233	6.703135625	Sch. road Osiakpu
5.292475711	6.702073921	Elite/Omoku road
5.275706838	6.700371259	Ohiugua/Elehia road
5.276744398	6.645065859	Hospital road Obigwe
5.295787149	6.652417305	Ahuda/Omoku road
5.311369973	6.653144164	Main road
5.238078968	6.651591642	elf Staff Quater's along Omoku road
5.234437807	6.642413808	palace of Adama Nwangwet Ogbogu
5.231815157	6.642589578	Ogbogu Health Centre along Omoku road
5.212832493	6.642436624	Eti-Oha road Akabuka
5.211161549	6.641523379	Akabuka Health Centre along Omoku road
5.211438649	6.642658701	Menjor road Akabuka
5.209168872	6.638710437	Community Pri. Sch. along School road Akabuka
5.211742915	6.640512720	Obiohuru Play Ground Akabuka
5.347041381	6.655173393	Customary Court Hall Omoku
5.346245988	6.652008723	Umuebe street Omoku
5.236268666	6.698585210	Akabta/Obiozumini road
5.238784125	6.698209201	Akabta/Obiozumini road

Appendix 6: Study Area Google Earth Image



APPENDIX 7 : ERROR MATRIXES

Table AP7.1a, b & c: AKABUKA Error Matrixes

Land use/cover	BU	OS	PR	UR	F	R	W	Grand Total	User's Accuracy
Buildings	58	5	7	9	10	4	0	93	62
Open Surface	6	54	7	2	6	3	0	78	69
Paved Roads	2	1	55	3	7	2	0	70	79
Unpaved Roads	4	9	8	71	4	2	0	98	72
Forest	7	3	6	1	63	3	0	83	76
Rangeland	5	5	3	3	10	62	0	88	70
Water	0	0	0	0	0	0	0	0	#DIV/0!
Grand Total	82	77	86	89	100	76	0	510	
Producer's Accuracy	71	70	64	80	63	82	#DIV/0!		
Overall Accuracy	71								
Overall Kappa index	0.654						363		

Land use/cover	BU	OS	PR	UR	F	R	W	Grand Total	User's Accuracy
Buildings	66	3	6	5	7	1	0	88	75
Open Surface	4	61	5	1	5	2	0	78	78
Paved Roads	4	1	65	1	3	2	0	76	86
Unpaved Roads	1	6	5	78	4	0	0	94	83
Forest	4	2	4	1	72	1	0	84	86
Rangeland	3	4	1	3	9	70	0	90	78
Water	0	0	0	0	0	0	0	0	#DIV/0!
Grand Total	82	77	86	89	100	76	0	510	
Producer's Accuracy	80	79	76	88	72	92	#DIV/0!		
Overall Accuracy	81								
Overall Kappa index	0.769						412		

Land use/cover	BU	OS	PR	UR	F	R	W	Grand Total	User's Accuracy
Buildings	77	2	3	2	3	0	0	87	89
Open Surface	2	67	1	1	3	2	0	76	88
Paved Roads	2	1	77	0	1	1	0	82	94
Unpaved Roads	1	3	2	84	1	0	0	91	92
Forest	2	1	3	1	91	0	0	98	93
Rangeland	0	3	0	1	1	73	0	78	94
Water	0	0	0	0	0	0	0	0	#DIV/0!
Grand Total	84	77	86	89	100	76	0	512	
Producer's Accuracy	92	87	90	94	91	96	#DIV/0!		
Overall Accuracy	92								
Overall Kappa index	0.899						469		

Tables AP7.2a, b & c – EGBEDA Error Matrixes

(a) Pixel Based	BU	OS	PR	UR	F	R	W	Grand Total	User's Accuracy
Buildings	58	4	4	4	4	6	0	80	73
Open Surface	6	59	6	2	4	1	0	78	76
Paved Roads	2	4	57	1	7	1	0	72	79
Unpaved Roads	4	6	1	61	2	1	0	75	81
Forest	4	3	0	2	59	2	0	70	84
Rangeland	6	7	1	4	4	63	0	85	74
Water	0	0	0	0	2	0	0	2	0
Grand Total	80	83	69	74	82	74	0	462	
Producer's Accuracy	73	71	83	82	72	85	#DIV/0!		
Overall Accuracy	77								
Overall Kappa index	0.728						357		

(b) OBIA - VHR	BU	OS	PR	UR	F	R	W	Grand Total	User's Accuracy
Buildings	67	3	1	2	1	5	0	79	85
Open Surface	3	68	3	2	2	0	0	78	87
Paved Roads	2	3	63	1	4	1	0	74	85
Unpaved Roads	4	3	1	68	1	1	0	78	87
Forest	0	3	0	1	69	2	0	75	92
Rangeland	4	2	1	0	4	65	0	76	86
Water	0	1	0	0	1	0	0	2	0
Grand Total	80	83	69	74	82	74	0	462	
Producer's Accuracy	84	82	91	92	84	88	#DIV/0!		
Overall Accuracy	87								
Overall Kappa index	0.839						400		

(c) OBIA - VHR & nDSM	BU	OS	PR	UR	F	R	W	G/ Total	User's Acc.
Buildings	76	2	0	2	0	3	0	83	92
Open Surface	1	78	3	1	2	0	0	85	92
Paved Roads	2	2	63	1	3	1	0	72	88
Unpaved Roads	1	0	2	69	1	0	0	73	95
Forest	0	0	0	1	74	2	0	77	96
Rangeland	0	0	1	0	2	68	0	71	96
Water	0	1	0	0	0	0	0	1	0
Grand Total	80	83	69	74	82	74	0	462	
Producer's Accuracy	95	94	91	93	90	92	#DIV/0!		
Overall Accuracy	93								
Overall Kappa index	0.912						428		

Tables AP7.3 a, b & c: IKIRI Error Matrixes

(a) Pixel Based	BU	OS	PR	UR	F	R	W	Grand Total	User's Accuracy
Buildings	54	2	3	2	3	2	6	72	75
Open Surface	3	61	8	2	6	0	9	89	69
Paved Roads	2	1	56	4	9	4	1	77	73
Unpaved Roads	3	7	4	60	9	3	9	95	63
Forest	3	2	5	1	60	3	7	81	74
Rangeland	4	5	1	5	7	60	1	83	72
Water	1	4	5	2	3	1	60	76	79
Grand Total	70	82	82	76	97	73	93	573	
Producer's Accuracy	77	74	68	79	62	82	65		
Overall Accuracy	72								
Overall Kappa index	0.670						411		

(b) OBIA - VHR	BU	OS	PR	UR	F	R	W	Grand Total	User's Accuracy
Buildings	61	2	2	2	3	1	5	76	80
Open Surface	2	68	5	0	3	0	6	84	81
Paved Roads	1	1	65	2	4	2	1	76	86
Unpaved Roads	2	2	2	65	7	1	9	88	74
Forest	1	2	1	1	70	2	3	80	88
Rangeland	3	3	2	4	7	66	1	86	77
Water	0	4	5	2	3	1	68	83	82
Grand Total	70	82	82	76	97	73	93	573	
Producer's Accuracy	87	83	79	86	72	90	73		
Overall Accuracy	81								
Overall Kappa index	0.776						463		

(c) OBIA - VHR & nDSM	BU	OS	PR	UR	F	R	W	Grand Total	User's Accuracy
Buildings	67	2	1	1	2	0	2	75	89
Open Surface	2	74	2	0	0	0	4	82	90
Paved Roads	0	1	76	2	2	1	0	82	93
Unpaved Roads	0	1	1	70	4	1	4	81	86
Forest	0	0	1	0	85	1	3	90	94
Rangeland	1	1	0	1	1	70	1	75	93
Water	0	3	1	2	3	0	80	89	90
Grand Total	70	82	82	76	97	73	94	574	
Producer's Accuracy	96	90	93	92	88	96	85		
Overall Accuracy	91								
Overall Kappa index	0.894						522		

Tables AP7.4 a, b & c: OBIDO Error Matrixes

(a) Pixel Based	BU	OS	PR	UR	F	R	W	Grand Total	User's Accuracy
Buildings	55	3	2	6	2	1	8	77	71
Open Surface	10	54	6	2	6	2	10	90	60
Paved Roads	3	0	56	3	8	1	2	73	77
Unpaved Roads	6	4	6	63	5	1	5	90	70
Forest	1	2	4	3	57	2	2	71	80
Rangeland	3	6	2	5	5	60	3	84	71
Water	3	7	5	2	1	3	62	83	75
Grand Total	81	76	81	84	84	70	92	568	
Producer's Accuracy	68	71	69	75	68	86	67		
Overall Accuracy	72								
Overall Kappa index	0.669						407		

(b) OBIA - VHR	BU	OS	PR	UR	F	R	W	Grand Total	User's Accuracy
Buildings	64	3	2	2	1	1	6	79	81
Open Surface	6	59	3	2	4	0	8	82	72
Paved Roads	1	0	64	3	5	1	2	76	84
Unpaved Roads	5	3	3	70	3	0	2	86	81
Forest	1	2	3	2	67	1	1	77	87
Rangeland	1	4	2	3	2	65	3	80	81
Water	3	5	4	2	2	2	70	88	80
Grand Total	81	76	81	84	84	70	92	568	
Producer's Accuracy	79	78	79	83	80	93	76		
Overall Accuracy	81								
Overall Kappa index	0.776						459		

(c) OBIA - VHR &nDSM	BU	OS	PR	UR	F	R	W	Grand Total	User's Accuracy
Buildings	75	3	1	1	0	1	2	83	90
Open Surface	1	67	2	0	2	0	5	77	87
Paved Roads	1	0	71	3	3	1	0	79	90
Unpaved Roads	2	0	3	77	2	0	0	84	92
Forest	0	1	1	1	76	1	1	81	94
Rangeland	0	3	2	2	0	65	3	75	87
Water	2	2	1	0	1	2	81	89	91
Grand Total	81	76	81	84	84	70	92	568	
Producer's Accuracy	93	88	88	92	90	93	88		
Overall Accuracy	90								
Overall Kappa index	0.885						512		

Tables AP7.5 a, b & c: OGBOGWU Error Matrixes

(a) Pixel Based	BU	OS	PR	UR	F	R	W	Grand Total	User's Accuracy
Buildings	61	4	2	6	1	3	10	87	70
Open Surface	6	58	7	3	6	2	6	88	66
Paved Roads	2	1	58	3	3	10	1	78	74
Unpaved Roads	9	4	5	65	3	2	2	90	72
Forest	5	2	5	1	68	3	5	89	76
Rangeland	4	6	1	2	4	59	1	77	77
Water	1	3	3	2	3	2	61	75	81
Grand Total	88	78	81	82	88	81	86	584	
Producer's Accuracy	69	74	72	79	77	73	71		
Overall Accuracy	74								
Overall Kappa index	0.692						430		

(b) OBIA - VHR	BU	OS	PR	UR	F	R	W	Grand Total	User's Accuracy
Buildings	70	2	2	2	0	3	4	83	84
Open Surface	4	65	6	2	2	0	4	83	78
Paved Roads	2	3	66	2	2	6	2	83	80
Unpaved Roads	5	2	2	71	2	2	2	86	83
Forest	2	2	3	1	76	2	1	87	87
Rangeland	4	2	0	3	3	67	1	80	84
Water	1	2	2	1	3	1	72	82	88
Grand Total	88	78	81	82	88	81	86	584	
Producer's Accuracy	80	83	81	87	86	83	84		
Overall Accuracy	83								
Overall Kappa index	0.806						487		

(c) OBIA - VHR & nDSM	BU	OS	PR	UR	F	R	W	Grand Total	User's Accuracy
Buildings	83	1	2	0	0	2	1	89	93
Open Surface	1	74	0	1	2	0	2	80	93
Paved Roads	0	1	77	1	0	3	0	82	94
Unpaved Roads	2	0	0	79	1	2	0	84	94
Forest	0	1	3	1	82	1	1	89	92
Rangeland	1	1	0	0	0	78	1	81	96
Water	1	0	1	0	3	0	78	83	94
Grand Total	88	78	83	82	88	86	83	588	
Producer's Accuracy	94	95	93	96	93	91	94		
Overall Accuracy	94								
Overall Kappa index	0.927						551		

Tables AP7.6 a, b & c: OMOKU Error Matrixes

(a) Pixel Based	BU	OS	PR	UR	F	R	W	Grand Total	User's Accuracy
Buildings	61	4	3	8	3	5	6	90	68
Open Surface	8	58	5	2	6	2	1	82	71
Paved Roads	3	1	55	5	7	8	6	85	65
Unpaved Roads	2	2	7	58	5	0	6	80	73
Forest	3	1	5	2	62	2	10	85	73
Rangeland	5	3	2	7	4	65	3	89	73
Water	2	7	3	3	2	3	57	77	74
Grand Total	84	76	80	85	89	85	89	588	
Producer's Accuracy	73	76	69	68	70	76	64		
Overall Accuracy	71								
Overall Kappa index	0.659						416		

(b) OBIA - VHR	BU	OS	PR	UR	F	R	W	Grand Total	User's Accuracy
Buildings	70	3	3	5	1	4	3	89	79
Open Surface	1	63	3	1	3	2	1	74	85
Paved Roads	3	1	67	1	2	3	4	81	83
Unpaved Roads	2	1	4	70	5	0	3	85	82
Forest	2	0	2	2	72	2	7	87	83
Rangeland	4	3	0	4	4	70	2	87	80
Water	2	5	1	2	2	2	69	83	83
Grand Total	84	76	80	85	89	83	89	586	
Producer's Accuracy	83	83	84	82	81	84	78		
Overall Accuracy	82								
Overall Kappa index	0.791						481		

(c) OBIA - VHR & nDSM	BU	OS	PR	UR	F	R	W	Grand Total	User's Accuracy
Buildings	80	1	2	1	1	2	2	89	90
Open Surface	0	71	1	0	2	1	2	77	92
Paved Roads	2	0	75	0	0	0	1	78	96
Unpaved Roads	1	1	1	80	2	0	1	86	93
Forest	1	0	1	1	83	2	4	92	90
Rangeland	0	0	0	2	0	77	1	80	96
Water	0	3	0	1	1	1	78	84	93
Grand Total	84	76	80	85	89	83	89	586	
Producer's Accuracy	95	93	94	94	93	93	88		
Overall Accuracy	93								
Overall Kappa index	0.916						544		

Tables AP7.7 a, b & c: OSIAKPU Error Matrixes

(a) Pixel Based	BU	OS	PR	UR	F	R	W	Grand Total	User's Accuracy
Buildings	60	5	4	3	3	5	5	85	71
Open Surface	10	61	3	4	6	2	2	88	69
Paved Roads	2	1	57	7	5	13	9	94	61
Unpaved Roads	8	6	2	64	3	2	5	90	71
Forest	8	2	7	2	61	2	2	84	73
Rangeland	8	4	3	5	10	64	2	96	67
Water	4	4	2	0	2	3	60	75	80
Grand Total	100	83	78	85	90	91	85	612	
Producer's Accuracy	60	73	73	75	68	70	71		
Overall Accuracy	70								
Overall Kappa index	0.647						427		

(b) OBIA - VHR	BU	OS	PR	UR	F	R	W	Grand Total	User's Accuracy
Buildings	78	4	3	1	2	5	5	98	80
Open Surface	4	69	1	2	1	0	2	79	87
Paved Roads	1	1	64	4	1	8	4	83	77
Unpaved Roads	4	1	1	73	3	1	4	87	84
Forest	3	2	5	2	75	1	2	90	83
Rangeland	6	3	3	3	8	73	0	96	76
Water	4	3	1	0	0	3	68	79	86
Grand Total	100	83	78	85	90	91	85	612	
Producer's Accuracy	78	83	82	86	83	80	80		
Overall Accuracy	82								
Overall Kappa index	0.786						500		

(c) OBIA - VHR & DSM	BU	OS	PR	UR	F	R	W	Grand Total	User's Accuracy
Buildings	88	1	2	0	2	2	2	97	91
Open Surface	3	77	1	2	0	0	2	85	91
Paved Roads	1	1	73	1	1	2	2	81	90
Unpaved Roads	0	0	0	79	1	0	2	82	96
Forest	0	1	0	1	84	0	2	88	95
Rangeland	5	2	1	2	2	85	0	97	88
Water	3	1	1	0	0	2	75	82	91
Grand Total	100	83	78	85	90	91	85	612	
Producer's Accuracy	88	93	94	93	93	93	88		
Overall Accuracy	92								
Overall Kappa index	0.903						561		

APPENDIX 8: Quantitative Values of the LU/LC classes achieved from different methods applied

Table AP8a: AKABUKA LU/LC Quantitative Values of Classes

Land Use	OB (VHR & nDSM)		OB (VHR)		PIXEL (ML)	
	Area	%	Area	%	Area	%
Buildings	21.57	18.08	25.26	21.17	16.60	13.91
Forest	48.35	40.52	8.81	7.38	40.16	33.66
Open Surfaces	13.13	11.00	7.50	6.29	23.26	19.50
Paved Roads	2.41	2.02	6.21	5.20	3.71	3.11
Rangeland	12.04	10.09	52.06	43.63	19.46	16.31
Unpaved Roads	7.60	6.37	12.18	10.21	6.34	5.31
Water	0.17	0.14	0.00	0.00	0.00	0.00
Shadow	14.04	11.77	7.3	6.12	9.79	8.20
TOTAL	119.31	100.00	119.31	100.00	119.31	100.00

Table AP8b: EGBEDA LU/LC Quantitative Values of Classes

Land Use	OB (VHR & nDSM)		OB (VHR)		PIXEL (ML)	
	Area	%	Area	%	Area	%
Buildings	69.66	11.46	89.54	14.73	56.11	9.23
Forest	309.24	50.86	91.72	15.08	266.89	43.89
Open Surfaces	48.16	7.92	2.70	0.44	65.77	10.82
Paved Roads	20.87	3.43	39.01	6.42	13.39	2.20
Rangeland	62.66	10.30	280.18	46.08	147.09	24.19
Unpaved Roads	21.56	3.55	28.99	4.77	35.15	5.78
Water	0.00	0.00	0.00	0.00	0.00	0.00
Shadow	75.92	12.49	75.92	12.49	23.65	3.89
TOTAL	608.07	100.00	608.07	100.00	608.07	100.00

Table AP8c: IKIRI LU/LC Quantitative Values of Classes

Land Use	OB (VHR & nDSM)		OB (VHR)		PIXEL (ML)	
	Area	%	Area	%	Area	%
Buildings	2.94	4.95	4.57	7.68	2.56	4.31
Forest	46.13	77.52	24.27	40.79	28.28	47.52
Open Surfaces	2.66	4.47	2.42	4.06	6.56	11.01
Paved Roads	1.15	1.94	1.53	2.58	0.58	0.97
Rangeland	3.48	5.84	22.75	38.23	9.14	15.36
Unpaved Roads	2.16	3.63	3.03	5.09	2.52	4.24
Water	0.98	1.65	0.93	1.57	0.83	1.40
Shadow	0	0.00	0	0.00	9.04	15.19
TOTAL	59.51	100.00	59.51	100.00	59.51	100.00

Table AP8d: OBIDO LU/LC Quantitative Values of Classes

Land Use	OB (VHR & nDSM)		OB (VHR)		PIXEL (ML)	
	Area	%	Area	%	Area	%
Buildings	8.03	8.22	22.88	23.40	2.16	2.21
Forest	27.33	27.95	15.48	15.84	17.78	18.18
Open Surfaces	20.65	21.12	3.19	3.26	20.03	20.48
Paved Roads	1.82	1.86	2.34	2.40	1.27	1.30
Rangeland	20.59	21.06	33.17	33.93	43.09	44.08
Unpaved Roads	5.07	5.18	6.91	7.07	5.88	6.01
Water	3.40	3.48	2.89	2.96	2.73	2.79
Shadow	10.89	11.14	10.89	11.14	4.84	4.95
TOTAL	97.77	100.00	97.77	100.00	97.77	100.00

Table AP8e: OGBOGWU LU/LC Quantitative Values of Classes

Land Use	OB (VHR & nDSM)		OB (VHR)		PIXEL (ML)	
	Area	%	Area	%	Area	%
Buildings	75.07	6.80	173.83	15.76	71.64	6.49
Forest	437.49	39.66	370.16	33.56	376.09	34.09
Open Surfaces	179.15	16.24	88.19	8.00	150.25	13.62
Paved Roads	41.03	3.72	59.08	5.36	56.00	5.08
Rangeland	139.30	12.63	167.33	15.17	310.44	28.14
Unpaved Roads	65.03	5.89	78.45	7.11	51.86	4.70
Water	9.52	0.86	9.52	0.86	6.97	0.63
Shadow	156.52	14.19	156.52	14.19	79.85	7.24
TOTAL	1103.10	100.00	1103.09	100.00	1103.09	100.00

Table AP8f: OMOKU LU/LC Quantitative Values of Classes

Land Use	OB (VHR & nDSM)		OB (VHR)		PIXEL (ML)	
	Area	%	Area	%	Area	%
Buildings	370.32	13.24	386.42	13.81	313.89	11.22
Forest	831.10	29.71	831.09	29.70	849.24	30.35
Open Surfaces	208.60	7.46	260.00	9.29	547.79	19.58
Paved Roads	87.27	3.12	166.61	5.96	159.13	5.69
Rangeland	712.33	25.46	526.33	18.81	690.42	24.68
Unpaved Roads	187.96	6.72	217.71	7.78	132.42	4.73
Water	13.96	0.50	23.36	0.83	5.46	0.20
Shadow	386.30	13.81	386.30	13.81	99.48	3.56
TOTAL	2797.84	100.00	2797.84	100.00	2797.84	100.00

Table AP8g: OSI AKPU LU/LC Quantitative Values of Classes

Land Use	OB (VHR & nDSM)		OB (VHR)		PIXEL (ML)	
	Area	%	Area	%	Area	%
Buildings	5.47	6.18	5.44	6.14	3.94	4.46
Forest	50.78	57.36	17.82	20.13	45.28	51.15
Open Surfaces	5.85	6.61	12.86	14.53	1.30	1.47
Paved Roads	0.92	1.04	2.83	3.20	1.58	1.79
Rangeland	5.75	6.50	28.08	31.72	21.91	24.75
Unpaved Roads	3.65	4.13	5.39	6.09	3.05	3.44
Water	0.74	0.84	0.74	0.84	0.76	0.86
Shadow	15.36	17.35	15.36	17.35	10.70	12.09
TOTAL	88.53	100.00	88.53	100.00	88.53	100.00